

Physical, Chemical and Biological Variability of the Sable Gully 2006-07

B.J.W. Greenan, B.D. Petrie, D.A. Cardoso, W.G. Harrison, E.J.H. Head
and W.K.W. Li

Ocean and Ecosystem Sciences Division
Maritimes Region
Fisheries and Oceans Canada

Bedford Institute of Oceanography
P.O. Box 1006
Dartmouth, Nova Scotia
Canada B2Y 4A2

2013

**Canadian Technical Report of
Hydrography and Ocean Sciences 293**

Canadian Technical Report of Hydrography and Ocean Sciences

Technical reports contain scientific and technical information of a type that represents a contribution to existing knowledge but which is not normally found in the primary literature. The subject matter is generally related to programs and interests of the Oceans and Science sectors of Fisheries and Oceans Canada.

Technical reports may be cited as full publications. The correct citation appears above the abstract of each report. Each report is abstracted in the data base *Aquatic Sciences and Fisheries Abstracts*.

Technical reports are produced regionally but are numbered nationally. Requests for individual reports will be filled by the issuing establishment listed on the front cover and title page.

Regional and headquarters establishments of Ocean Science and Surveys ceased publication of their various report series as of December 1981. A complete listing of these publications and the last number issued under each title are published in the *Canadian Journal of Fisheries and Aquatic Sciences*, Volume 38: Index to Publications 1981. The current series began with Report Number 1 in January 1982.

Rapport technique canadien sur l'hydrographie et les sciences océaniques

Les rapports techniques contiennent des renseignements scientifiques et techniques qui constituent une contribution aux connaissances actuelles mais que l'on ne trouve pas normalement dans les revues scientifiques. Le sujet est généralement rattaché aux programmes et intérêts des secteurs des Océans et des Sciences de Pêches et Océans Canada.

Les rapports techniques peuvent être cités comme des publications à part entière. Le titre exact figure au-dessus du résumé de chaque rapport. Les rapports techniques sont résumés dans la base de données *Résumés des sciences aquatiques et halieutiques*.

Les rapports techniques sont produits à l'échelon régional, mais numérotés à l'échelon national. Les demandes de rapports seront satisfaites par l'établissement auteur dont le nom figure sur la couverture et la page de titre.

Les établissements de l'ancien secteur des Sciences et Levés océaniques dans les régions et à l'administration centrale ont cessé de publier leurs diverses séries de rapports en décembre 1981. Vous trouverez dans l'index des publications du volume 38 du *Journal canadien des sciences halieutiques et aquatiques*, la liste de ces publications ainsi que le dernier numéro paru dans chaque catégorie. La nouvelle série a commencé avec la publication du rapport numéro 1 en janvier 1982.

**Canadian Technical Report of
Hydrography and Ocean Sciences 293**

2013

Physical, Chemical and Biological Variability of the Sable Gully 2006-07

by

**B.J.W. Greenan, B.D. Petrie, D.A. Cardoso, W.G. Harrison,
E.J.H. Head and W.K.W. Li**

**Ocean and Ecosystems Sciences Division
Maritimes Region
Fisheries and Oceans Canada**

**Bedford Institute of Oceanography
P. O. Box 1006
Dartmouth, Nova Scotia
Canada B2Y 4A2**

© Minister of Supply and Services 2013

Cat. No. Fs 97-18/293E ISSN 0711-6764 (print version)

Cat. No. Fs 97-18/293E-PDF ISSN 1488-5417 (on-line version)

Correct Citation for this publication:

Greenan, B.J.W., B.D. Petrie, D.A. Cardoso, W.G. Harrison, E.J.H. Head and W.K.W. Li. 2013. Physical, chemical and biological variability of the Sable Gully 2006-07. Can. Tech. Rep. Hydrogr. Ocean. Sci. 293: x+261 pp.

TABLE OF CONTENTS

TABLE CAPTIONS	V
FIGURE CAPTIONS	V
ABSTRACT	VIII
RÉSUMÉ	IX
1. INTRODUCTION	1
2. DATA AND METHODS	3
2.1 Field Program Overview	3
2.2 CTD Surveys	3
2.2.1 Lowered-Acoustic Doppler Current Profiler	3
2.2.2 BIONESS and Ring Net Tows	3
2.3 Current Meter Moorings	4
2.3.1 Mooring Data Return	4
2.4 Other Field Observations not Included in this Report	5
2.4.1 Vessel-Mounted-Acoustic Doppler Current Profiler	5
2.4.2 Sediment Grabs	5
2.4.3 Seabird Observations	5
2.4.4 CO ₂ Sampling	5
2.5 Data Processing	6
2.6 Data Analysis	6
2.6.1 Richardson Number	7
2.6.2 Tidal analysis	7
2.6.3 Spectral analysis	7
2.6.4 Atmospheric Data	7
2.6.5 Biological Data	8
2.6.6 Remote Sensing	8
3. RESULTS	8
3.1 Hydrographic Sections	8
3.2 Section-averaged profiles	9
3.3 Nutrient Profiles	10
3.4 Distribution of microbial plankton	11
3.5 Annual cycle of surface chlorophyll derived from SeaWiFS observations	11
3.6 Zooplankton Tow Results	13
3.7 Mooring Results	14
3.8 Sable Island Winds	17
4. DISCUSSION	17
5. CONCLUSIONS	21

ACKNOWLEDGMENTS	24
REFERENCES	25
TABLES	30
FIGURES	36
APPENDIX 1: MOORING DIAGRAMS	56
APPENDIX 2: CTD AND LOWERED-ACOUSTIC DOPPLER CURRENT PROFILER	61
APPENDIX 3: CTD SECTIONS, INCLUDING CHLOROPHYLL, FLUORESCENCE, AND NITRATE	87
APPENDIX 4: BIOLOGICAL DATA FROM CTD STATIONS, 2007	110
APPENDIX 5: ACOUSTIC DOPPLER CURRENT PROFILER (ADCP) MOORED CURRENT METER	118
APPENDIX 6: RCM SINGLE POINT MOORED CURRENT METER	140
APPENDIX 7: MOORED TEMPERATURE-SALINITY TIME SERIES	167
APPENDIX 8: CURRENT METER DATA SYNTHESIS	186
APPENDIX 9: TIDAL ANALYSIS	241
APPENDIX 10: SPECTRAL ANALYSIS	257

Table Captions

Table 1: Summary of Sable Gully mooring configuration. Nominal depths (m) of the instruments are indicated by the numbers in each of the mooring columns. Numbers with asterisks indicate that the RCM8 did not have sensors installed for pressure or conductivity. Water depth at each of the mooring sites is given by the number in brackets at the top of each column.

Table 2: Summary for each instrument type of the estimated accuracy (Acc) and resolution (Res) of the variables speed, direction, temperature and conductivity.

Table 3: ADCP bin depth used for plotting and percent data return for each bin.

Table 4: Percent data return for ADCP bins 16 to 24 on each of the four moorings SG2, SG10, SG11 and SG12.

Table 5: Parameters derived from the average annual cycle for the Gully and nearby areas. Under the heading “Linear Regression”, I stands for intercept, S for slope; under Gaussian fit, the peak corresponds to the largest value of surface chlorophyll concentrations, b the day of the peak bloom, and the duration the time span for the fitted bloom of rise/fall to 0.5 times the peak concentration.

Table 6: Ratio of SG11 to Slope variance from moored current meter data (see Figure 18) at various depths listed on the column headings. The rows represent different frequency bands.

Figure Captions

Figure 1: Schematic (depth in m) of the Sable Gully field program with CTD stations (grey dots) and mooring sites (red dots) indicated. The inset shows the eastern North America shelf break region with other canyons which have been studied: Carson (C), Lydonia (L), Hudson (H) and Baltimore (B).

Figure 2: Mean currents averaged in three layers in the Sable Gully region from BIO archived data. The three layers presented are 0-50 m (black), 50-100 m (red) and 100-150 m (green).

Figure 3: April 2006 CTD section (Stations 14-21) across the mouth of Sable Gully showing (a) temperature ($^{\circ}\text{C}$), (B) salinity (with σ_T density contours, kg m^{-3}), and (C) dissolved oxygen (% saturation).

Figure 4: August 2007 CTD section of Stations 14-21 across the mouth of Sable Gully showing (A) temperature ($^{\circ}\text{C}$), (B) salinity (with σ_T density contours kg m^{-3}), and (C) dissolved oxygen (% saturation).

Figure 5: Section-averaged salinity and temperature (°C) profiles for the 2006 (A, B) and 2007 (C, D) CTD surveys. The vertical range has been limited to depths below the canyon rim (200 m) and above 1000 m.

Figure 6: Temperature-salinity plots based on the CTD surveys in 2006 (A) and 2007 (B) for 200-1000 m. Profiles for each section are color-coded. Isopycnals are shown as sloping, gray shaded lines. T-S envelopes, based on Gatién (1976), are presented for Labrador Slope Water (LSW, magenta) and Warm Slope Water (WSW, cyan).

Figure 7: Nitrate, phosphate and silicate concentrations for the Gully (black) for April 2006 (upper panels) and August 2007 (lower panels) and for three adjacent areas (Banquereau, Middle and Sable Island Banks, grey) in April-May (upper panels) and July-August (lower panels).

Figure 8: Station-averaged values for the Gully in August 2007. (A) temperature, (B) salinity, (C) density, (D) chlorophyll *a*, (E) *Synechococcus*, (F) picoeukaryotic algae, (G) nanophytoplankton, and (H) bacteria. Individual samples are shown as grey dots; 10m depth-binned average and standard deviations are shown in red colour. (I) Full depth profile of bacteria.

Figure 9: Phytoplankton and bacteria on the Scotian Shelf and the Gully. Values across the Scotian Shelf are station-average measurements of 100m-integrated abundance from AZMP surveys in the spring (April, green circles) and fall (October, orange squares) from 1997-2011 on the 21 core stations of the Browns Bank Line (Western Scotian Shelf), the Halifax Line (Central Scotian Shelf), and the Louisbourg Line (Eastern Scotian Shelf). Values in the Gully are station-average measurements of 100m-integrated abundance from the 2007 summer survey (August, pink diamond).

Figure 10: Annual variation of surface chlorophyll based on SeaWiFS observations from 1997-2009.

Figure 11: Gaussian fit (G) to and observed (O) spring bloom for Middle Bank and the Gully.

Figure 12: Zooplankton biomass in the Gully in April 2006 and August 2007. Black symbols show the biomass in the 0-100 m depth range, red symbols show the biomass for greater depth ranges.

Figure 13: Seasonal cycle of zooplankton biomass in the Gully, constructed from average monthly values derived from cruises between 1984 and 2009, together with values averaged over all sampling stations in April 2006 and August 2007. The numbers by each point of the 1984-2009 data show the number of tows that were made in each month over the 15 year period; some years there were several tows in one or more months.

Figure 14: Average estimates from SG10, SG11 and SG12 moorings for the (A) across-canyon speed (m s^{-1} , positive northeast), (B) along-canyon speed (m s^{-1} , positive northwest), (C) across-canyon variance of speed ($\text{m}^2 \text{s}^{-2}$) and (D) along-canyon variance ($\text{m}^2 \text{s}^{-2}$). Grey lines in the top two panels represent the 0 m s^{-1} contour.

Figure 15: Progressive vector diagrams for (A) SG2, (B) SG11, (C) SG12 and (D) SG10 moorings. The approximate direction of the Sable Gully axis is shown as a light gray line. The scale in (A) shows the distance travelled over the entire observation period for an average speed of 0.05 m s^{-1} . Lines are color-coded based on instrument depth: red ($<200 \text{ m}$, shallower than the canyon rim), green (mid-depth) and blue (deep). The number at the end of each line denotes the nominal instrument depth.

Figure 16: Variances derived from instruments at mooring sites (A) SG2, (B) SG11, (C) SG12 and (D) SG10. Variances from Scotian Slope moorings at comparable bottom depths are shown for comparison. Variance is presented as low frequency (subtidal) and total components.

Figure 17: Tidal ellipses for the (A) K1 and (B) M2 tidal constituents. The ellipses have been plotted such that tidal excursions correspond to map geometry. Record depths are colour-coded.

Figure 18: Spectra of depth-averaged currents for two locations within the Sable Gully (black, red dots) and three locations on the Scotian Slope. Site C, not shown on the inset, is located at approximately 42.67°N , 63.5°W . Observations from sites A and B are from 2000-04 (Loder and Geshelin, 2009); observations from Site C are from 1975-78 (Smith and Petrie, 1982). Vertical grey lines correspond to tidal and inertial frequencies. Ninety-five percent confidence levels are shown for the Gully Head record at diurnal, semi-diurnal and 5 cpd frequencies.

Figure 19: Sable Island hourly wind speed (m s^{-1}), direction ($^\circ\text{T}$), along-shore wind stress (Pa) and across-shore wind stress (Pa). The numbers on the wind stress panels indicate the value for those points that extend beyond the limits of the y-axis.

Figure 20: Progressive vector diagram for Sable Island hourly wind from April 2006 to September 1, 2007.

Figure 21: (A) Loadings for the first mode of a principal component analysis (PCA) based on the covariance matrix of the along-Gully monthly currents for depths = 150 m, moorings SG10-12. (B) Time series of PCA1 for the period of the mooring deployment.

ABSTRACT

Greenan, B.J.W., B.D. Petrie, D.A. Cardoso, W.G. Harrison, E.J.H. Head and W.K.W. Li. 2013. Physical, chemical and biological variability of the Sable Gully 2006-07. Can. Tech. Rep. Hydrogr. Ocean. Sci. 293: x+261 pp.

The Sable Gully, a broad, shelf break submarine canyon approximately 40 km east of Sable Island on the eastern Scotian Shelf, separates Banquereau and Sable Island Banks. Unique among canyons on the eastern Canadian continental shelf because of its depth, steep slopes and extension far onto the shelf, its ecological significance and increasing human pressures led to its designation in 2004 under Canada's *Oceans Act* as the first Marine Protected Area (MPA) in the Atlantic Region.

To improve the state of knowledge of the Gully MPA, a multi-disciplinary field program was carried out in 2006-07; this consisted of the deployment (April 2006) and recovery (August 2007) of four current meter moorings, and CTD surveys during the 2006 and 2007 cruises. Analysis of this 16-month mooring deployment demonstrates that the mean circulation above the canyon rim (~200 m) is characterized by a southwestward flow which appears unaffected by the canyon topography. There is also some indication of the existence of an eddy at rim depth. Below 500 m, the circulation is dominated by an up-canyon flow (of order 0.02 m s^{-1}) at the mooring array (halfway between the canyon head and mouth). The mean, 200 m–bottom transport towards the head of the Gully was estimated as $35,500 \text{ m}^3 \text{ s}^{-1}$, implying an upwelling velocity of $1.7 \times 10^{-4} \text{ m s}^{-1}$ (14 m d^{-1}) over the area between the mooring array and the head of the Gully. Results also show bottom-intensified tidal flows and non-linear constituents due to the interaction of K1, O1, M2 and S2 components along the thalweg of the canyon; the strong overtimes and compound tides observed in the Gully makes it unique among canyons. Further analyses provide evidence of enhanced vertical mixing in the Gully ($K_v \sim 180 \times 10^{-4} \text{ m}^2 \text{ s}^{-1}$), which is approximately 20 times that observed on the adjoining Scotian Shelf. Total variance of the currents in the Gully is about 2.5 times greater than that observed on the nearby continental slope with an equivalent water depth.

The vertical distribution of phytoplankton and bacteria in the Gully appear, as elsewhere, to be constrained by the surface layer nutrient regime imposed by density stratification. Maximum microbial cell abundance is located at the top of the pycnocline/nitracline, but maximum phytoplankton biomass is somewhat deeper. On a seasonally adjusted basis, there is no strong evidence of enhanced phytoplankton or bacterial concentrations in the Gully compared to the Scotian Shelf as a whole. Observations of surface chlorophyll derived from SeaWiFS observations were compiled for the Gully as well as for 5 adjacent or nearby areas. Results of this analysis indicate that the Gully does not appear to be distinct relative to the other nearby regions. Surface to 250 m profiles of nitrate, phosphate and silicate concentrations in Gully did not differ from those on the surrounding shelf. Zooplankton were collected in vertical net tows (200 μm mesh) between 100 m and the surface at nine stations in April 2006 and at eleven stations in August 2007.

RÉSUMÉ

Greenan, B.J.W., B.D. Petrie, D. Cardoso, W.G. Harrison, E.J.H. Head et W.K.W. Li. 2013. Variabilité physique, chimique et biologique du goulet de l'île de Sable 2006-2007. Rapp. tech. can. hydrogr. sci. océan. 293: x+261 pp.

Gully est un large canyon sous-marin au bord de la plateforme continentale, situé à environ 40 km à l'est de l'île de Sable sur à l'est du plateau néo-écossais, qui sépare le banc Banquereau et le banc de l'île de Sable. Il se distingue parmi les canyons du plateau continental de l'est du Canada en raison de sa profondeur, de ses parois abruptes et du fait qu'il s'étend sur une bonne distance sur le plateau. Son importance écologique et les pressions humaines croissantes ont conduit en 2004 à sa désignation comme première zone de protection marine (ZPM) de la région de l'Atlantique en vertu de la *Loi sur les océans* du Canada.

Afin d'améliorer l'état des connaissances sur la ZPM du Gully, un programme multidisciplinaire a été mis en œuvre sur le terrain en 2006-2007. Ce programme a consisté à mettre en place en avril 2006 quatre bouées amarrées de courantomètres et à effectuer des études sur la conductivité, la température et la profondeur durant les croisières de 2006 et 2007. Ces bouées ont été récupérées en août 2007. L'analyse des 16 mois durant lesquels les bouées ont été mouillées montre que la circulation moyenne au-dessus du bord du canyon (environ 200 m de profondeur) est caractérisée par un flux s'écoulant vers le sud-ouest qui ne semble pas affecté par la topographie du canyon. Il y a également quelques indications de l'existence d'un tourbillon à la profondeur du bord. À 500 m de profondeur, la circulation est dominée par un courant remontant le canyon (de l'ordre de $0,02 \text{ m s}^{-1}$) à hauteur du poste d'amarrage (à mi-chemin entre la tête et la sortie du canyon). Le transport moyen (entre 200 m de profondeur et le fond) vers la tête du Gully a été estimé à $35\,500 \text{ m}^3 \text{ s}^{-1}$, ce qui implique une vitesse de remontée des eaux de $1,7 \times 10^{-4} \text{ m s}^{-1}$ (14 m d^{-1}) dans la zone située entre le poste d'amarrage et la tête du Gully. Les résultats montrent également la présence de courants de marée plus forts au niveau du fond et de constituants non linéaires en raison des interactions entre les composants K1, O1, M2 et S2 le long du creux barométrique du canyon. Les fortes ondes supérieures de marée et ondes composées observées dans le Gully le distinguent des autres canyons. Des analyses approfondies apportent la preuve d'un accroissement du mélange vertical dans le Gully ($K_v \sim 180 \times 10^{-4} \text{ m}^2 \text{ s}^{-1}$), ce qui représente environ 20 fois ce qui a été observé sur le plateau néo-écossais adjacent. L'écart total entre les courants dans le Gully est environ 2,5 fois plus grand que ce qui a été observé sur la pente continentale à proximité à une profondeur de l'eau équivalente.

La répartition verticale du phytoplancton et des bactéries dans le Gully semble, tout comme ailleurs, être entravée par le régime des éléments nutritifs de la couche de surface imposé par stratification de la densité. L'abondance maximum de cellules microbiennes se situe au sommet de la pycnocline/nitracline, mais la biomasse maximale du phytoplancton se trouve un peu plus en profondeur. Sur une base ajustée en fonction des saisons, il n'y a pas de preuve solide d'accroissement du phytoplancton ou des concentrations bactériennes dans le Gully en comparaison avec l'ensemble du plateau néo-écossais. Les observations de la chlorophylle à la surface dérivées d'observations SeaWiFS ont été compilées pour le Gully ainsi que pour cinq zones adjacentes ou à proximité. Les résultats de cette analyse indiquent que le Gully ne semble pas être différent des autres régions à proximité. Les profils des concentrations de

nitrate, de phosphate et de silicate entre la surface de l'eau et 250 m de profondeur dans le Gully ne diffèrent pas de celles du plateau autour du canyon. Du zooplancton a été collecté dans des traits de filets verticaux (mailles de 200 μm) entre 100 m de profondeur et la surface à neuf stations en avril 2006 et à onze stations en août 2007.

1. Introduction

Submarine canyons are common features of the continental margins off both coasts of North America (Harris and Whiteway, 2011). They have been shown to act as sediment pathways, transporting material from the shelf to the continental slope (Shephard et al., 1974; Carson et al., 1986; Nittrouer and Wright, 1994); furthermore, it has been argued that the canyons are sites of enhanced species diversity and bioproductivity (Hickey, 1995; Hooker et al., 1999; De Leo et al., 2010; Moors-Murphy, 2013; Kenchington et al., 2013) which could be driven by increased nutrient fluxes generated by upwelling (Freeland and Denman, 1982). Theoretical and numerical studies have shown that strong upwelling occurs on the downstream rim of canyons narrower than half the Rossby radius (Klinck, 1988, 1989, 1996; Allen, 1996; Chen and Allen, 1996). Geostrophic flow is predicted and observed to follow isobaths in broader canyons (width \sim Rossby radius; Kinsella et al., 1987; Maso et al., 1990).

Enhanced turbulent mixing has been identified as an alternative mechanism to upwelling for supplying nutrients to the euphotic zone in canyons (Carter and Gregg, 2002). Canyons may be effective conduits for funneling open-ocean internal wave energy onto the inner shelf (Gordon and Marshall, 1976) and sites for the generation of internal waves through topographic scattering of surface tides (Bell, 1975; Baines, 1982, 1983). These waves in turn may lead to increased mixing. Large internal wave fluctuations have been reported in canyons (Shephard et al., 1974; Gardner, 1989; Hotchkiss and Wunsch, 1982; Petruncio et al., 1998; Garcia Lafuente et al., 1999). Near-inertial period oscillations are suppressed by the proximity of steep canyon topography, while internal tides and their harmonics can be enhanced. Kunze et al. (2012) inferred horizontal upslope flows of $10\text{--}50\text{ m day}^{-1}$ in Monterey and Soquel Canyons based on an advective-diffusive balance. Hall et al. (2013) demonstrate that changes in the near-surface stratification can modify the behavior of the internal tides in upper Monterey Canyon; this seasonal transition was from a partly standing wave during pre-upwelling conditions to a progressive wave during upwelling condition.

Xu and Noble (2009) combined current meter measurements from three deployments in Monterey Canyon to provide an overview of the mean, subtidal and tidal flows for depths ranging from 250 to 3300m. Their conclusion was that the spatial variations in the flow fields were primarily controlled by the topography of the canyon. The flows were dominated by tidal currents, especially the semidiurnal constituents M2 and S2, which typically accounted for more than 90% of the variance. Pulses of strong currents, attributed to intense baroclinic processes, were observed near the canyon floor over periods of several days with magnitudes as high as 0.6 m s^{-1} . The subtidal and mean currents were relatively weak (typically less than 0.05 m s^{-1}) with the higher along-canyon speeds being observed in the narrow upper reaches.

On the east coast of North America, observational studies have been carried out in Hudson, Baltimore, Lydonia and Carson Canyons, all four of which lie on the same equatorward advective pathway as the Sable Gully (Figure 1). Hotchkiss and Wunsch (1982) observed that available potential energy increased by a factor of 10 toward the bottom and by 100 toward the head of Hudson Canyon on the New York Bight. Tidal flows were the main components of the overall current variance which was about $0.03\text{ m}^2\text{ s}^{-2}$ near the bottom at mid-canyon. The

currents within Baltimore Canyon were complex, making it difficult to establish a well-determined circulation (Hunkins, 1988). However, this study demonstrated a near-bottom amplification of semi-diurnal tidal flows throughout the mooring period. Tidal currents dominated the flow over the entire study area with M4 and MS4 harmonic constituents evident at the head (bottom depth 275 m) and near mid-canyon (bottom depth 600 m). Along the axis of the canyon, total current variance near the bottom ranged from $0.014 \text{ m}^2 \text{ s}^{-2}$ (565 m) to $0.002 \text{ m}^2 \text{ s}^{-2}$ (993 m). The Lydonia Canyon study on the southern flank of Georges Bank indicated that mean currents in the Canyon were weaker than those over the adjacent shelf and slope (Noble and Butman, 1989). In addition, the amplitude of the sub-tidal flow was 2 to 6 times weaker in the Canyon than on the shelf and slope; tidal flows were the strongest components of the current field. During a mooring deployment of about 2 weeks, Kinsella et al. (1987) found that when a baroclinic shelf break jet (Labrador Current) encountered the abrupt topography of Carson Canyon on the eastern slope of the Grand Banks, the flow was deflected by about 15° and led to an on-shelf transport of $\sim 0.02 \text{ Sv}$.

The Sable Gully is a submarine canyon located approximately 40 km east of Sable Island on the eastern Scotian Shelf and separates Banquereau and Sable Island Banks (Figure 1). It is unique among canyons on the eastern Canadian continental shelf because of its depth, ($Z_{\text{max}} \sim 2000 \text{ m}$) steep slopes (0.2) and extension far onto the shelf ($\sim 110 \text{ km}$). It can be divided into two general areas, the trough and the canyon. The trough is a wide, long (30 km x 70 km) shallow basin at the head of the canyon, which links the continental slope with the inner Scotian Shelf. The canyon is a narrower, shorter feature (10 km x 40 km) extending onshore from the shelf break and characterized by steep sides extending to depths greater than 2000 m. The width of the canyon, relative to the Rossby radius ($R \sim 14 \text{ km}$; Swart et al. (2011)), suggests that upwelling on the Gully's downstream rim is possible (Allen and Hickey, 2010). The Gully's unique physical attributes and its ecological significance led to its designation in 2004 as a Marine Protected Area (MPA) under Canada's *Oceans Act*. Greenan et al (2013) provide an introduction to the physical oceanography of the Sable Gully.

An analysis of archived data which focused on the circulation, current variability, cross-shelf exchange, tides and low frequency variability of hydrographic properties suggested that circulation in the Gully contributes to localized retention of materials and large-scale, cross-shelf transport (Petrie et al., 1998). However, many of the conclusions depended solely on computer simulations of the circulation with few supporting data. While current meter databases do not contain records from within the Gully, nearby data indicate that the upper (0-50 m) ocean mean flows are less than 0.15 m s^{-1} (23 of 25 records, 15 of which are $< 0.1 \text{ m s}^{-1}$) and predominantly towards the southwest (Figure 2). The currents generally decrease with increasing depth with a median speed of 0.04 m s^{-1} for the combined 50-100 m and 100-150 m layers. These records also provide some evidence of the clockwise circulation around Sable Bank, to the west of the Gully.

From April 2006 to August 2007, a field program was mounted to address basic issues in the Sable Gully including its mean circulation, evidence for enhanced mixing and vertical fluxes, and processes that may be unique to the Gully relative to the areas of similar depth on the adjacent Scotian Shelf and Slope. The data and analysis methods are summarized in Section 2 and results are presented in Section 3. A discussion of the findings is given in Section 4, and a

summary of conclusions is presented in Section 5. A series of 10 appendices present plots of basic data as well as some derived data products.

2. Data and Methods

2.1 Field Program Overview

The field program consisted of four moorings (deployment April 23-24, 2006, recovery August 3, 2007) and two shipboard conductivity, temperature, depth (CTD) surveys. The CTD surveys (April 22-26, 2006; August 2-8, 2007) included nutrient, chlorophyll, bacteria, phytoplankton and zooplankton sampling, and lowered-acoustic Doppler current profiling.

2.2 CTD Surveys

Profiles of water properties were obtained using a Sea-Bird 911 CTD-rosette equipped with dual temperature, conductivity, oxygen and fluorescence sensors, and single a PAR sensor. The CTD surveys were completed for sites SG1-SG21 in 2006 and SG1-SG29 in 2007 (Figure 1). The temperature and conductivity sensors were calibrated annually at the Bedford Institute of Oceanography. Salinity samples were collected during the surveys using the CTD rosette and were subsequently analyzed with an Autosol; these results were incorporated into the calibration of the CTD data. The oxygen, fluorescence and PAR sensor outputs are based on the manufacturer's calibration for each instrument.

2.2.1 Lowered-Acoustic Doppler Current Profiler

A narrowband 150 kHz RDI Lowered-ADCP system (LADCP) was mounted and lowered on the CTD rosette. It was loaned to BIO by Daniel Torres at the Woods Hole Oceanographic Institution (WHOI) and is normally used on our CTD system during the annual AR7W survey of the Labrador Sea. Repeated LADCP profiles were collected over a 12-hour period at stations (SG18, SG11, SG6 and SG2) along the Gully axis during the last two working days of the 2007 survey.

2.2.2 BIONESS and Ring Net Tows

Zooplankton were collected in vertical net tows (200 μ m mesh) between 100 m and the surface at nine stations in April 2006 (Stations 2, 4, 6, 9, 11, 13, 14, 16, 18, and a station off the main grid located east of 19 and south of 20) and at eleven stations in August 2007 (2, 6, 9, 11, 13, 14, 16, 18, 20, 22 and one located between 24 and 25). During deployment one deep ring net tow was carried out at SG11 and during recovery ring net tows to 1000 m were completed at SG11, SG18, SG25 and SG26.

BIONESS tows for plankton concentration measurements were carried out during recovery in the central Gully, northwest and northeast arms of Gully. The multiple opening-closing net system BIONESS enabled vertical resolution of the water column with 10 nets (202 \sim m mesh).

2.3 Current Meter Moorings

One mooring was deployed at each of the sites SG2 (1050 m), SG10 (475 m), SG11 (1640 m) and SG12 (723 m) (see Figure 1). The moorings consisted of one upward-looking Teledyne RDI 300 kHz Workhorse acoustic Doppler current profiler (ADCP), 3 to 6 Aanderaa RCM8 current meters, 2 to 4 Sea-Bird SBE37 MicroCAT temperature/conductivity sensors, and 2 to 3 Vemco Minilog temperature recorders (for details, see Table 1). The moorings were designed to provide near-complete depth coverage; a sub-surface Braincon float, equipped with an upward-looking ADCP, provided the main buoyancy. For the moorings on the Gully slopes (SG10 & SG12), there was no instrumentation above the Braincon; on SG2 and SG11, a streamlined buoyancy package equipped with a MicroCAT was placed 45 m above the main float. All moorings were deployed with either a 3 or 4-trainwheel anchor and a Benthos 965A acoustic release.

The ADCPs recorded vertical profiles of currents in 24 4-m bins; samples were recorded hourly with a setting of 80 pings per ensemble in burst mode. The estimated resolution of the ADCP with this setup is summarized in Table 2. The time series were binned into 25-m averages for analysis purposes. The RCMs recorded currents and temperatures hourly at a single depth; some shallower RCMs also recorded pressure and salinity. The Minilogs recorded temperature hourly; the MicroCATs recorded temperature, salinity and pressure in 10-min intervals. Three different MicroCAT pressure sensors, with resolutions of 0.02, 0.04 and 0.06 dbar and accuracies of 1, 2 and 3 dbar, were paired with the temperature and salinity sensors. Nominal resolutions and accuracies of these sensors are summarized in Table 2.

Bottom depths change profoundly over short horizontal distances within the Gully; this led to moorings SG2 and SG12 being deployed 100 m deeper than intended and compromised the resolution of near-surface currents.

2.3.1 Mooring Data Return

The array provided high quality data for the full deployment with a few exceptions. Firstly, the surface to 150 m depth range was not well sampled at SG2, 11 and 12; only SG10 had significant data return from the upper 150 m (Table 3, Table 4). Secondly, the upper 200 m of mooring SG11 broke away on 17 June 2007 due to a wire failure, resulting in the temporary loss of an ADCP, one Minilog and two MicroCATs. All remaining instruments continued to function; however, their data were compromised due to the loss of the primary buoyancy. Backup buoyancy allowed the recovery of these instruments on 3 August 2007. The upper part of this mooring was recovered by a fisherman and returned to BIO with data intact.

A third significant issue arose from the unexpectedly strong currents along the canyon axis, currents which caused substantial knockdown of moorings SG2 and SG11. For example, the SG11 (bottom depth 1640 m) mooring frequently had knockdowns as large as 500 m. This complicated the processing and quality control of the data from these sites. In this paper, the standard depths of the RCM8s and Minilogs were determined from the pressure record of the closest MicroCAT using the known distances between instruments. Further, the 4-m resolution ADCP data were binned and averaged every $25 \text{ m} \pm 2 \text{ m}$ to minimize gaps in the records.

As a result of the large mooring knockdowns, the flotation in the streamlined buoyancy above the Braincon on the SG2 and SG11 moorings imploded during deployment causing the upper MicroCAT and Minilog to sink about 90 m deeper than intended. A Minilog on SG2 also imploded because it exceeded its design depth.

Finally, the MicroCAT at 660 m (SG11) did not record salinity or pressure; the MicroCAT at 225 m (SG2) did not record salinity.

2.4 Other Field Observations not Included in this Report

2.4.1 Vessel-Mounted-Acoustic Doppler Current Profiler

A vessel-mounted 75 kHz RDI Acoustic Doppler Current Profiler Ocean Surveyor (VM-ADCP) was run continuously in narrowband mode from the ship's departure at BIO until the start of the Lowered-ADCP (LADCP) survey. Its primary purpose was to record volume backscattering for biological studies. The sampling period was normally 30 seconds; long-term averaging was set to 5 minutes. At the beginning of the LADCP survey, the vessel-mounted profiler was switched to broadband mode to give the best quality current estimates in the upper 650 m while the LADCP was deployed to get full-depth current profiles.

2.4.2 Sediment Grabs

Sediment samples were collected at four of the eight planned sites (SED2, SED3, SED4, and SED5) during recovery. These four sites were at the heads of active feeder canyons on the northwest side of the Gully. Two samples were collected with the van Veen grab at each site. One sample will be used for hydrocarbon and the other for metals analyses. All samples were frozen immediately and have been analyzed by Dr. Ken Lee's lab at the Centre for Offshore Oil, Gas and Energy Research at BIO.

2.4.3 Seabird Observations

Seabird observations were carried out during the 2006 cruise by David Fifield and during the 2007 cruise by Susan Abbott, both under contract to the Canadian Wildlife Service (CWS). Contact Carina Gjerdum at CWS for more information.

2.4.4 CO₂ Sampling

CO₂ sampling was conducted at stations SG2, SG6, SG11, SG17, SG22, SG24, SG27 and SG29 at all depths in 2007. A solution of HgCl₂ was added to the samples to prevent further biological activity from altering the in situ carbon content; the bottles were returned to the lab for analysis of dissolved inorganic carbon (DIC) and alkalinity. An underway system was run throughout the cruise; an open path atmospheric sensor mounted above the ship's bridge measured the CO₂ levels of the air, while corresponding wind speed and direction measurements were recorded by the ship's internal meteorological monitoring system. An underway system was installed in the geochemistry lab to monitor surface water CO₂ continuously using the seawater intake located

~3 meters below the surface. These data were collected by Elizabeth Shadwick and Dr. Helmuth Thomas of Dalhousie University.

2.5 Data Processing

All shipboard profile data and moored time series were processed using standard methodologies employed by the Ocean Data and Information Services (ODIS) group at the Bedford Institute of Oceanography. These procedures include spike removal and checks for other quality control issues such as low signal-to-noise ratio. The data are archived in a self-described ASCII file in the Ocean Data Format and are publically available.

While knockdown of the SG11 and SG2 moorings caused vertical displacement of the individual instruments, it did not cause significant data quality issues. This can be partially attributed to the manner in which the instruments were mounted on the mooring; the ADCPs were installed in streamlined buoyancy packages which maintain a specified orientation into the flow. The pitch/roll time series for the ADCPs indicated that none of the instruments exceeded 10 degrees tilt during the deployments. The RCMs were mounted in gimbals, which ensured that they remained close to vertical even if the mooring tilted during knockdown.

2.6 Data Analysis

Data analysis was mostly conducted using MATLAB[®]. CTD profiles are plotted for each station for the deployment and recovery periods and presented in Appendix 2. Section plots were created for CTD-measured temperature, salinity, density, dissolved oxygen and fluorescence using the primary CTD sensors; the data were compared with those from the secondary sensors and no significant differences were found except for the near-surface observations at site 26. The Brunt-Väisälä frequencies ($=\{-g/\rho_0\}\partial\rho/\partial z$) and percent saturations of dissolved oxygen were calculated and plotted. The Brunt-Väisälä frequencies were computed from CTD data using the Properties of Sea Water MATLAB toolbox available from the SEA-MAT website (<http://woodshole.er.usgs.gov/operations/sea-mat/>).

Section plots were also generated for chlorophyll, nitrate, bacteria, *Synechococcus*, picoeukaryotes, and nanophytoplankton data collected using the rosette bottle system. Surface to 100 m integrated bubble plots were generated for these data with the exception of nitrate. Scatter plots were generated for nitrate versus salinity and chlorophyll versus fluorescence. All contour and scatter plots are presented in Appendix 3. During the deployment period in April 2006 only every second station was sampled for chlorophyll.

Contoured time series are plotted for currents, vertical shear and percent of good pings for the ADCP data. Stick plots of daily averaged U (positive eastward) and V (positive northward) current are plotted as well as current time series for depth-binned data, approximately every 25 m, with the percent of data return given on each plot. All ADCP plots are shown in Appendix 4. Time series plots were generated for pressure, temperature, salinity and currents for RCM data and are presented in Appendix 5.

Time series plots of Microcat pressure, temperature and salinity and Minilog temperature are presented in Appendix 6. In addition, temperature and salinity contour plots versus time for each mooring generated by combining all records, and daily averaged temperature/salinity scatter plots for RCM and Microcat instruments are provided in Appendix 6.

Monthly and overall mean current velocity and variance section plots were created for the middle section of the canyon using the data from moorings 1589, 1590 and 1591. The 25 m binned ADCP data along with the RCM data were used; any ADCP bin with less than 60% data return was not included. Currents were resolved along and across the Gully; the along-(across-)Gully direction was 60°(150°)T. Monthly current roses were plotted showing the current velocity and direction distributions (Appendix 7).

2.6.1 Richardson Number

Both the CTD and LADCP data sets were used to estimate the gradient Richardson number, $Ri = -g\partial\rho\partial z / \{\rho_0(\partial u/\partial z)^2\}$ where g is the gravitational acceleration, ρ is the water density, z is vertical distance, and u is the water velocity. The magnitude of Ri is an indicator of the potential for vertical mixing. The vertical shear was computed using a first-differencing method. Values of shear below the precision of the LADCP were removed from the data set. The buoyancy frequency, $N^2 (= -g/\rho_0\partial\rho\partial z)$, was calculated using density computed from the CTD data. The data from individual CTD profiles were matched with co-occurring LADCP data to estimate Ri in 16 m vertical bins. These results, presented in Fig. A-29, show that Ri values typically are in the range of 1 to 5.

2.6.2 Tidal analysis

Harmonic tidal analyses of the RCM8 and the ADCP 25 m binned currents time series were conducted using the t-tide package (Pawlowicz et al., 2002) and MATLAB[®]. These tidal analyses provide the semi-major and semi-minor axis current amplitudes, ellipse orientation and phase with confidence intervals for each tidal constituent (Appendix 9). Tidal ellipses of the dominant tidal constituents are also shown in Appendix 9 for selected depths.

2.6.3 Spectral analysis

Spectral analyses of the currents time series were done using the Hamming window of 1024 points sampled hourly and Welch's averaged modified periodogram method (Welch, 1967). Results of these analyses are provided in Appendix 10.

2.6.4 Atmospheric Data

Hourly wind speed data for Sable Island concurrent with the mooring program were obtained from Environment Canada (<http://climate.weatheroffice.gc.ca/>). The data were filtered and subsampled every 6 hours using a Cartwright low pass filter with a half power point of ~28 hours.

2.6.5 Biological Data

Water samples were collected using a 24-bottle rosette attached to a CTD (SeaBird SBE 911). Nutrients (nitrate, silicate and phosphate) were analyzed colourimetrically using standard chemical methods and a Technicon Autoanalyzer; chlorophyll was determined from acetone-extracted samples by fluorometry (Mitchell et al. 2002). Nanophytoplankton, picophytoplankton and bacterial abundance were determined by flow cytometry according to methods outlined in Li and Dickie (2001). Vertical plankton net tows were analyzed for zooplankton.

Fluorescence data from the CTD sensor were processed using the manufacturer's calibration; bottle chlorophyll samples collected during both cruises were compared to the simultaneously measured fluorescence observations (Fig. A-51). The comparison for cruise HUD2006/008 shows a weak negative correlation ($r^2 = 0.35$, $\text{Chl} = -2.2 \cdot \text{Fluor} + 11.6$), indicating a poor relationship of fluorescence with in situ chlorophyll. There is some improvement for the recovery cruise; the comparison for HUD2007/033 shows a positive correlation, a large slope and an intercept of approximately 0 ($r^2 = 0.65$, $\text{Chl} = 2.9 \cdot \text{Fluor} + 0.03$). From Figure A-51 it is apparent that the scatter of in situ chlorophyll and fluorescence increases for values of fluorescence > 0.5 ; for fluorescence values < 0.5 , the linear regression has a slope of 2.6 an intercept of 0.04 and an $r^2 = 0.75$.

2.6.6 Remote Sensing

Sea surface temperature and ocean colour data (SeaWiFS, MODIS), converted to chlorophyll *a* for periods corresponding to the deployment and recovery CTD surveys, were obtained from the OESD database (http://www2.mar.dfo-mpo.gc.ca/science/ocean/database/data_query.html) where details of the raw data sources and processing are provided.

3. Results

3.1 Hydrographic Sections

Sections in the Gully were only sampled once each year and, therefore, represent a snapshot of the hydrographic variability over a 4-day period in 2006 and a 6-day period in 2007. Representative mean currents in the 200 to 1000 m depth interval, i.e. below the rim of the Gully, are of order 0.01 m s^{-1} (see Figure 14). Given the Gully's length of about 30 km along the deep central axis, an advective time scale would be about 30 days. Repeat sections over this time scale might give a reasonable average and allow interpretation of the section-to-section variability. The present CTD dataset may not allow this; nonetheless, it is useful to examine sections to determine if consistent patterns emerge.

Temperature, salinity, density and oxygen saturation sections across the mouth of the Gully indicate a 3-layer structure in 2006 and 2007 (Figure 3, Figure 4). The upper 100 m features varying temperatures and salinities in response to the annual changes in heat flux and freshwater inflow (Petrie et al. (1996)); oxygen saturations were generally $> 90\%$ in 2006 and $> 80\%$ in 2007. Temperatures and salinities were highest in the layer from about 100 to 350 m during both years due to the presence of Warm Slope Water (WSW, $T = 9\text{--}13^\circ\text{C}$, $S = 34.73\text{--}35.56$; Gatién (1976),

Petrie and Drinkwater (1993)). This layer features a minimum of oxygen saturations; these relatively low values are also characteristic of WSW (Petrie and Yeats (2000)). The deeper part of the section is dominated by Labrador Slope Water (LSW, $T = 4-9^{\circ}\text{C}$, $S = 34.3-35$; Gatién (1976), Petrie and Drinkwater (1993)) and higher oxygen saturation. In both years, the density surfaces are relatively flat, indicating no strong baroclinic circulation during the surveys.

For a complete summary of the CTD observations, individual profiles of temperature salinity and sigma-t, organized by section (see Figure 1) are compiled in Appendix 2; the profiles are combined and shown as section plots in Appendix 3. An additional derived variable, the Brunt-Vaisälä frequency derived from the profiles and an indication of the vertical gradient of density, is also shown.

3.2 Section-averaged profiles

The along-Gully variation of temperature and salinity can be simplified by averaging the profiles across the sections from the depth of the rim (200 m) and, subsequently, displaying their depth dependence (Figure 5 (A-D)). We then examined the section-to-section variability in vertically averaged layers. Figure 5 (A, C, D) – 2006 S , 2007 S and T – show the same pattern, namely increasing, depth-averaged values (200-1000 m, to 881 m in 2006, 866 m in 2007, the deepest depths at the shallowest section, stations 1-3) from the head to the mouth of the Gully (T , S versus distance along the Gully) that were strongly linear as indicated by their correlations (2006 S , $r^2 = 0.99$; 2007 S , 0.95; T , 0.96), amounting to changes of 0.055 and 0.087 for S in 2006 and 2007, and 0.43°C for T in 2007. Similarly, the 0-200 m averaged salinities were strongly linear ($r^2 = 0.97$, for both years) with increases of 0.45 (2006) and 0.43 (2007) from the head to the mouth of the Gully. Increasing salinities offshore in both layers implies two-way exchange between them, similar to classical estuarine dynamics. However, linearity is not expected if the mixing were uniform along the axis of the Gully; moreover, the salinity structure in the 200-400 m depth range, particularly in 2007, implies more complex mixing processes are occurring than one might conclude from gross layer averages.

Figure 6(A, B) show the T - S structure in the 200-1000 m range. In both years, LSW is the dominant water mass in this depth range, a consequence of the large-scale advection pattern in this region (Petrie and Drinkwater (1993)); there is a minor contribution from WSW. This supports the finding of MacIsaac et al. (2013) who report that the fauna of the Gully is dominated by cold temperate species typical of mid- to high-latitudes in the North Atlantic. In 2006, the T - S structure shows an orderly pattern: the section (Stations 14-21) at the mouth of the Gully generally features higher temperatures and salinities than the other sections; this pattern progresses systematically with decreasing temperatures and salinities towards the head of the Gully, where the lowest values are found (Stations 1-3). The detailed variability is more complex, with overlapping T - S structure for the middle sections between 200-275 m ($7.35-7.25^{\circ}\text{C}$) and roughly 475-575 m ($5.5-5.1^{\circ}\text{C}$); the outermost sections T - S structure overlaps between approximately 275-390 m ($7.25-5.95^{\circ}\text{C}$) and finally the inner three sections' properties overlap over varying depth ranges, which span 430 m (Stations 1-3) and 990 m (Stations 9-14). Consequently, deep along-Gully isopycnals tend to be shallowest at the mouth and head and deepest at the two middle sections. The overlapping T - S structure between sections implies an

advective connection; on the other hand, the differences may be due to more complex spatial variability in the flow field.

Similar behaviour is seen in the 2007 survey, though overall, the waters are fresher and cooler than in 2006. Moreover, the layering appears to be simpler with the only appreciable overlap of T - S properties between the two outer sections observed in the range of 220-360 m (7.8-5.9°C). Deep isopycnals along the Gully axis tended to be flat. In both years, the 1000 m observations converge to about 4.2°C and 34.9, with temperatures and salinities slightly higher at the mouth of the Gully.

An examination of T - S variation across the Gully for each section did not reveal a consistent pattern in either 2006 or 2007.

3.3 Nutrient Profiles

Nutrient samples were collected in the Gully in late April 2006 and early August 2007 during the deployment and recovery cruises. It has been suggested that physical processes such as enhanced mixing could drive greater primary productivity in the Gully and result in greater biodiversity (Harrison and Fenton, 1998). This could lead to differing nutrient profiles in the upper layers of the Gully compared to those in surrounding areas. Consequently, we examined archived nitrate, silicate and phosphate data from three adjacent regions surrounding the Gully: Banquereau Bank to the northeast; Middle Bank to the north-northwest; and Sable Island Bank to the southwest (Figure 1). Polygons defining these areas are shown in the on-line hydrological atlas of the Scotian Shelf and Gulf of Maine (<http://www2.mar.dfo-mpo.gc.ca/science/ocean/tsdata.html>). Archived nutrient data were recovered from the on-line database BIOCHEM maintained by the Integrated Science Data Management group (ISDM, DFO Ottawa) at <http://www.meds-sdmm.dfo-mpo.gc.ca/BioChem/biochem-eng.htm>.

Archived data are presented for the months of April-May and July-August because of the timing of the 2006 (late April) and 2007 (early August) cruises. The comparisons are for 0-250 m only because the three adjacent regions are on the shelf and are shallow relative to the maximum depth of the Gully. Moreover, this is the depth range where primary productivity is expected to play an important role. While identical vertical profiles indicate that the inventory of nutrients is the same, it does not necessarily mean that the vertical fluxes and primary productivity are equivalent.

Figure 7 shows that the concentrations of nutrients in the Gully for both periods are comparable to those in the three adjacent areas. There are slight deviations (determined by averaging the observations in 10-m bins beginning with 0 m): spring phosphate levels are slightly lower (on average -0.1 µM; a typical standard deviation for the adjacent areas is 0.3 µM), as are summer silicate values (-1.3 µM; a typical SD is 3 µM) in the Gully. Overall we conclude that the 0-250 m nutrient profiles in the Gully are not significantly different from those in the adjacent shelf areas. Comparisons of standing crops of chlorophyll (not shown) show no significant differences between the levels observed in 2006 and 2007 and archived data from the adjacent shelf. The similar nutrient profiles and standing crops of chlorophyll imply that primary productivity in the Gully is not enhanced relative to that of the surrounding areas.

3.4 Distribution of microbial plankton

In August 2007, the surface layer was warm (Figure 8A) and relatively fresh (Figure 8B). The top of the pycnocline (Figure 8C) and nitracline (Figure 8D) at 20m coincided with the depth of maximum microbial abundance, which included the picoplanktonic *Synechococcus* (Figure 8E), the picoeukaryotic algae (Figure 8F), the nanophytoplankton (Figure 8G); and the heterotrophic bacteria (Figure 8H). Total phytoplankton biomass, indicated by the concentration of chlorophyll *a*, was maximum at 40m (Figure 8D), where nutrients were not depleted (Figure 7). Section plots (Figures A52-A57) of microbial abundance show a persistence of these depth patterns across the entire Gully region. Near-surface, summer average concentrations (in units of \log_{10} cells ml^{-1}) for bacteria, *Synechococcus*, picoeukaryotes and nanophytoplankton were 6.0 (range of 0.3), 4.1 (0.8), 3.7 (1.3) and 3.1 (0.5) (Figure 8). The integrals over the upper 100 m using the average concentration for all stations and expressed as \log cells m^2 were 13.8, 12.1, 11.6 and 10.9. Bacterial abundance decreased sharply from about 2,000,000 cells ml^{-1} near the surface to $\sim 350,000$ cells ml^{-1} at 100 m and then approximately linearly to $\sim 65,000$ cells ml^{-1} at 1800 m (Figure 8I).

A comparison of chlorophyll concentration and microbial abundance in the Gully (measured in summer) with values on the Scotian Shelf as a whole (measured on annual spring and fall surveys of the AZMP) must recognize strong seasonality in the annual cycle of planktonic organisms. It appears that the August 2007 chlorophyll and microbial values in the Gully are generally similar to the fall (October) values elsewhere on the Shelf (Figure 9). There is an indication that the summer Gully value for *Synechococcus* is slightly lower than the general fall Shelf value (Figure 9B); and that the summer Gully value for bacteria is slightly higher than the general fall Shelf value (Figure 9E). Although these differences require confirmation by repeat sampling of the Gully in summer, it can be noted that in Bedford Basin, climatological values of summer *Synechococcus* are indeed lower than fall values; and that climatological values of summer bacteria are indeed higher than fall values (Li 1998; Li and Harrison 2008; O'Brien et al. 2012).

Taken together, chlorophyll and microbial levels in the Gully do not show strong evidence of seasonally adjusted enhancements over regional values across the Scotian Shelf.

3.5 Annual cycle of surface chlorophyll derived from SeaWiFS observations

Estimates of surface chlorophyll derived from SeaWiFS observations (48/year, 1997-2009) were compiled for the Gully as well as for 5 adjacent or nearby areas: Misaine Bank, Banquereau Bank, Middle Bank, Sable Bank and the Northern Slope. The boundaries of these areas are defined by Petrie et al. (1996). Annual cycles for each area were computed by averaging all available observations in each of the 48 time windows (Figure 10) and compared using linear regression (Table 5). The linear regression is given by:

$$\text{Area value} = \text{Intercept} + \text{Slope} * \text{Gully Value}.$$

If a selected area had the same annual cycle as the Gully then the intercept would be 0, and the slope and R^2 would be 1. For all areas the intercepts are small; the slopes for Misaine and Middle Banks are greater than 1, indicating enhanced concentrations relative to the Gully. The slopes for Sable and Banquereau Banks are close to 1, whereas the slope for the Northern continental slope region is less than 1, implying reduced concentrations relative to the Gully. The R^2 values range from about 0.7 to 0.8 indicating reasonable fits for the regressions.

The integrated chlorophyll concentration over the year from largest to smallest is Middle Bank (47 mg m^{-3}), Sable Bank (47), Misaine Bank (46), Gully (39), Banquereau Bank (36) and Northern Slope (29). In terms of the annual cycle, there is no indication of enhanced chlorophyll concentrations over the Gully.

We further examined the averaged observations by focusing on the spring bloom. We expect that the averaging will broaden the bloom period if the timing of its peak varies from year to year. Additional analysis could involve examining the bloom within each year. Nonetheless, this analysis will provide some sense of the average timing and duration (or variation of timing) of the bloom. To this end, we fit a Gaussian function to the bloom and examined its suitability by comparing the variance accounted for by it. The Gaussian function took the form:

$$\text{Chl concentration} = k + a \cdot \exp\{-(x-b)^2/(2 \cdot c^2)\}$$

where k is a constant that can account for a background residual concentration, a is a constant, x is the variable year day for which observations are available, b is the day of peak chlorophyll concentration fitted by the function, and c is constant that normalizes the exponential argument. Fits for the Gully and Middle Bank (the best fit) are shown in Figure 11. The results are presented in Table 5 where the key parameters are the peak concentration, b , the day of the peak bloom, and the duration, defined as the time for the fitted bloom to reach concentrations of $0.5 \cdot \text{peak}$. Data from day 67 to 135 were fitted after examining the annual cycle (Figure 10); an additional calculation was made for Sable Bank data as the initial fit using days 67-135 indicated that the bloom reached $0.5 \cdot \text{peak}$ earlier than day 67. The second fit for the Sable Bank observations was made using data from days 46-128; the fitted parameters were only slightly affected relative to those using days 67-135. We emphasize again that the definition of the bloom duration is arbitrary (we chose $0.5 \cdot \text{peak}$); secondly, the value for the duration includes not only the true duration of the bloom but also is influenced by when the bloom occurs in each year. A bloom of 20 days duration but occurring ± 30 days about a central date may, when the 12 years of data are analyzed as we have done, appear to be 50 days long.

With this caveat in mind, what does the analysis show? First the Gaussian function does a good job of fitting the data with R^2 values of 0.83 to 0.98. The peak value of the fit to the bloom period is smallest for the Gully save for the Northern Slope region. Only Sable Bank has an earlier bloom (peak on day 87) than the Gully (day 97), but the peaks in the remaining areas follow soon after (day 101-108; recall that the temporal resolution of the data is about 7 days). Finally the “duration” of the bloom is long (49-62 days) for 3 areas including the Gully and considerably shorter for the other 3 (26-28 days). This indicates that it may be useful to examine each year individually to determine more definitively the source of these differences. With this first examination however, we conclude that the Gully does not appear to be distinct relative to

the other regions. Moreover, the data indicate that the Gully surface concentrations, if anything, appear lower than some of the surrounding areas.

3.6 Zooplankton Tow Results

Zooplankton were collected in vertical net tows (200 μm mesh) between 100 m and the surface at nine stations in April 2006 and at eleven stations in August 2007. In this layer the biomass range was 29-71 g m^{-2} (wet weight) in April 2006 and much lower at 1-6 g m^{-2} in August 2007 (Figure 12). Two vertical tows were made to greater depths in April 2006 and four in August 2007. The biomass in the 0-1500 m range was the same as that in the 0-100 m range in the central Gully in April, whereas the biomass in the 0-384 m range at a station near the head of the Gully, was larger (by a factor of 1.7) than that in the 0-100 m depth range. In August, zooplankton biomass in deep tows (0-1000 m) at the stations within and downstream (to the southwest) of the Gully along the shelf-break were more-or-less the same (range 61-74 g m^{-2}). At a station upstream (to the northeast) of the Gully along the shelf-break the biomass was somewhat lower (32 g m^{-2}) than at the other stations.

There has been sampling in the Gully by means of vertically towed ring nets or obliquely towed BIONESS net systems during several months of the year since 1984. Since biomass is more-or-less constant over the entire region in the 0-100 m depth range (Figure 12), a seasonal cycle of zooplankton biomass for the 0-100 m layer was constructed, using monthly values obtained by averaging over all stations and all years, but excluding the values from April 2006 and August 2007 (Figure 13). The average biomass values for April 2006 and August 2007 were consistent with the average 1984-2009 seasonal cycle.

A seasonal cycle for zooplankton biomass at depth could not be constructed to compare with the results of the deep tows in April 2006 and August 2007. This is partly because most sampling stations in other years were not in the central Gully, where depths are >800 m, but at a station along the southern wall, where the bottom depth is between 450 and 600 m. The two tows that were in the central Gully showed that in September 1985 and October 1984 most of the zooplankton biomass was found between 600 and 800 m. These tows gave lower estimates of zooplankton biomass (53 and 32 g m^{-2} , respectively) than did the 0-1000 m tows in August 2007, but this might be because the BIONESS system has a maximum towing depth of 800 m. The BIONESS profiles of zooplankton biomass did show, however, that highest biomass concentrations are in the 0-100 m layer in April with an increasing proportion of biomass being found at increasingly greater depths through the summer and fall.

The seasonal differences in zooplankton biomass depth distribution between April and August reflect the changes in the vertical distribution of one dominant species, the copepod *Calanus finmarchicus*. In the spring *C. finmarchicus* are feeding on phytoplankton in the surface layers and are reproducing, developing and growing. The biomass peak is apparently in May (Figure 13) and at that time and thereafter individual *C. finmarchicus* are leaving the surface layers as they reach the pre-adult CV stage in their life history. By August, most are found at greater depths, probably concentrated in the deep portions of the Gully. There they spend the fall and winter in a resting state (diapause) waiting for the following spring when they will ascend to the surface, mature, mate and start the production cycle again. Throughout the year at all depths,

individual *C. finmarchicus* are undoubtedly subject to varying levels of predation mortality and advection into and out of the Gully region.

3.7 Mooring Results

The overall mean current velocity and variance for the Gully spanned by moorings SG10, SG11 and SG12 are presented in Figure 14. The 25-m binned ADCP and the RCM data were used; any ADCP bin with less than 60% data return was excluded. The velocity data were rotated such that the resulting components were in the along- and across-Gully directions, which were 330° ($=V_{330}$) and 60° ($=U_{60}$), respectively. The results were linearly interpolated between moorings for those depths above the seabed on the canyon walls at SG12 and SG10. For deeper depths, the velocity and variance were linearly interpolated with depth along the central mooring; this result was then assumed to represent the flow at that depth across the canyon.

The across-canyon mean speed (U_{60}) is enhanced near the bottom at SG12 and SG11. The flow shallower than 500 m is characterized by two features: firstly, in mid-layer, the U_{60} flow ranges from 0.01 m s^{-1} on the eastern side of the Gully to near zero on the western side; at shallower depths, the flow is directed to the southwest (negative U_{60}) at a rate of 0.02 m s^{-1} , which is consistent with nearby archived current observations near the shelf edge (Figure 2). Current magnitude from between the shallowest depth and 200 m averaged -0.04 m s^{-1} at SG10, 11 and -0.01 m s^{-1} at SG12.

The along-Gully mean component (V_{330}) indicates that below 500 m the flow is predominantly towards the head of the canyon. There is a layer ($\sim 200\text{-}300 \text{ m}$) of on-shelf flow in the western section that weakens eastward, becoming negative on the eastern wall. On the western side, a wedge of current is primarily off-shelf below $\sim 300 \text{ m}$. This pattern suggests the possibility of the existence of a rim-depth eddy over the canyon, however, it is difficult to make a definitive statement based on the available data set.

The variance of the across-canyon component is highest at shallow depths, decreasing to about half its maximum value at roughly 250 m. An analysis of the time series for the 222 m RCM at SG10 indicates that 60% of the variance can be attributed to the tidal/inertial band, 35% to the 1-10 day wind-driven band, and 5% to lower frequencies. Earlier studies of the role of meteorological forcing on the low-frequency variability and circulation of the Scotian Shelf were carried out by Petrie and Lively (1979) and Smith and Petrie (1982). Topographic steering of the circulation in the deep Gully and the restrictive nature of the sidewalls leads to the low variance observed in the U_{60} component. The variance in the along-canyon velocity V_{330} increases with depth at the SG11 mooring site, over the canyon thalweg, as a result of bottom-intensified tidal amplification; this will be discussed further in Section 4. There is no increase in variance evident from the mooring records on the canyon sidewalls. Peak variance in the along-canyon direction is about five times larger than that observed in the across-canyon direction.

The mean along-Gully transport through moorings SG10-12 over the entire mooring period from 200 m to the bottom was $35,500 \text{ m}^3 \text{ s}^{-1}$ toward the head of the Gully. At mooring SG2 near the head of the Gully, the mean velocity was also positive at 0.004 m s^{-1} . These results imply net

upwelling over the section of the Gully from the outer array to the head and the potential for on-shelf flow.

A progressive vector diagram (PVD, Figure 15) created from the hourly time series provides an overview of the flow at each of the four moorings sites. The lines have been color-coded to be representative of above-rim (<200 m), mid-depth (200-500 m) and deep (below 500 m) layers. The above-rim flow at SG2 (canyon head) is primarily in the northwest direction (along canyon axis) but weakens at shallower depths. Northwestward flow is observed at other depths with the exception of the currents at 562 and 761 m, which are to the southeast and east adding complexity to the circulation at this site.

The mooring array (Figure 15(B-D)) indicates that the above-rim flow is primarily to the southwest (across the canyon) in agreement with the archived data (Figure 2). The above-rim currents appear to weaken from east to west across the canyon; the flows at SG11 and SG12 are perpendicular to the canyon axis, whereas at SG10 the flow has a stronger off-shelf component. For SG11, the flow below 500 m is primarily along the canyon axis towards the shelf but weaker than at SG2. The low-frequency current on the western side (SG12) rotates clockwise with increasing depth for the upper 220 m and is strongest at that depth; below this the flow rotates anti-clockwise. At SG10 for depths exceeding 200 m, the circulation rotates counter-clockwise to westward flow near the bottom.

The low frequency (subtidal) and total variance of the current meter data were computed for each of the four mooring sites, and for moorings on the Scotian Slope adjacent to the Gully (Figure 16, Figure 18). The subtidal variance generally decreases with increasing depth at all sites. It is evident that the two mooring sites (SG2, 11) along the Gully axis are unique because the total variance increases markedly with depth. The total variance at SG11 (Figure 16B) reaches a maximum $0.062 \text{ m}^2 \text{ s}^{-2}$ at 50 m above the seabed. The SG2 total variance profile (Figure 16A) is more noisy, however, its magnitude is $\sim 3\text{x}$ larger than at SG11, reaching a peak value of $0.15 \text{ m}^2 \text{ s}^{-2}$ at 761 m, approximately 300 m above bottom. At the eastern and western mooring sites, the total variance profile mirrors the low frequency profile and is about 2x larger. It was evident from the raw data that the source of this enhanced variance seen at SG2 and SG11 was tidal variability.

At the Halifax tide gauge, the K1 tidal amplitude is 0.1038 m; the O1 amplitude is 0.0483 m (P. MacAulay, Cdn. Hydrographic Service, Bedford Institute, pers. comm.). If these elevations were solely due to on-shelf flow, then at the SG2 mooring we would expect barotropic tidal currents of about 0.0015 m s^{-1} for K1 and about half that for O1. A tidal analysis of the individual current meter time series is presented in Figure 17 for the tidal constituents K1 and M2. The K1 tidal velocities increase with depth and indicate that the Gully acts to amplify these high-frequency flows (see Swart et al. (2011)). At the SG2 site, 761 m, the K1 major axis current is the largest at about 0.31 m s^{-1} , and the O1 flow is 0.26 m s^{-1} (not shown). At SG11, 1542 m the K1 component is 0.19 m s^{-1} , while the O1 major current is 0.16 m s^{-1} . These flows far exceed the expected on-shelf currents which could account for the surface tide at Halifax. The tidal ellipses at SG2 and SG11 are aligned with the local topography, especially below the rim (>200 m). The sites on the canyon walls (SG10, SG12) have lower tidal velocities compared to those at similar depths along the axis; these sites also show no indication of bottom-enhancement of the diurnal tides. Based

on all of the current meter data, the O1 constituent is approximately 0.82 of the K1 amplitude; this is consistent at both the SG2 and SG11 sites ($r^2 = 0.99$ for K1 vs. O1 amplitude).

For depths >200m at SG2, the tidal excursions range from 4.4 km (O1, 355 m) to 8.5 km (K1, 761 m); excursions of this length at the head of the Gully could force an alternating upslope-downslope flow and enhance vertical mixing. The K1 and O1 phases decrease by about 30° with increasing depth at the SG2 site. The phase lag of K1 relative to its forcing is on average 27° greater than that of the O1 tidal constituent. Similar trends in phase are observed at SG11 with an average K1-O1 offset of 23°. The orientation of the K1 and O1 diurnal constituents is virtually identical at all depths below the canyon rim and shifts to higher values as depth increases; the trend with depth is more evident at the SG2 location.

The semi-diurnal M2 constituent also shows the influence of topography through the orientation of the tidal ellipses below 500 m (Figure 17B); however, these ellipses are not as rectilinear as those of the diurnal tides. There is some evidence of amplification of the M2 component with depth. At SG2 for depths >200 m, the M2 major component increases from 0.049 m s⁻¹ at 355 m to 0.116 m s⁻¹ at 761 m before decreasing to 0.063 m s⁻¹ near the bottom; at SG11, the M2 major currents increase from 0.04 m s⁻¹ at 444 m to 0.094 m s⁻¹ at 1549 m. As for K1 and O1, the M2 major flows exceed the expected on-shelf current of about 0.017 m s⁻¹. The diurnal constituents in the deep layer are significantly larger at the SG2 site compared to the SG11 site; this is not the case for the M2 constituent where the magnitude is very similar at both sites. The orientation of the M2 tidal ellipses is quite variable above 500 m.

The change in phase of the M2 constituent with depth is significantly more variable than observed for the diurnal constituents; below 400 m the phase decreases with depth which is consistent with the trends observed for K1 and O1. The orientation of the M2 ellipses is relatively constant with depth; however, there is large variability at mid-depth at both SG2 and SG11.

Depth-averaged spectra were generated for the two Gully mooring sites along the canyon axis (SG2 at the head and SG11 at the center) and for three sites on the Scotian Slope (Figure 18). These spectra were based on observations from 150 m (i.e., well below the mixed layer) to the deepest current meter from the site (typically 50 m above the seabed). These results indicate that the Gully is indeed a unique ocean environment in which rarely observed compound tidal frequencies (e.g. M2+K1 = MK3) generated by non-linear interactions among diurnal and semi-diurnal components are clearly evident in both the SG2 and SG11 records. The analysis of slope mooring sites is substantially different from the two Gully sites with the only common features being spectral peaks at the semi-diurnal frequencies (N2, M2, S2) and weaker peaks at diurnal periods. The slope sites also have a significant response at the inertial frequency, as well as a modest peak at the diurnal frequencies O1 and K1. The largest peak in the Gully mooring spectra are at these diurnal frequencies.

At the two Gully sites, the ratios of the response (spectral estimate) to the forcing (Halifax sea level), which we designate the gains, were determined for the diurnal components O1 (period 25.819 h) and K1 (23.934 h). If the response to forcing were the same, then the ratio of the gains should be 1. For SG2 at the head of the Gully, the gain for O1 divided by the gain for K1 was

1.44; for SG11 it was 1.46. This implies that the resonance frequency for the Gully is closer to the O1 frequency, than to that of K1.

Rough estimates of the potential of the M2, K1 and O1 tidal constituents to generate harmonics can be made through consideration of the non-linear terms such as $v(M2)\partial v(K1)/\partial y$, where v represents the along-Gully current and y the distance (see, e.g., Petrie (1975)). Using the spectral estimates, one can predict the spectral energies at frequencies corresponding to MK3 and MO3. Alternatively, the distance Y required to give the observed spectral energy can be estimated. For the SG2 mooring at the head of the Gully, the distances are 1.5 and 1.6 km for MO3 and MK3; for the outer mooring SG11, the distances are 5.2 and 6 km. These are reasonable given the proximity of the head of the Gully to the SG2 mooring, whereas the SG11 mooring is located farther from the head.

The spectral energy distributions at both the SG2 and SG11 sites are very similar except for the energy level, which is measurably higher at the head of the canyon. Spectral peaks are clearly evident at frequencies as high as almost 7 cycles per day (MK7), and beyond this the variance is a factor of about 3 times higher at the canyon head versus the deep central mooring at SG11, consistent with the profiles of total variance (Figure 16). The unique topography of the Gully is obviously a key factor in the non-linear interaction of tidal constituents, which produces the spectra observed (overtides and compound tides) at SG2 and SG11.

3.8 Sable Island Winds

The hourly data provided by the Environment Canada weather station on Sable Island are presented in Figure 19 for the period corresponding to the mooring deployment. The seasonal cycle in wind speed and stress is evident from these time series. The peak in wind stress occurs during the winter period and is at a minimum during the summer. This is also apparent in the progressive vector diagram (PVD) in Figure 20 with larger spatial gaps during the winter months. The PVD shows the seasonal change in the predominant wind direction from the southwest in the summer period to being from the northwest during the winter.

4. Discussion

Previous studies (e.g., Harrison and Fenton, 1998) have raised a number of key questions related to the Sable Gully which include the following: is there evidence of significant retention which could explain the inferred enriched productivity; is there significant transport of slope water onto the Scotian Shelf; how does the current variability compare to the nearby slope regions; is there evidence of enhanced internal tides and waves; and, is the Gully an area of stronger vertical mixing and upwelling potential that would support higher primary productivity? We shall attempt to address these questions in the remainder of this section.

It has long been speculated that one of the possible explanations for the high biodiversity and productivity of the Gully was that the mean circulation fostered enhanced retention of water within the Gully, and that this would enable biological communities to thrive. The current meter data collected in the upper 200 m, as part of this mooring program, indicates that the Gully has

little impact on the upper ocean circulation, which is predominantly influenced by the shelf-break current flowing to the southwest. Similarly, Hunkins (1988) noted that the southwestward, near-surface flow over Baltimore Canyon appeared unaffected by canyon topography; Noble and Butman (1989) also found dominant southwestward flow over the inner portion of Lydonia Canyon, transitioning seaward to northeastward flow likely caused by the presence of warm-core eddies. For the Gully, this decoupling does not appear to be related to the seasonal stratification as the 50-100 m currents in surrounding areas strongly resemble those in the 0-50 m layer (Figure 2). Moreover, Shan et al. (2013a, b) show the Gully only weakly affects the flow for depths less than 200 m. Upper layer (<200 m) flow is to the southwest at all three outer moorings and ranges from 0.01 (SG12) to 0.04 m s⁻¹ (SG10, 11); this gives a transit time of about 3 days, considerably less than retention times of > 40 days for specific areas of the Gully determined from numerical simulations (Petrie et al. (1998)). At the SG2 site, the mean flows are to the NW at about 0.01 m s⁻¹, leading to a transit time of about 12 days and indicating a longer retention time at least near the head of the Gully. An analysis (not shown) of the satellite sea surface temperature (SST) and ocean colour imagery (<http://www.bio.gc.ca/science/newtech-technouvelles/sensing-teledetection/index-eng.php>) does not provide any indication of differences between the Gully and the surrounding region. The annual means and annual harmonics of SSTs for the nearby Banquereau, Middle and Sable Island Banks are within 0.5°C of the Gully values; the annual harmonic phases are within 0.03 months. If there were enhanced mixing by a factor of 2 over the Gully compared to the surrounding Banks, then differences of SST exceeding 1°C could occur from June to September with the maximum difference ~3-4°C in August. Differences of these magnitudes are not generally seen. Overall, the evidence seems to indicate that if there are processes occurring at depth to generate enhanced productivity, they are not influencing the surface waters over the Gully.

There is some evidence supporting the presence of a rim-depth eddy between 200 and 300 m depth; however, given the sparse spatial coverage of the moorings, it is difficult to be conclusive. The PVDs (Figure 15) indicate that the depth-averaged mean velocity below the Gully rim (< 200 m) is on the order of 0.01 m s⁻¹. With a distance of ~30 km from the mouth to the head of the canyon, the advective time scale is approximately 30 days which is significantly longer than the observed residence time above the canyon rim. Shan et al. (2013a) suggest that particles released in their computer simulation near the head of the Gully are retained much longer than those released elsewhere.

The mean, 200 m–bottom transport towards the head of the Gully through the SG10-12 array was estimated as 35,500 m³ s⁻¹ (Section 3.4). Hunkins (1988) also observed deep flow towards the head of Baltimore Canyon; in contrast, Noble and Butman (1989) found weak (spatial average, -0.006 m s⁻¹), along-canyon mean flow with a slight tendency for flow out of the canyon. For the Gully, the bottom transport implies an upwelling velocity of 1.7x10⁻⁴ m s⁻¹ over the area from the mooring to its head near the SG2 site. This upwelling could give rise to a nitrate flux into the upper 200 m of 2 to 4x10⁻³ kg m⁻² day⁻¹ (see Figure 7). If distributed uniformly over the upper 200 m, this flux could potentially generate a chlorophyll concentration of ~1.7 mg Chl m⁻³, a significant amount (Greenan et al., 2002). However, a flow of 0.01 m s⁻¹ out of the western side of the Gully alone from SG2 to SG11 (19 km by 200 m) could offset the upwelled nitrate flux. For depths less than 200 m, the mean flows at all mooring sites are ≥ 0.01 m s⁻¹. Thus, the 0-200 m currents could on average advect this nitrate flux from the region before

it entered the euphotic zone, reducing its impact over the Gully, but this could be a potential nutrient source for areas downstream.

A plot of the along-axis density field (not shown) based on the deployment and recovery cruises shows very little evidence of upwelling occurring within the canyon (i.e., the isopycnal surfaces are flat from the Gully mouth to the head), despite the long-term observation that the mean flow is directed towards the head of the Gully. While these only represent two snapshots, the results are consistent for both cruises.

An intrusion of colder, fresher water at 290 m depth was observed at the SG11 mooring site for the period of 1 January to 6 April 2007. Through investigation of the correlation between the temperature at 290 m with MicroCAT measurements at 355 m (SG2), 444 m (SG11) and 562 m (SG2), we can provide estimates of upper bounds on the vertical eddy diffusivity (K_v) as well as the mean horizontal flow speed (v) between the SG11 and SG2 mooring sites. Based on the maximum correlation for lagged time series for the 290 and 444 m temperature time series, it is estimated that K_v is $180 \times 10^{-4} \text{ m}^2 \text{ s}^{-1}$, which is about 20 times the typical value observed on the Scotian Shelf (Umoh and Thompson, 1994). The speed of propagation of the cold, fresh intrusion from SG11 to SG2 is estimated to be 0.02 m s^{-1} based on the distance between the two mooring sites and the time lag observed and is consistent with the current meter measurements.

The linear increases of salinity in both the shallow (0-200 m) and deep (>200 m) layers towards the mouth of the Gully described in Section 3.2 suggests estuarine-like dynamics with mixing between the two layers. We considered an advective-diffusive balance, $v \partial S / \partial y = K_v \partial^2 S / \partial z^2$, where v is the deep flow towards the head of the canyon, y is the along-canyon direction, and z is the vertical coordinate. Using the average of the salinity gradients from Section 3.2 and estimating the $\partial^2 S / \partial z^2$ term across the 200 m interface (averaging over each section), we get $K_v = 0.9 \times 10^{-4} \text{ m}^2 \text{ s}^{-1}$, 200 times less than the value estimated from tracking the cold, fresh event described above. However, if we incorporate the mean upwelling velocity, $w = 1.7 \times 10^{-4} \text{ m s}^{-1}$, we obtain $K_v = 45 \times 10^{-4} \text{ m}^2 \text{ s}^{-1}$, in better agreement with the other estimate of $180 \times 10^{-4} \text{ m}^2 \text{ s}^{-1}$. Greater vertical mixing is necessary to overcome the mean upwelling to produce the salinity gradient in the lower layer. These estimates represent a high rate of vertical mixing likely driven by the exceptionally strong tidal flows, particularly the diurnal components. However, this simple salt balance based on vertically averaged properties, which has worked for other canyons, gives at best a sense of the level of mixing. From the averaged profiles, we can see that the salinity gradient changes sign in the upper 400 m (Figure 5), casting doubt on the estimates of vertical salinity gradients based on representing the Gully as two layers; moreover, there is both vertical and horizontal current shear in the Gully. At best, we can say that the vertical mixing appears to be strong.

A principal component analysis (PCA) of the monthly mean, along-Gully currents was carried out for each of the mooring sites using data from 150 m to bottom to determine the overall coherency of the low frequency circulation (Figure 21). For the outer array alone, the PCA1 accounts for 56% of the variance; loadings were generally in phase for SG11 and SG12, but out of phase for SG10. The loadings were high for depths < 400 m and mirror the pattern of the mean, along-Gully flow (Figure 14B, Figure 21A). The time series of PCA1 has a large amplitude for the initial month but weak variability thereafter; the amplitudes are negative for all

but 1 month (Figure 21B). Thus seasonal variability is not a major factor and the currents described by this mode change sign only for that one month; for all other months, the flow is towards the head of the Gully where loadings are negative and towards the mouth where they are positive. It is not surprising then that the loadings which describe coherent variability resemble the mean flow and that there is a tendency for upwelling at the head of the Gully. If SG2 is included in the analysis, then PCA1 for the whole array accounts for 44% of the variance, 80% by the first three modes. Overall, this indicates highly coherent low frequency current variability in the Gully. For comparison, the PCA1 for the Lydonia Canyon moorings only accounted for 25% of the variance (Noble and Butman, 1989).

Current variance along the axis of the Gully for depths greater than 200 m is high, showing peaks of $0.15 \text{ m}^2 \text{ s}^{-2}$ at mooring SG2 (head) and $0.062 \text{ m}^2 \text{ s}^{-2}$ at SG11 (Figure 14, Figure 16). Baltimore and Lydonia Canyons have values of about $0.014 \text{ m}^2 \text{ s}^{-2}$, as much as a factor of 10 lower than observed in the Gully (Hunkins, 1988; Noble and Butman, 1989). On the other hand, in Hudson Canyon current variances reach $\sim 0.05 \text{ m}^2 \text{ s}^{-2}$, comparable to those observed in the Gully. For the 200 m to bottom, depth-averaged spectra (Figure 18), about 95% of the variance is accounted for by the tides. Tidal flows are noted as strong or the strongest components in the current fields in Baltimore, Hudson and Lydonia Canyons (Hunkins, 1988; Hotchkiss and Wunsch, 1982; Noble and Butman, 1989) and as contributing 90% of the overall variance in Monterey Canyon (Xu and Noble, 2009).

A computation of the ratios of variance from the SG11 and Slope moorings (Table 6) provides some further insight into the differences between the Gully and surrounding slope region. It is evident that at low frequencies (less than diurnal), the depth dependence of the Gully and Slope variance is similar. In sharp contrast to this, the diurnal ratios range from 4.1 at 150 m to 548 at 1500 m, reflecting the resonant or near-resonant conditions that prevail in the Gully. At the inertial frequency, the variance in the Gully ranges from 0.2 to 0.8 of the Slope value, indicating the inhibiting effect of the Gully walls in the generation of currents at this frequency. For the semi-diurnal and higher frequencies, the ratios in the upper 1000 m are relatively constant at about 1 and 2, respectively, and then jump to about a factor of 10 at 1500 m. It is evident from this analysis that the Gully is an environment which is quite unique from the surrounding slope region, and that this is in large part attributable to amplification of the diurnal and semi-diurnal tides along the Gully axis. Length scales ($L = 35 \text{ km}$, $W_{head} = 1/10 W_{mouth}$, $R = 14 \text{ km}$) suggest that the diurnal tide should be resonant in the canyon. Swart et al. (2011) used an analytical framework to explain the mechanisms behind the strong diurnal currents observed by the moored array. They suggested that an along-shelf barotropic flow sets up a double Kelvin wave response in the canyon, generating along-canyon velocities that are subsequently amplified by resonance. The double Kelvin wave model predicts that the velocity will increase from the canyon walls to a maximum at the center of the Gully; this is consistent with the observations from the Gully mooring array. The nature of the velocity profile in the along-canyon direction depends on the canyon geometry, the forcing frequency, and the strength of the stratification. Swart et al. (2011) state that the Gully represents a special case in this regard as the diurnal frequency is very near to resonant for the observed stratification.

A surprising feature of the spectra from sites SG2 and SG11 is the occurrence of a large number of peaks corresponding to overtides (higher harmonics) and compound tides (resulting from the

interaction of two or more astronomical constituents); such peaks that are typically seen in near-shore areas (Parker, 1991; Aubrey and Speer, 1985; Speer and Aubrey, 1985), but not in the offshore at depths up to 1500 m, and underline the unique tidal response in the Gully in comparison to other submarine canyons (Xu and Noble, 2009; Hotchkiss and Wunsch, 1982). Hunkins (1988) notes that quarter-diurnal tides were evident at sites near the head of Baltimore Canyon, but did not indicate their strength. This implies that tidal resonance is the likely source of energy driving the enhanced vertical mixing indicated by the simple models we have employed. The strength of the compound tides at moorings SG2 in particular and SG11 also implies tidal residual flows of $\sim 0.01 \text{ m s}^{-1}$ which could contribute significantly to the long-term mean flow (see Figure 14).

Shan et al. (2013a,b) have developed a high-resolution, nested model to study the circulation and hydrography of the Gully. This model suggested that the deep portion of the canyon is characterized by a weak, but persistent, northwestward flow indicating cross-shelf transport of deep slope water into the Gully. This is consistent with the moored current meter records from the array. The model is also able to demonstrate significant tide-topography interaction within the canyon, and suggested that circulation and hydrography above the canyon rim is influenced significantly by wind forcing.

5. Conclusions

The physical environment of the Sable Gully is in some ways similar to other canyons along the eastern seaboard of North America; however, there are several features which make it unique. The circulation above the Gully rim ($< 200 \text{ m}$) flowed relatively undisturbed over the canyon and is primarily influenced by the southwestward shelf-break current. This decoupling does not appear to be related to seasonal stratification and is similar to observations for other canyons on the Atlantic coast. There is limited evidence supporting the existence of a rim-depth eddy. The depth-averaged mean velocity below the Gully rim is on the order of 0.01 m s^{-1} ; given the distance from the mouth to the head of the Gully, the advective time scale in the deep part of the canyon is approximately 30 days which is significantly longer than the observed residence time above the rim.

The mean 200 m–bottom transport towards the head of the Gully measured by the mid-canyon array leads to an estimated upwelling velocity of $1.7 \times 10^{-4} \text{ m s}^{-1}$ over the inner half of the Gully. This should produce a significant vertical nitrate flux and potentially generate a chlorophyll concentration of $\sim 1.7 \text{ mg Chl m}^{-3}$ over the upper 200 m. However, the currents immediately above the Gully rim would advect this nitrate out of the region relatively quickly and reduce the impact on production within the canyon. Nevertheless, this could be a potential nutrient source for areas downstream.

An intrusion of colder, fresher water into the Gully during the mooring deployment enabled an estimate of an upper bound on the vertical eddy diffusivity ($K_v \leq 180 \times 10^{-4} \text{ m}^2 \text{ s}^{-1}$); this is about 20 times the typical value observed on the Scotian Shelf. The speed of propagation of this cold, fresh intrusion from SG11 (mid-canyon) to SG2 (head) was estimated to be $\sim 0.02 \text{ m s}^{-1}$, based on the distance between the mooring sites and the time lag observed; this is consistent with the current meter measurements.

A principal component analysis of the along-Gully velocities observed at the main array found that PCA1 accounts for 56% of the variance; loadings were generally in phase for SG11 and SG12, but out of phase for SG10. If SG2 is included in the analysis, PCA1 accounts for 44% of the variance and the first three modes account for 80%. This is much higher than observed in Lydonia Canyon where PCA1 accounted for 25% of the variance. Seasonal variability is not a major factor in the low frequency circulation. It is evident that at low frequencies (less than diurnal), the depth dependence of current variance of the Gully and nearby open, continental slope area is similar. This is in sharp contrast to the diurnal ratios (Gully/open slope velocities) which range from 4.1 at 150 m to 548 at 1500m. For 200 m to bottom, the tides account for 95% of the measured variance in the Gully.

The amplification of diurnal and semi-diurnal tides along the Gully axis results in a physical environment which is unique relative to the surrounding slope region at depths below 200 m. A surprising and exceptional feature of the spectra derived from current meter measurements at SG2 and SG11 is the large number of peaks corresponding to overtides and compound tides. This extensive non-linear interaction of tidal constituents has not been observed in other canyons. The strength of these compound tides also implies that the tidal residual flows of $\sim 0.01 \text{ m s}^{-1}$ could contribute significantly to the long-term mean flow.

The vertical distribution of phytoplankton and bacteria in the Gully appears, as elsewhere, to be constrained by the surface layer nutrient regime imposed by density stratification. Maximum microbial cell abundance is located at the top of the pycnocline/nitracline, but maximum phytoplankton biomass is somewhat deeper. On a seasonally adjusted basis, there is no strong evidence of enhanced phytoplankton or bacterial concentrations in the Gully compared to the Scotian Shelf as a whole. These concentrations in the Gully appear to be constrained within the envelope of annual variability of the wider Scotian Shelf (Li 1998; 2009; Li and Harrison 2001; Li et al. 2006; Li et al. 2011).

Observations of surface chlorophyll derived from SeaWiFS observations (48/year, 1997-2009) were compiled for the Gully as well as for 5 adjacent or nearby areas: Misaine Bank, Banquereau Bank, Middle Bank, Sable Bank and the Northern Slope. The peak value of the fit to the bloom period is smallest for the Gully save for the Northern Slope region. Only Sable Bank has an earlier bloom (peak on day 87) than the Gully (day 97), but the peaks in the remaining areas follow soon after (day 101-108). The “duration” of the bloom is long (49-62 days) for 3 areas including the Gully and considerably shorter for the other 3 (26-28 days). We conclude that the Gully does not appear to be distinct relative to the other regions. Moreover, the data indicate that the surface concentrations, if anything, appear lower than some of the surrounding areas.

Zooplankton were collected in vertical net tows (200 μm mesh) between 100 m and the surface at nine stations in April 2006 and at eleven stations in August 2007. In this layer the biomass range was 29-71 g m^{-2} (wet weight) in April 2006 and much lower at 1-6 g m^{-2} in August 2007. Two vertical tows were made to greater depths in April 2006 and four in August 2007. The biomass in the 0-1500 m range was the same as that in the 0-100 m range in the central Gully in April, whereas the biomass in the 0-384 m range at a station near the head of the Gully, was larger (by a factor of 1.7) than that in the 0-100 m depth range. In August, zooplankton biomass

971 in deep tows (0-1000 m) at the stations within the Gully and downstream (to the southwest) of it
972 along the shelf-break were more-or-less the same (range 61-74 g m⁻²). At a station upstream (to
973 the northeast) of the Gully along the shelf-break the biomass was somewhat lower (32 g m⁻²)
974 than at the other stations.

975
976

977

978 **Acknowledgments**

979 This project was funded through the Fisheries and Oceans Canada (DFO) Oceans Action Plan
980 Phase 1 and the Health of the Oceans (HOTO). We also thank the officers and crew of CCGS
981 Hudson for their assistance with the field program. The Technical Operation Section at BIO
982 provided excellent field support for this project; in particular, the authors thank Murray Scotney,
983 Rick Boyce, Adam Hartling, Jay Barthelotte and Bob Ryan. Norman Cochrane and Yongsheng
984 Wu provided helpful reviews.

985

986

References

- Allen, S. E., 1996. Topographically generated, subinertial flows within a finite-length canyon. *J. Phys. Oceanogr.* 26, 1608–1632.
- Allen, S. E., Hickey, B. M., 2010. Dynamics of advection-driven upwelling over a shelf break submarine canyon. *J. Geophys. Res.* 115, C08018, doi:10.1029/2009JC005731.
- Aubrey, D.G., Speer, P.E., 1985. A study of non-linear tidal propagation in shallow inlet/estuarine systems Part I: Observations. *Estuarine Coastal Shelf Sci.*, 21, 185–205, doi:10.1016/0272-7714(85)90096-4.
- Baines, P.G., 1982. On internal tide generation models. *Deep-Sea Res.* 29, 307–318.
- Baines, P.G., 1983. Tidal motions in submarine canyons—A laboratory experiment. *J. Phys. Oceanogr.* 13, 310–328.
- Bell, T. H., 1975. Topographically-generated internal waves in the open ocean. *J. Geophys. Res.* 80, 320–327.
- Carson, B., Baker, E. T., Hickey, N. M., Nittrouer, C. A., DeMaster, D. J., Thorbjarnarson, K. W., Snyder, G. W., 1986. Modern sediment dispersal and accumulation in Quinault Submarine Canyon—A summary. *Mar. Geol.*, 71, 1–13.
- Carter, G. S., Gregg, M. C., 2002. Intense, variable mixing near the head of Monterey Canyon. *J. Phys. Oceanogr.* 32, 3145–3165.
- Chen, X., Allen, S. E., 1996. The influence of canyons on shelf currents: A theoretical study. *J. Geophys. Res.* 101, 18043– 18059.
- De Leo, F. C., Smith, C. R., Rowden, A. A., Bowden, D. A., Clark, M. R., 2010. Submarine canyons: hotspots of benthic biomass and productivity in the deep sea. *Proc. R. Soc. B.* 277, 2783–2792. doi: 10.1098/rspb.2010.0462.
- Freeland, H. L., Denman, K. L., 1982. A topographically-induced upwelling center off southern Vancouver Island. *J. Mar. Res.*, 40, 1069–1093.
- Garcia Lafuente, J., Sarhan, T., Vargas, M., Vargas, J. M., Plaza, F., 1999. Tidal motions and tidally-induced fluxes through La Linea submarine canyon, western Alboran Sea. *J. Geophys. Res.* 104, 3109–3119.
- Gardner, W. D., 1989. Periodic resuspension in Baltimore Canyon by focussing of internal waves. *J. Geophys. Res.* 94, 18185– 18194.
- Gatien, M. G. , 1976. A study in the Slope Water Region South of Halifax. *J. Fish. Res. Bd. Canada* 33, 2213–2217.

- Gordon, R. L., Marshall, N. F., 1976. Submarine canyons: Internal wave traps? *Geophys. Res. Lett.* 3, 622–624.
- Greenan, B.J.W., Petrie, B.D., Cardoso, D.A. Mean circulation and high-frequency flow amplification in the Sable Gully. *Deep-Sea Res. II* (2013)
<http://dx.doi.org/10.1016/j.dsr2.2013.07.011>
- Greenan, B.J.W., Petrie, B. D., Harrison, W. G., Oakey, N. S., 2002. Short-term physical, chemical and biological variability on the Scotian Shelf. *Can. Tech. Rep. Hydrogr. Ocean. Sci.* 218:xi + 106 pp.
- Hall, R. A., Alford, M. H., Carter, G. S., Gregg, M. C., Lien, R.-C., Wain, D. J., Zhao, Z., 2013. Transition from partly standing to progressive internal tides in Monterey submarine canyon. *Deep-Sea Res. II*.
- Harrison, W.G., Fenton, D.G., 1998. The Gully: A scientific review of its environment and ecosystem. Department of Fisheries and Oceans, Ottawa. Canadian Science Advisory Secretariat Research Document. 98/83, 282 pp.
- Harris, P. T., Whiteway, T., 2011. Global distribution of large submarine canyons: Geomorphic differences between active and passive continental margins. *Mar. Geol.* 285, 69–86.
- Hickey, B. M., 1995. Coastal submarine canyons. Topographic effects in the ocean: ‘Aha Huliko’a Hawaiian Winter Workshop. University of Hawaii at Manoa, Honolulu, HI, pp. 95–110.
- Hooker, S. K., Whitehead, H., Gowans, S., 1999. Marine protected area design and the spatial and temporal distribution of cetaceans in a submarine canyon. *Conserv. Biol.* 13 (3), 592–602.
- Hotchkiss, F. S., Wunsch, C., 1982: Internal waves in Hudson Canyon with possible geological implications. *Deep-Sea Res.*, **29**, 415–442.
- Hunkins, K., 1988: Mean and tidal currents in Baltimore Canyon. *J. Geophys. Res.*, **93**, 6917–6929.
- Kenchington, E., Cogswell, A., MacIsaac, K., Beazley, L., Law, B., Kenchington, T., 2013. Bathyal epibenthic megafauna of the Gully submarine canyon, northwest Atlantic. *Deep-Sea Res. II*, in press.
- Kinsella, E. D., Hay, A. E., Denner, W. W., 1987: Wind and topographic effects on the Labrador Current at Carson Canyon. *J. Geophys. Res.*, **92**, 10,853–10,869.
- Klinck, J. M., 1988. The influence of narrow transverse canyon on initially geostrophic flow. *J. Geophys. Res.* 93, 509–515.

- Klinck, J. M., 1989. Geostrophic adjustment over submarine canyons. *J. Geophys. Res.* 94, 6133–6144.
- Klinck, J. M., 1996. Circulation near submarine canyons: A modeling study. *J. Geophys. Res.* 101, 1211–1223.
- Kunze, E., MacKay, C., McPhee-Shaw, E. E., Morrice, K., Girton, J. B., Terker, S. R., 2012. Turbulent Mixing and Exchange with Interior Waters on Sloping Boundaries. *J. Phys. Oceanogr.* 42, 910–927.
- Li, W. K. W. 1998. Annual average abundance of heterotrophic bacteria and *Synechococcus* in surface ocean waters. *Limnol. Oceanogr.* 43, 1746–1753.
- Li, W. K. W. 2009. From cytometry to macroecology: a quarter century quest in microbial oceanography. *Aquat. Microb. Ecol.* doi: 10.3354/ame01328.
- Li, W. K. W., Harrison, W. G. 2001. Chlorophyll, bacteria and picophytoplankton in ecological provinces of the North Atlantic. *Deep-Sea Research II* 48:2271–2293.
- Li, W. K. W., Harrison, W. G. 2008. Propagation of an atmospheric climate signal to phytoplankton in a small marine basin. *Limnol. Oceanogr.* 53:1734–1745.
- Li, W. K. W., Harrison, W. G., Head, E. J. H. 2006. Coherent assembly of phytoplankton communities in diverse temperate ocean ecosystems. *Proc. R. Soc. B.* 273:1953–1960.
- Li, W. K. W., Andersen, R. A., Gifford, D. J., Incze, L. S., Martin, J. L., Pilskaln, C. H., Rooney-Varga, J. N., Sieracki, M. E., Wilson, W. H., Wolff, N. H. 2011. Planktonic microbes in the Gulf of Maine area. *PLoS ONE* 6(6): e20981. doi:10.1371/journal.pone.0020981.
- Loder, J., Geshelin, Y., 2009. Currents and temperature variability from moored measurements on the outer Halifax Line in 2000–2004. *Atlantic Zone Monitoring Program Bulletin* 8, 44–50. http://www.meds-sdmm.dfo-mpo.gc.ca/isdm-gdsi/azmp-pmza/docs/bulletin_8_07.pdf.
- MacIsaac, K. G., Kenchington, T., Kenchington, E. L. R., Best, M., 2013. The assemblage of larger pelagic crustacea at the Gully submarine canyon: major patterns and a comparison to the adjacent continental shelf. *Deep-Sea Res. II*, in press
- Maso, M., La Violatte, P. E., Tintore, J., 1990. Coastal flow modification by submarine canyons along the NE Spanish coast. *Sci. Mar.* 54, 343–348.
- Moors-Murphy, H. B., 2013. Submarine canyons as important whale habitat: a review of cetacean associations with the Gully and other submarine canyons. *Deep-Sea Res. II*.
- Nittrouer, C. A., Wright, L. D., 1994. Transport of particles across continental shelves. *Rev. Geophys.* 32 (1), 85–113.

- Noble, M., Butman, B., 1989. The structure of subtidal currents within and around Lydonia Canyon: evidence for enhanced cross-shelf fluctuations over the mouth of the canyon. *J. Geophys. Res.* 94, 8091-8110.
- O'Brien, T.D., Li, W.K.W., Moran, X.A.G. (Eds.) 2012. ICES Phytoplankton and Microbial Plankton Status Report 2009/2010. ICES Cooperative Research Report No. 313, 196pp.
- Parker, B. B. (Ed.), 1991. *Tidal Hydrodynamics*. John Wiley & Sons, New York, 883 pages.
- Pawlowicz, R., Beardsley, B., Lentz, S., 2002. Classical tidal harmonic analysis including error estimates in MATLAB using T_TIDE. *Comput. Geosci.* 28, 929-937.
- Petrie, B., 1975. M2 surface and internal tides on the Scotian shelf and slope. *J. Mar. Res.* 33, 303-323.
- Petrie, B., Lively, R. R., 1979. Offshore meteorological measurements with a CODS discus buoy. *Atmos.-Ocean.* 17, 117-140.
- Petrie, B., Drinkwater, K., 1993. Temperature and salinity variability on the Scotian Shelf and in the Gulf of Maine 1945-1990. *J. Geophys. Res.* 98, 20079-20089.
- Petrie, B., Drinkwater, K., Gregory, D., Pettipas, R., Sandström, A., 1996. Temperature and salinity atlas for the Scotian Shelf and Gulf of Maine. *Can. Tech. Rep. Hydrogr. Ocean Sci.* 171: v + 398 pp.
- Petrie, B., Shore, J., Hannah, C., Loder, J., 1998. Physical Oceanography. In *The Gully: A scientific review of its environment and ecosystem*. A. G. Harrison and D. G. Fenton, Editors, pp 20-57. Department of Fisheries and Oceans, Ottawa. Canadian Science Advisory Secretariat Research Document. 98/83, 282 pp.
- Petrie, B., Yeats, P., 2000. Annual and interannual variability of nutrients and their estimated fluxes in the Scotian Shelf-Gulf of Maine region. *Can. J. Fish. Aquat. Sci.* 57, 2536-2546.
- Petruncio, E. T., Rosenfeld, L. K., Paduan, J. D., 1998. Observations of the internal tide in Monterey Canyon. *J. Phys. Oceanogr.* 28, 1873-1903.
- Shan, S., Sheng, J., Greenan, B. J. W., 2013a. Modelling study of three-dimensional circulation and particle movement over the Sable Gully of Nova Scotia, *Ocean Dynamics*, submitted.
- Shan, S., Sheng, J., Greenan, B. J. W., 2013b. Physical processes affecting circulation and hydrography in the Sable Gully of Nova Scotia, *Deep Sea Res. II*, in press.
- Shephard, F.P., Marshall, N.F., McLoughlin, P.A., 1974. Currents in the submarine canyons. *Deep-Sea Res.* 21, 691-706.
- Smith P. C., Petrie, B. D., 1982. Low-frequency circulation at the edge of the Scotian Shelf. *J. Phys. Oceanogr.* 12, 28-46.

- Speer, P.E., Aubrey, D.G., 1985. A study of non-linear tidal propagation in shallow inlet/estuarine systems Part II: Theory. *Estuarine Coastal Shelf Sci.*, 21, 207-224, [doi: 10.1016/0272-7714\(85\)90097-6](https://doi.org/10.1016/0272-7714(85)90097-6).
- Swart, N. C., Allen, S. E., Greenan, B. J. W., 2011. Resonant amplification of subinertial tides in a submarine canyon, *J. Geophys. Res.*, 116, C09001, [doi:10.1029/2011JC006990](https://doi.org/10.1029/2011JC006990).
- Umoh, J. U., Thompson, K. R., 1994. Surface heat flux, horizontal advection, and the seasonal evolution of water temperature on the Scotian Shelf. *J. Geophys. Res.*, 99, C10, 20,403-20,416.
- Welch, P.D., 1967. The use of fast Fourier transform for the estimation of power spectra: a method based on time averaging over short, modified periodograms, *IEEE Transactions on Audio Electroacoustics*, AU-15, 70–73.
- Xu, J. P., Noble, M. A., 2009. Currents in Monterey submarine canyon. *J. Geophys. Res.*, 114, C03004, [doi: 10.1029/2008JC004992](https://doi.org/10.1029/2008JC004992).

TABLES

Table 1: Summary of Sable Gully mooring configuration. Nominal depths (m) of the instruments are indicated by the numbers in each of the mooring columns. Numbers with asterisks indicate that the RCM8 did not have sensors installed for pressure or conductivity. Water depth at each of the mooring sites is given by the number in brackets at the top of each column.

Instrument	Parameters	SG2 (1054 m)	SG11 (1640 m)	SG12 (723 m)	SG10 (476 m)
Vemco Minilog	Temperature	208 250 273	154 203 230	245 270	123 148
Aanderaa RCM8	Speed Direction Temperature Conductivity Pressure	355 562* 761* 1007*	290 444* 635* 945* 1249* 1542*	345 546 673*	222 323* 424*
TRDI Workhorse ADCP (300 kHz)	Speed Direction Temperature Pressure	225	178	220	95
Sea-Bird SBE37 MicroCAT	Temperature Conductivity Pressure	188 225 562 761	134 178 444 635	220 546	95 424

Table 2: Summary for each instrument type of the estimated accuracy (Acc) and resolution (Res) of the variables speed, direction, temperature and conductivity.

Instrument	Speed		Direction		Temperature		Conductivity	
	Acc	Res	Acc	Res	Acc	Res	Acc	Res
RDI ACDP	0.5%	0.1 cm s ⁻¹	2°	0.01°	0.4°C	0.01°C		
Sea-Bird SBE37 MicroCat					0.002°C	0.001°C	0.003 mS cm ⁻¹	0.0001 mS cm ⁻¹
Aanderaa RCM8	N/A	> of 4% spd or 1 cm s ⁻¹	5°	0.35°	0.05°C	0.02°C	0.074 mS cm ⁻¹	0.074 mS cm ⁻¹
Vemco Minilog					0.2°C	0.1°C		

Table 3: ADCP bin depth used for plotting and percent data return for each bin.

SG2 (1588)		SG11 (1589)		SG10 (1590)		SG12 (1591)	
Bin depth (m)	% return	Bin depth (m)	% return	Bin depth (m)	% return	Bin depth (m)	% return
130	24	100	21	130	45	25	90
150	64	125	63	150	91	50	100
175	90	150	89	175	100	75	100
200	95	175	91	200	100	90	100
225	27	200	28	220	100	-	-

Table 4: Percent data return for ADCP bins 16 to 24 on each of the four moorings SG2, SG10, SG11 and SG12.

Bin #	SG2 (1588)	SG11 (1589)	SG10 (1590)	SG12 (1591)
24	15	26	0	0
23	21	30	37	1.4
22	27	35	44	1.6
21	34	41	53	1.7
20	40	48	65	18
19	44	55	75	77
18	53	64	82	85
17	63	73	88	88
16	72	82	92	91
15	80	89	95	93
14	87	93	97	95
13	91	96	98	97
12	94	98	99	98

Table 5: Parameters derived from the average annual cycle for the Gully and nearby areas. Under the heading “Linear Regression”, I stands for intercept, S for slope; under Gaussian fit, the peak corresponds to the largest value of surface chlorophyll concentrations, b the day of the peak bloom, and the duration the time span for the fitted bloom of rise/fall to 0.5 times the peak concentration.

Area	Integrated Chl (mg m ⁻³)	Linear Regression			Gaussian Fit to Spring Bloom			
		I	S	R ²	Peak (mg m ⁻³)	b (day)	Duration (day)	R ²
Gully	39	n/a	n/a	n/a	2.1	97	49	0.92
N Slope	29	0.1	0.6	0.72	1.5	101	62	0.83
Banq	36	0	0.9	0.73	2.7	108	26	0.92
Misaine	46	-0.1	1.3	0.66	3.7	106	28	0.91
Middle	47	-0.1	1.3	0.81	3.7	101	28	0.98
Sable	47	0.2	1	0.70	2.6	87	49	0.92

Table 6: Ratio of SG11 to Slope variance from moored current meter data (see Figure 18) at various depths listed on the column headings. The rows represent different frequency bands.

	150 m	500 m	1000m	1500m
Low Frequency	0.6	1.1	1.1	1.8
Diurnal	4.1	94	140	548
Inertial	0.4	0.2	0.3	0.8
Semi Diurnal	0.5	1.7	1.5	7.5
High Frequency	2.3	2.3	1.5	9.5

FIGURES

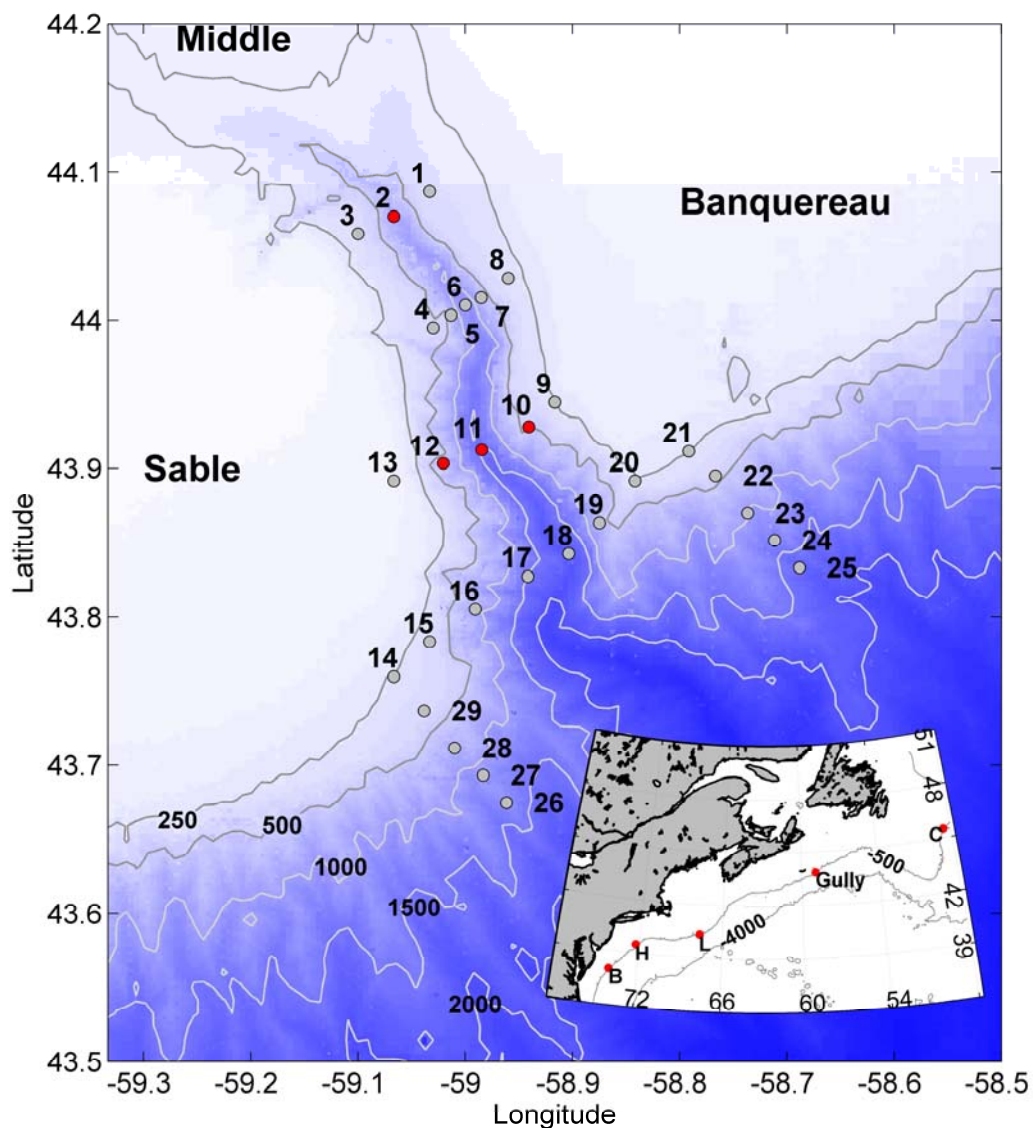


Figure 1: Schematic (depth in m) of the Sable Gully field program with CTD stations (grey dots) and mooring sites (red dots) indicated. The inset shows the eastern North America shelf break region with other canyons which have been studied: Carson (C), Lydonia (L), Hudson (H) and Baltimore (B).

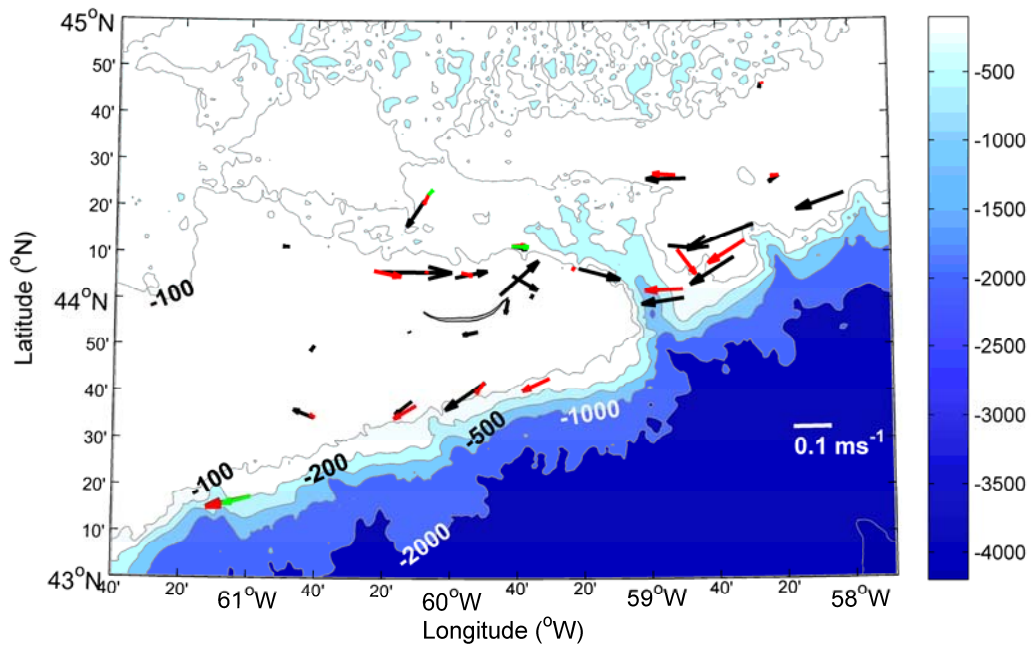


Figure 2: Mean currents averaged in three layers in the Sable Gully region from BIO archived data. The three layers presented are 0-50 m (black), 50-100 m (red) and 100-150 m (green).

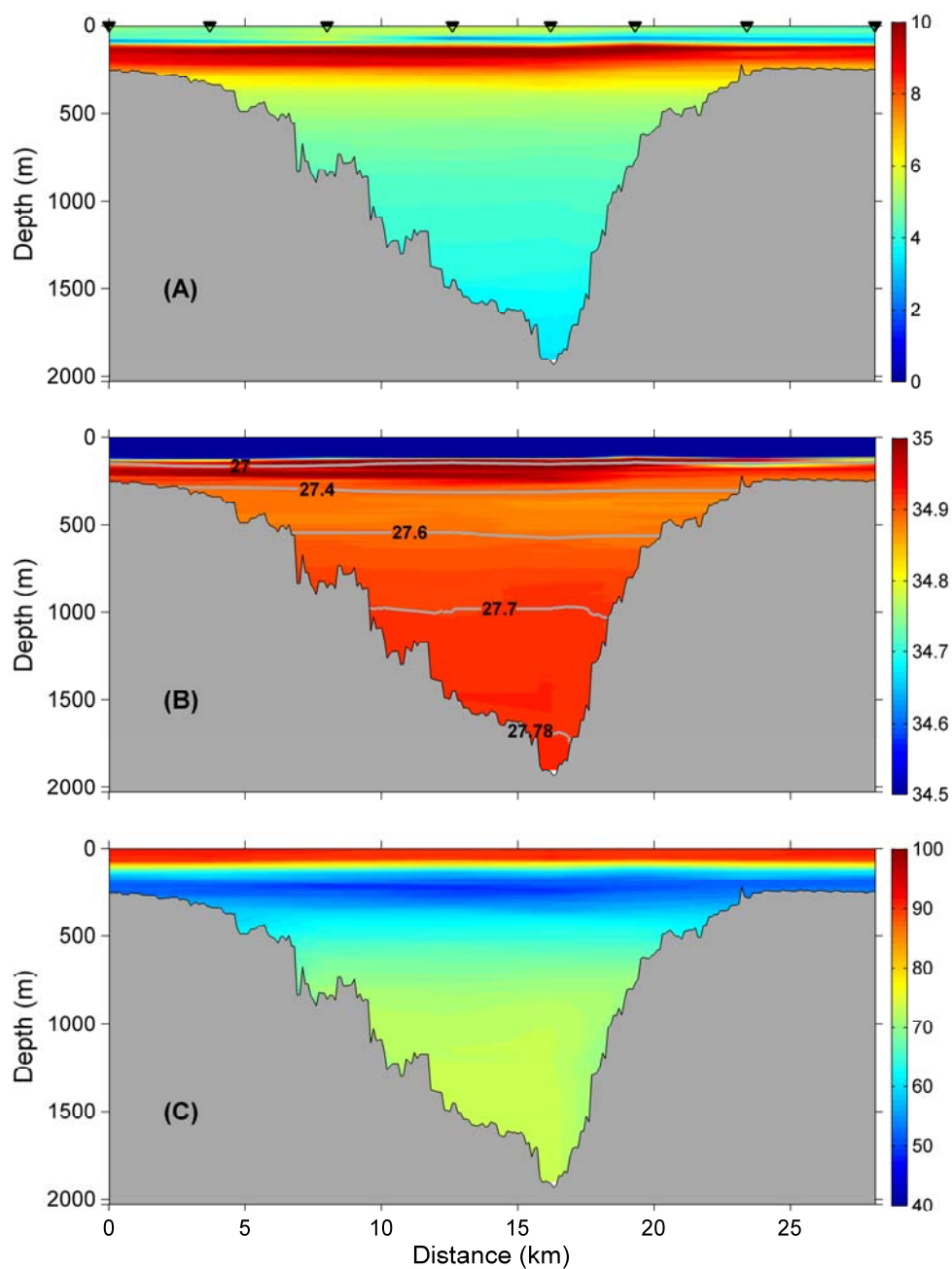


Figure 3: April 2006 CTD section (Stations 14-21) across the mouth of Sable Gully showing (a) temperature (°C), (B) salinity (with σ_T density contours, kg m⁻³), and (C) dissolved oxygen (% saturation).

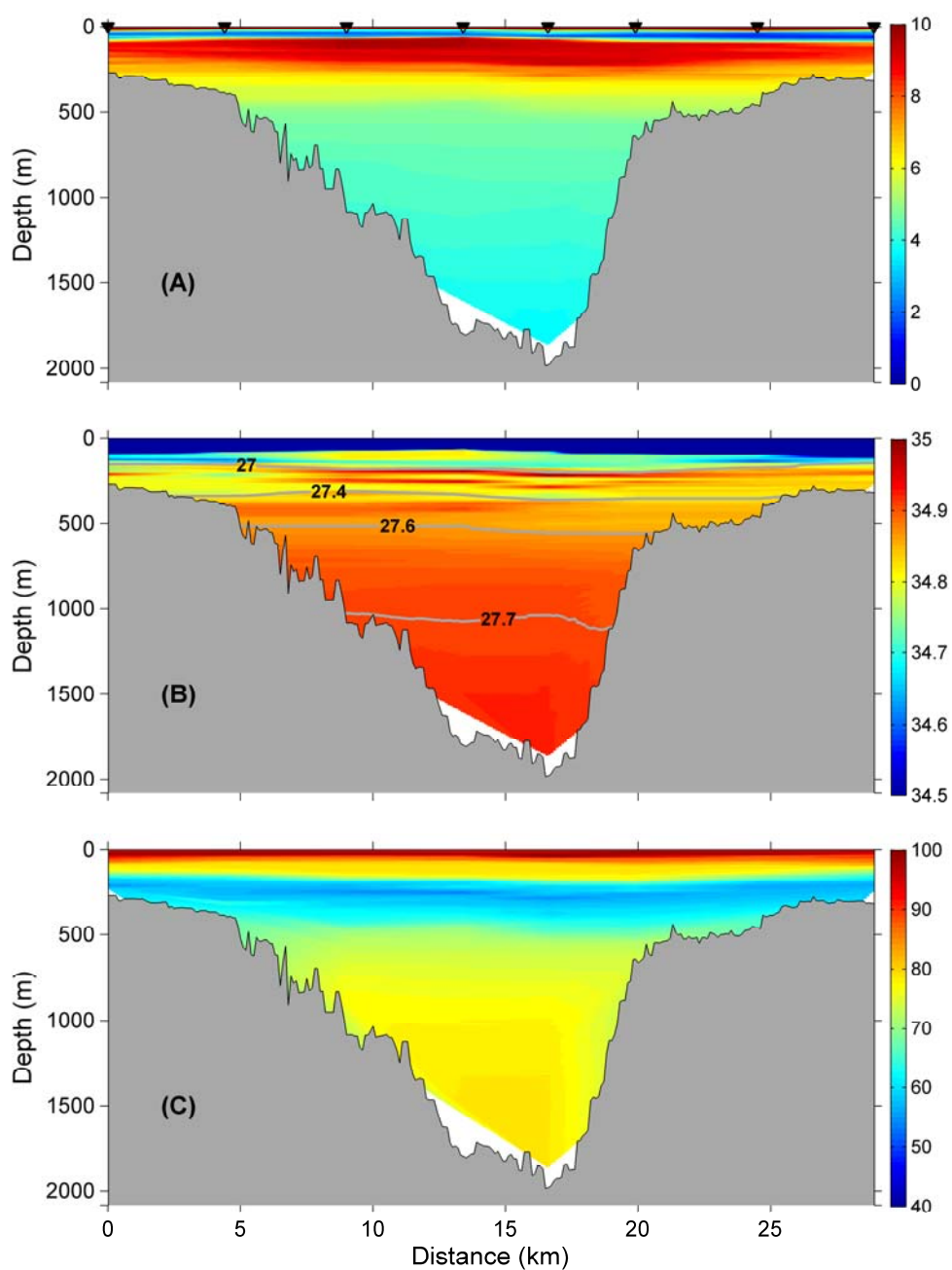


Figure 4: August 2007 CTD section of Stations 14-21 across the mouth of Sable Gully showing (A) temperature (°C), (B) salinity (with σ_T density contours kg m⁻³), and (C) dissolved oxygen (% saturation).

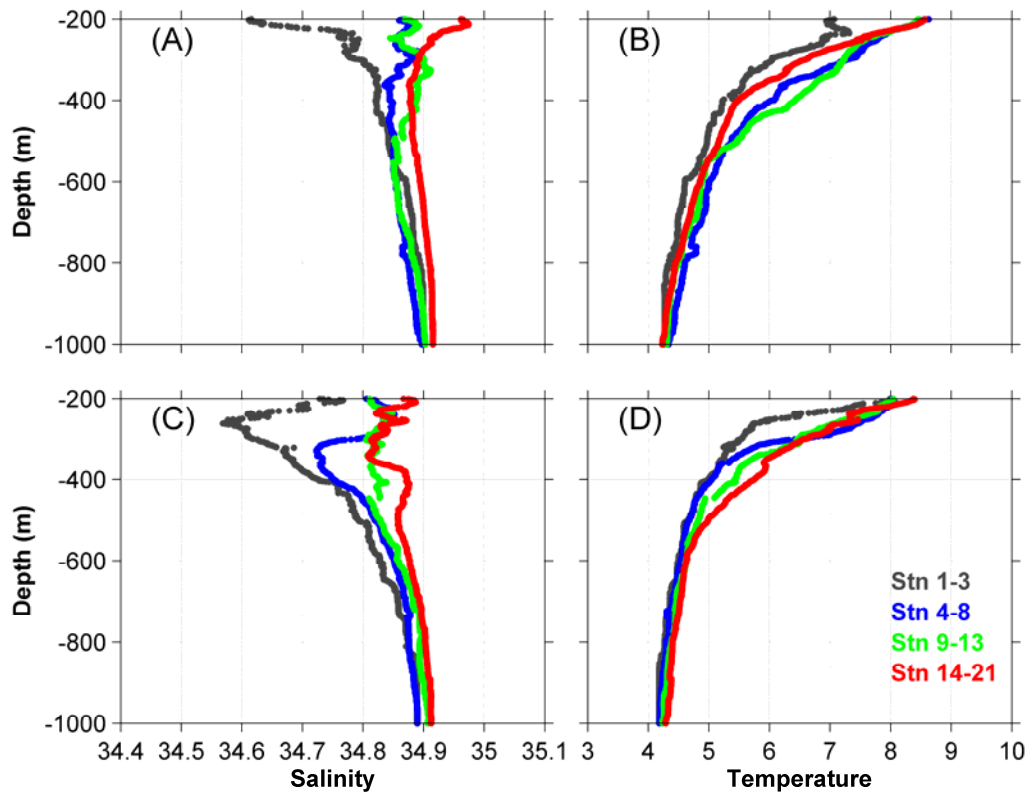


Figure 5: Section-averaged salinity and temperature (°C) profiles for the 2006 (A, B) and 2007 (C, D) CTD surveys. The vertical range has been limited to depths below the canyon rim (200 m) and above 1000 m.

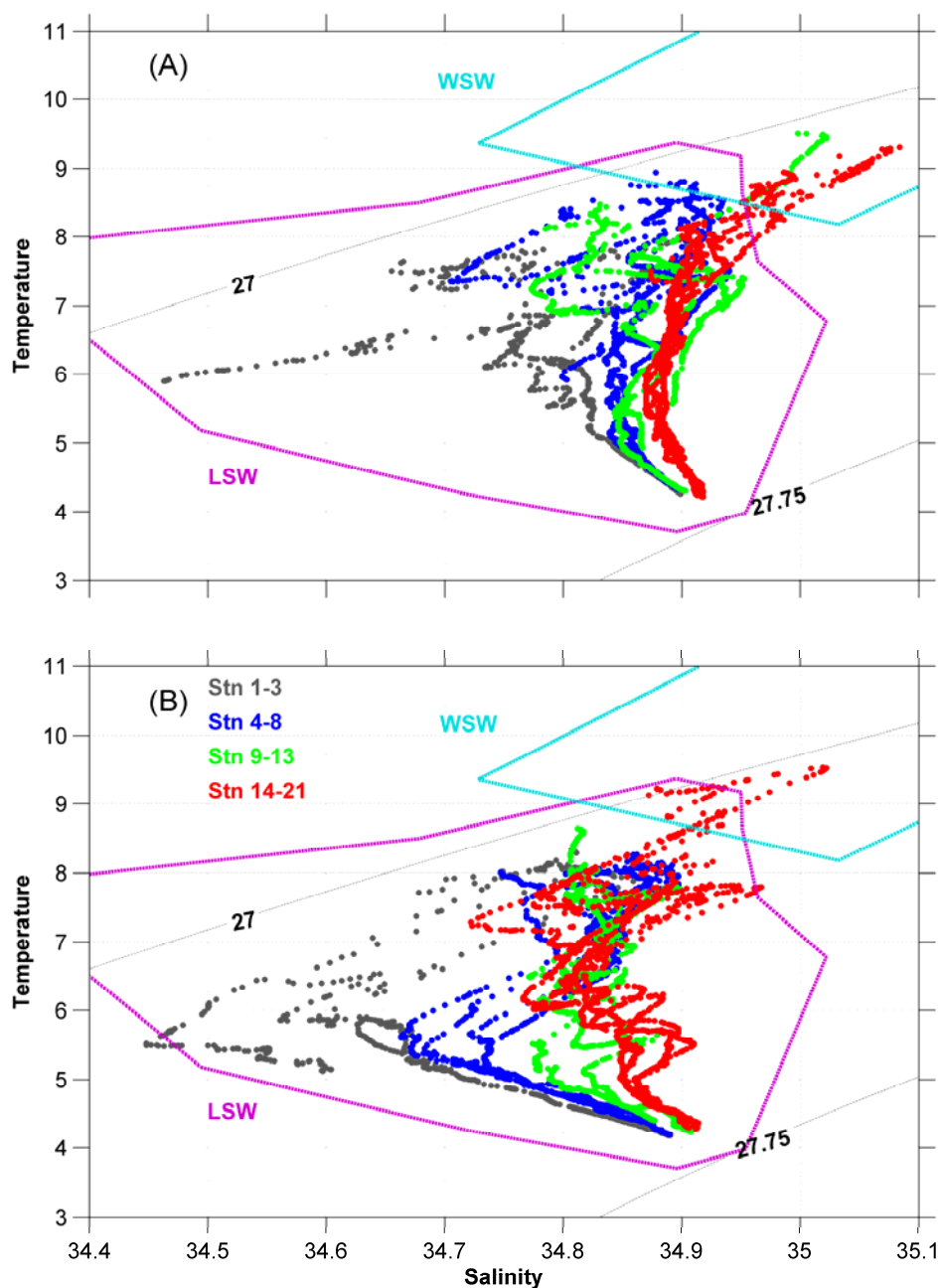


Figure 6: Temperature-salinity plots based on the CTD surveys in 2006 (A) and 2007 (B) for 200-1000 m. Profiles for each section are color-coded. Isopycnals are shown as sloping, gray shaded lines. T-S envelopes, based on Gatién (1976), are presented for Labrador Slope Water (LSW, magenta) and Warm Slope Water (WSW, cyan).

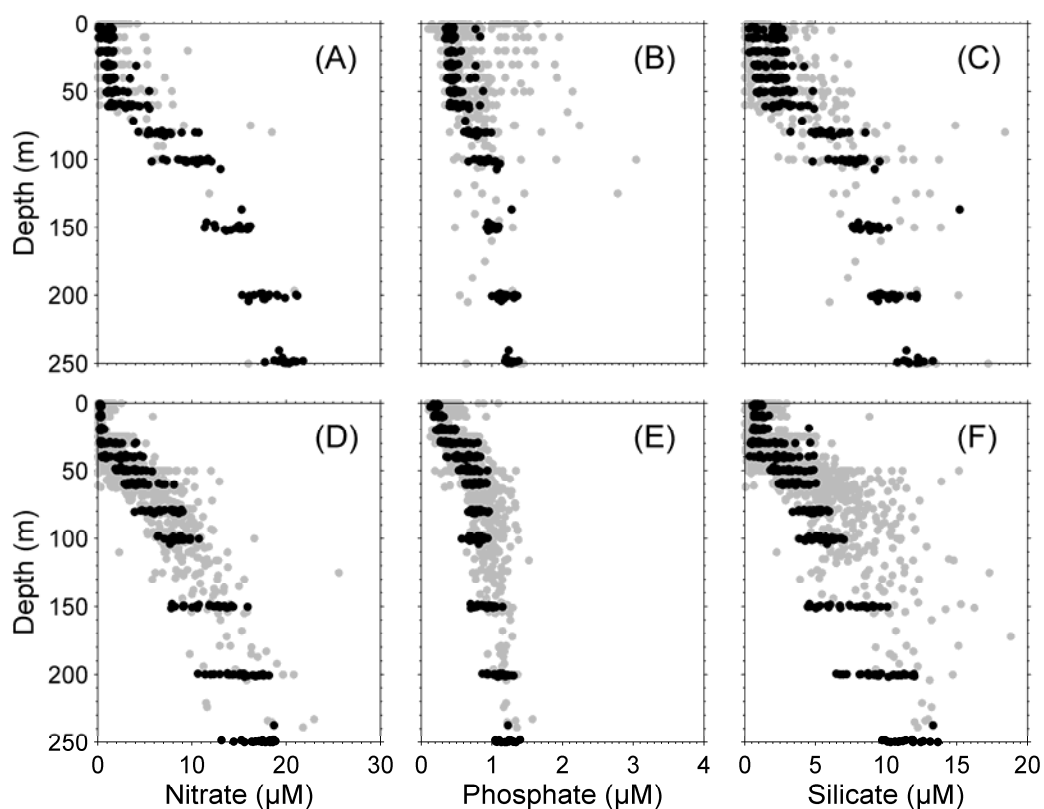


Figure 7: Nitrate, phosphate and silicate concentrations for the Gully (black) for April 2006 (upper panels) and August 2007 (lower panels) and for three adjacent areas (Banquereau, Middle and Sable Island Banks, grey) in April-May (upper panels) and July-August (lower panels).

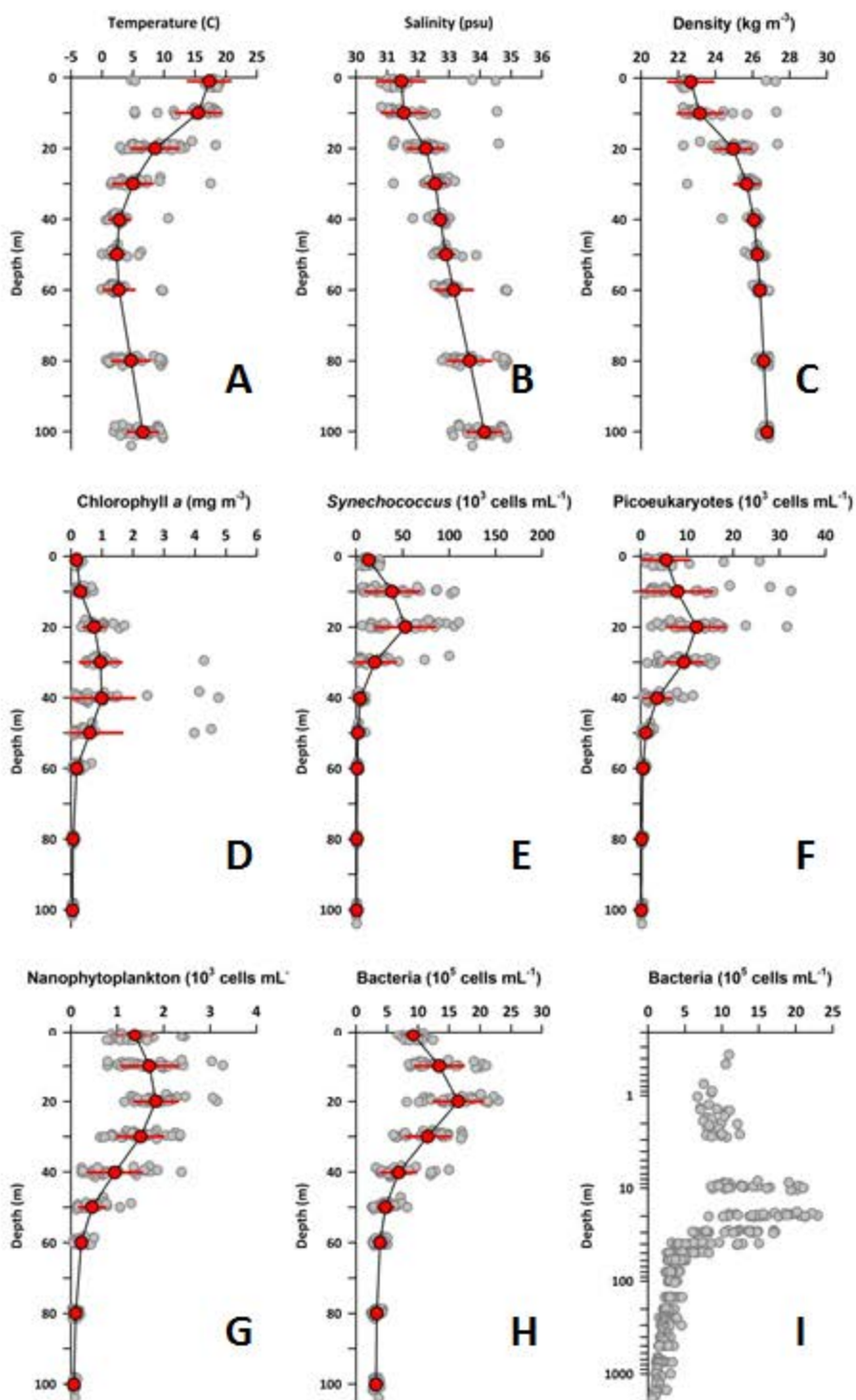


Figure 8: Station-averaged values for the Gully in August 2007. (A) temperature, (B) salinity, (C) density, (D) chlorophyll *a*, (E) *Synechococcus*, (F) picoeukaryotic algae, (G) nanophytoplankton, and (H) bacteria. Individual samples are shown as grey dots; 10m depth-binned average and standard deviations are shown in red colour. (I) Full depth profile of bacteria.

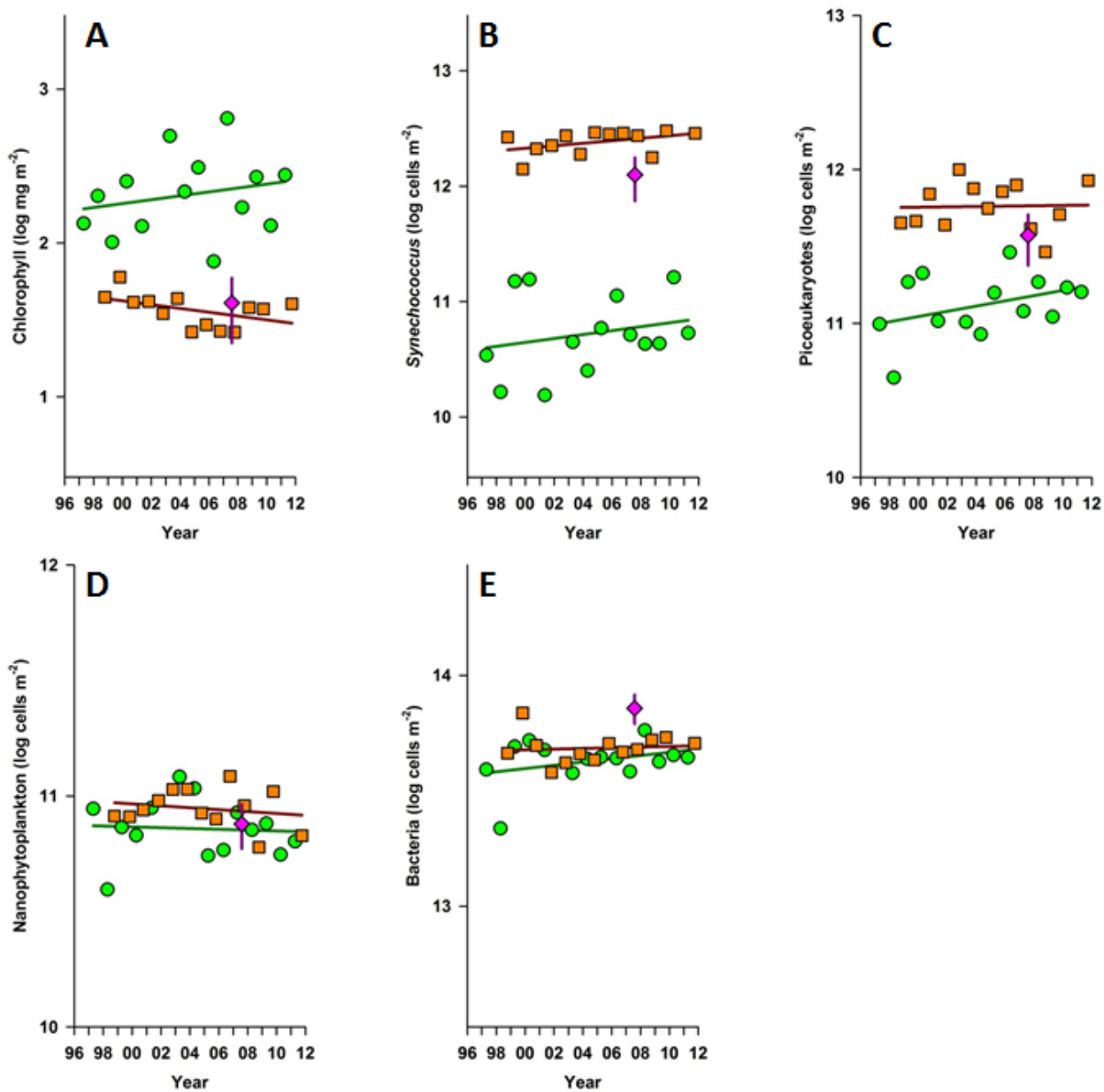


Figure 9: Phytoplankton and bacteria on the Scotian Shelf and the Gully. Values across the Scotian Shelf are station-average measurements of 100m-integrated abundance from AZMP surveys in the spring (April, green circles) and fall (October, orange squares) from 1997-2011 on the 21 core stations of the Browns Bank Line (Western Scotian Shelf), the Halifax Line (Central Scotian Shelf), and the Louisbourg Line (Eastern Scotian Shelf). Values in the Gully are station-average measurements of 100m-integrated abundance from the 2007 summer survey (August, pink diamond).

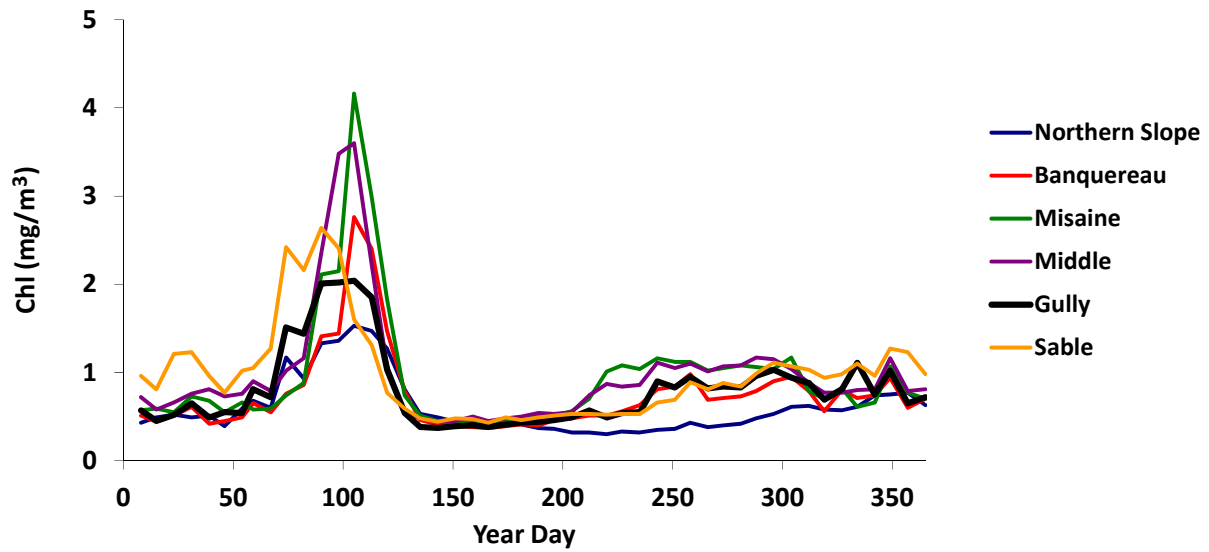


Figure 10: Annual variation of surface chlorophyll based on SeaWiFS observations from 1997-2009.

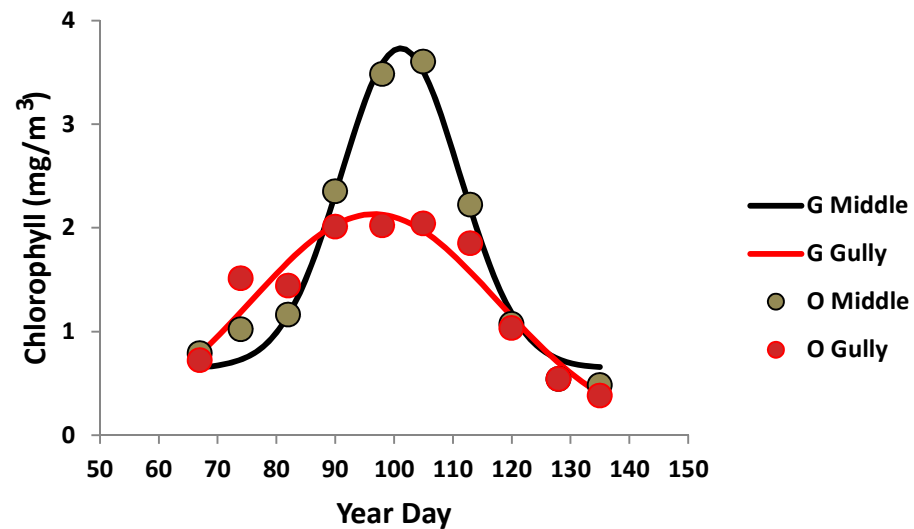


Figure 11: Gaussian fit (G) to and observed (O) spring bloom for Middle Bank and the Gully.

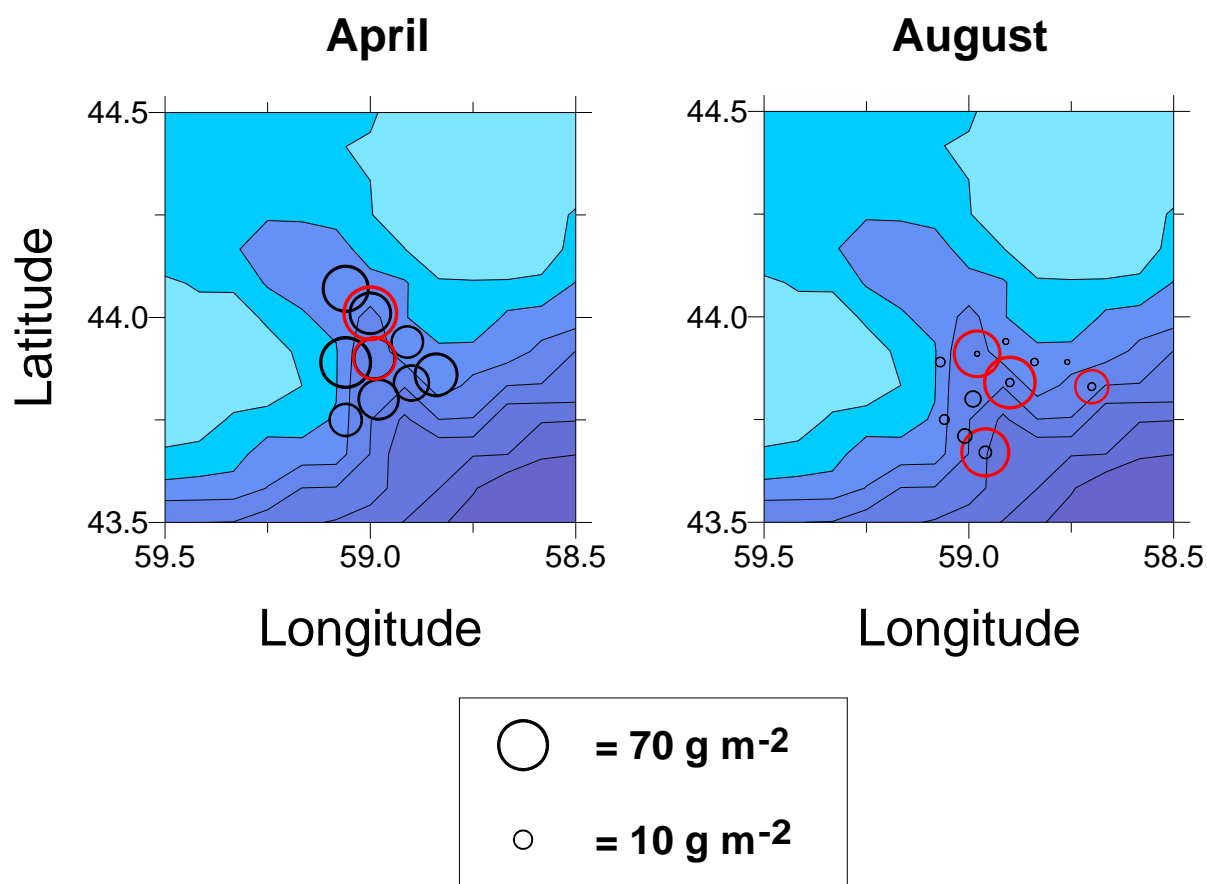


Figure 12: Zooplankton biomass in the Gully in April 2006 and August 2007. Black symbols show the biomass in the 0-100 m depth range, red symbols show the biomass for greater depth ranges.

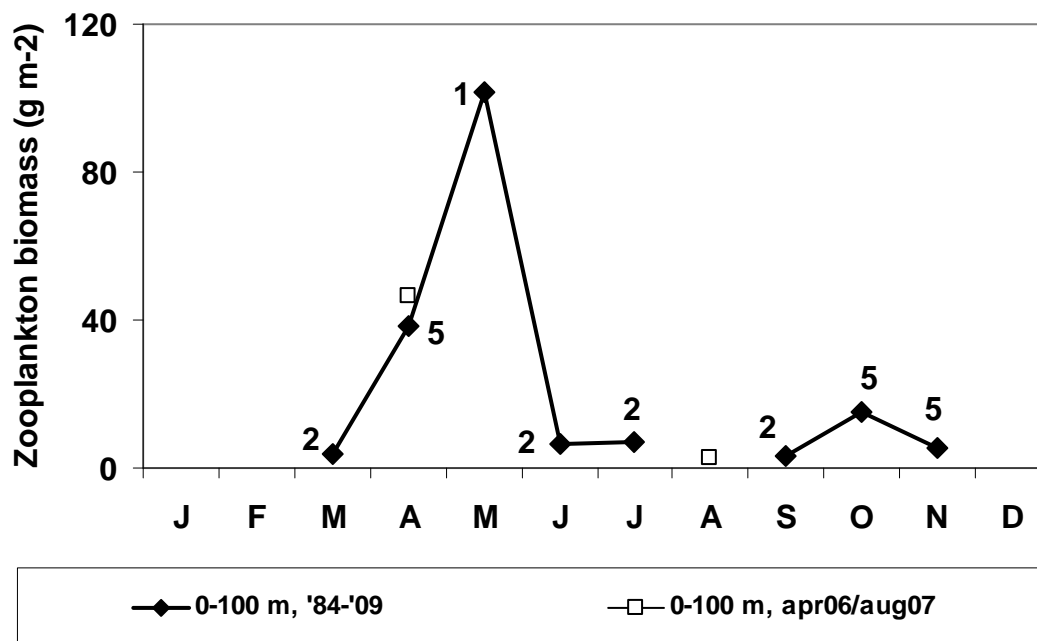


Figure 13: Seasonal cycle of zooplankton biomass in the Gully, constructed from average monthly values derived from cruises between 1984 and 2009, together with values averaged over all sampling stations in April 2006 and August 2007. The numbers by each point of the 1984-2009 data show the number of tows that were made in each month over the 15 year period; some years there were several tows in one or more months.

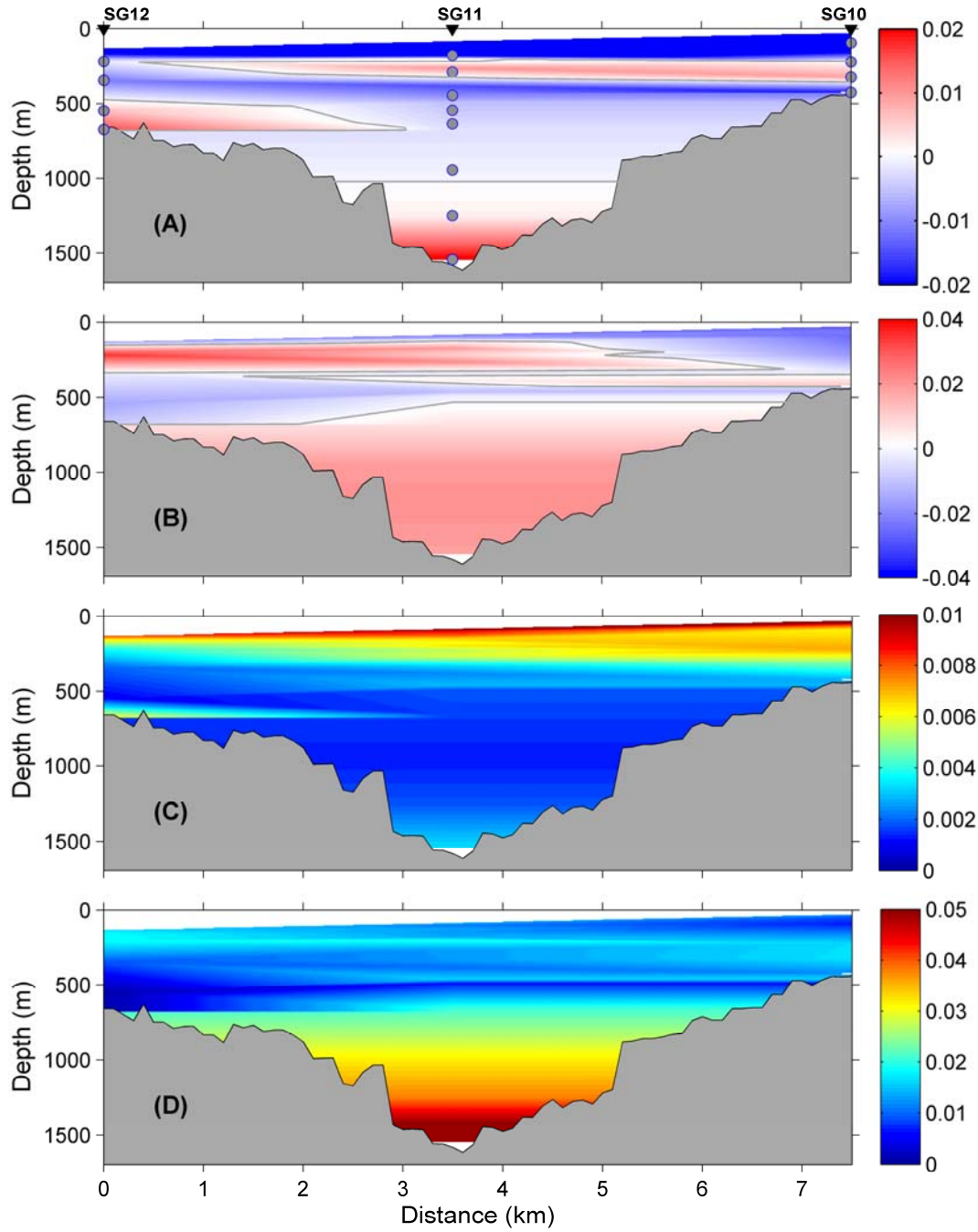


Figure 14: Average estimates from SG10, SG11 and SG12 moorings for the (A) across-canyon speed (m s^{-1} , positive northeast), (B) along-canyon speed (m s^{-1} , positive northwest), (C) across-canyon variance of speed ($\text{m}^2 \text{s}^{-2}$) and (D) along-canyon variance ($\text{m}^2 \text{s}^{-2}$). Grey lines in the top two panels represent the 0 m s^{-1} contour.

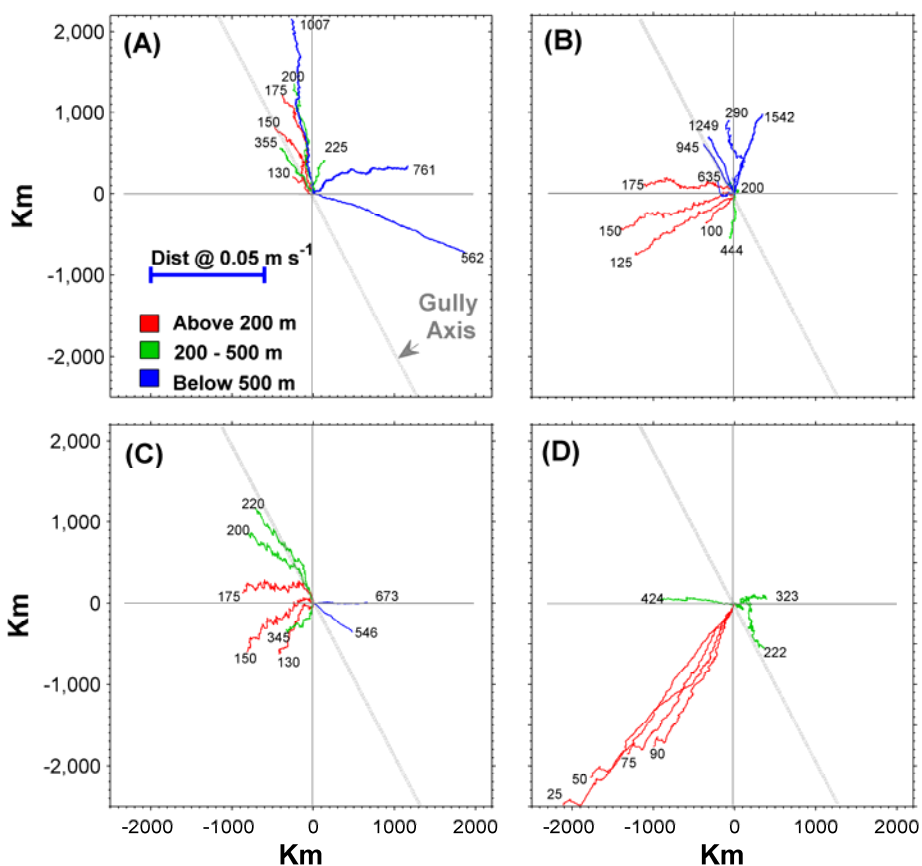


Figure 15: Progressive vector diagrams for (A) SG2, (B) SG11, (C) SG12 and (D) SG10 moorings. The approximate direction of the Sable Gully axis is shown as a light gray line. The scale in (A) shows the distance travelled over the entire observation period for an average speed of 0.05 m s⁻¹. Lines are color-coded based on instrument depth: red (<200 m, shallower than the canyon rim), green (mid-depth) and blue (deep). The number at the end of each line denotes the nominal instrument depth.

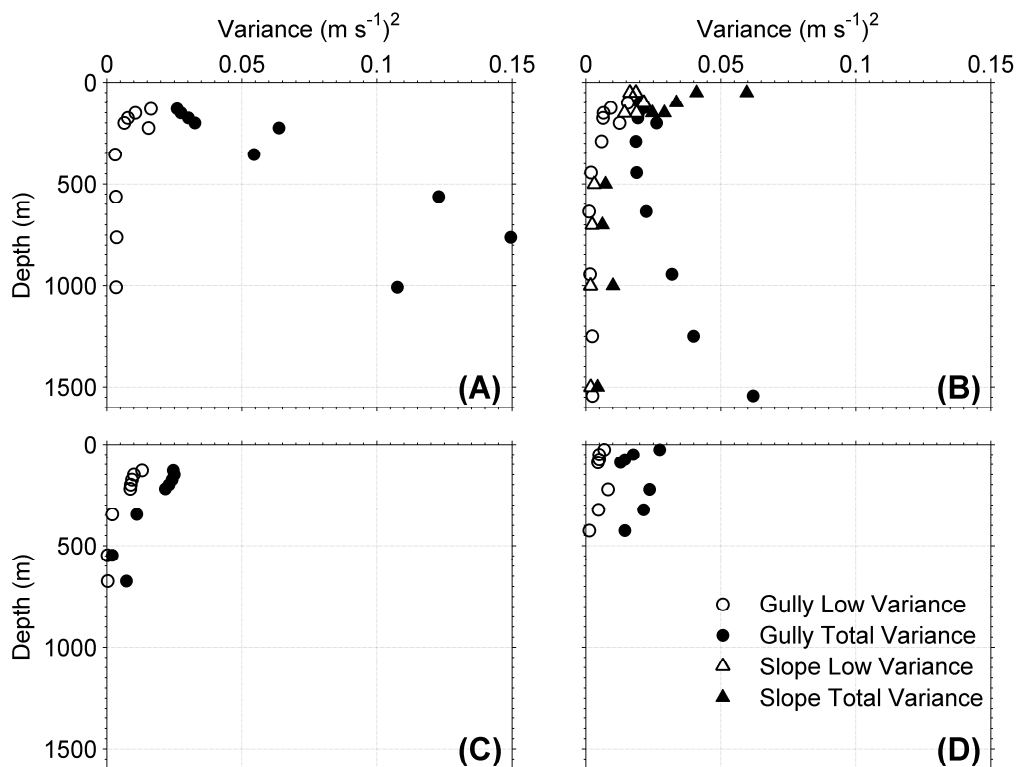


Figure 16: Variances derived from instruments at mooring sites (A) SG2, (B) SG11, (C) SG12 and (D) SG10. Variances from Scotian Slope moorings at comparable bottom depths are shown for comparison. Variance is presented as low frequency (subtidal) and total components.

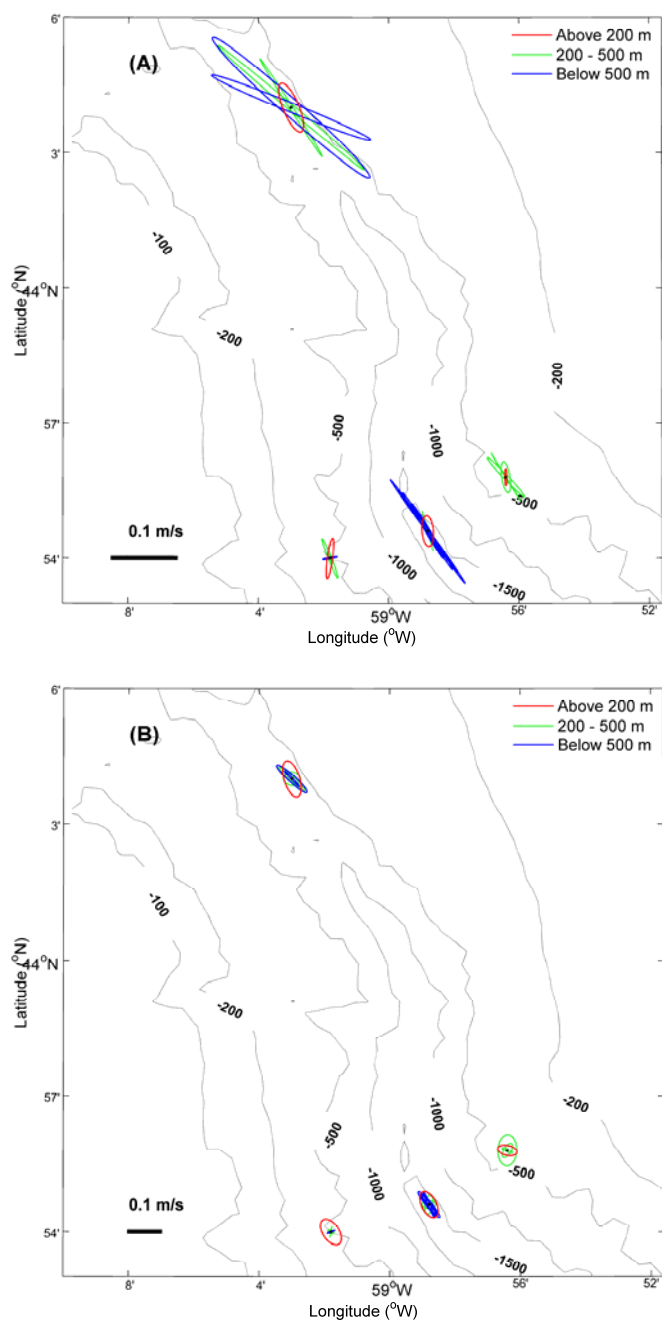


Figure 17: Tidal ellipses for the (A) K1 and (B) M2 tidal constituents. The ellipses have been plotted such that tidal excursions correspond to map geometry. Record depths are colour-coded.

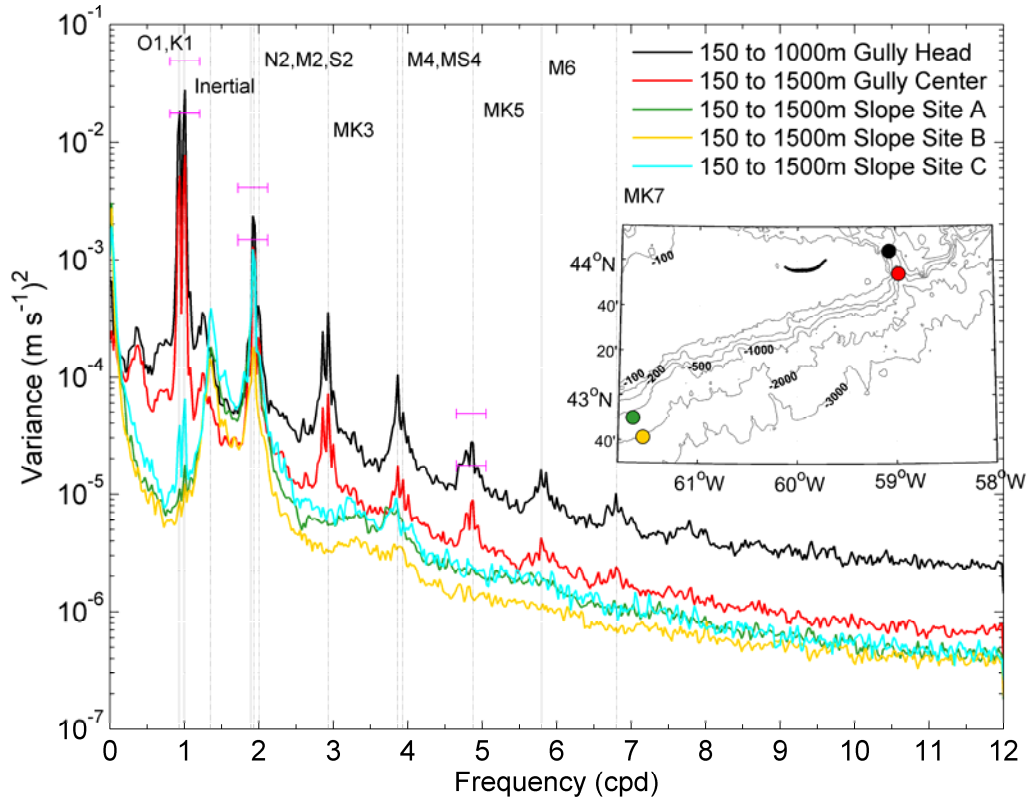


Figure 18: Spectra of depth-averaged currents for two locations within the Sable Gully (black, red dots) and three locations on the Scotian Slope. Site C, not shown on the inset, is located at approximately 42.67°N, 63.5°W. Observations from sites A and B are from 2000-04 (Loder and Geshelin, 2009); observations from Site C are from 1975-78 (Smith and Petrie, 1982). Vertical grey lines correspond to tidal and inertial frequencies. Ninety-five percent confidence levels are shown for the Gully Head record at diurnal, semi-diurnal and 5 cpd frequencies.

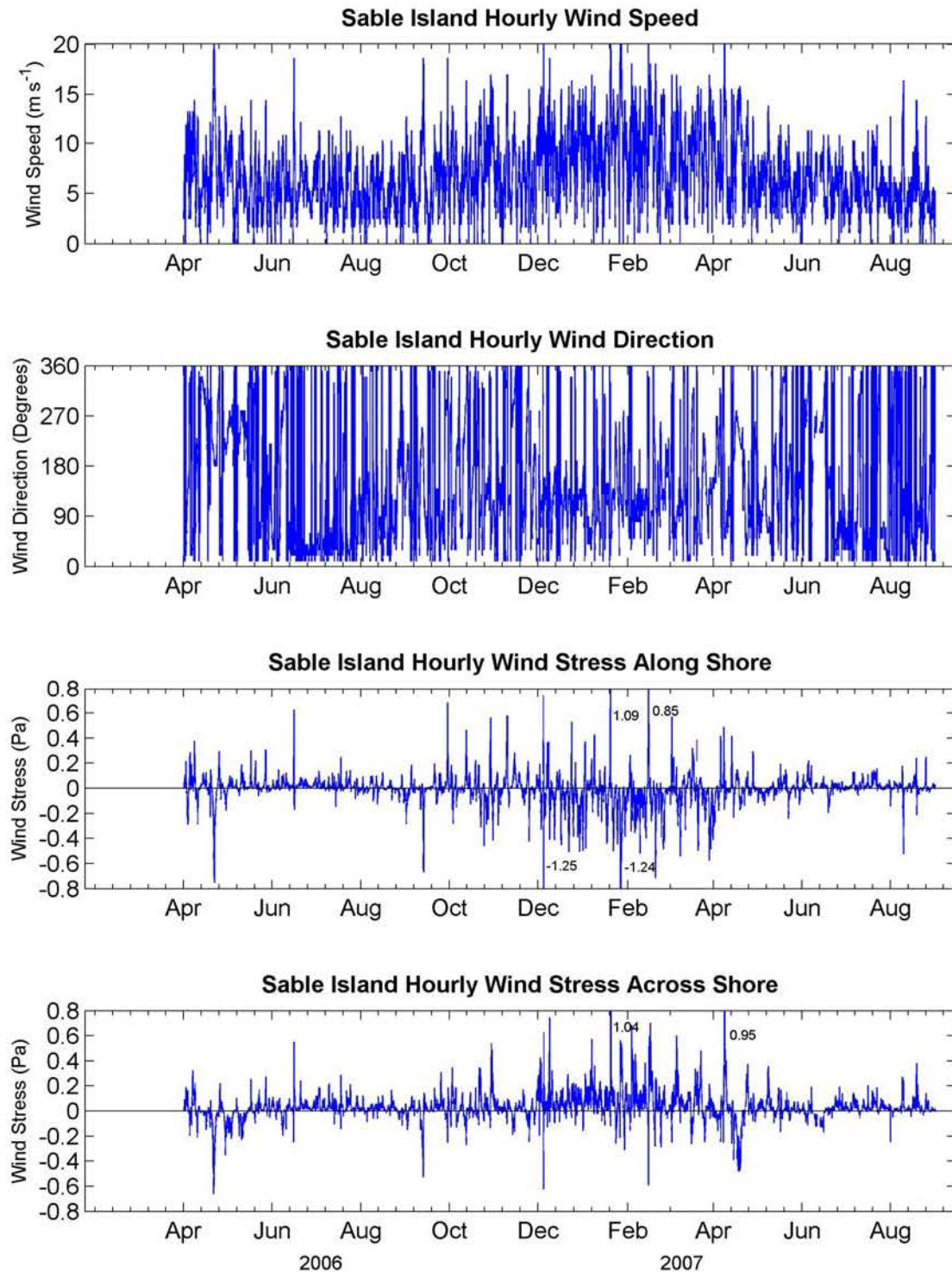


Figure 19: Sable Island hourly wind speed (m s^{-1}), direction ($^{\circ}\text{T}$), along-shore wind stress (Pa) and across-shore wind stress (Pa). The numbers on the wind stress panels indicate the value for those points that extend beyond the limits of the y-axis.

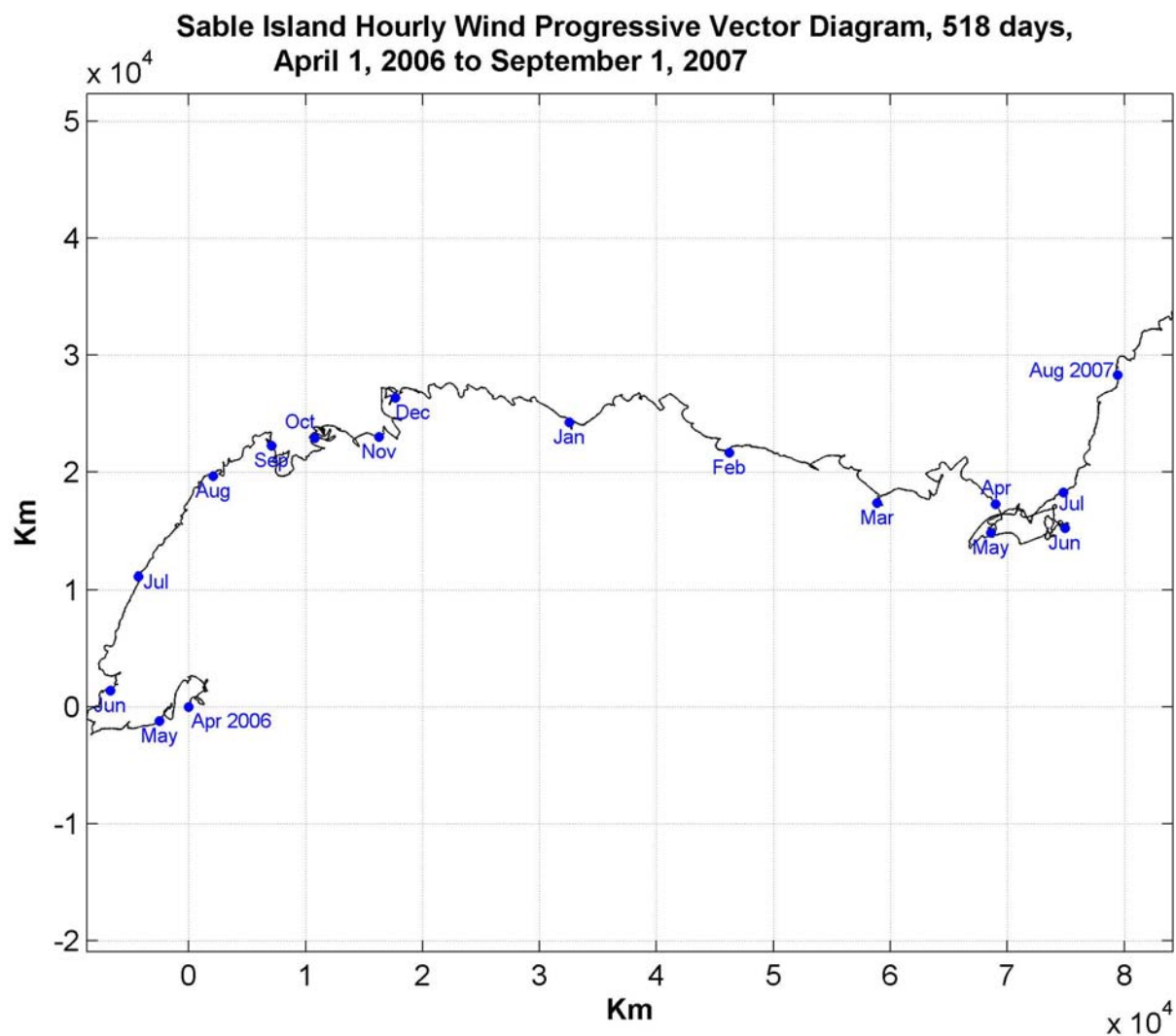


Figure 20: Progressive vector diagram for Sable Island hourly wind from April 2006 to September 1, 2007.

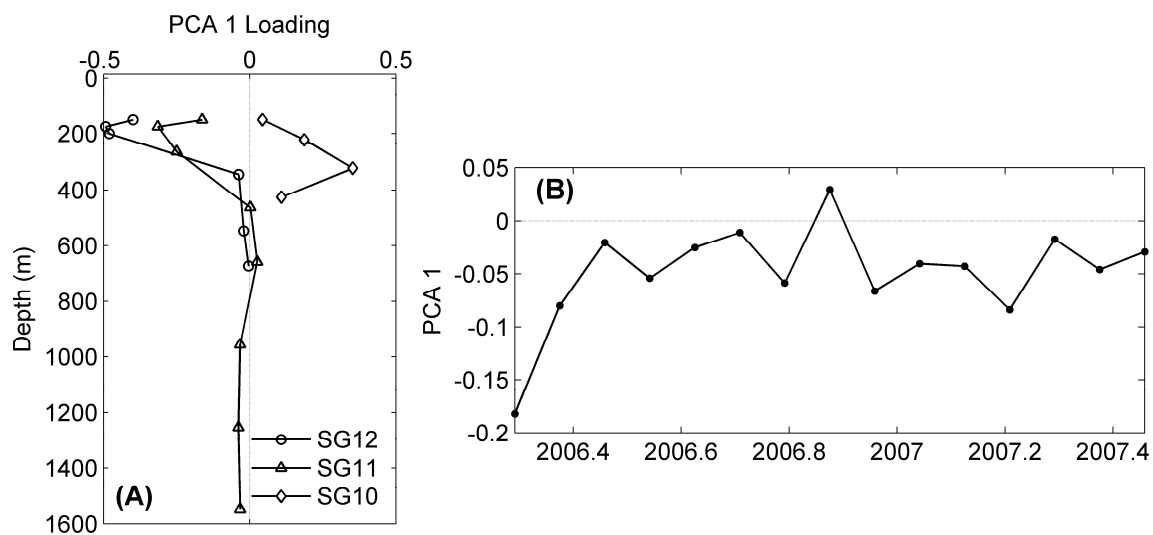


Figure 21: (A) Loadings for the first mode of a principal component analysis (PCA) based on the covariance matrix of the along-Gully monthly currents for depths = 150 m, moorings SG10-12. (B) Time series of PCA1 for the period of the mooring deployment.

Appendix 1: Mooring Diagrams

Four moorings were deployed at the sites SG2, SG10, SG11, SG12 in Zone 1 of the Gully (Figure 1). These moorings consisted of RDI ADCPs, Aandarra RCM8 current meters, Sea-Bird Microcat sensors and Vemco Minilog temperature recorders. These figures were created by Mr. Rick Boyce using TurboCAD.

Mooring Locations

Mooring	Latitude	Longitude	Bottom Depth (m)
SG2 (1588)	44.0424	59.0381	1054
SG10 (1591)	43.9281	58.9408	476
SG11 (1589)	43.9127	58.9846	1640
SG12 (1590)	43.9033	59.0205	800

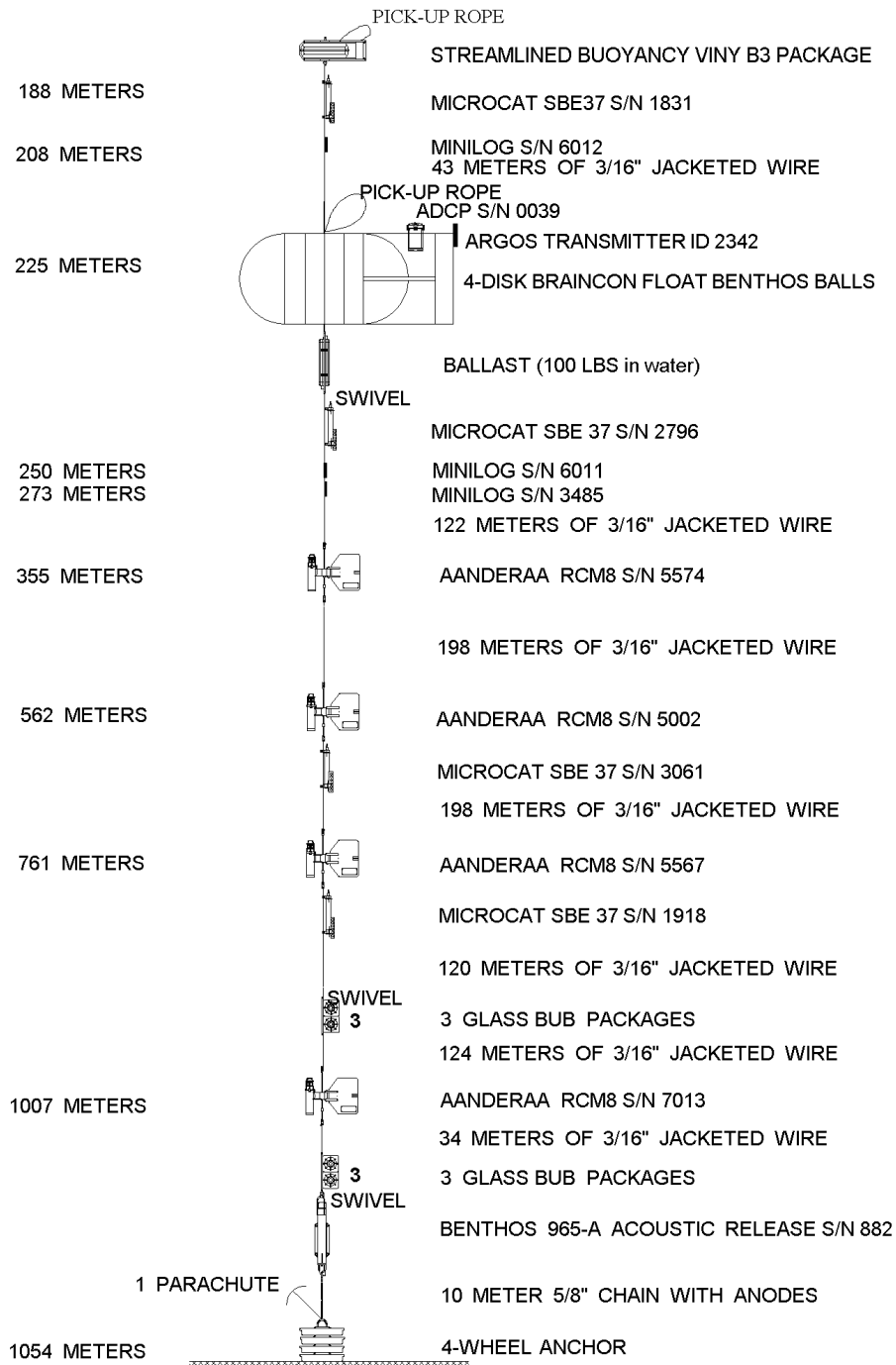
MOORING # 1588 SG2 B. GREENAN UPPER GULLY APRIL 2006

Figure A- 1: Schematic of mooring 1588 deployed at SG2 site.

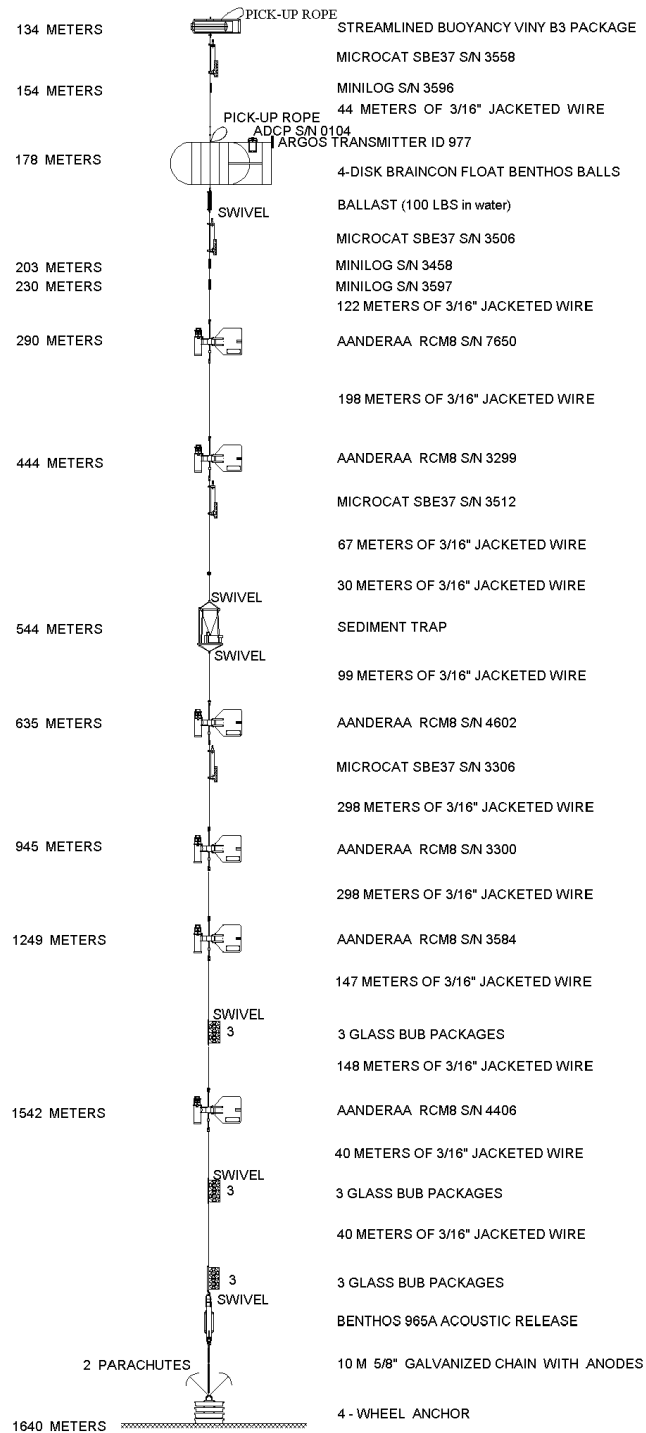
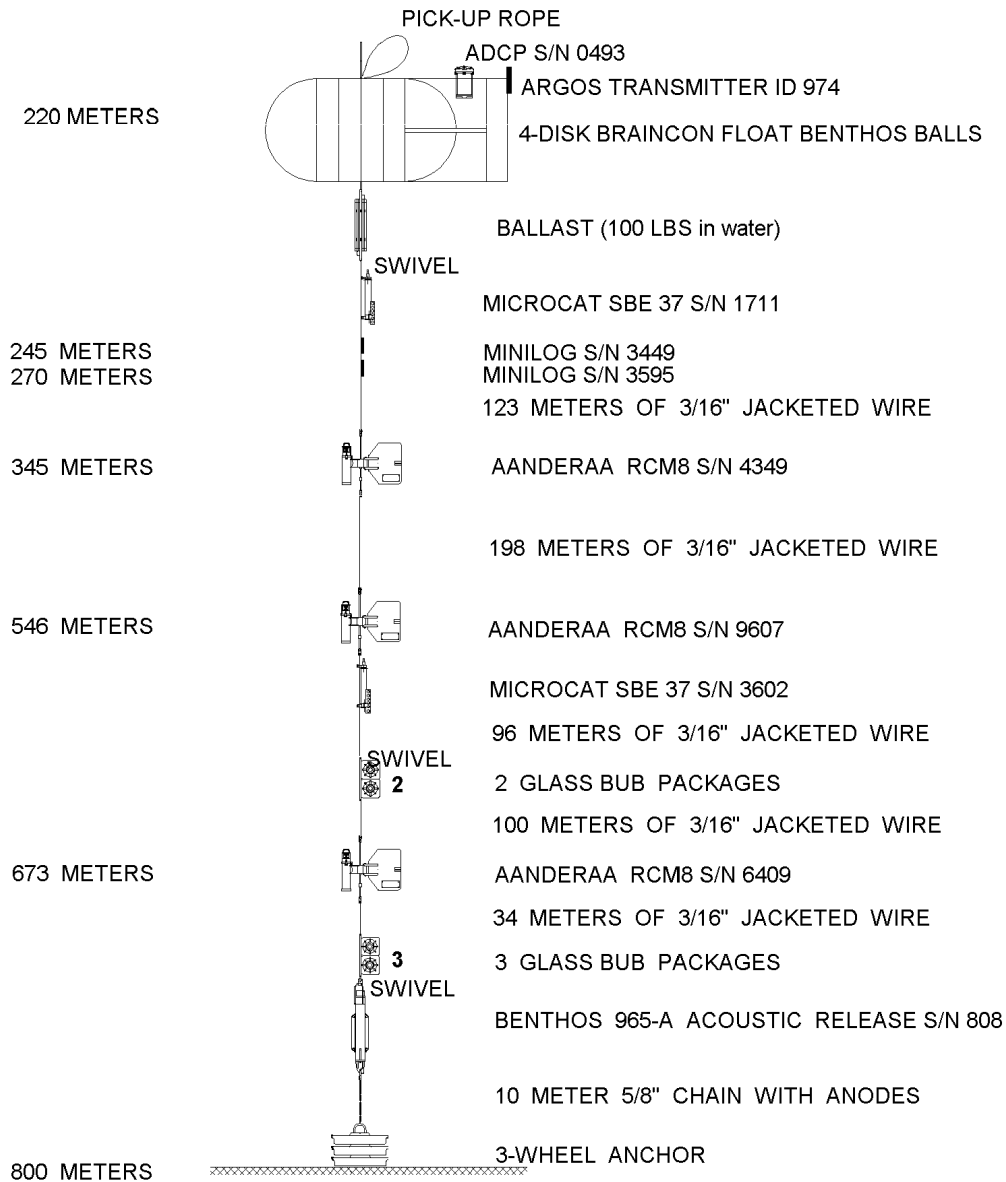
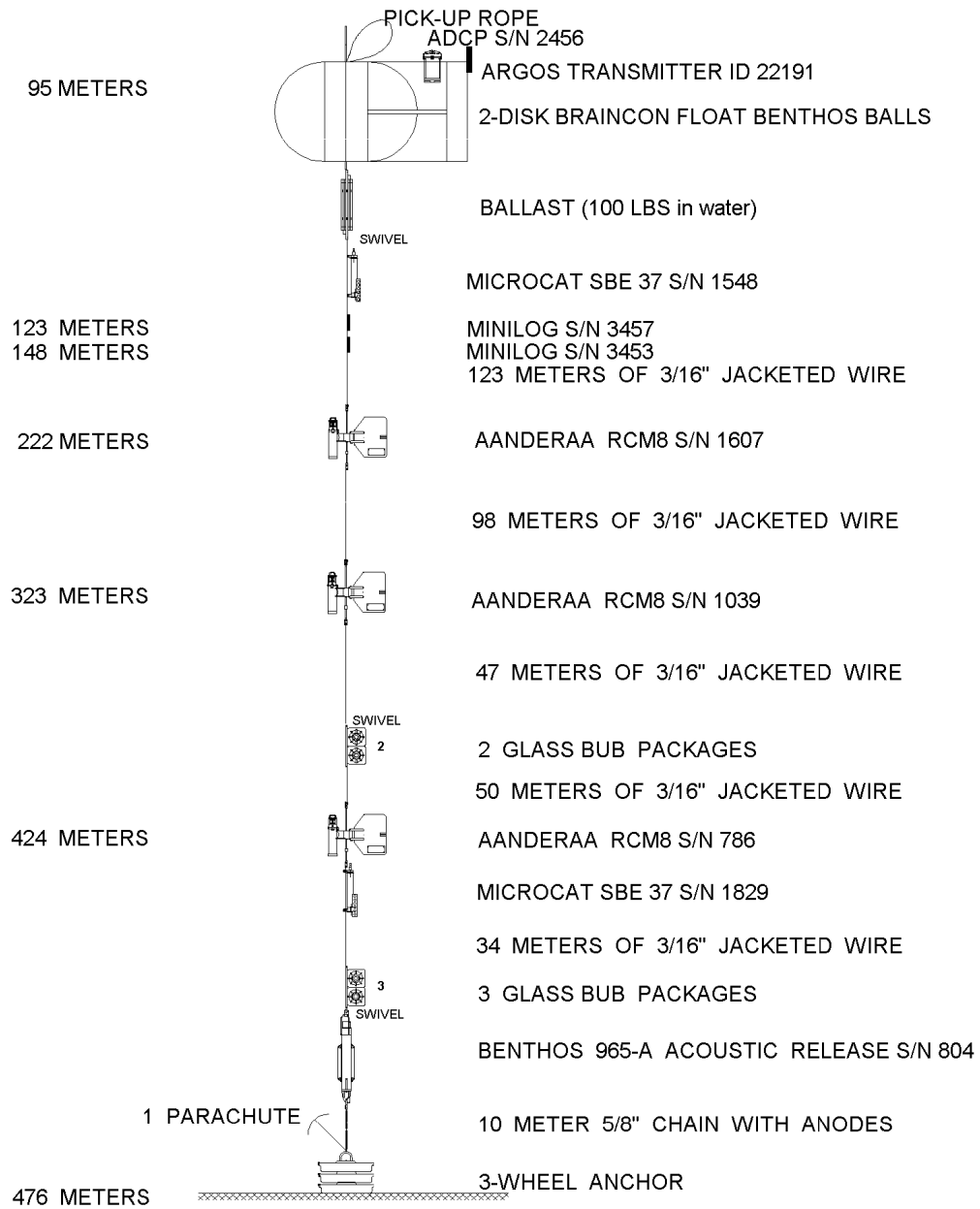
MOORING # 1589 GREENAN GULLY DEEP CENTRAL APRIL 2006

Figure A- 2: Schematic of mooring 1589 deployed at SG11 site.

MOORING # 1590 SG12 B. GREENAN WEST WALL APRIL 2006**Figure A- 3: Schematic of mooring 1590 deployed at SG12 site.**

MOORING # 1591 SG10 B. GREENAN EAST WALL APRIL 2006**Figure A- 4: Schematic of mooring 1591 deployed at SG10 site.**

Appendix 2: CTD and Lowered-Acoustic Doppler Current Profiler

CTD surveys were completed with Sea-Bird 911 CTD and 24-bottle rosette. These were conducted on two separate cruises HUD2006-008 from April 20-26, 2006 at sites SG1 through SG21 and HUD2007-033 from August 2-8, 2007 at sites SG1 through SG29 (Figure 1). The CTD had dual temperature, conductivity and pressure sensors as well as oxygen and fluorescence sensors. The following plots are for both the HUD2007-033 and HUD2006-008 cruises. These profiles show the temperature (black line), salinity (red line) and density (blue line) from the first sensor however the data were compared with that from the second sensor and no differences were found except for the near surface data at SG26. Percent saturation of dissolved oxygen (blue line) and fluorescence (black line) were also plotted.

A map is included for each section where the red dots show all the CTD sites and the yellow dots are the section CTD sites depicted in the plots on that given page.

The depth is kept consistent for each group of section profile plots, however there are 6 deep water sites, SG11, SG17, SG18, SG24-SG26, that exceed 1200 m; these are potted together in Figure A- 17, Figure A- 18, Figure A- 27 and Figure A- 28.

Lowered ADCP profiles are shown in Figure A- 29.

All plots were created using MATLAB R2008b.

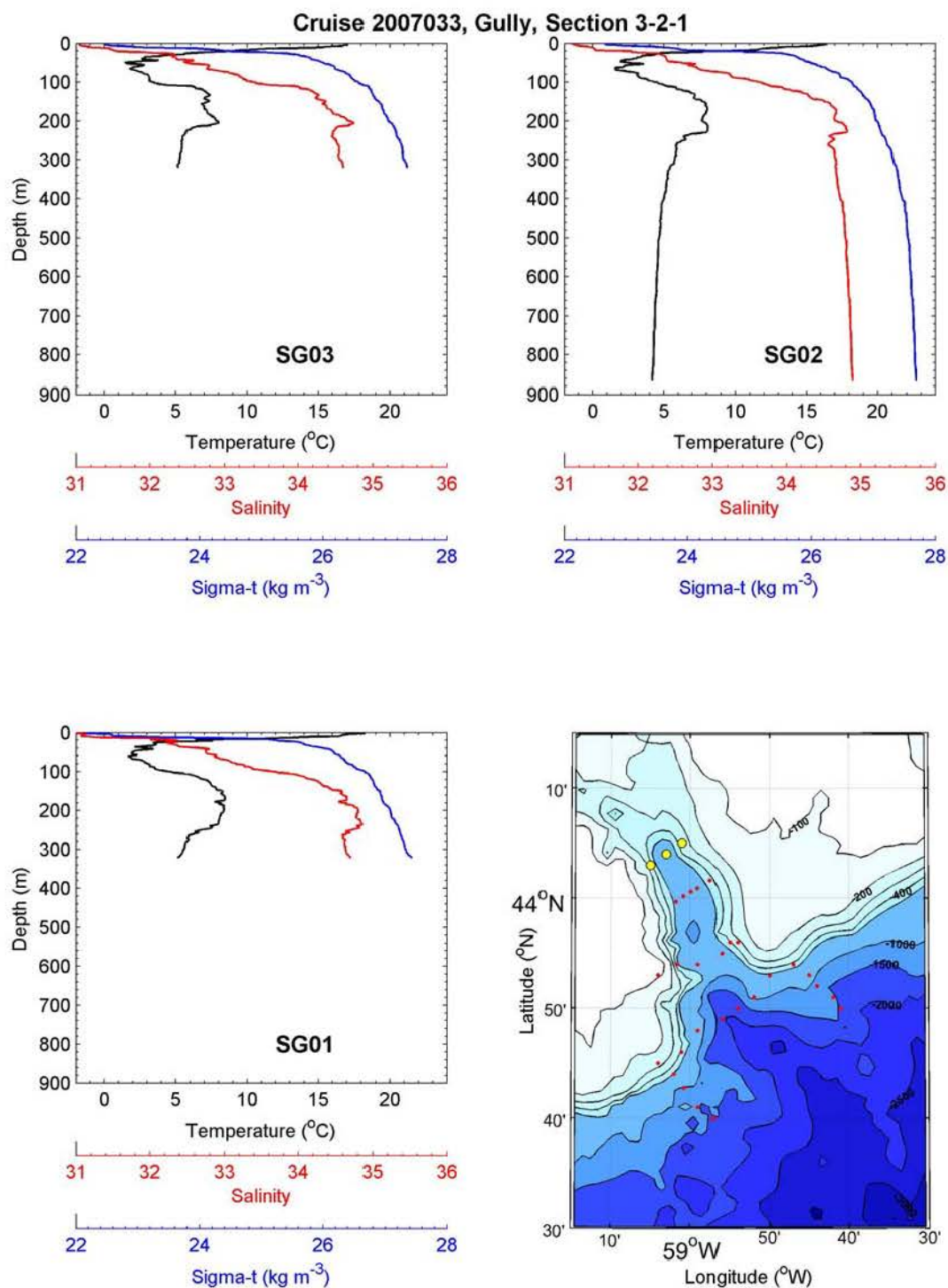


Figure A- 5: Profiles of temperature, salinity and density for the stations highlighted in yellow in the lower right-hand panel. Refer to Figure 1 for numbering of the CTD stations.

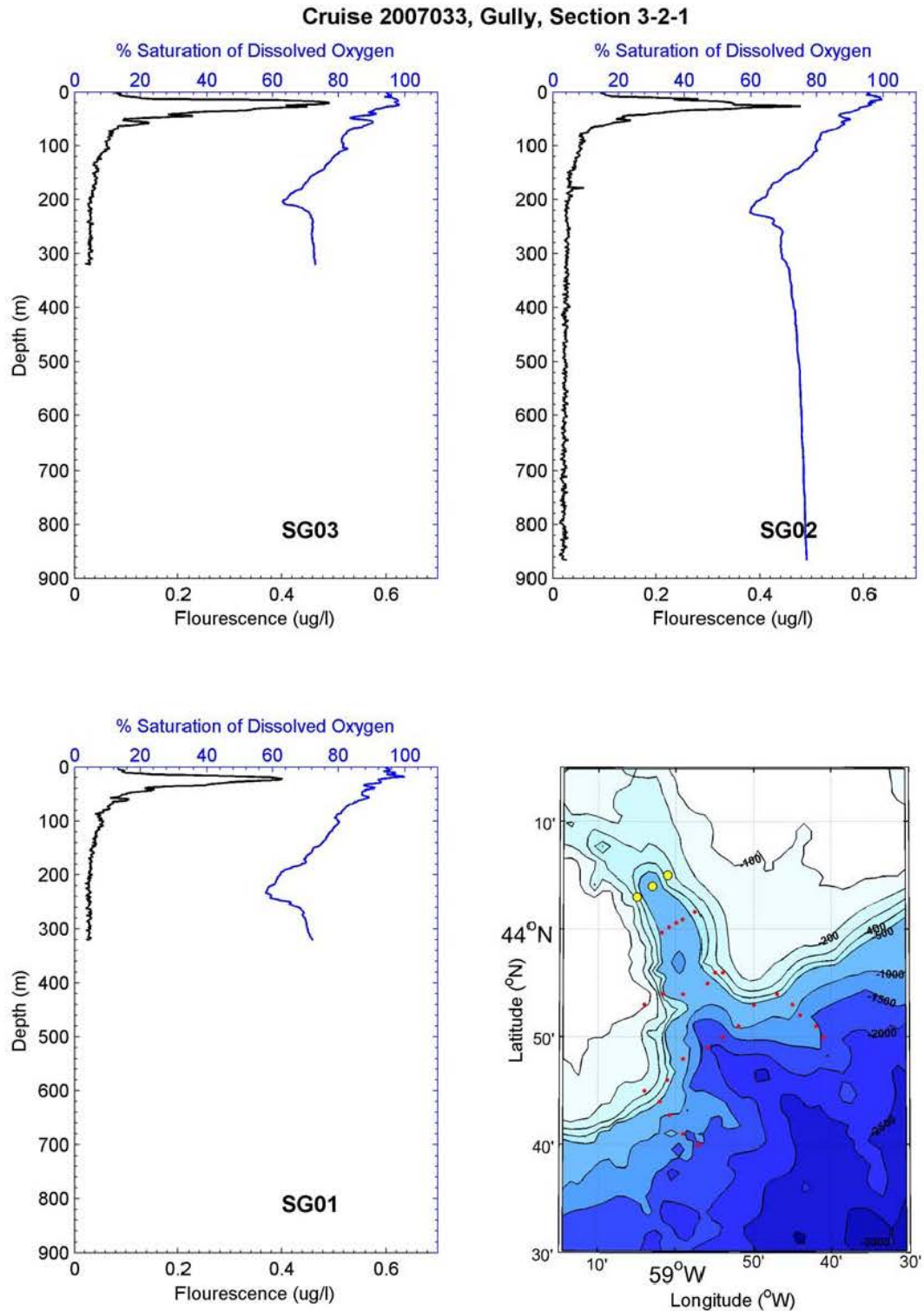


Figure A- 6: Profiles of dissolved oxygen from the CTD SBE43 sensor for the stations highlighted in yellow in the lower right-hand panel. Refer to Figure 1 for numbering of the CTD stations.

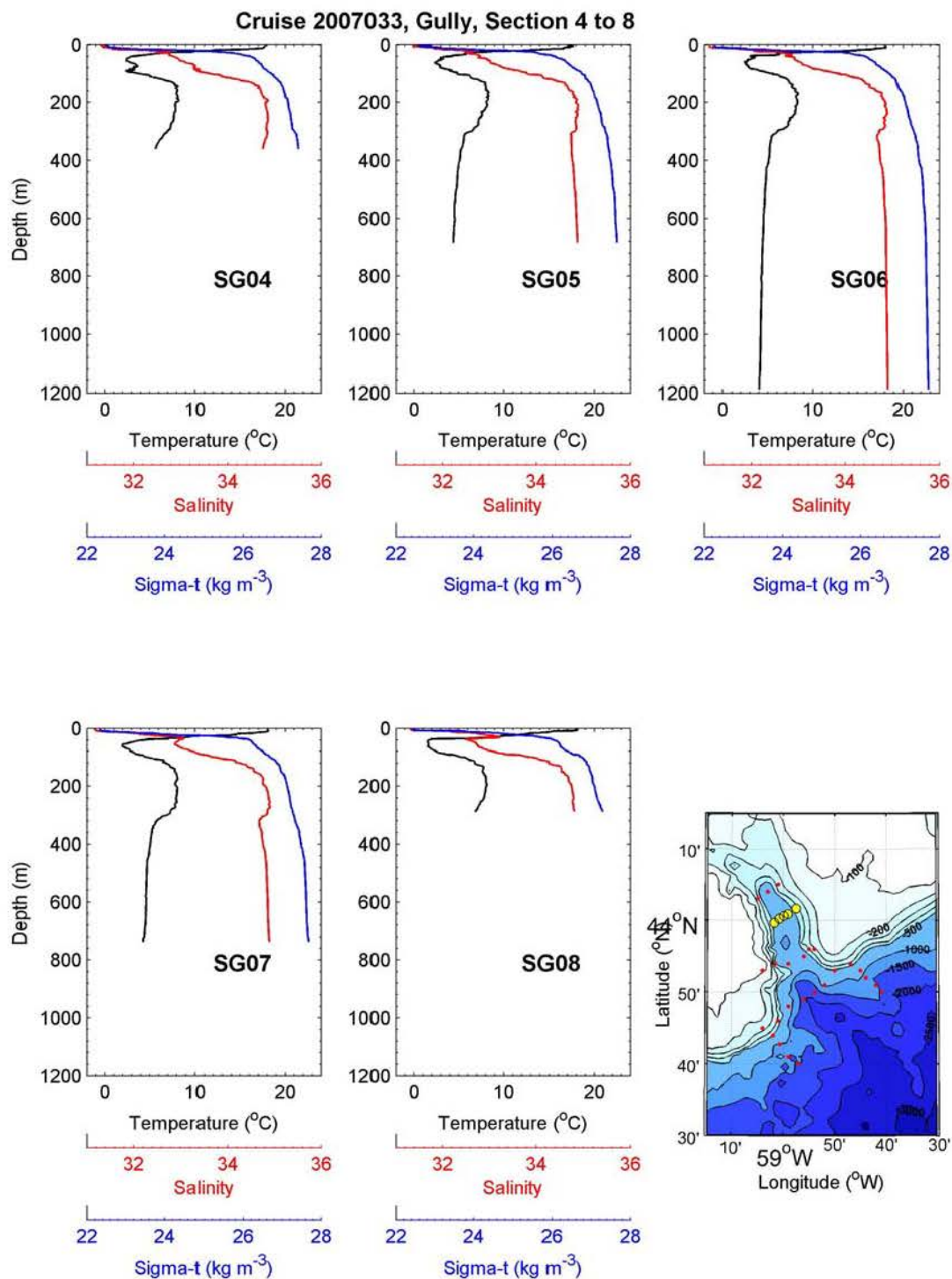


Figure A- 7: Profiles of temperature, salinity and density for the stations highlighted in yellow in the lower right-hand panel. Refer to Figure 1 for numbering of the CTD stations.

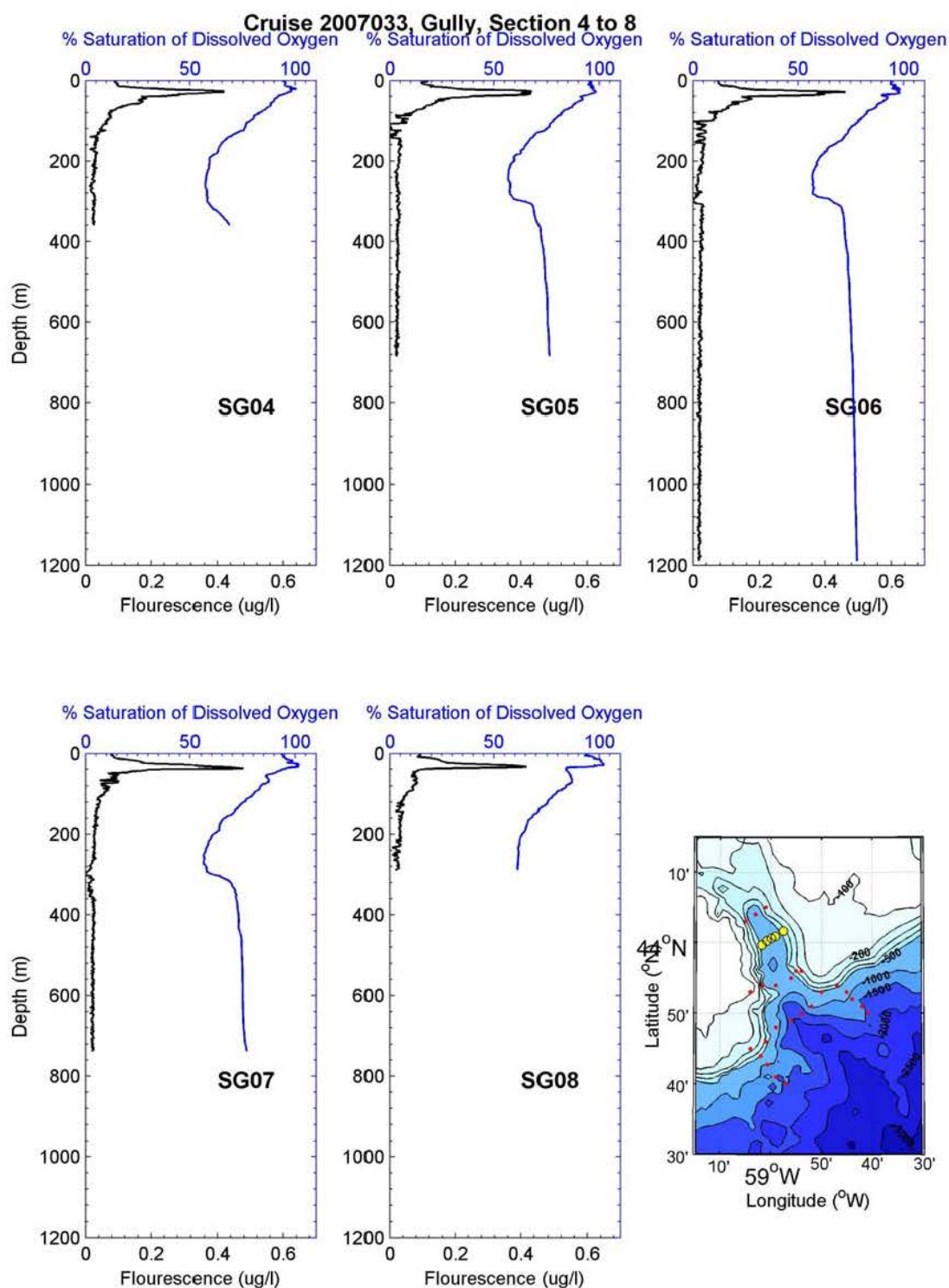


Figure A- 8: Profiles of dissolved oxygen from the CTD SBE43 sensor for the stations highlighted in yellow in the lower right-hand panel. Refer to Figure 1 for numbering of the CTD stations.

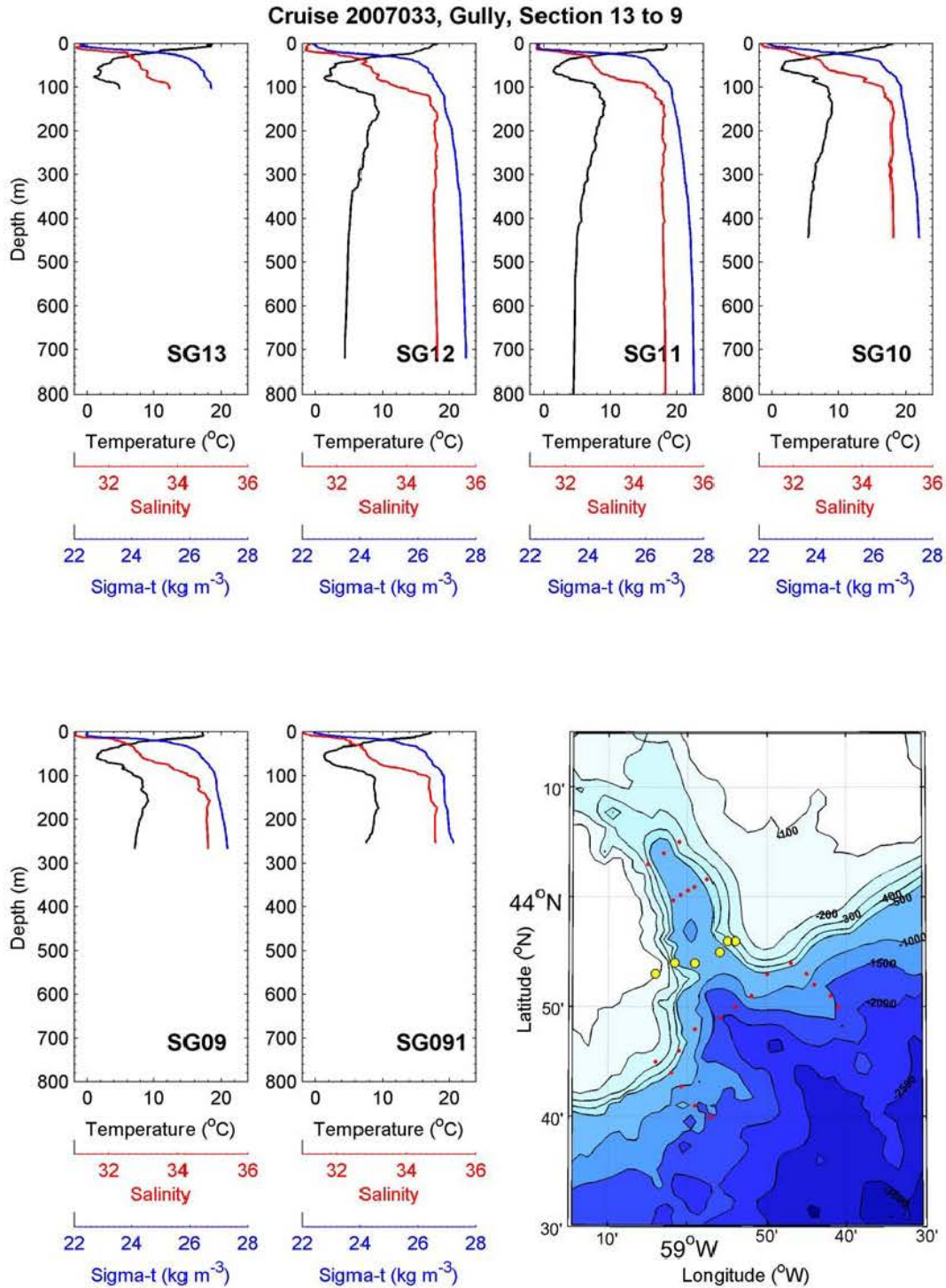


Figure A- 9: Profiles of temperature, salinity and density for the stations highlighted in yellow in the lower right-hand panel. Refer to Figure 1 for numbering of the CTD stations.

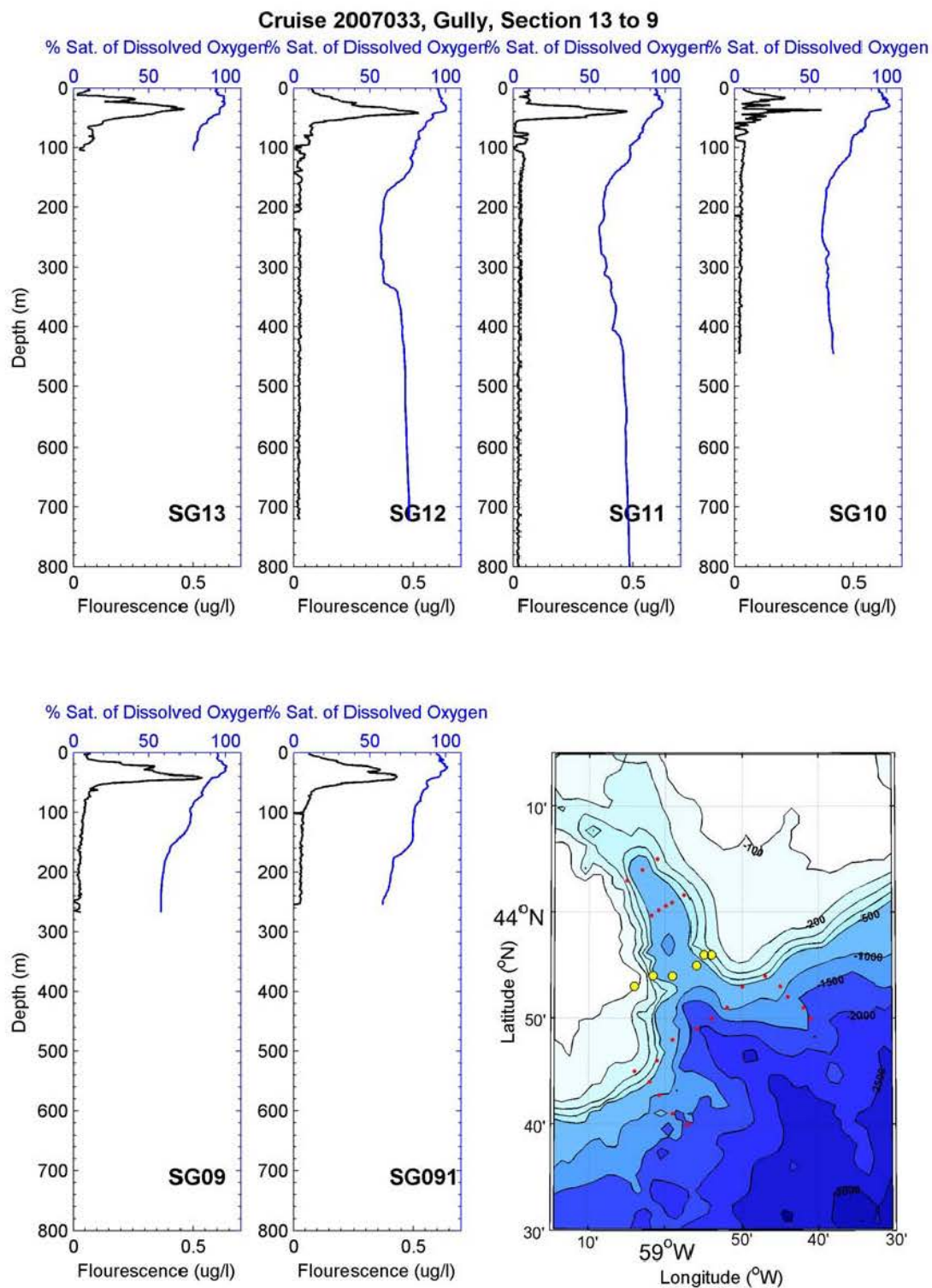


Figure A- 10: Profiles of dissolved oxygen from the CTD SBE43 sensor for the stations highlighted in yellow in the lower right-hand panel. Refer to Figure 1 for numbering of the CTD stations.

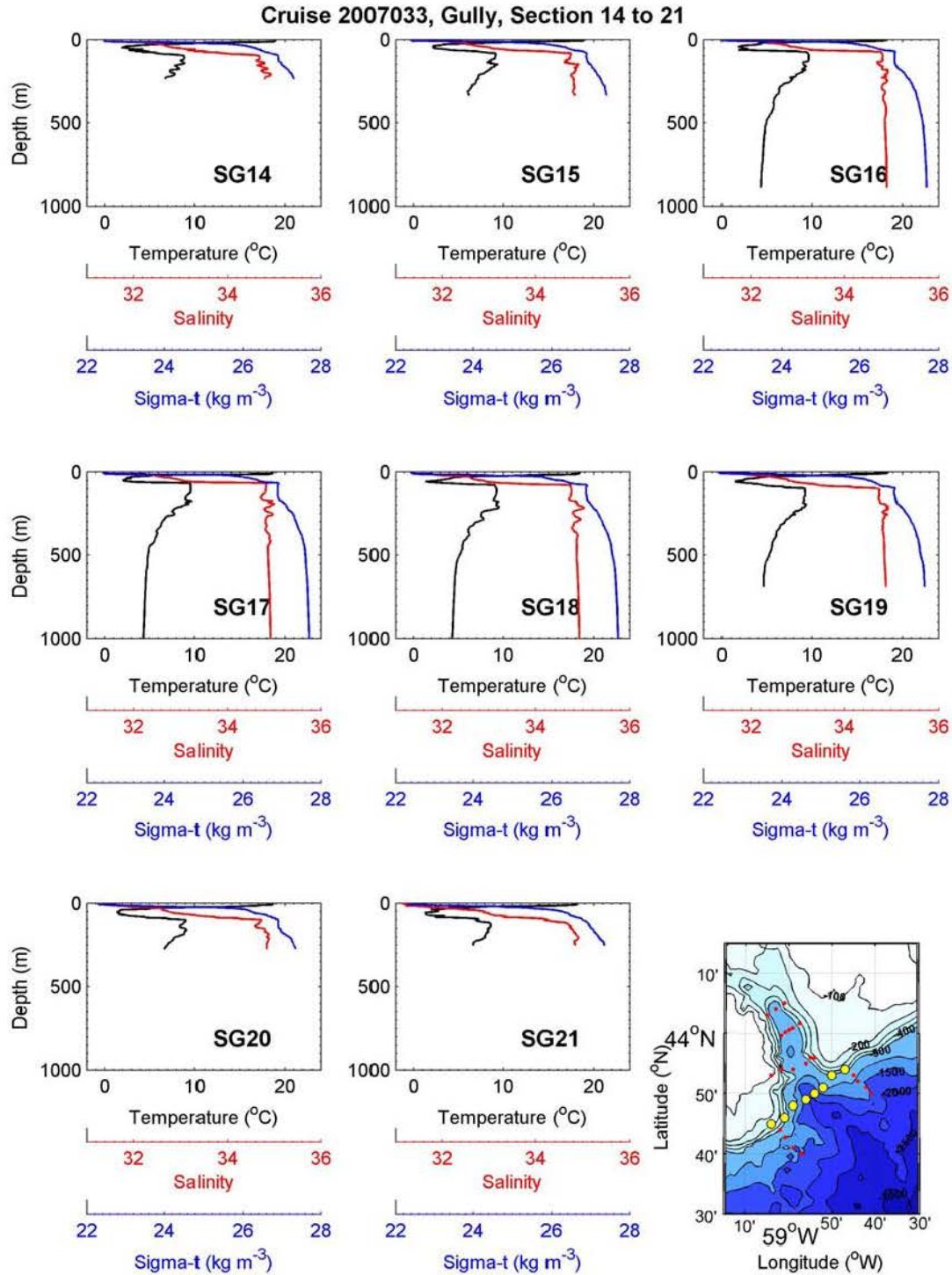


Figure A- 11: Profiles of temperature, salinity and density for the stations highlighted in yellow in the lower right-hand panel. Refer to Figure 1 for numbering of the CTD stations.

Cruise 2007033, Gully, Section 14 to 21

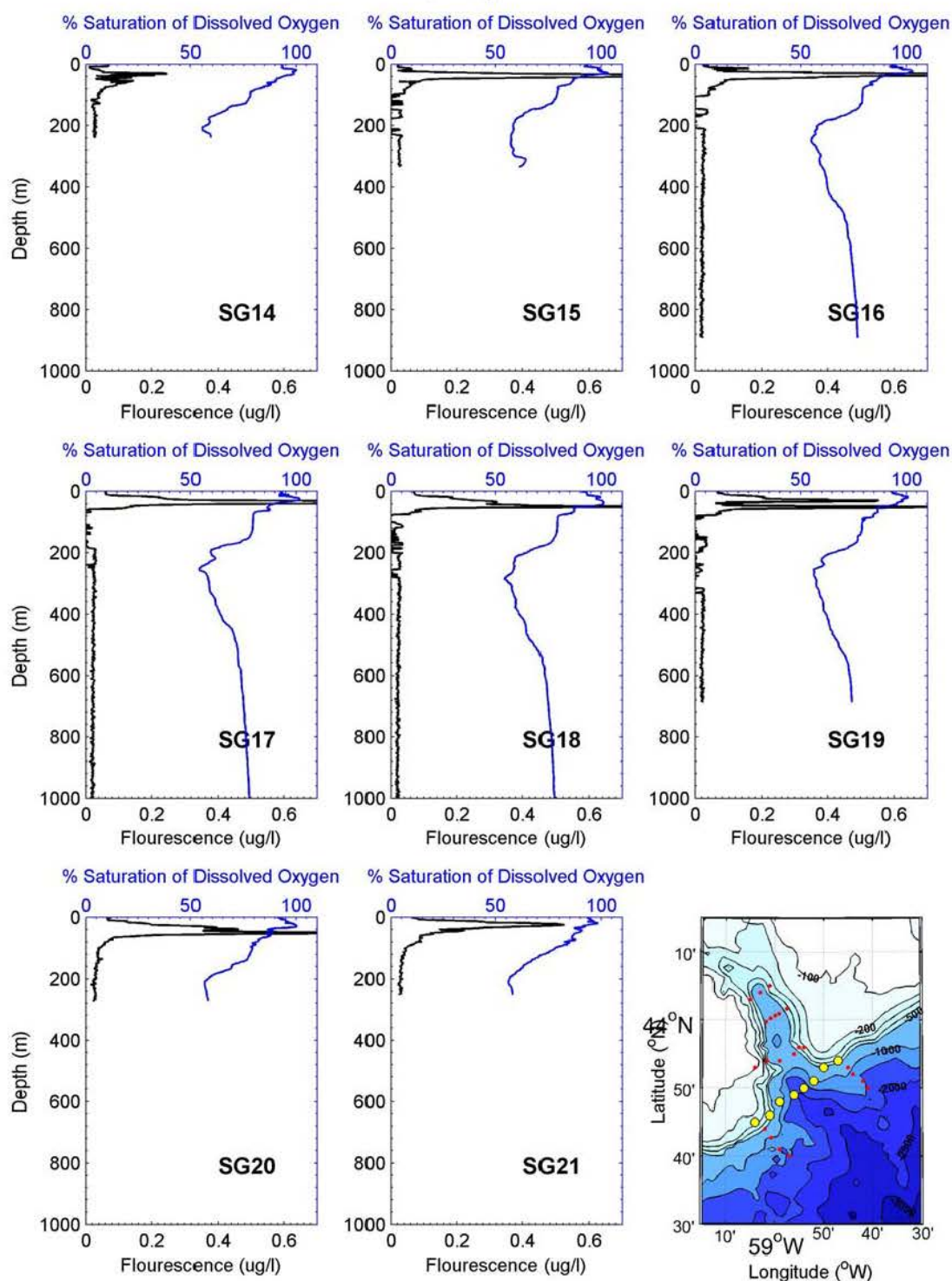


Figure A- 12: Profiles of dissolved oxygen from the CTD SBE43 sensor for the stations highlighted in yellow in the lower right-hand panel. Refer to Figure 1 for numbering of the CTD stations.

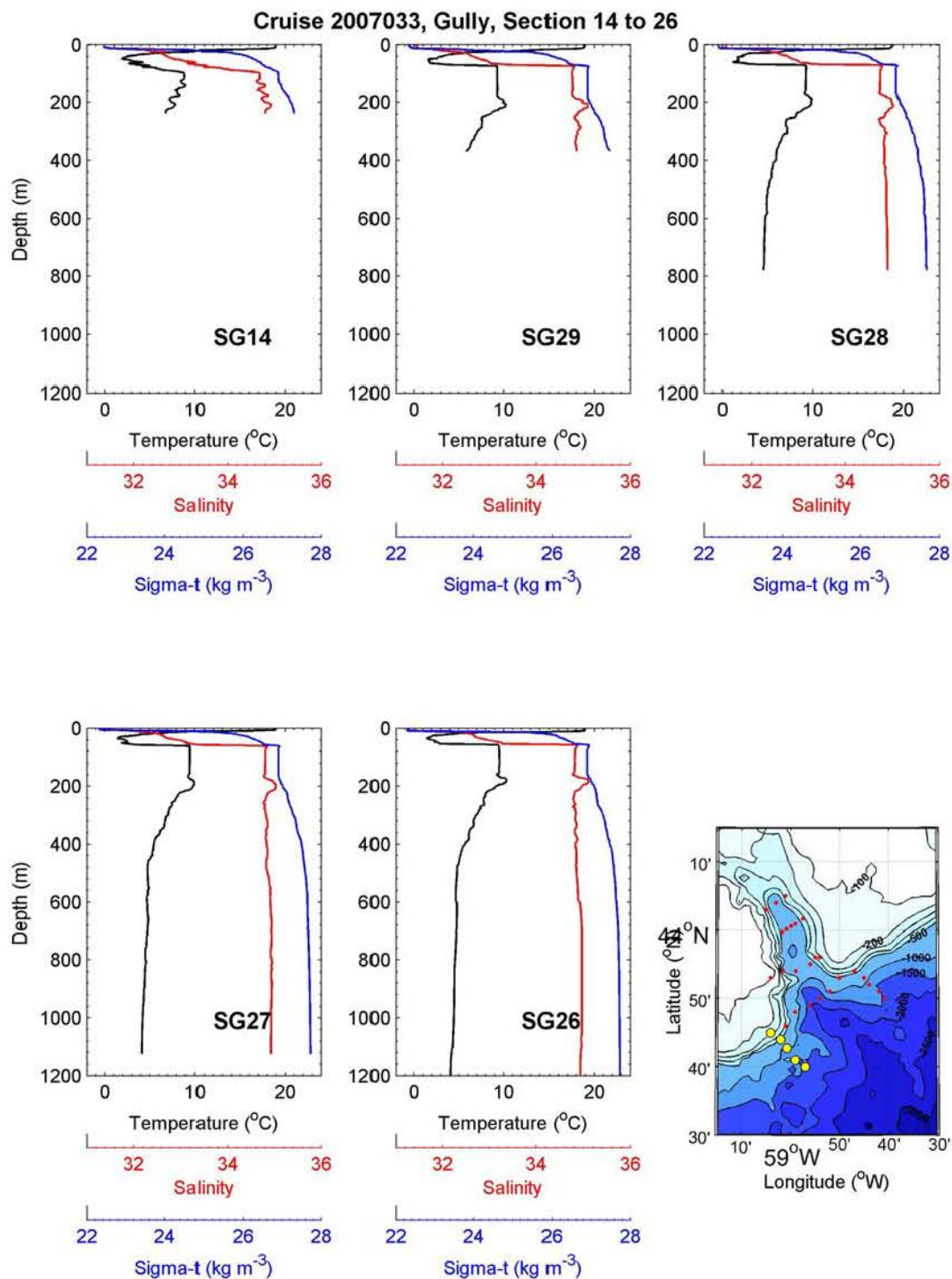


Figure A- 13: Profiles of temperature, salinity and density for the stations highlighted in yellow in the lower right-hand panel. Refer to Figure 1 for numbering of the CTD stations.

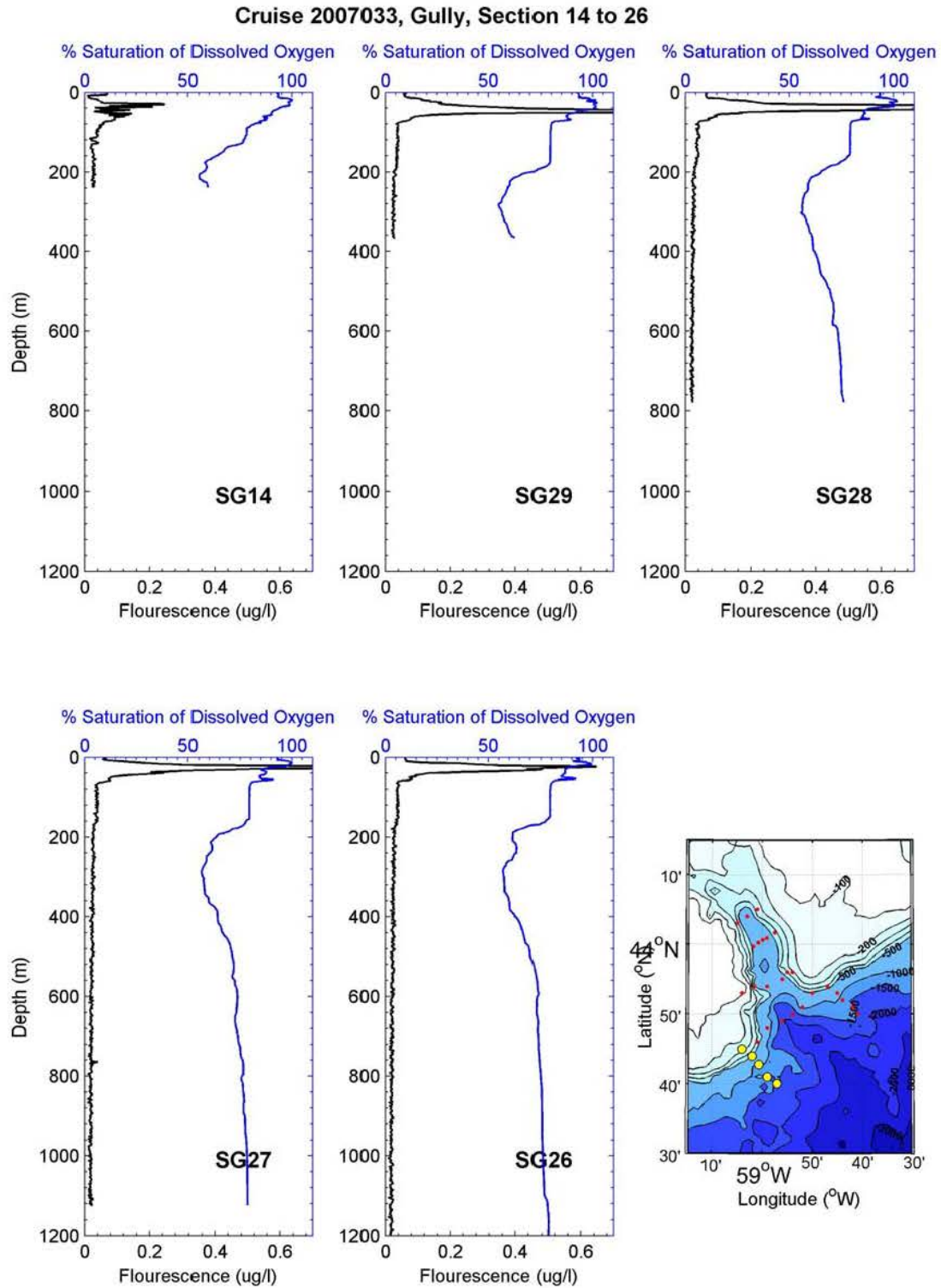


Figure A- 14: Profiles of dissolved oxygen from the CTD SBE43 sensor for the stations highlighted in yellow in the lower right-hand panel. Refer to Figure 1 for numbering of the CTD stations.

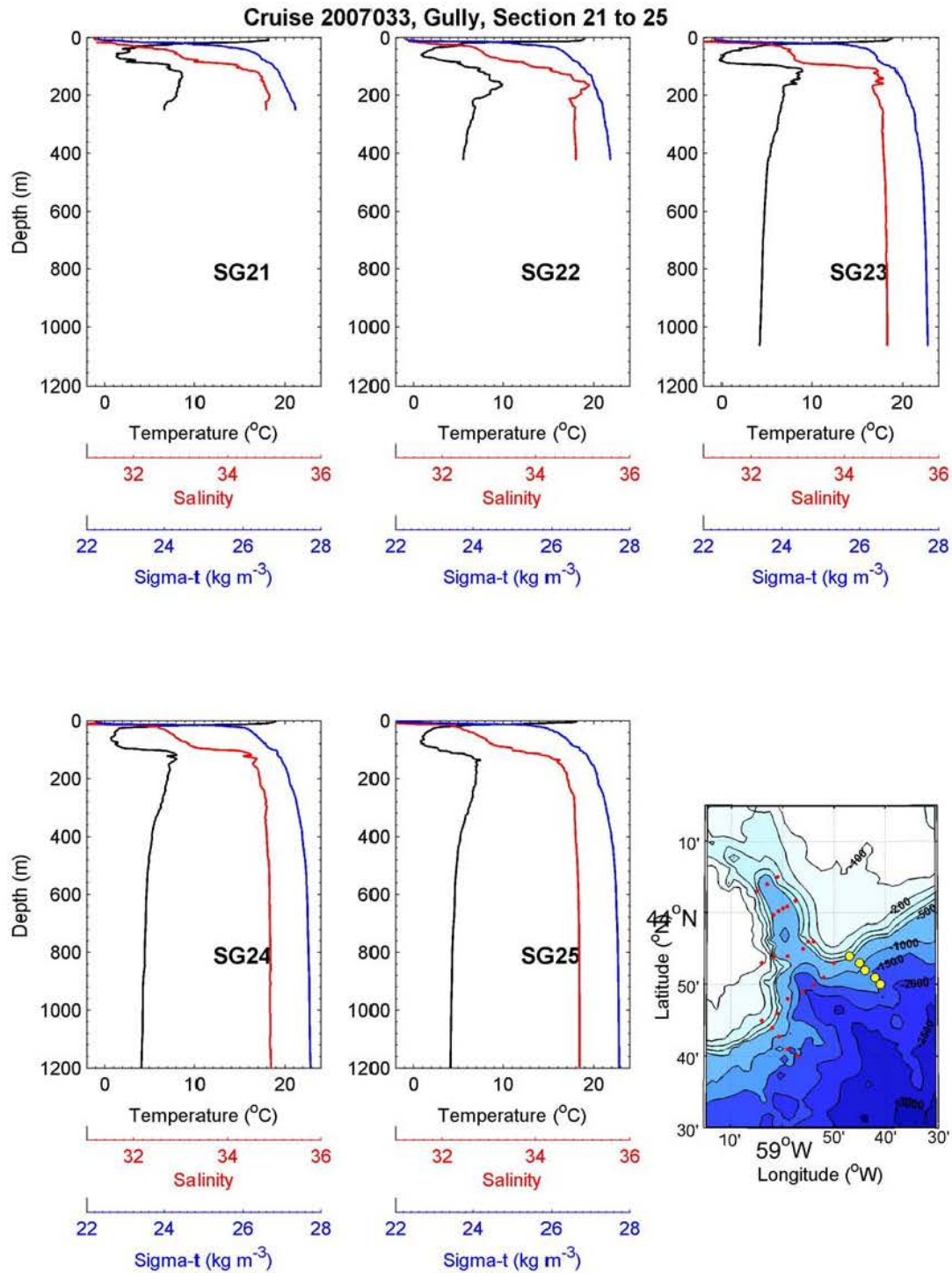


Figure A- 15: Profiles of temperature, salinity and density for the stations highlighted in yellow in the lower right-hand panel. Refer to Figure 1 for numbering of the CTD stations.

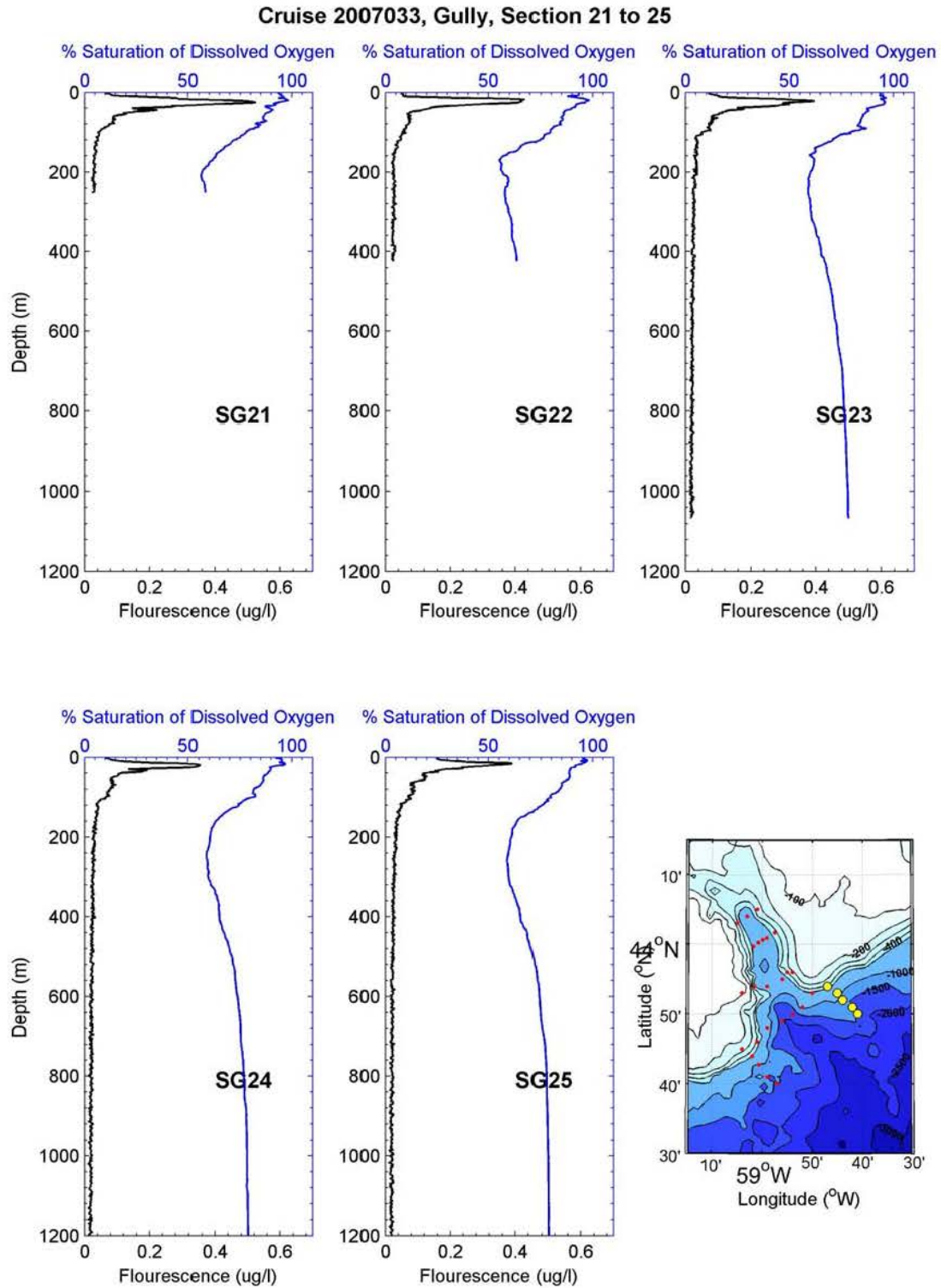


Figure A- 16: Profiles of dissolved oxygen from the CTD SBE43 sensor for the stations highlighted in yellow in the lower right-hand panel. Refer to Figure 1 for numbering of the CTD stations.

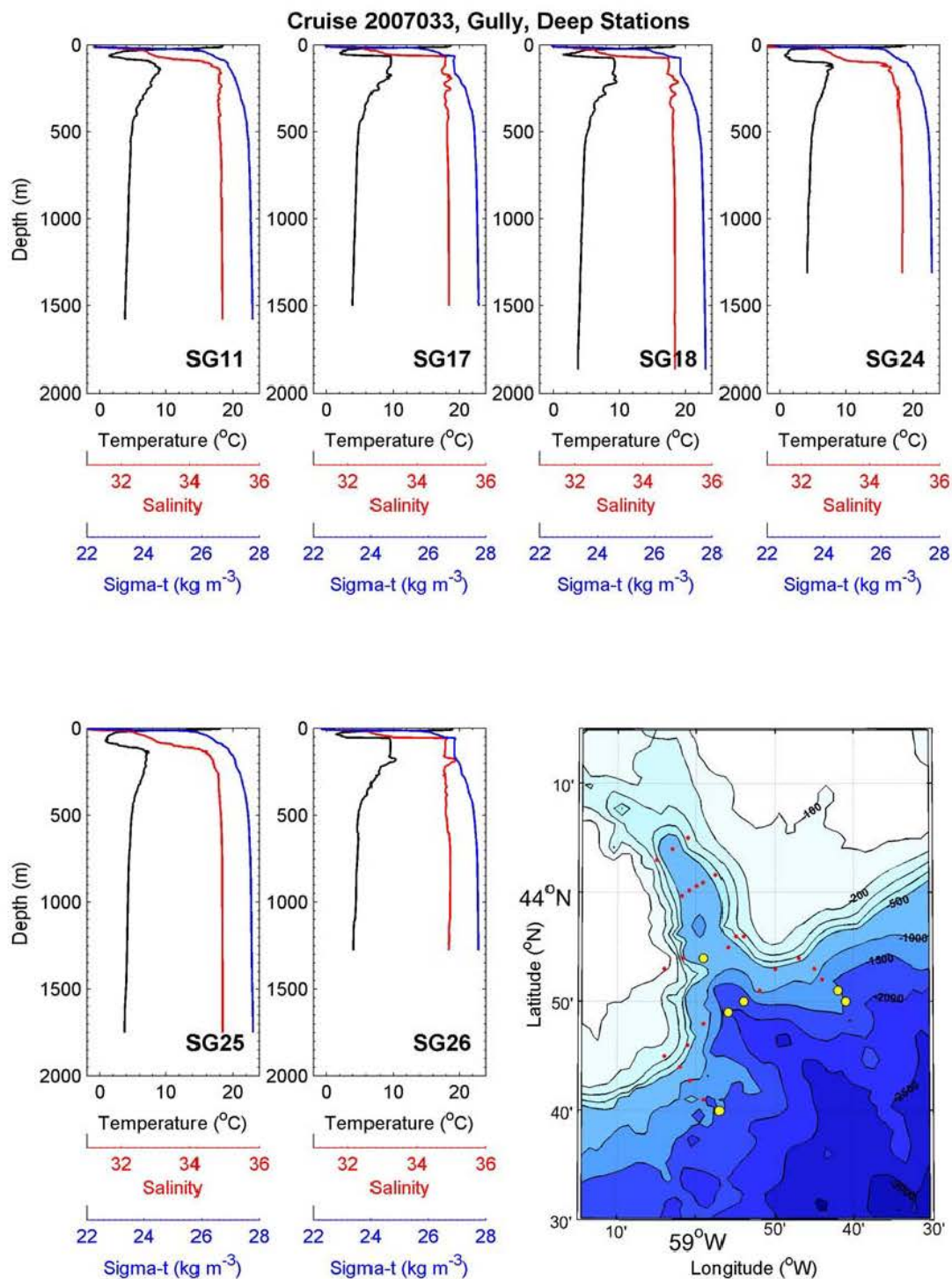


Figure A- 17: Profiles of temperature, salinity and density for the stations highlighted in yellow in the lower right-hand panel. Refer to Figure 1 for numbering of the CTD stations.

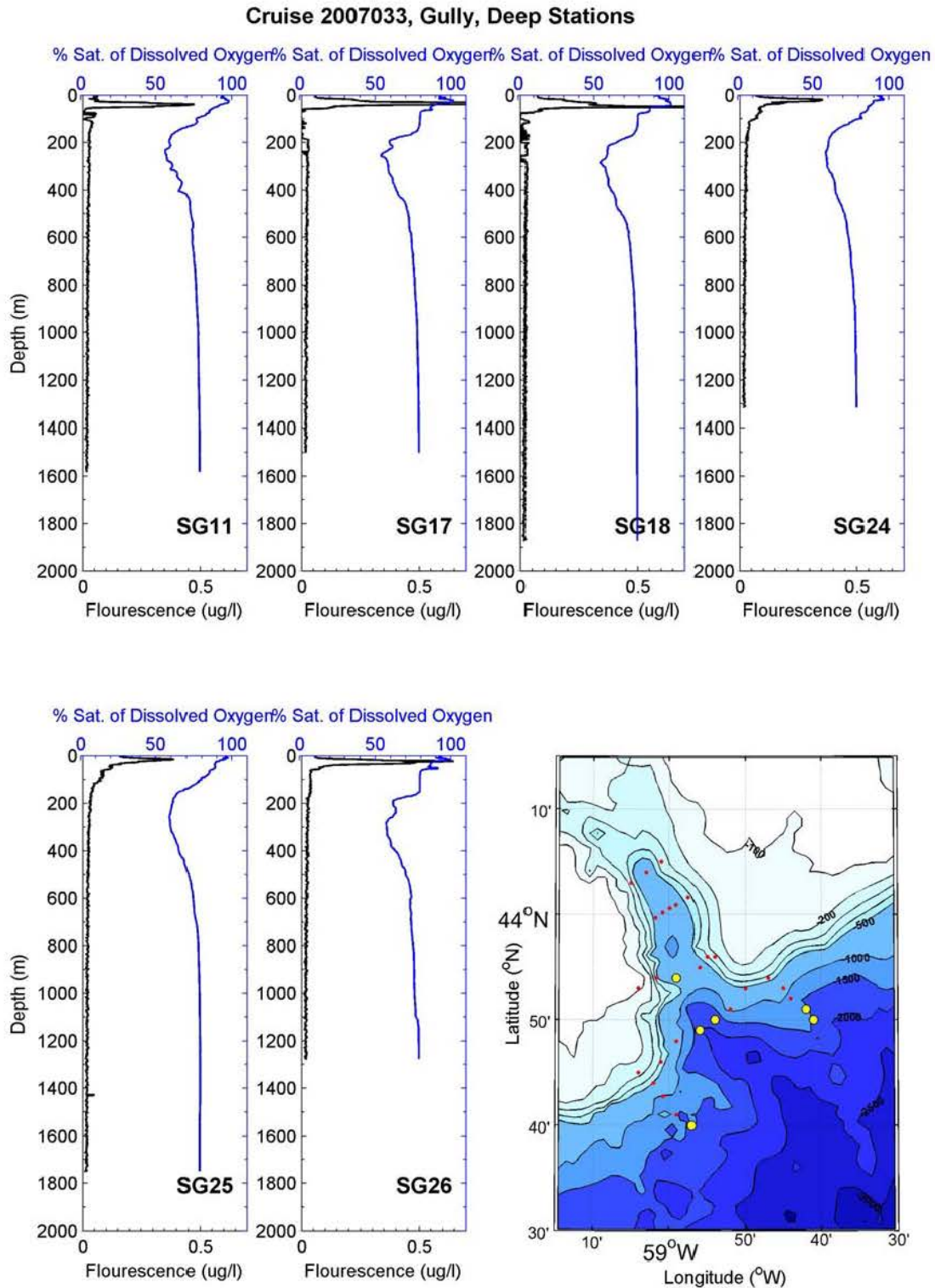


Figure A- 18: Profiles of dissolved oxygen from the CTD SBE43 sensor for the stations highlighted in yellow in the lower right-hand panel. Refer to Figure 1 for numbering of the CTD stations.

Cruise 2006008, Gully, Section 3-2-1

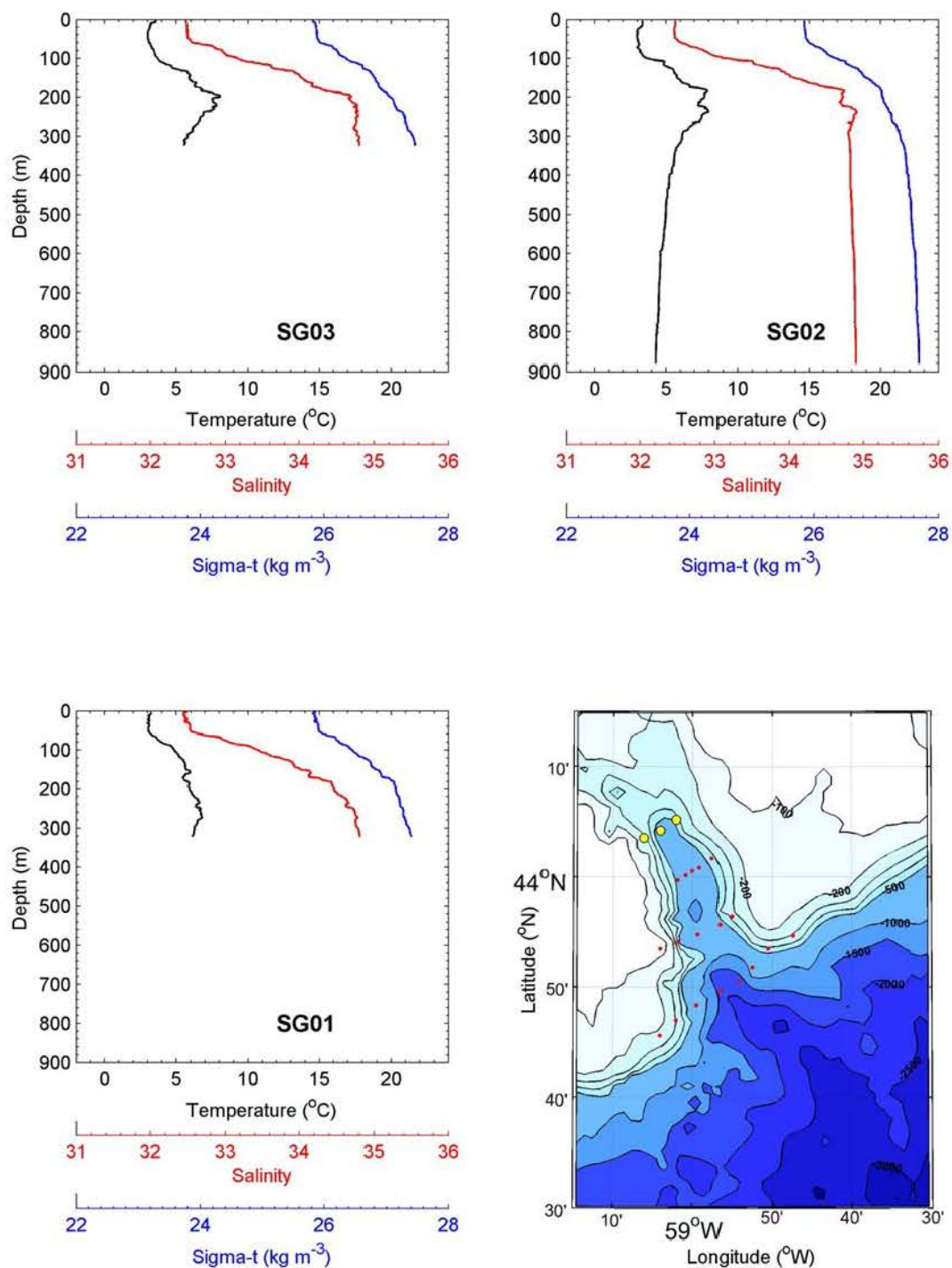


Figure A- 19: Profiles of temperature, salinity and density for the stations highlighted in yellow in the lower right-hand panel. Refer to Figure 1 for numbering of the CTD stations.

Cruise 2006008, Gully, Section 3-2-1

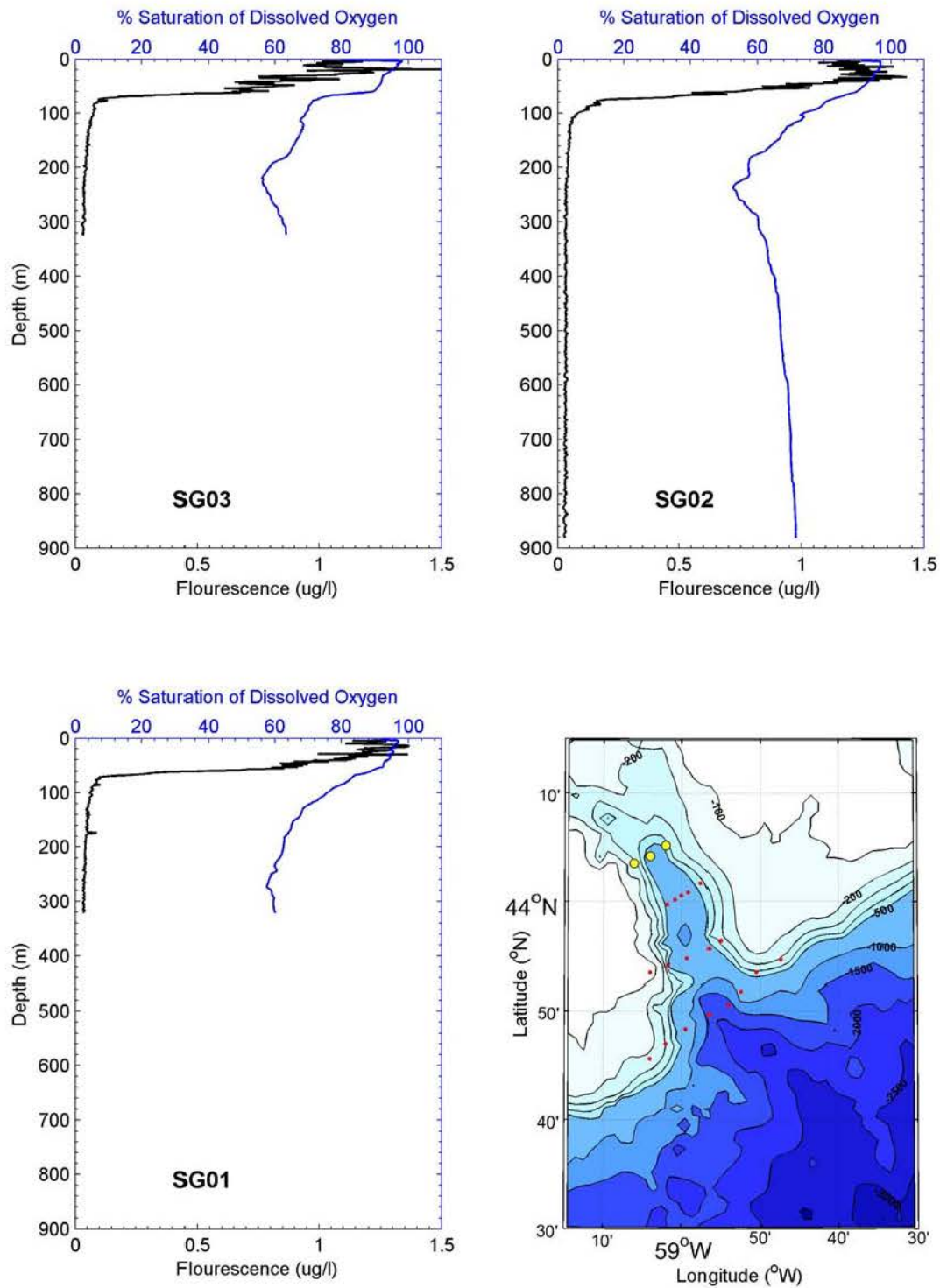


Figure A- 20: Profiles of dissolved oxygen from the CTD SBE43 sensor for the stations highlighted in yellow in the lower right-hand panel. Refer to Figure 1 for numbering of the CTD stations.

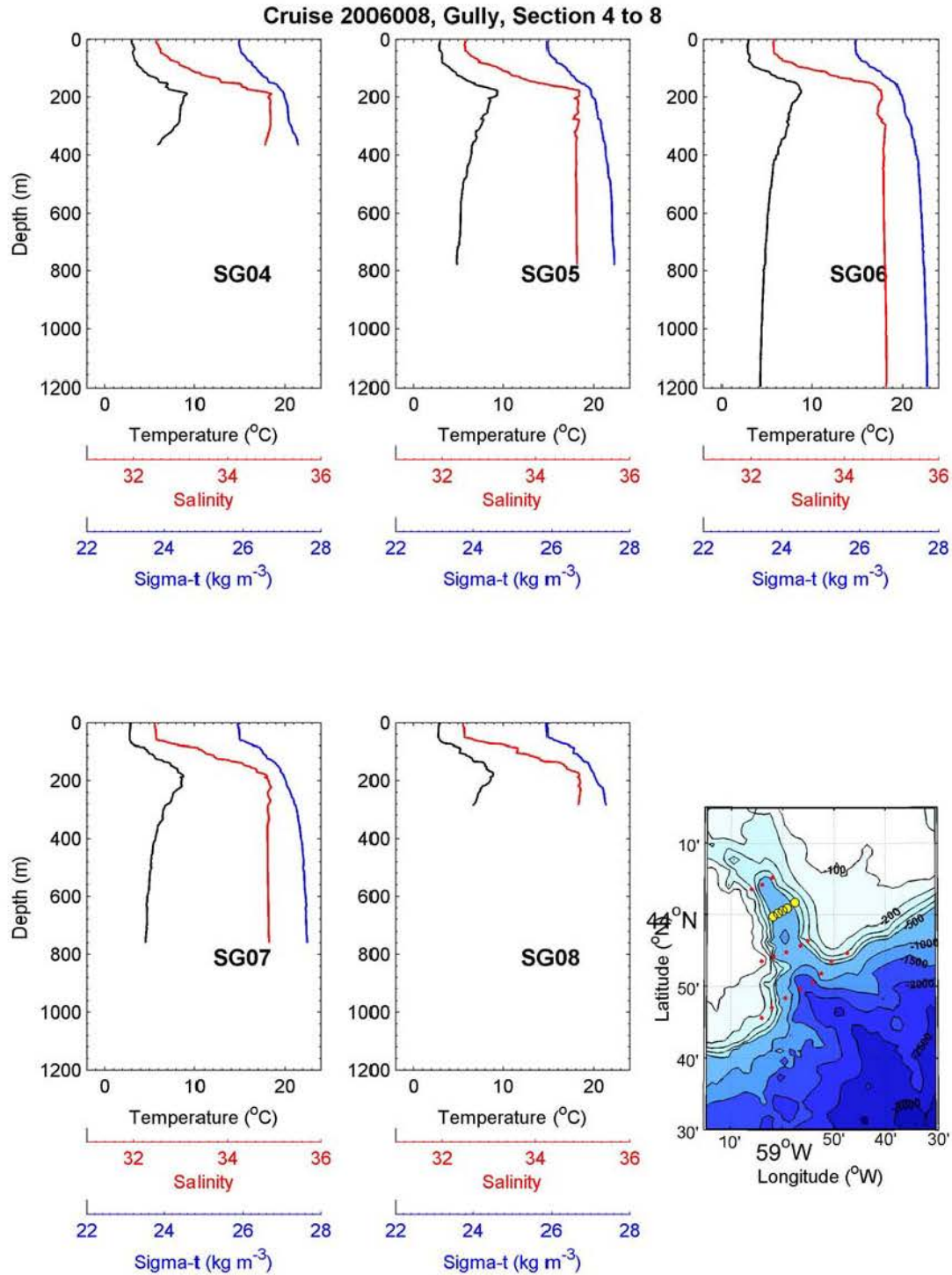


Figure A- 21: Profiles of temperature, salinity and density for the stations highlighted in yellow in the lower right-hand panel. Refer to Figure 1 for numbering of the CTD stations.

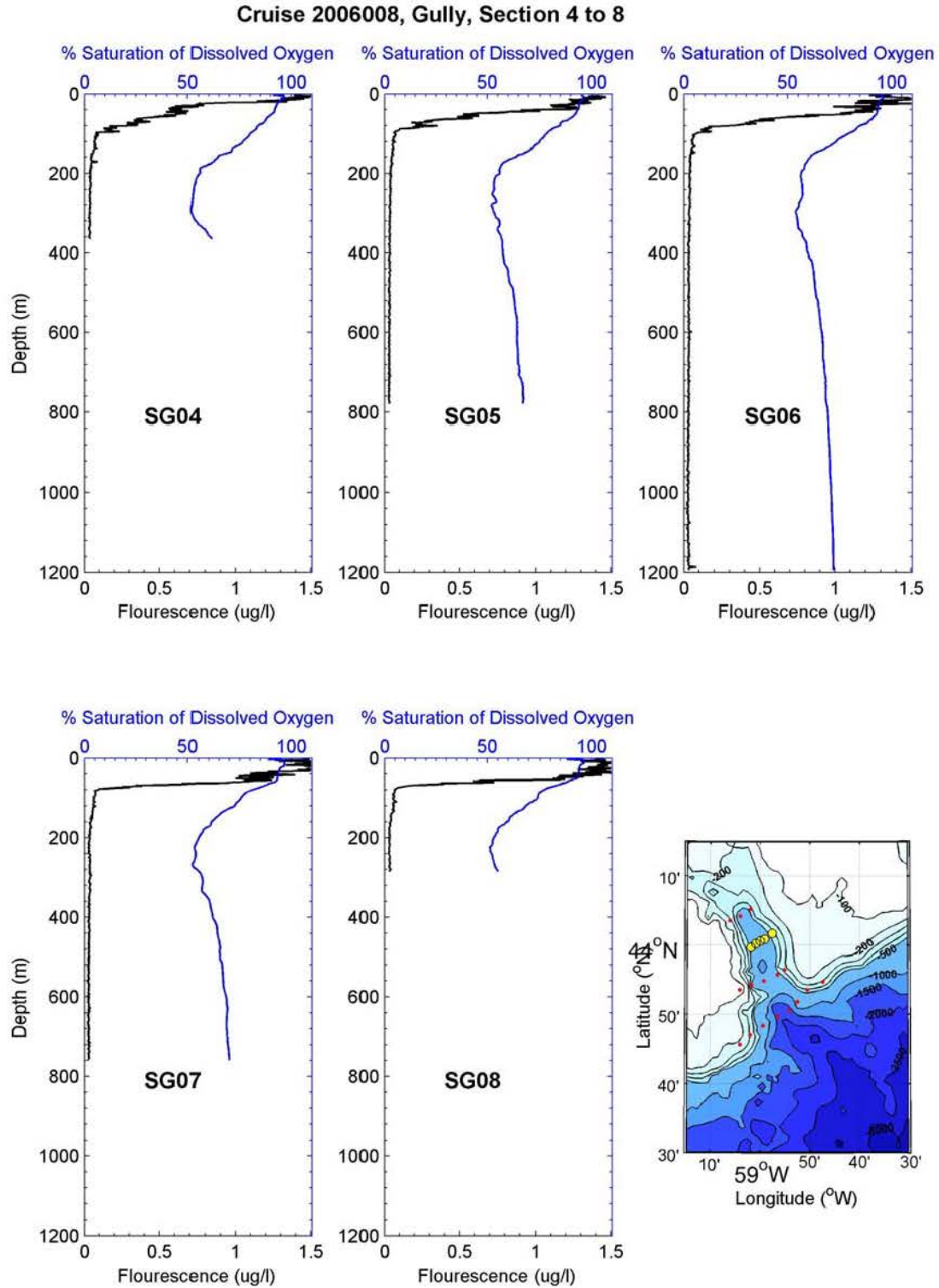


Figure A- 22: Profiles of dissolved oxygen from the CTD SBE43 sensor for the stations highlighted in yellow in the lower right-hand panel. Refer to Figure 1 for numbering of the CTD stations.

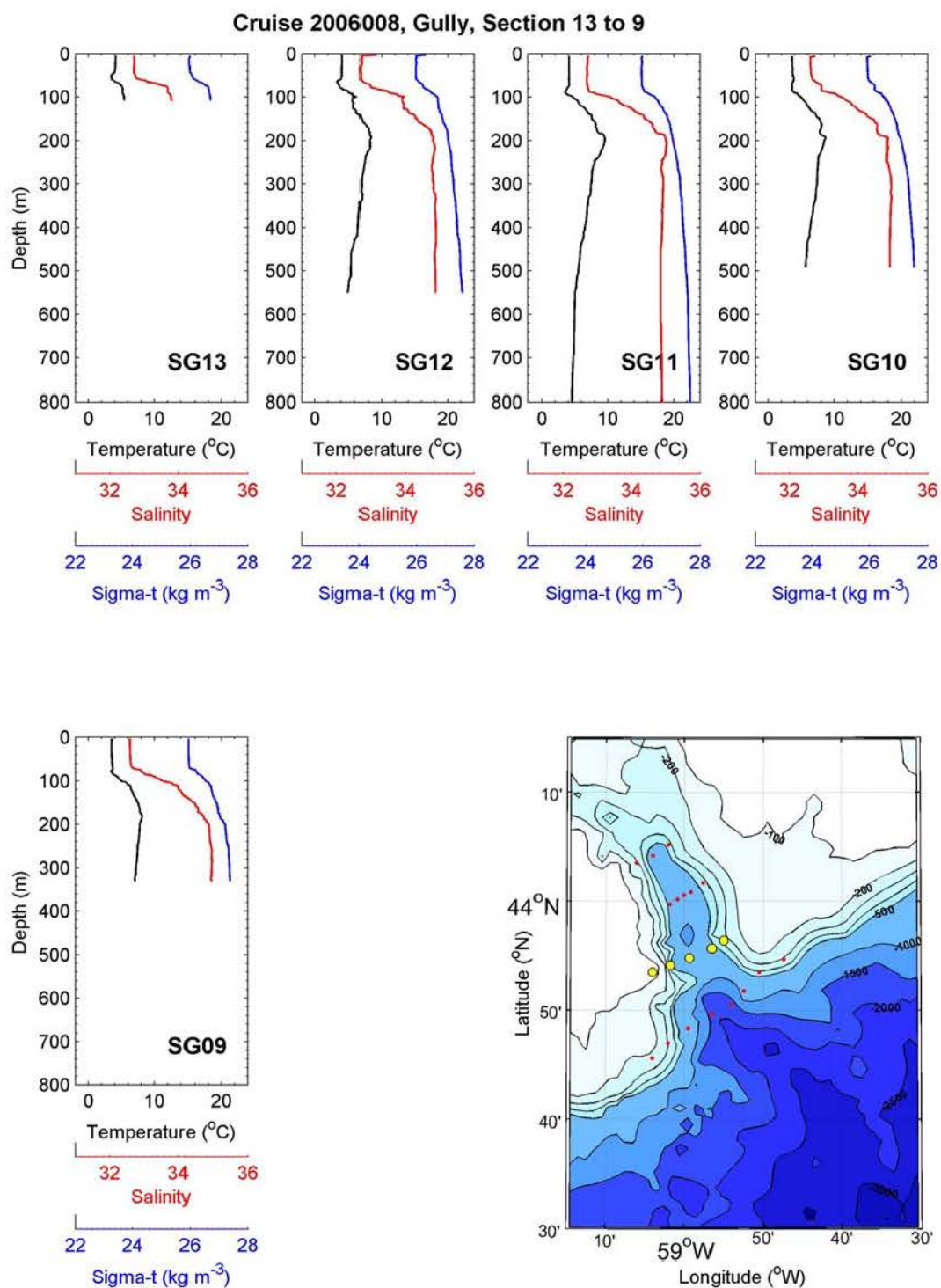
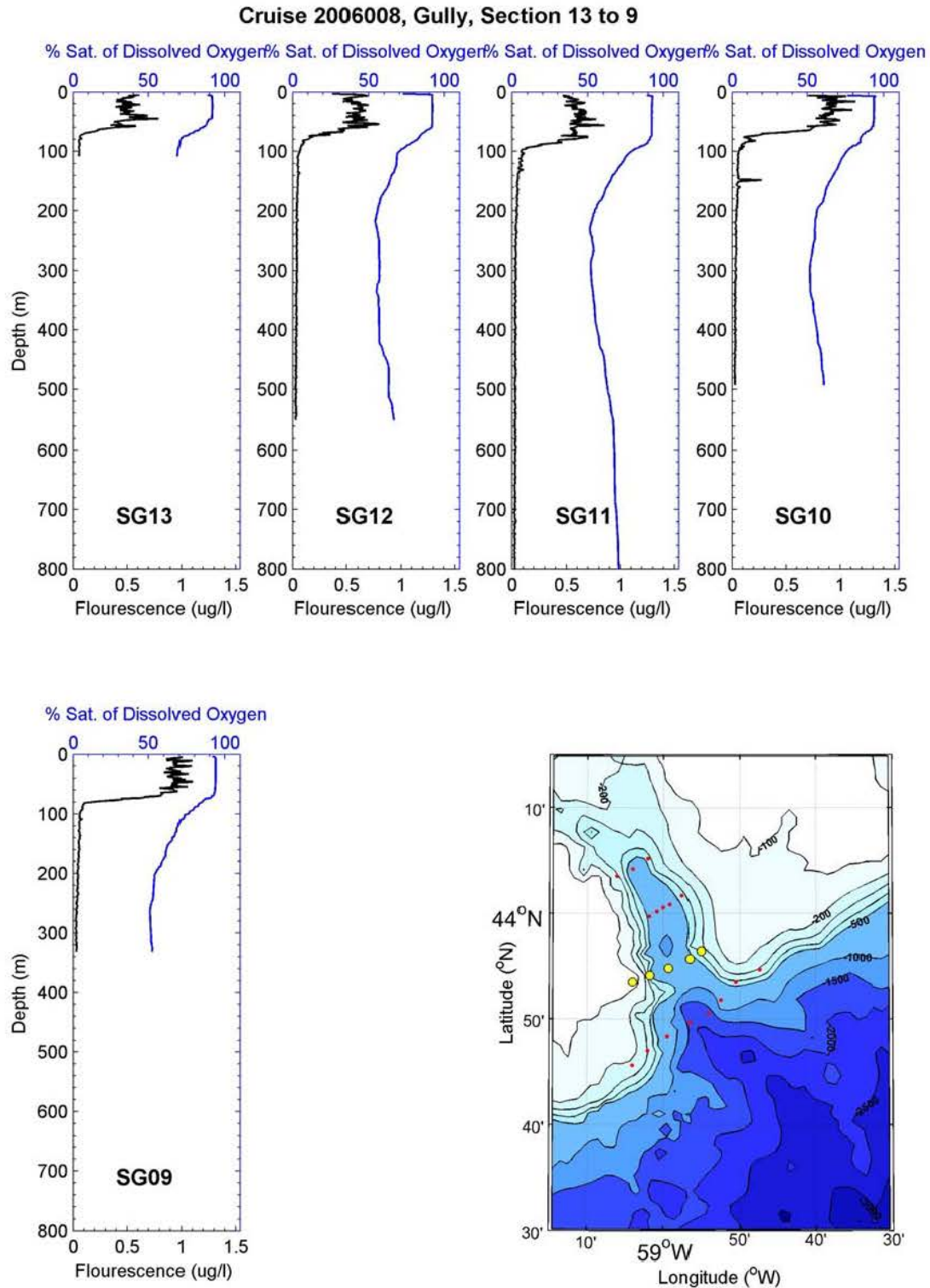


Figure A- 23: Profiles of temperature, salinity and density for the stations highlighted in yellow in the lower right-hand panel. Refer to Figure 1 for numbering of the CTD stations.



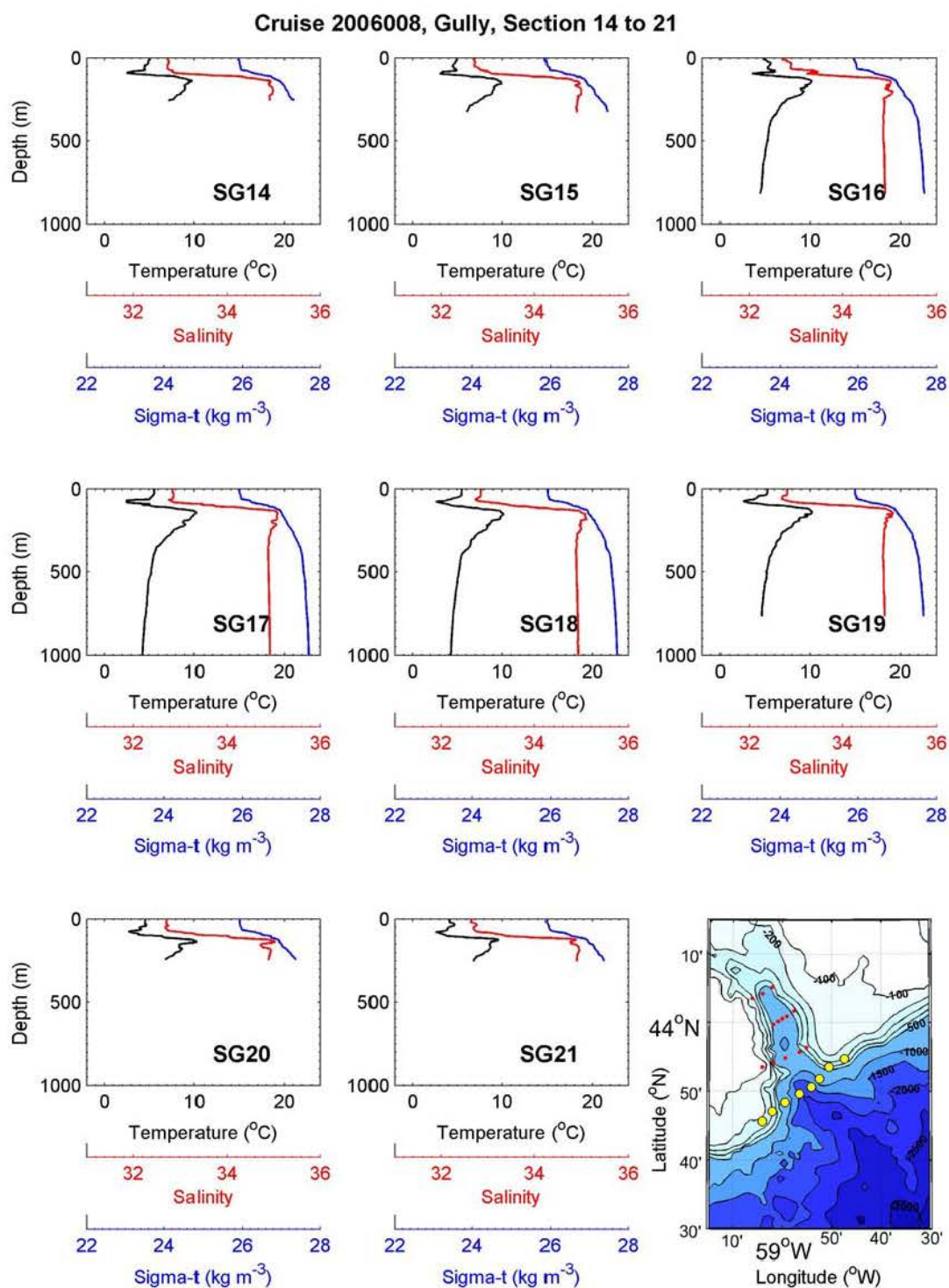


Figure A- 25: Profiles of temperature, salinity and density for the stations highlighted in yellow in the lower right-hand panel. Refer to Figure 1 for numbering of the CTD stations.

Cruise 2006008, Gully, Section 14 to 21

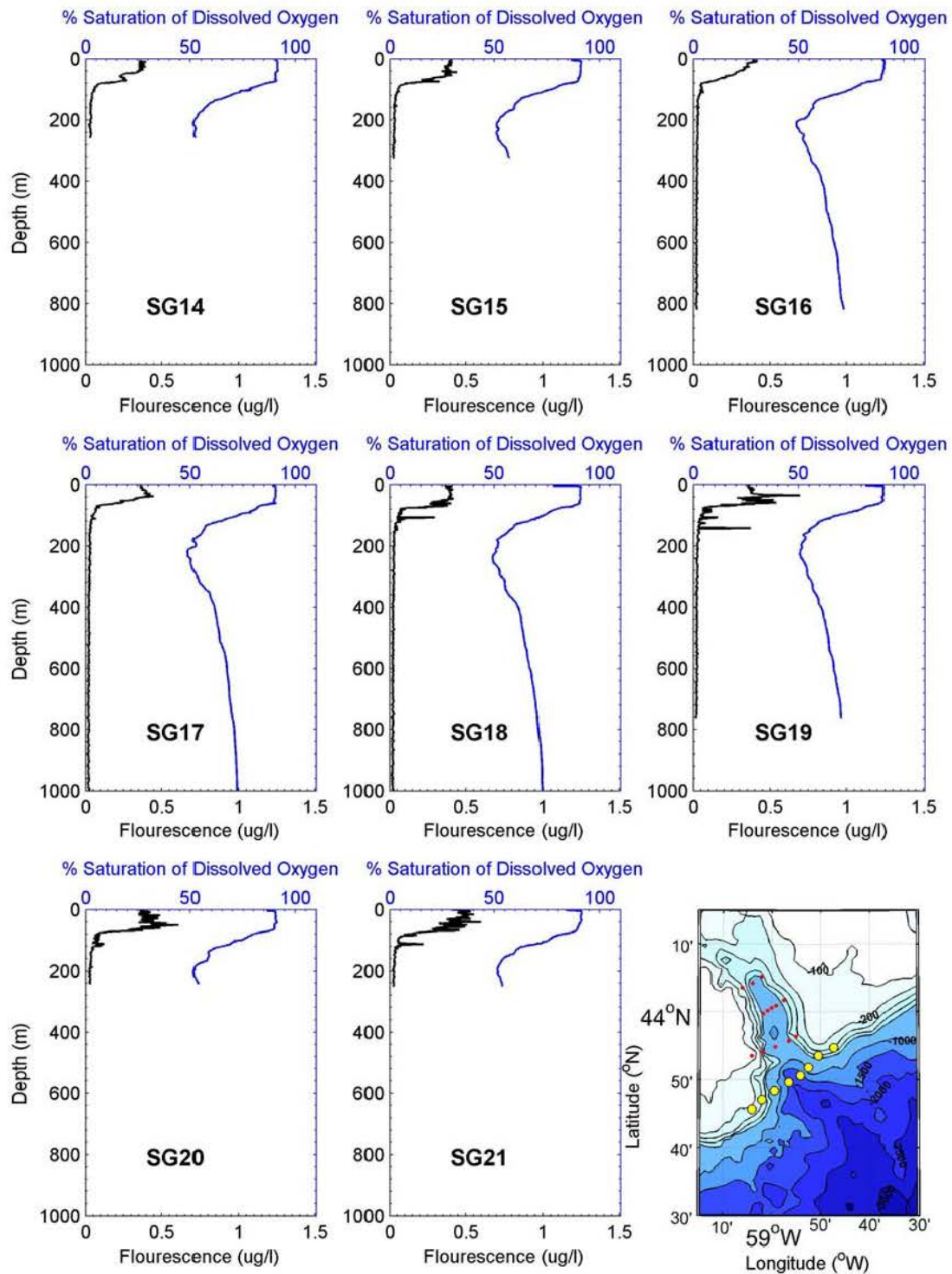


Figure A- 26: Profiles of dissolved oxygen from the CTD SBE43 sensor for the stations highlighted in yellow in the lower right-hand panel. Refer to Figure 1 for numbering of the CTD stations.

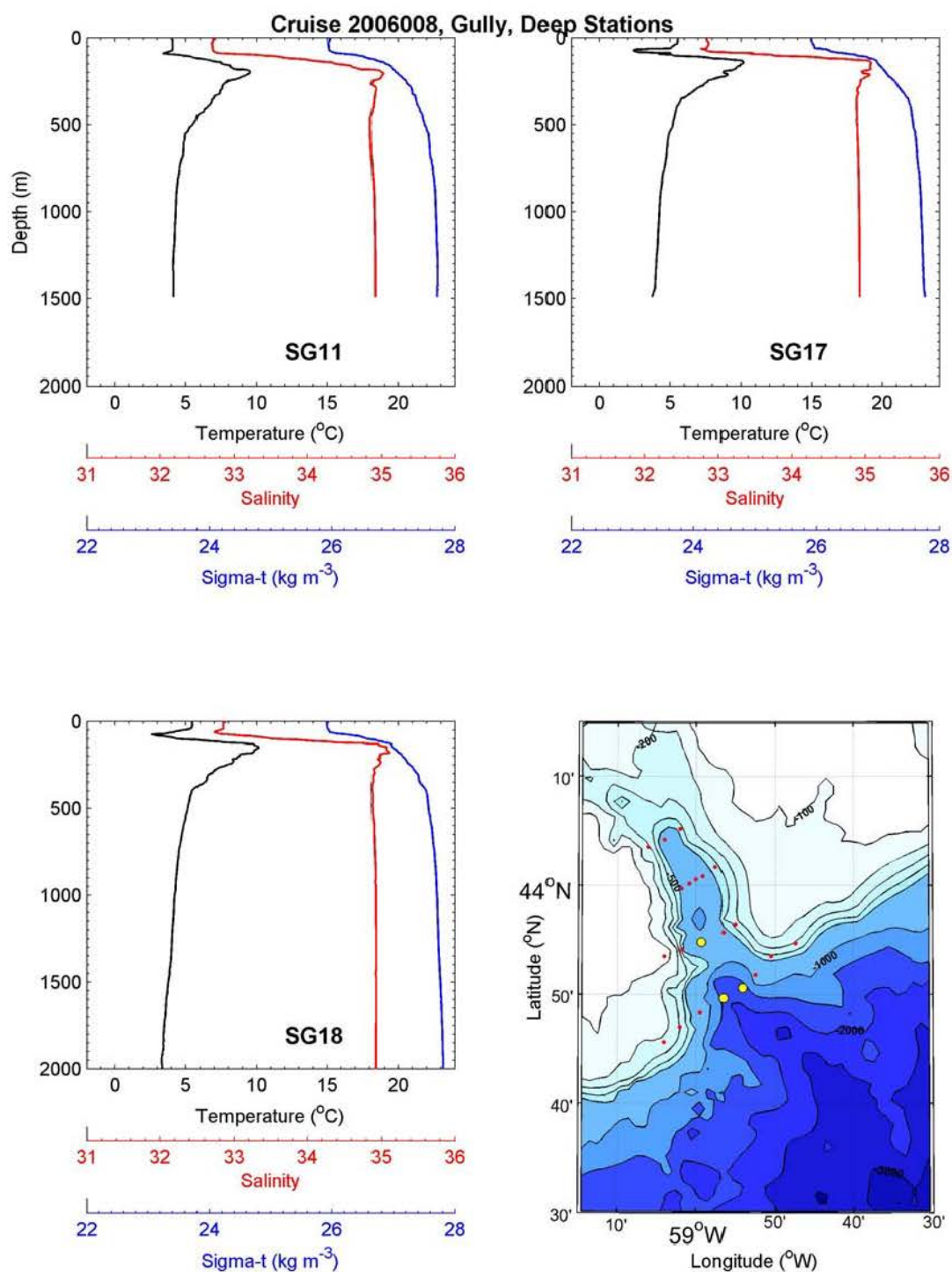


Figure A- 27: Profiles of temperature, salinity and density for the stations highlighted in yellow in the lower right-hand panel. Refer to Figure 1 for numbering of the CTD stations.

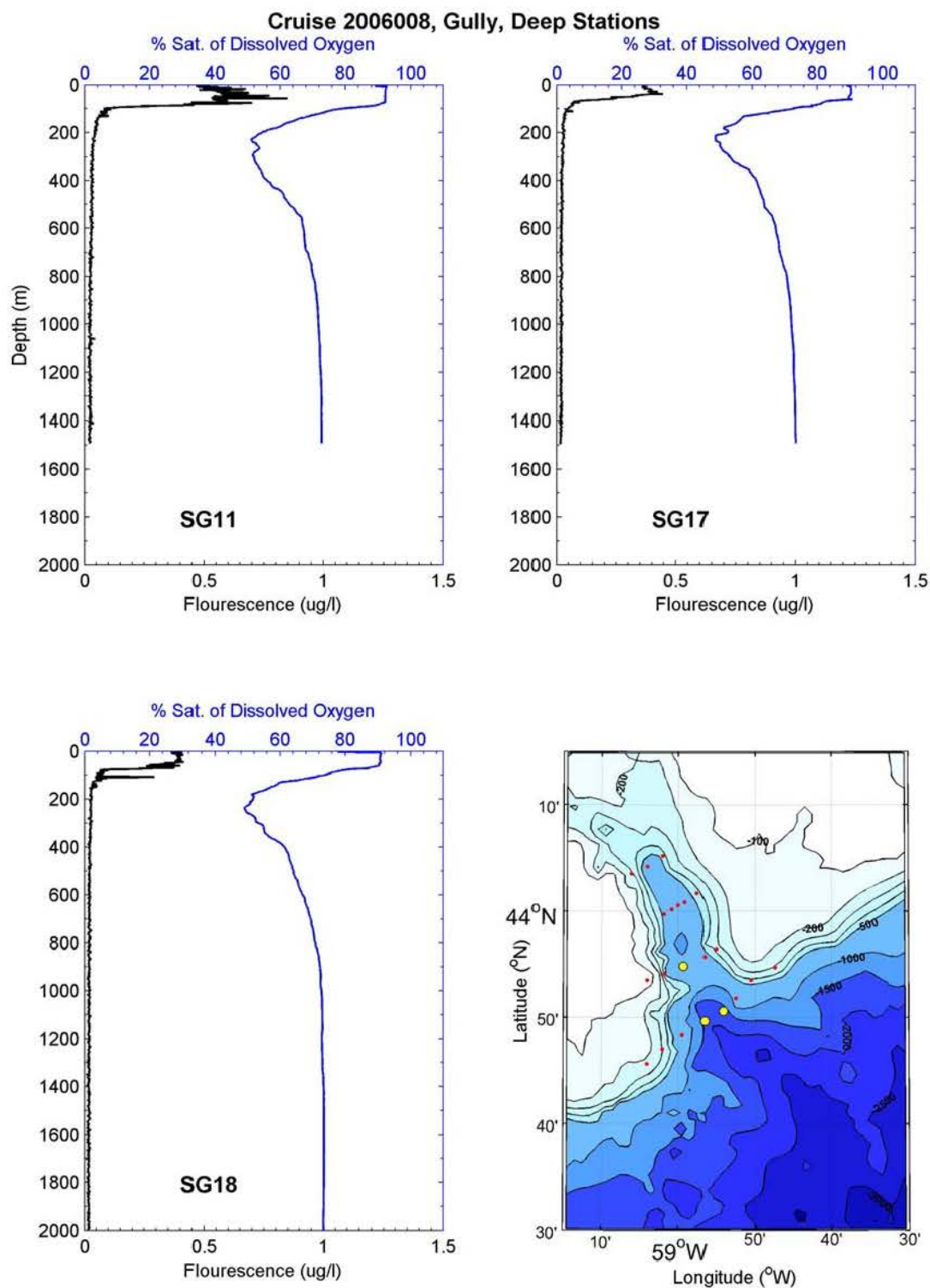


Figure A- 28: Profiles of dissolved oxygen from the CTD SBE43 sensor for the stations highlighted in yellow in the lower right-hand panel. Refer to Figure 1 for numbering of the CTD stations.

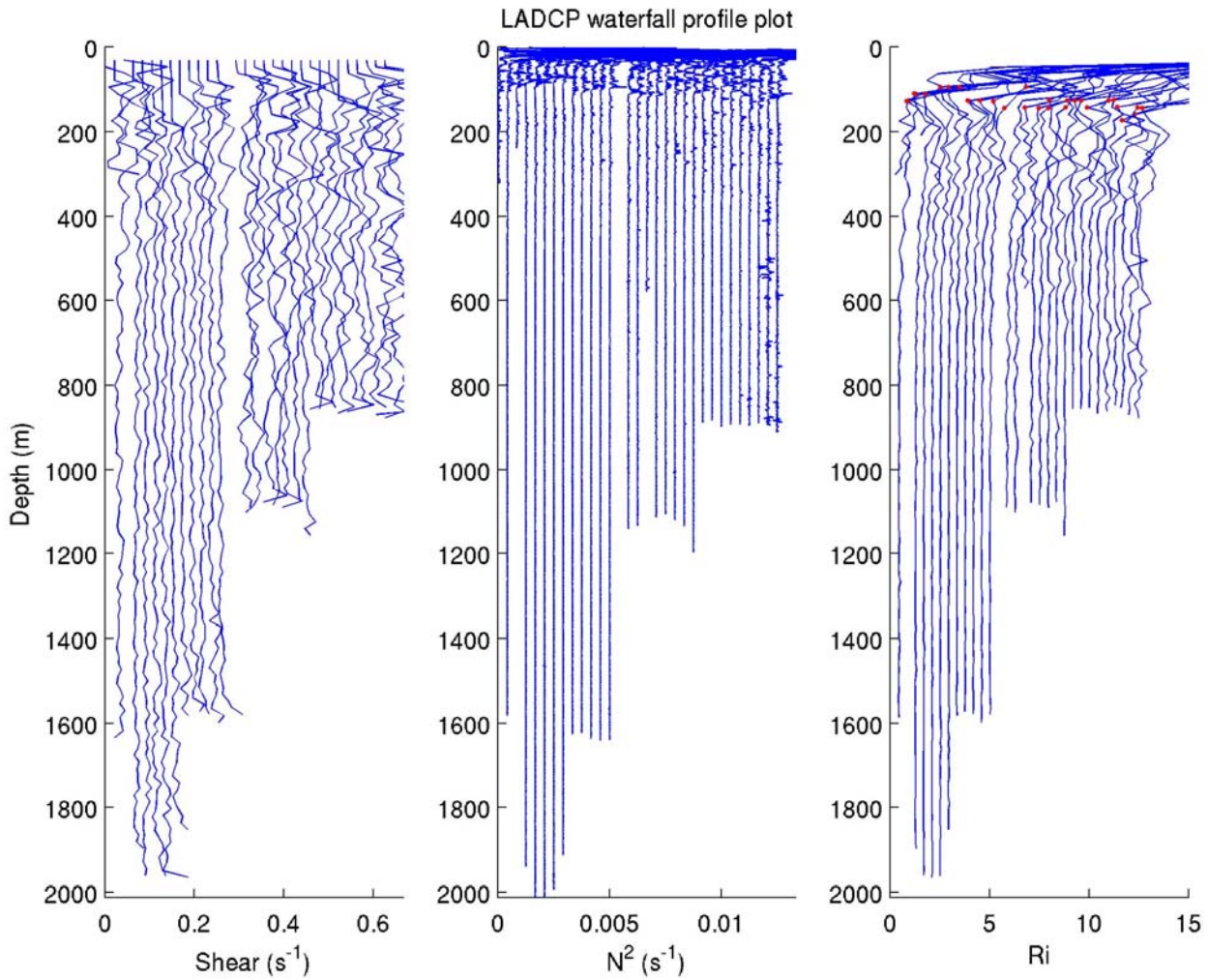


Figure A- 29: Waterfall plot of vertical shear computed from the Lowered-ADCP data using a first-differencing method (left panel), buoyancy frequency calculated from the corresponding CTD profile (middle panel), and estimate of the gradient Richardson number, Ri , in 16 m vertical bins (right panel). These results show that Ri values typically are in the range of 1 to 5. Waterfall plots are a composite of 4 occupations of 12-hour periods at stations SG18, SG11, SG6 and SG2. The change in station location is evident from the change in depth of the casts (aside from the first two casts at SG18 which were stopped well above bottom).

Appendix 3: CTD Sections, including Chlorophyll, Fluorescence, and Nitrate

CTD surveys were completed with Sea-Bird 911 CTD and 24-bottle rosette. These were conducted on two separate cruises HUD2006-008 from April 20-26, 2006 at sites SG1 through SG21 and HUD2007-033 from August 2-8, 2007 at sites SG1 through SG29 (Figure 1). The CTD had dual temperature, conductivity and pressure sensors as well as oxygen and fluorescence sensors. The following plots are for both the HUD2007-033 and HUD2006-008 cruises. Contour plots were created for each section for temperature, salinity and density observations from the first sensor package versus distance; however, these data were compared with those from the second sensor package and no differences were found except for the near surface data at SG26. Brunt Vaisala, dissolved oxygen, percent saturation of dissolved oxygen and fluorescence from CTD measurements were also plotted. Bottle data were plotted for chlorophyll and nitrate (Figure A- 30 to Figure A- 49).

Scatter plots were also generated for nitrate versus salinity and chlorophyll versus fluorescence all from bottle data with the exception of salinity which was from CTD. The colour bars show the depth (Figure A- 50 to Figure A- 51).

All plots were created using MATLAB R2008b.

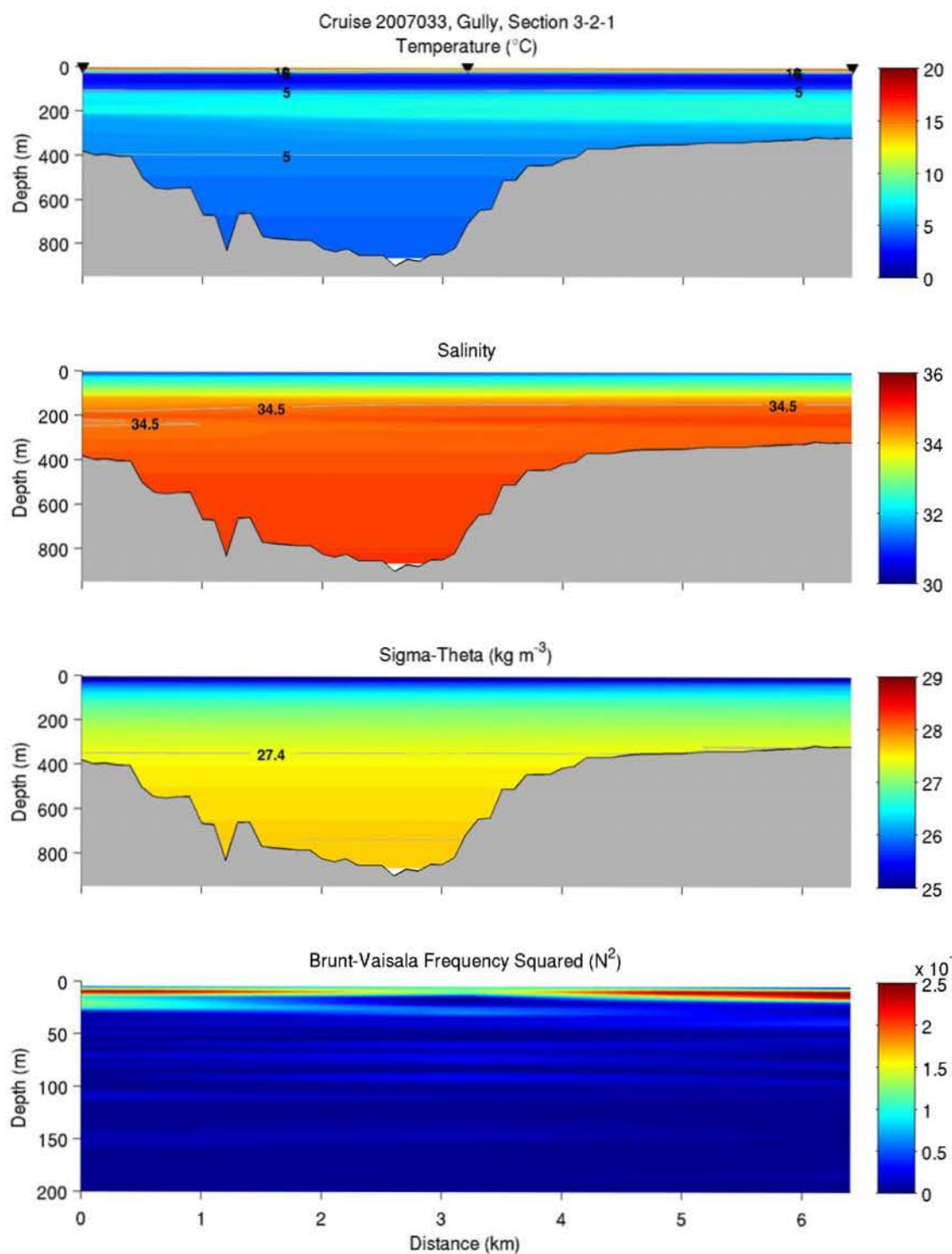


Figure A- 30: Section plots of temperature, salinity, density and Brunt-Vaisala frequency squared. Refer to Figure 1 for numbering of the CTD stations.

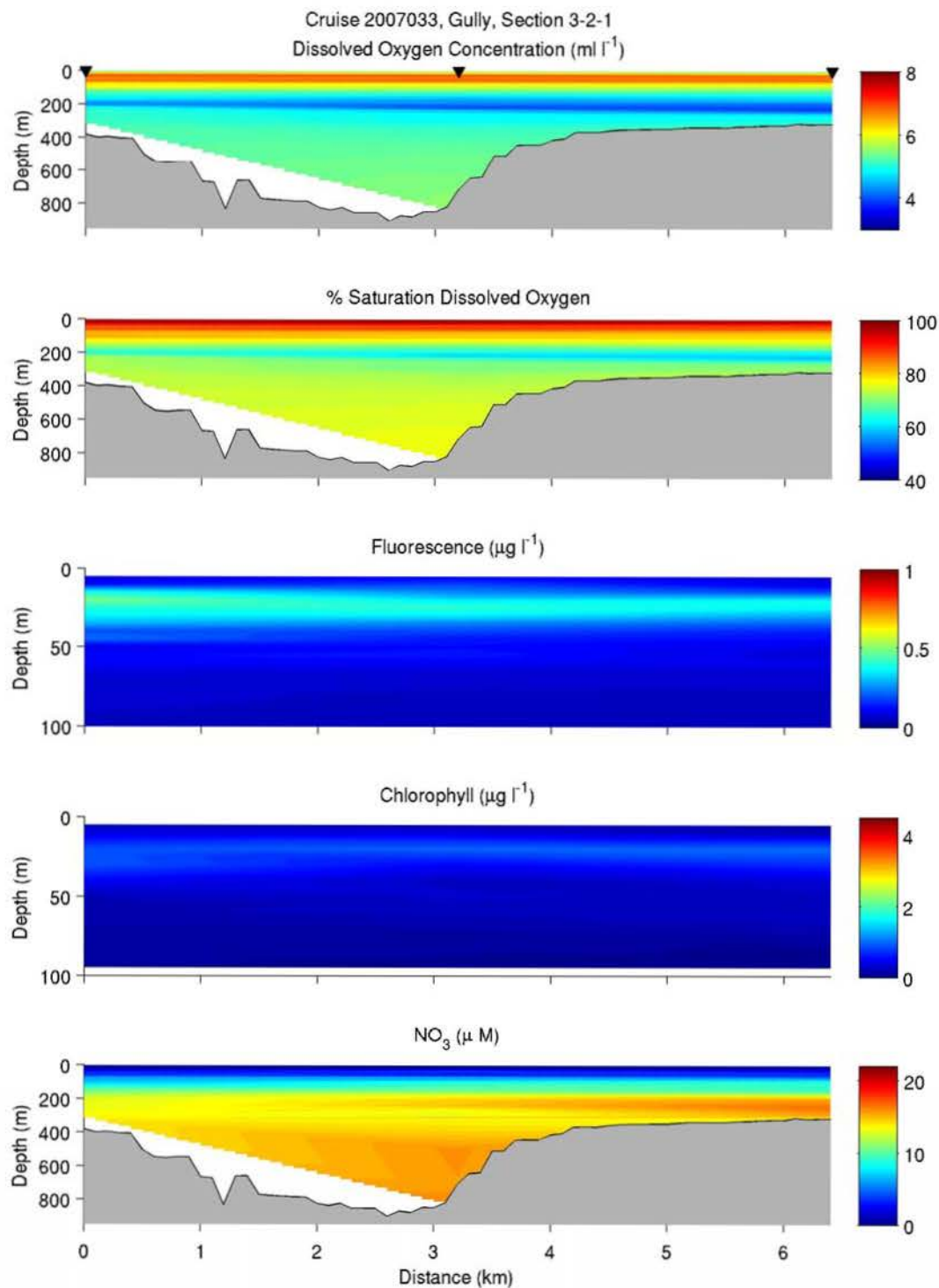


Figure A- 31: Section plots of dissolved oxygen concentration, percent saturation dissolved oxygen, fluorescence, chlorophyll from water samples and nitrate from water samples. Refer to Figure 1 for numbering of the CTD stations.

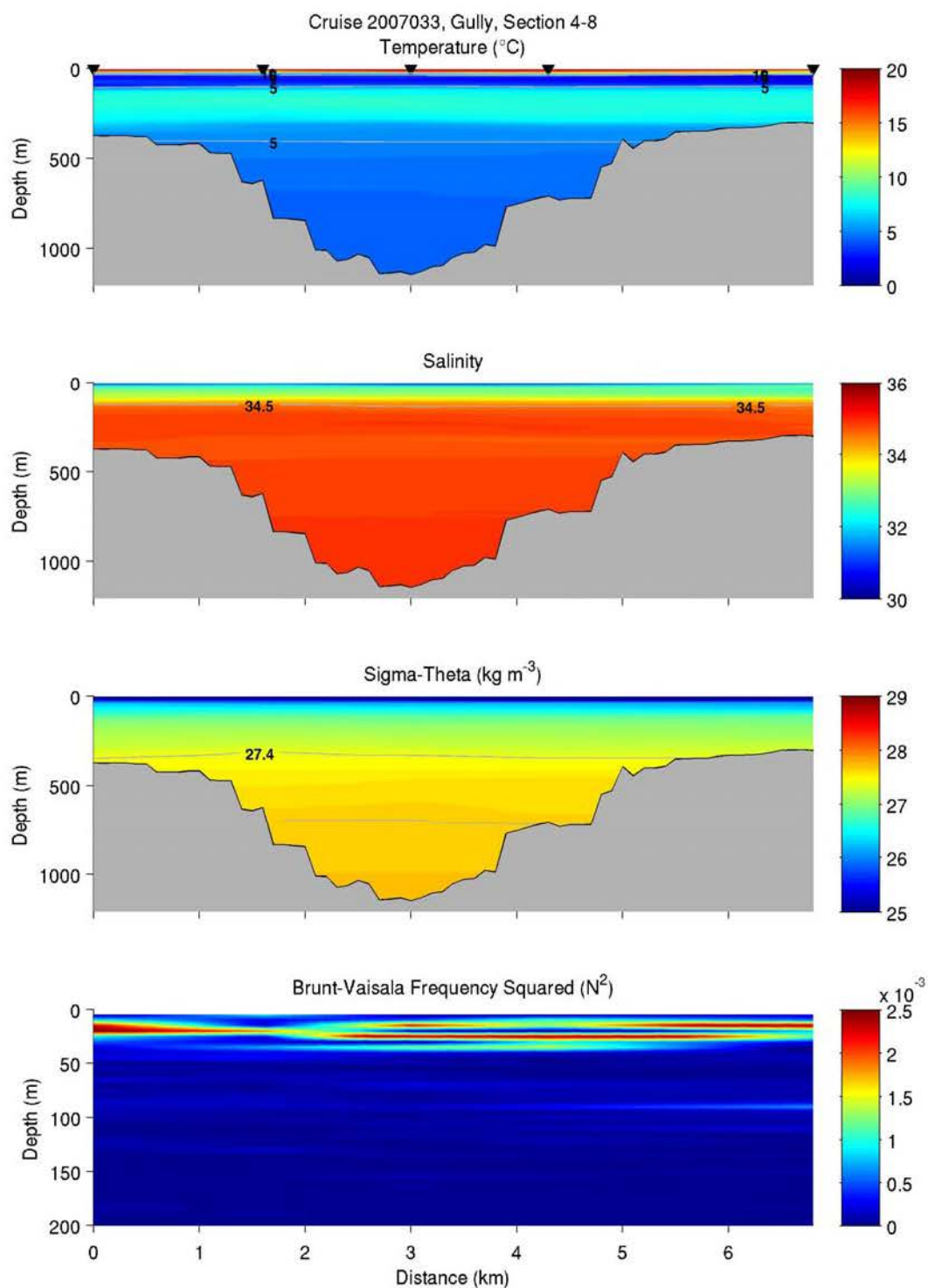


Figure A- 32: Section plots of temperature, salinity, density and Brunt-Vaisala frequency squared. Refer to Figure 1 for numbering of the CTD stations.

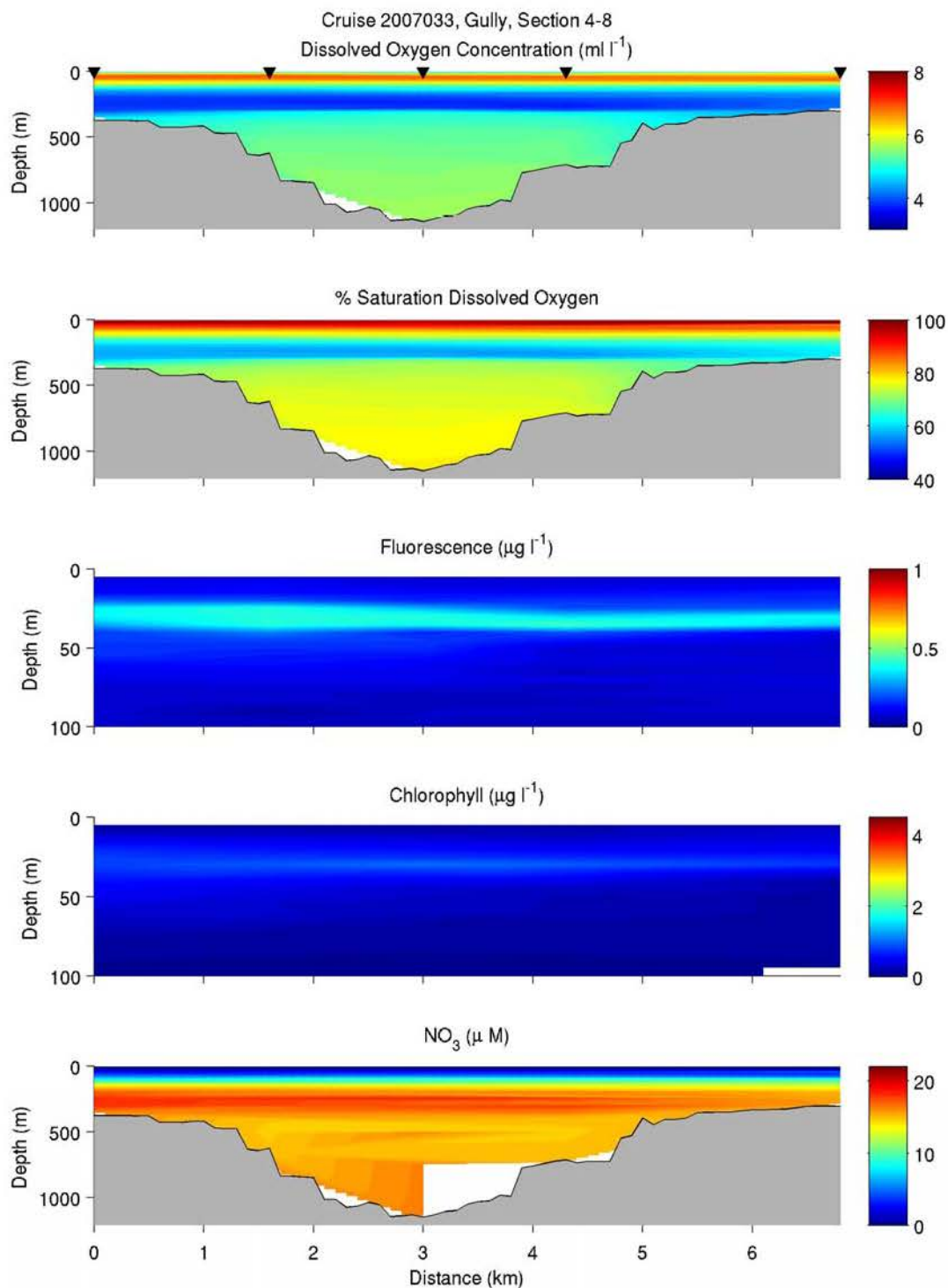


Figure A- 33: Section plots of dissolved oxygen concentration, percent saturation dissolved oxygen, fluorescence, chlorophyll from water samples and nitrate from water samples. Refer to Figure 1 for numbering of the CTD stations.

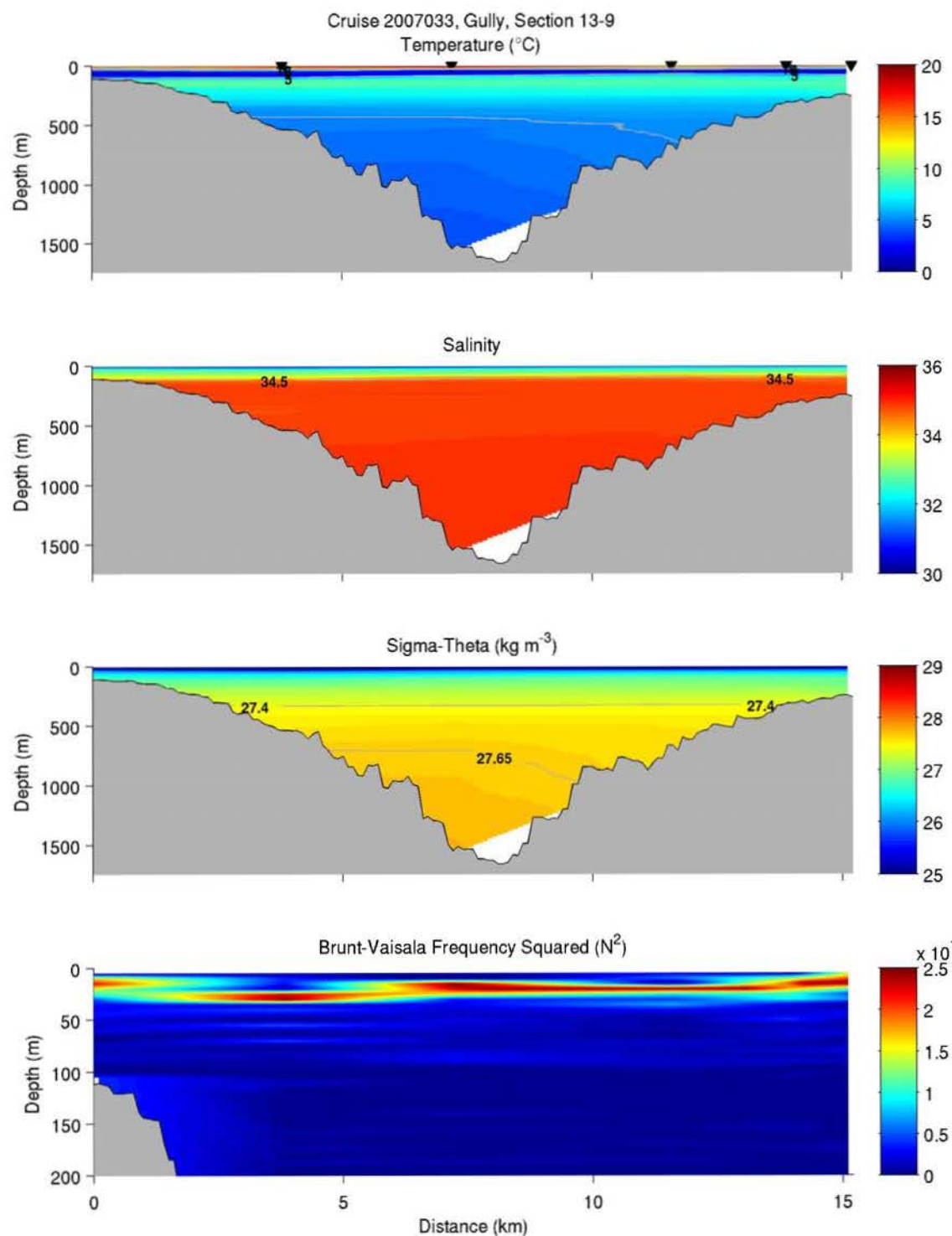


Figure A- 34: Section plots of temperature, salinity, density and Brunt-Vaisala frequency squared. Refer to Figure 1 for numbering of the CTD stations.

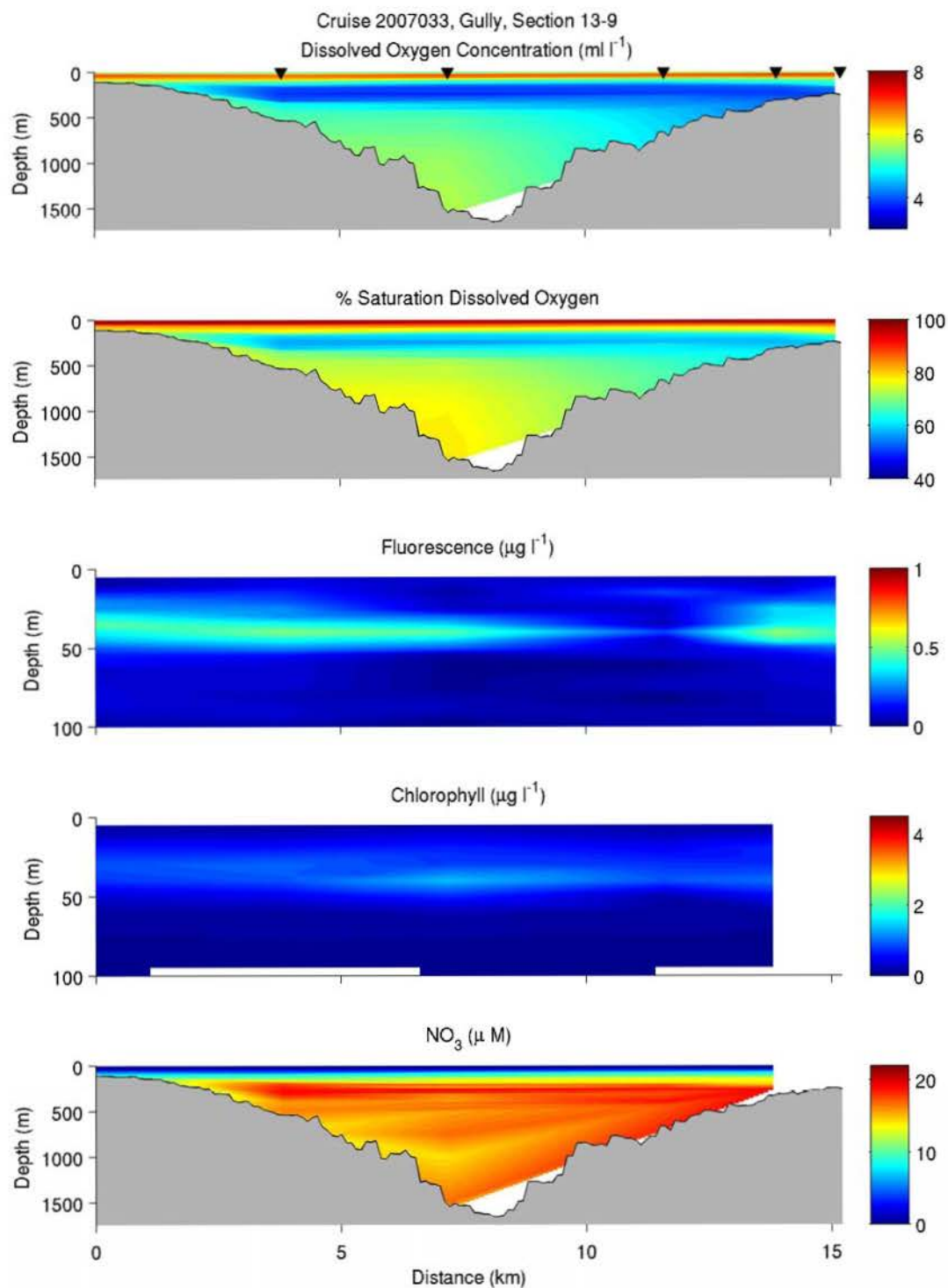


Figure A- 35: Section plots of dissolved oxygen concentration, percent saturation dissolved oxygen, fluorescence, chlorophyll from water samples and nitrate from water samples. Refer to Figure 1 for numbering of the CTD stations.

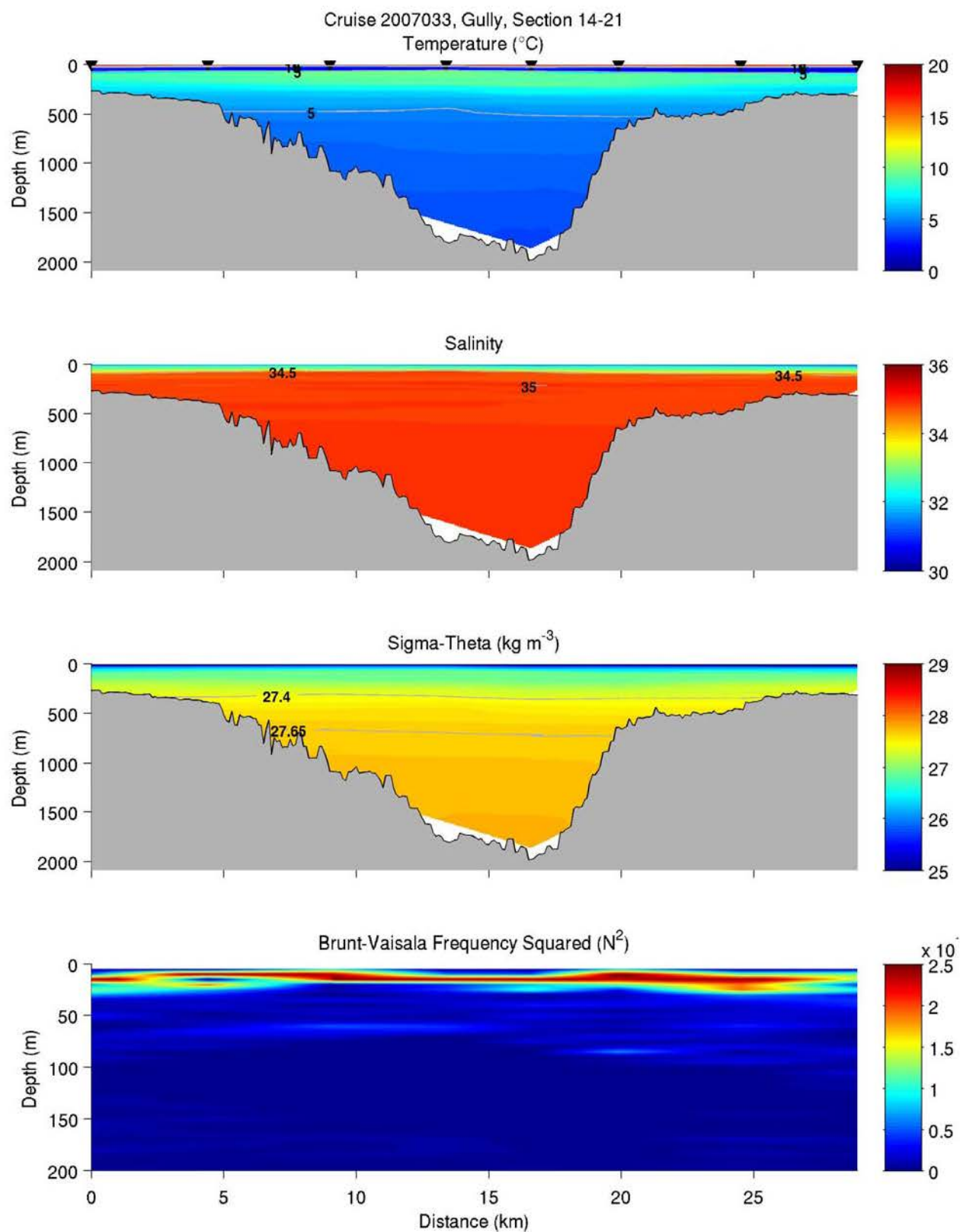


Figure A- 36: Section plots of temperature, salinity, density and Brunt-Vaisala frequency squared. Refer to Figure 1 for numbering of the CTD stations.

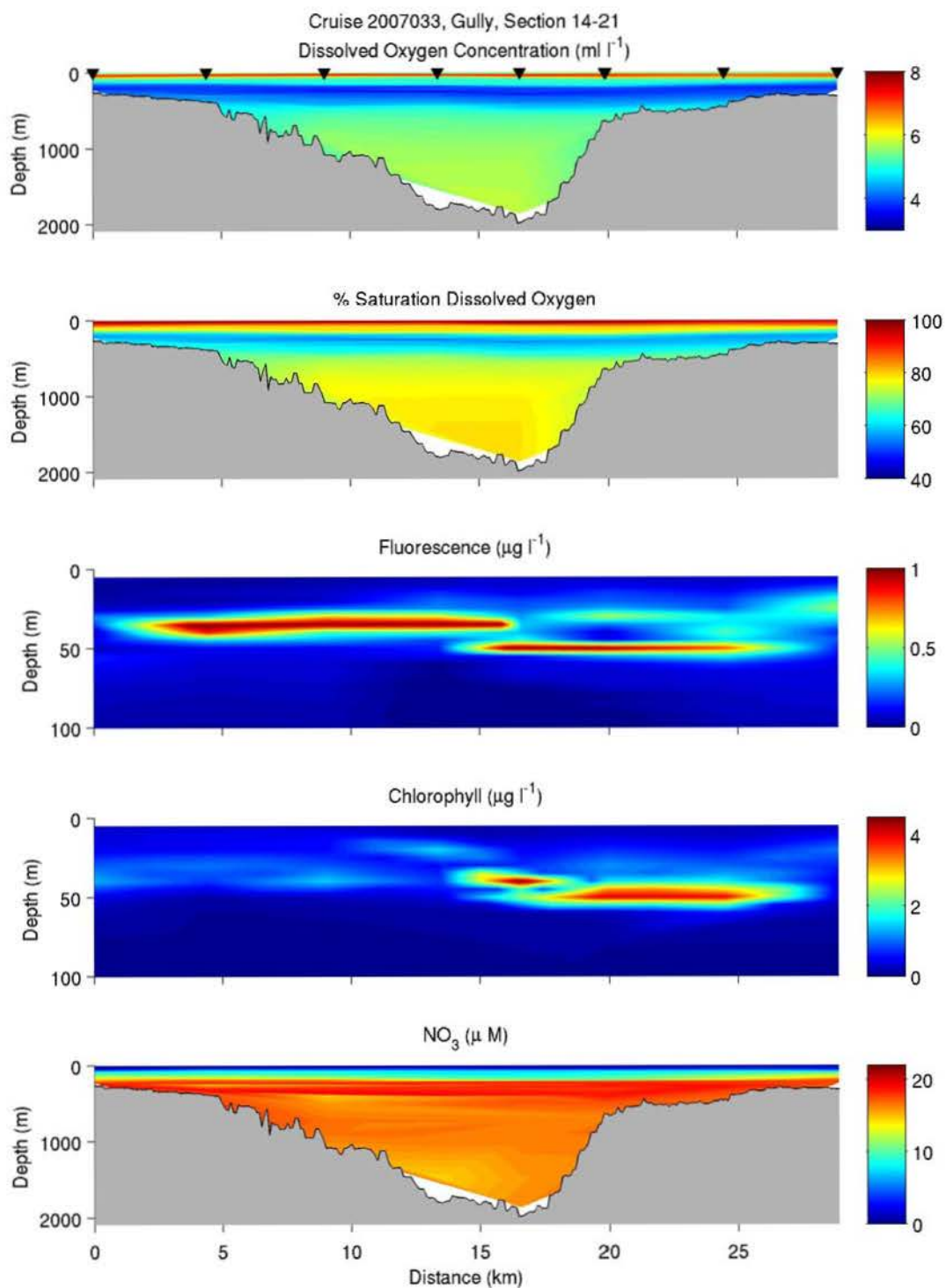


Figure A- 37: Section plots of dissolved oxygen concentration, percent saturation dissolved oxygen, fluorescence, chlorophyll from water samples and nitrate from water samples. Refer to Figure 1 for numbering of the CTD stations.

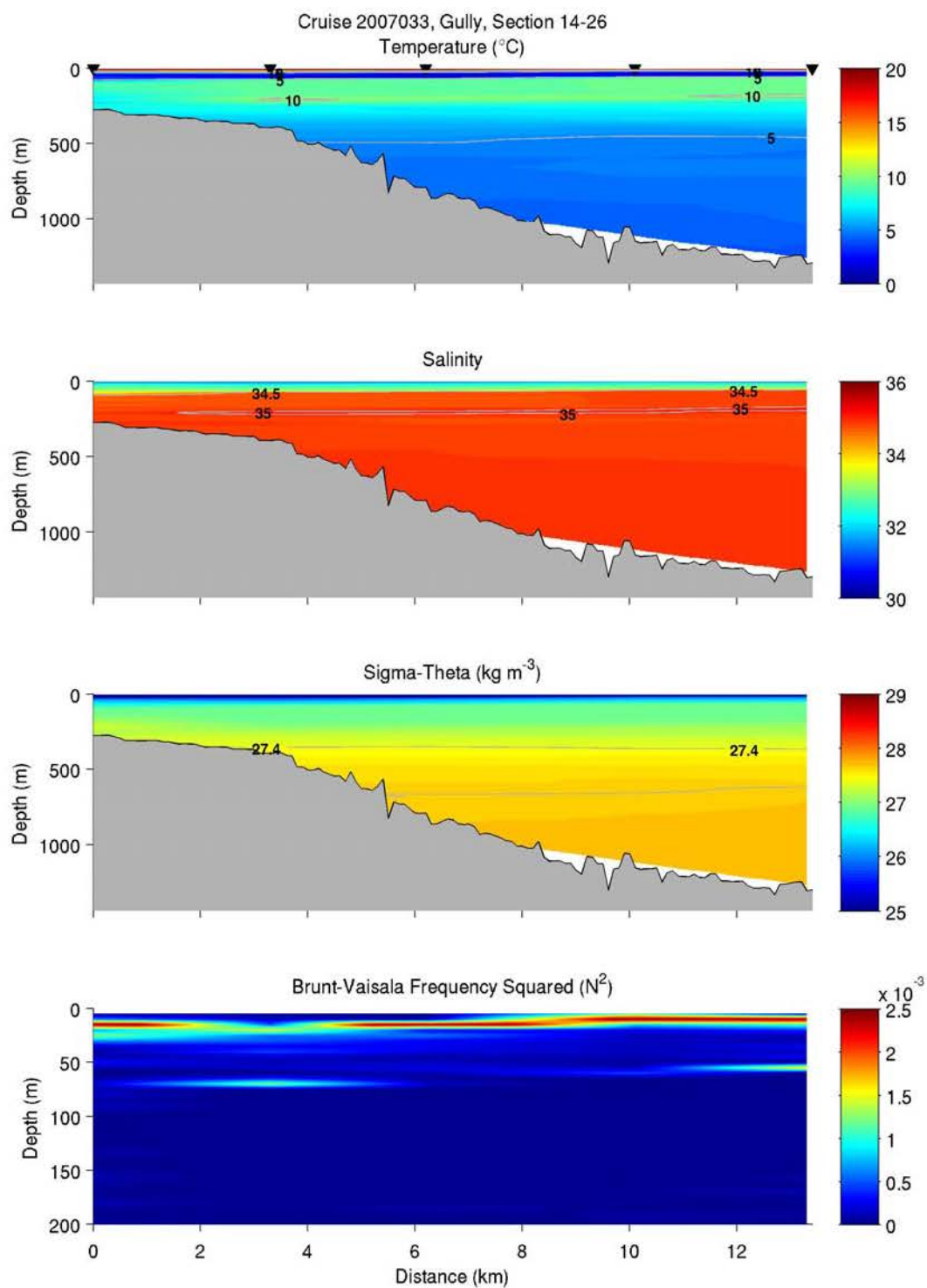


Figure A- 38: Section plots of temperature, salinity, density and Brunt-Vaisala frequency squared. Refer to Figure 1 for numbering of the CTD stations.

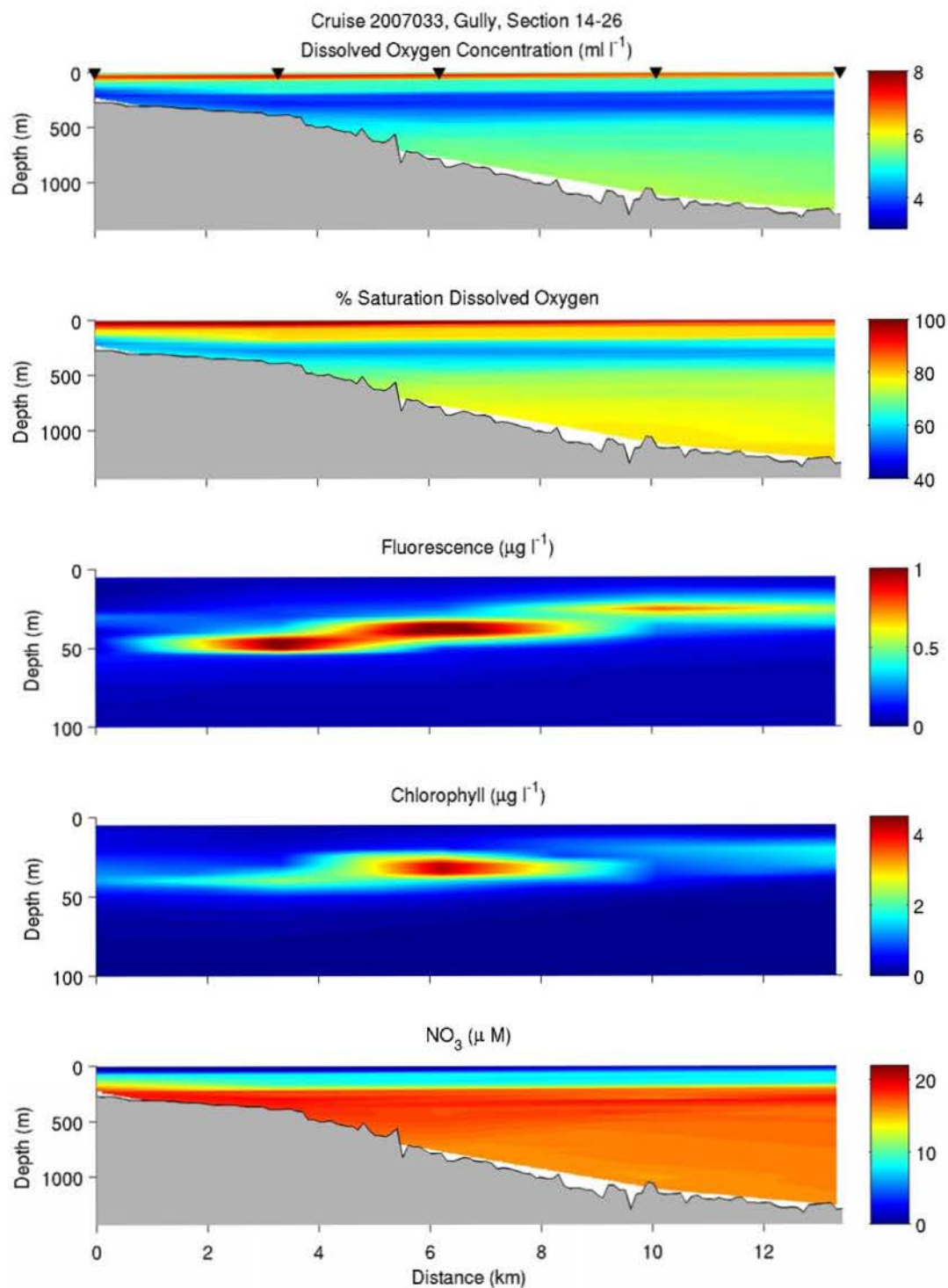


Figure A- 39: Section plots of dissolved oxygen concentration, percent saturation dissolved oxygen, fluorescence, chlorophyll from water samples and nitrate from water samples. Refer to Figure 1 for numbering of the CTD stations.

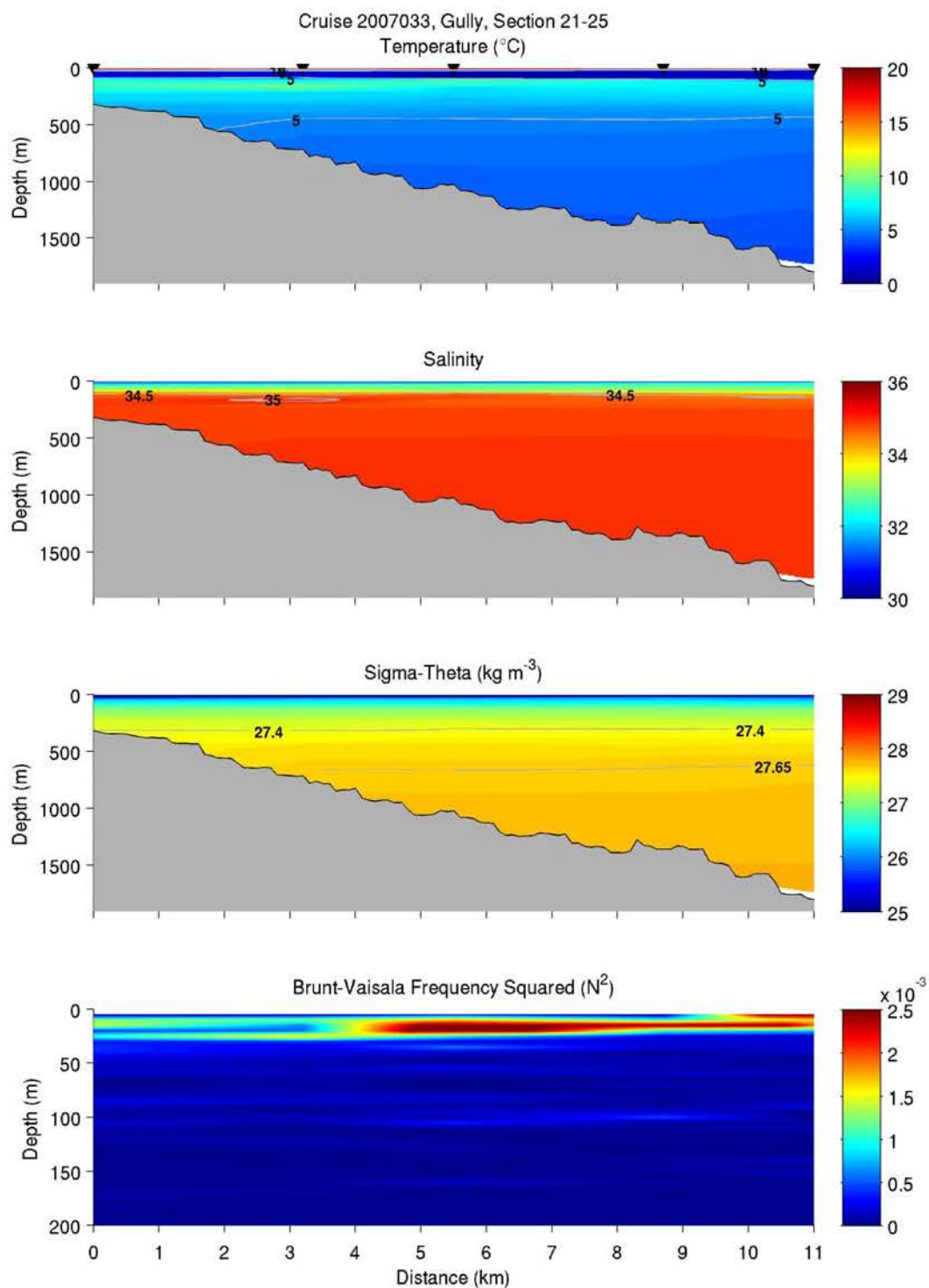


Figure A- 40: Section plots of temperature, salinity, density and Brunt-Vaisala frequency squared. Refer to Figure 1 for numbering of the CTD stations.

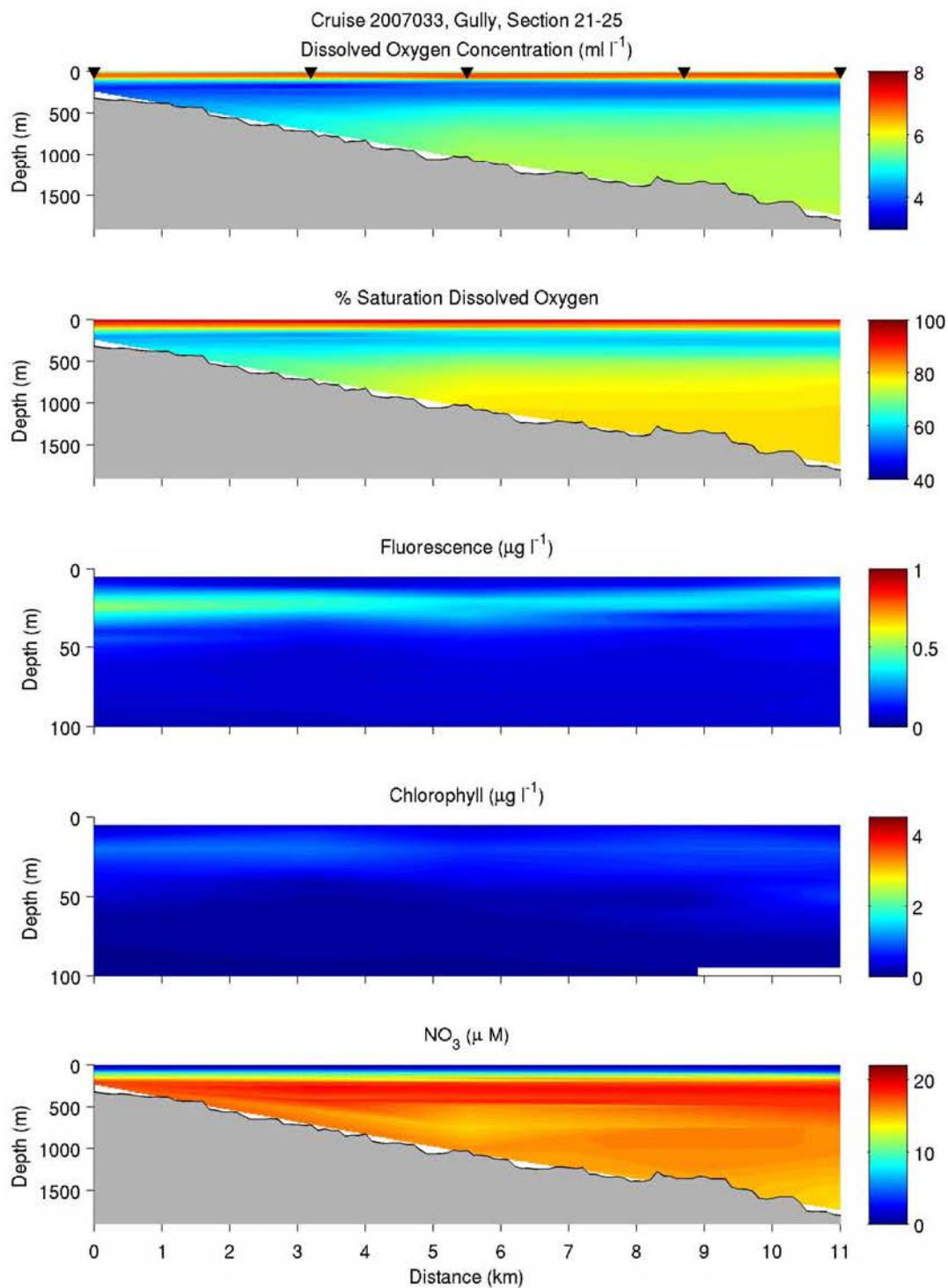


Figure A- 41: Section plots of dissolved oxygen concentration, percent saturation dissolved oxygen, fluorescence, chlorophyll from water samples and nitrate from water samples. Refer to Figure 1 for numbering of the CTD stations.

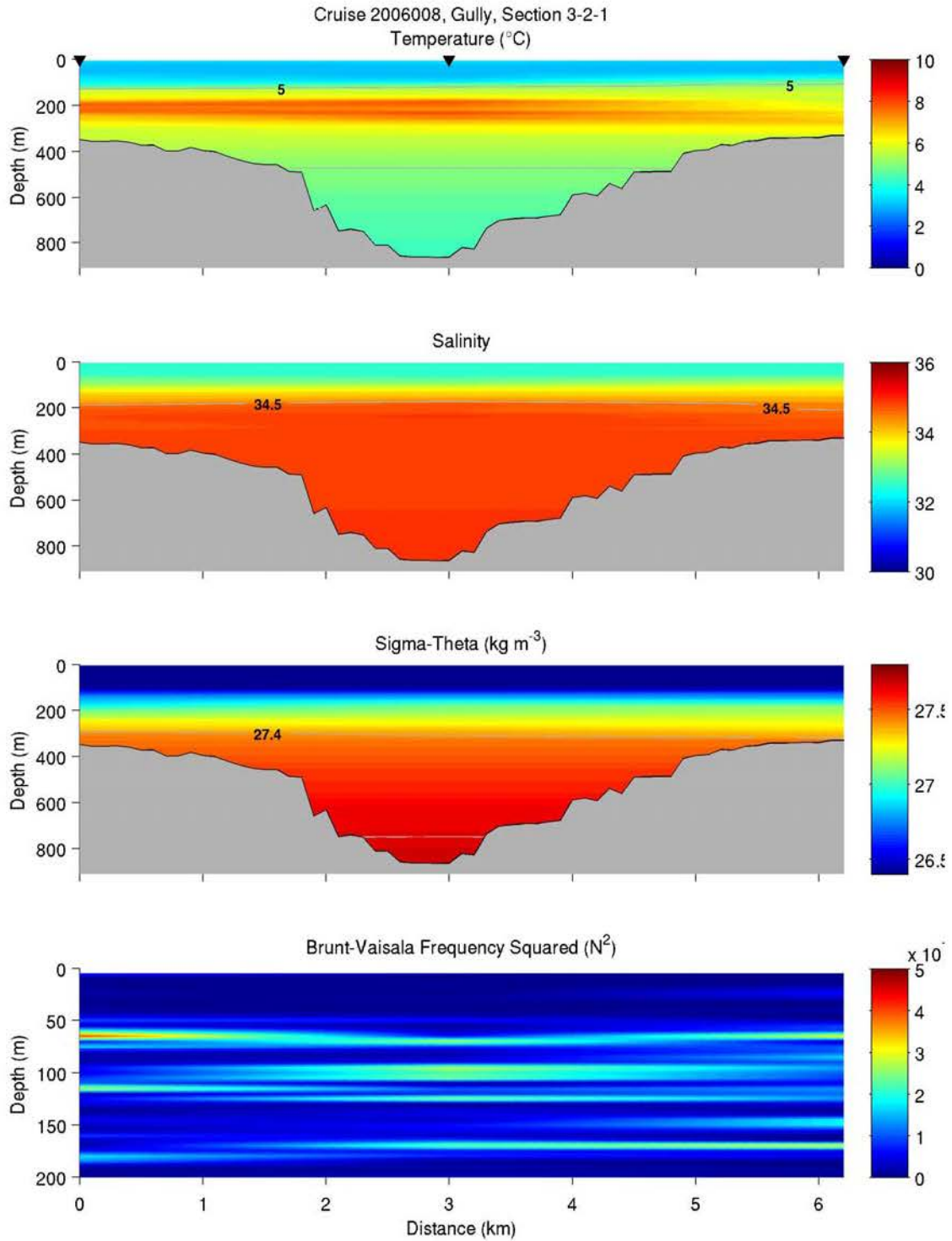


Figure A- 42: Section plots of temperature, salinity, density and Brunt-Vaisala frequency squared. Refer to Figure 1 for numbering of the CTD stations.

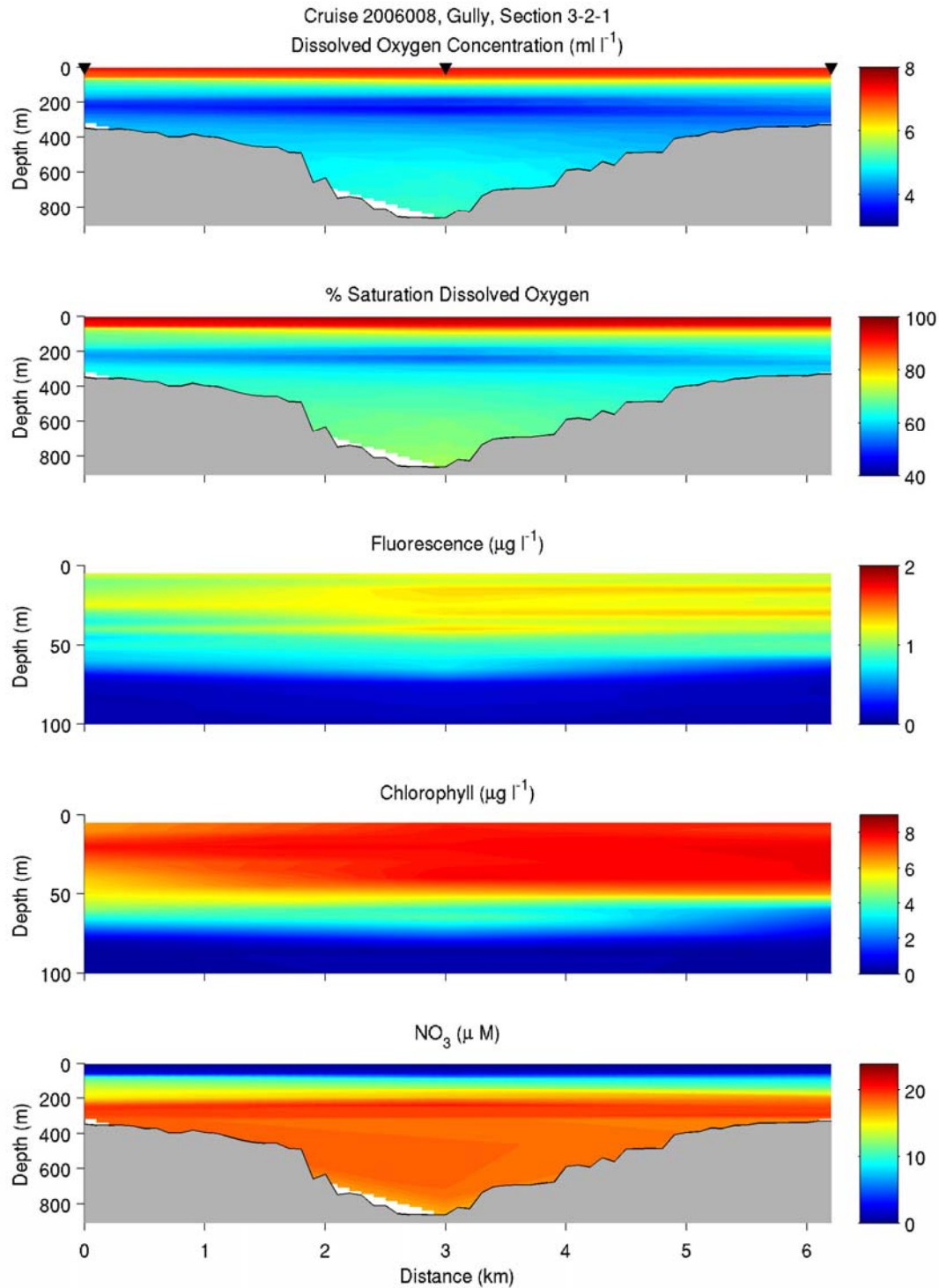


Figure A- 43: Section plots of dissolved oxygen concentration, percent saturation dissolved oxygen, fluorescence, chlorophyll from water samples and nitrate from water samples. Refer to **Figure 1** for numbering of the CTD stations.

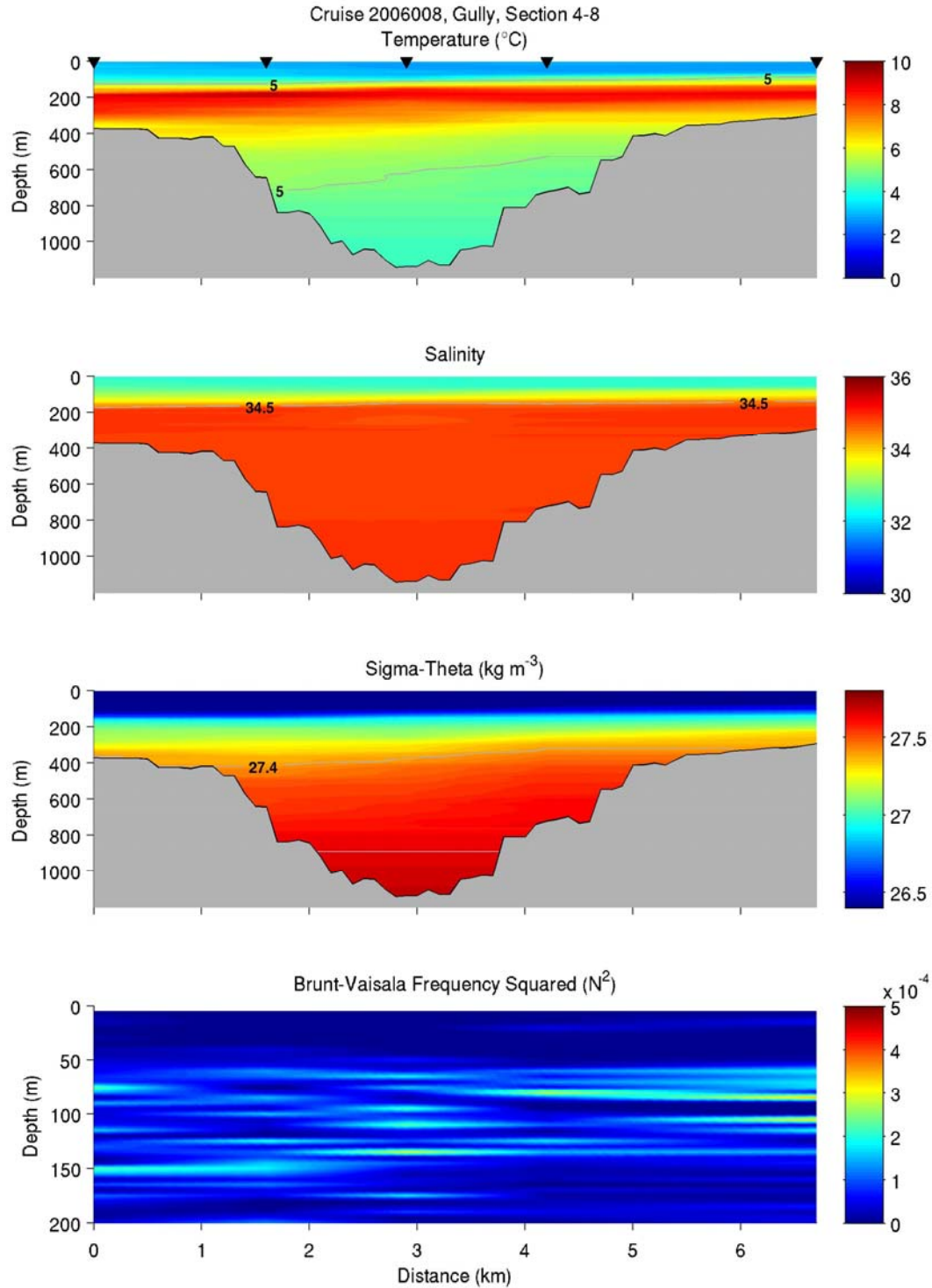


Figure A- 44: Section plots of temperature, salinity, density and Brunt-Vaisala frequency squared. Refer to **Figure 1** for numbering of the CTD stations.

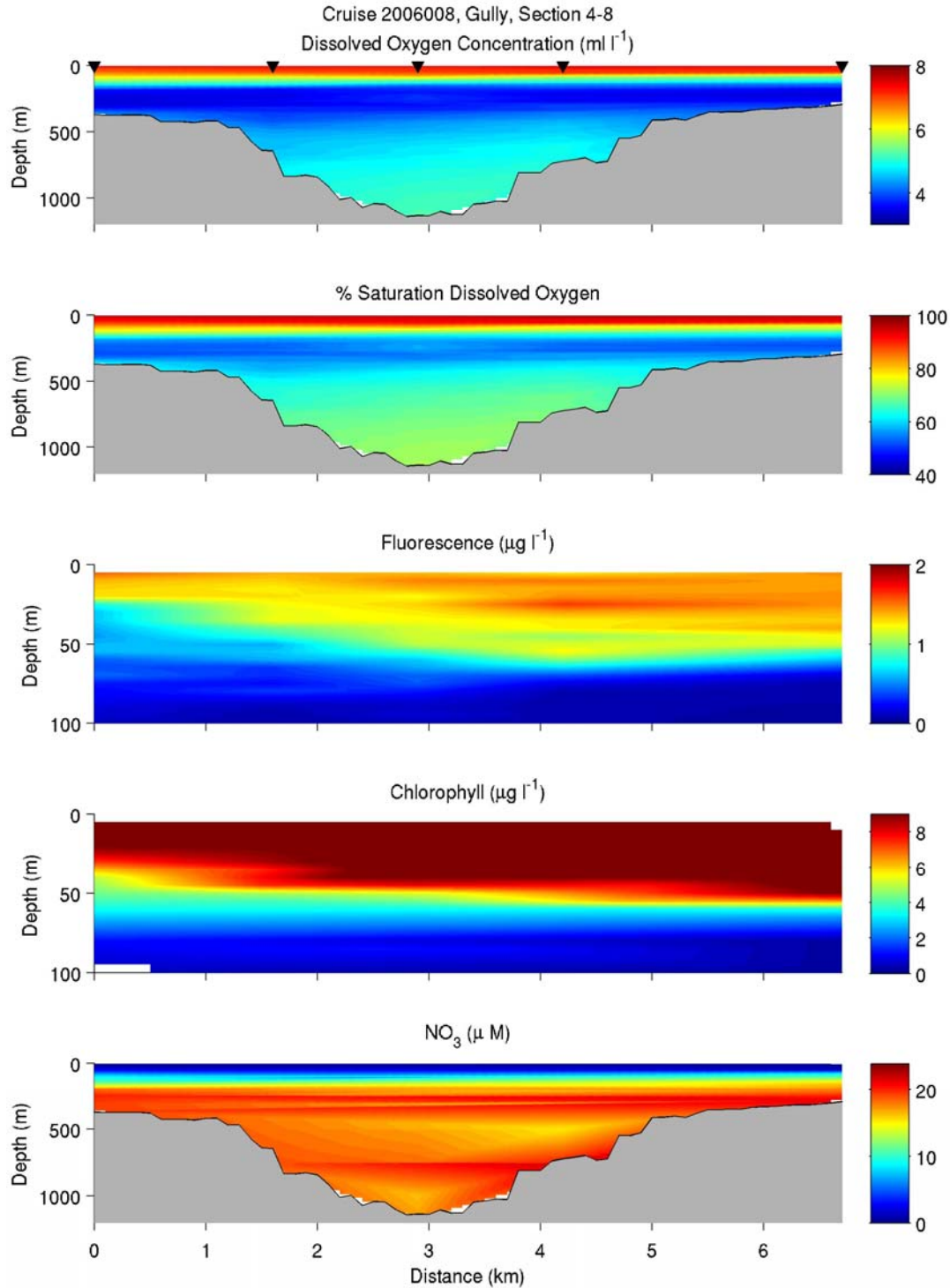


Figure A- 45: Section plots of dissolved oxygen concentration, percent saturation dissolved oxygen, fluorescence, chlorophyll from water samples and nitrate from water samples. Refer to **Figure 1** for numbering of the CTD stations.

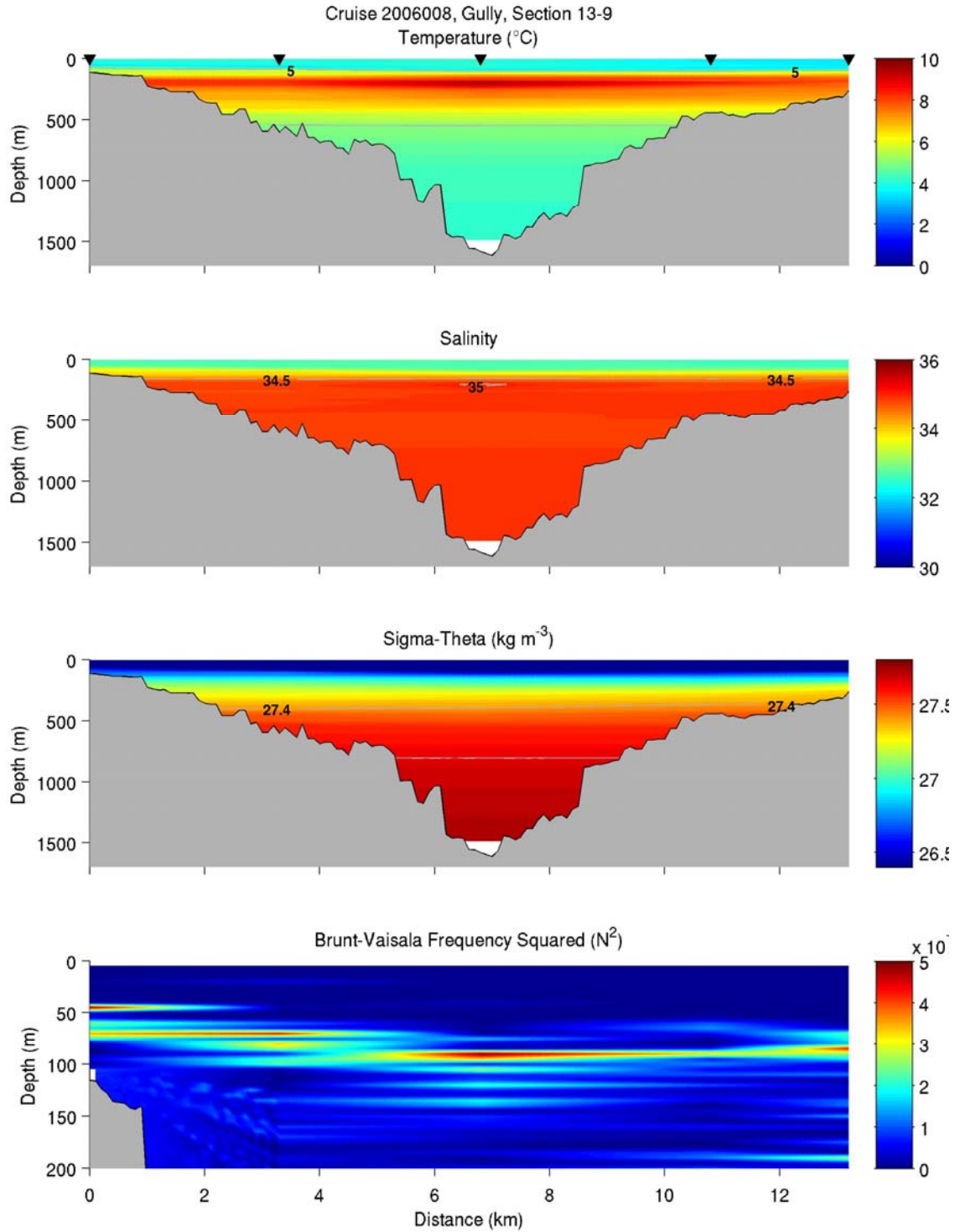


Figure A- 46: Section plots of temperature, salinity, density and Brunt-Vaisala frequency squared. Refer to **Figure 1** for numbering of the CTD stations.

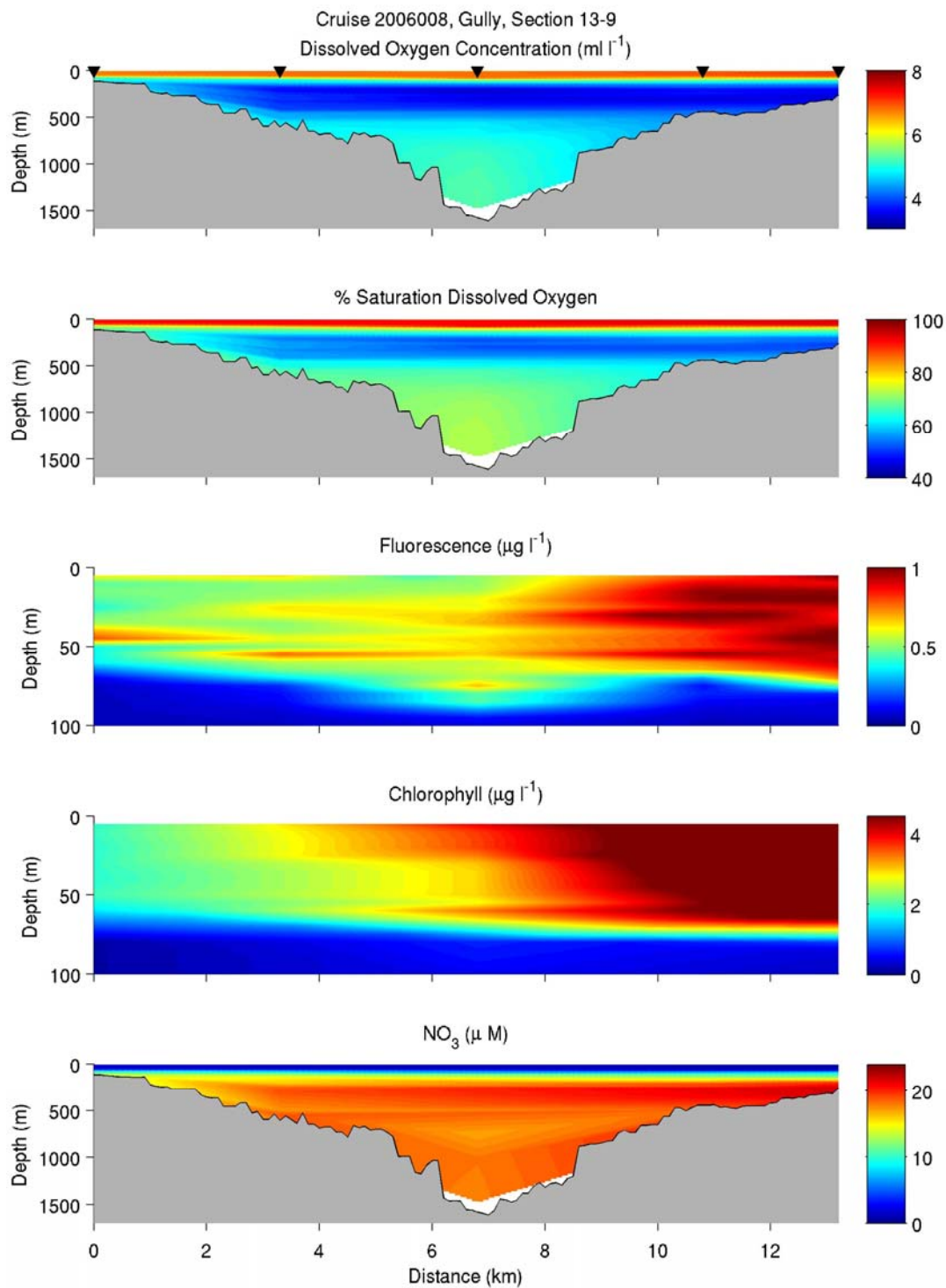


Figure A- 47: Section plots of dissolved oxygen concentration, percent saturation dissolved oxygen, fluorescence, chlorophyll from water samples and nitrate from water samples. Refer to **Figure 1** for numbering of the CTD stations.

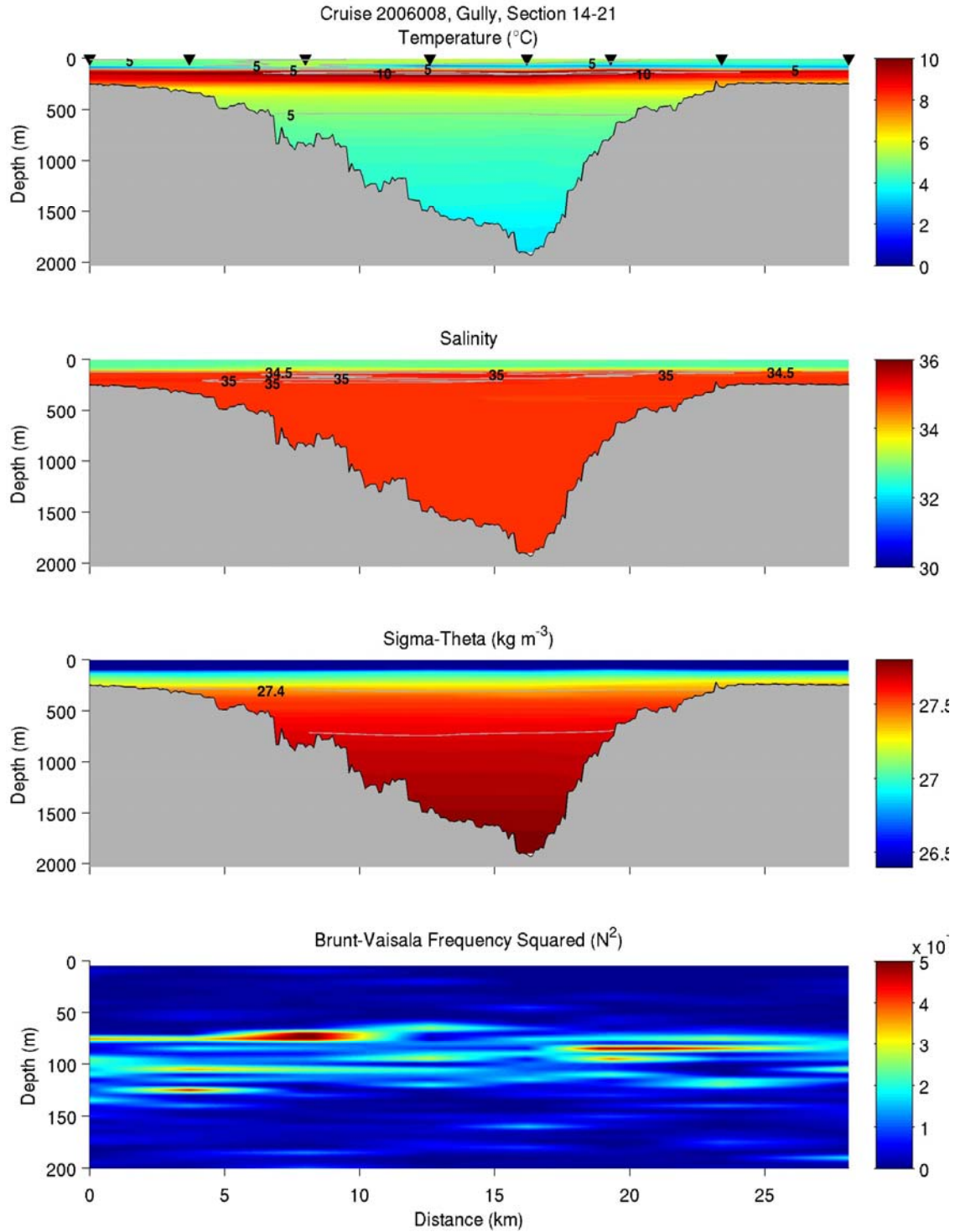


Figure A- 48: Section plots of temperature, salinity, density and Brunt-Vaisala frequency squared. Refer to **Figure 1** for numbering of the CTD stations.

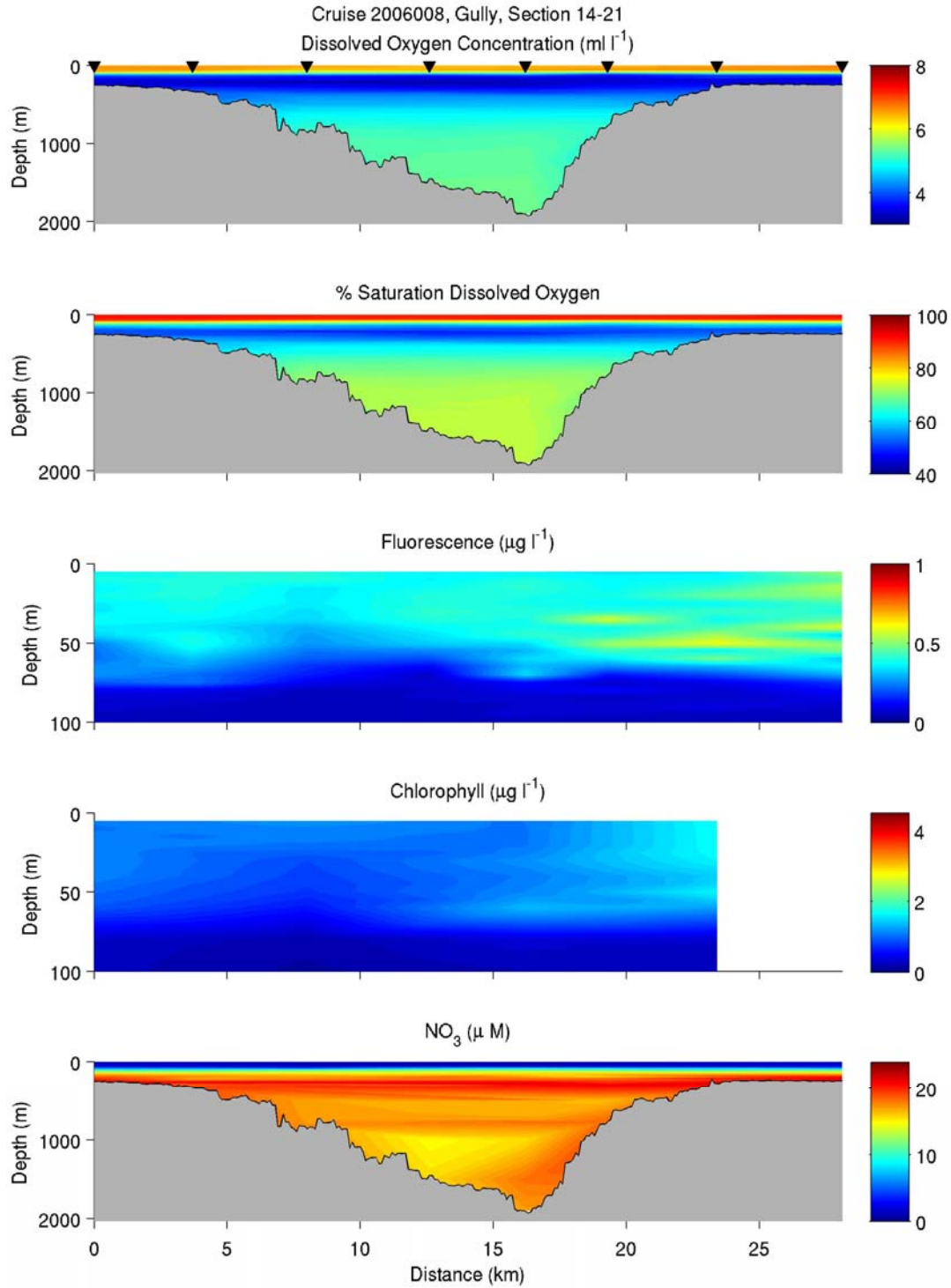


Figure A- 49: Section plots of dissolved oxygen concentration, percent saturation dissolved oxygen, fluorescence, chlorophyll from water samples and nitrate from water samples. Refer to **Figure 1** for numbering of the CTD stations.

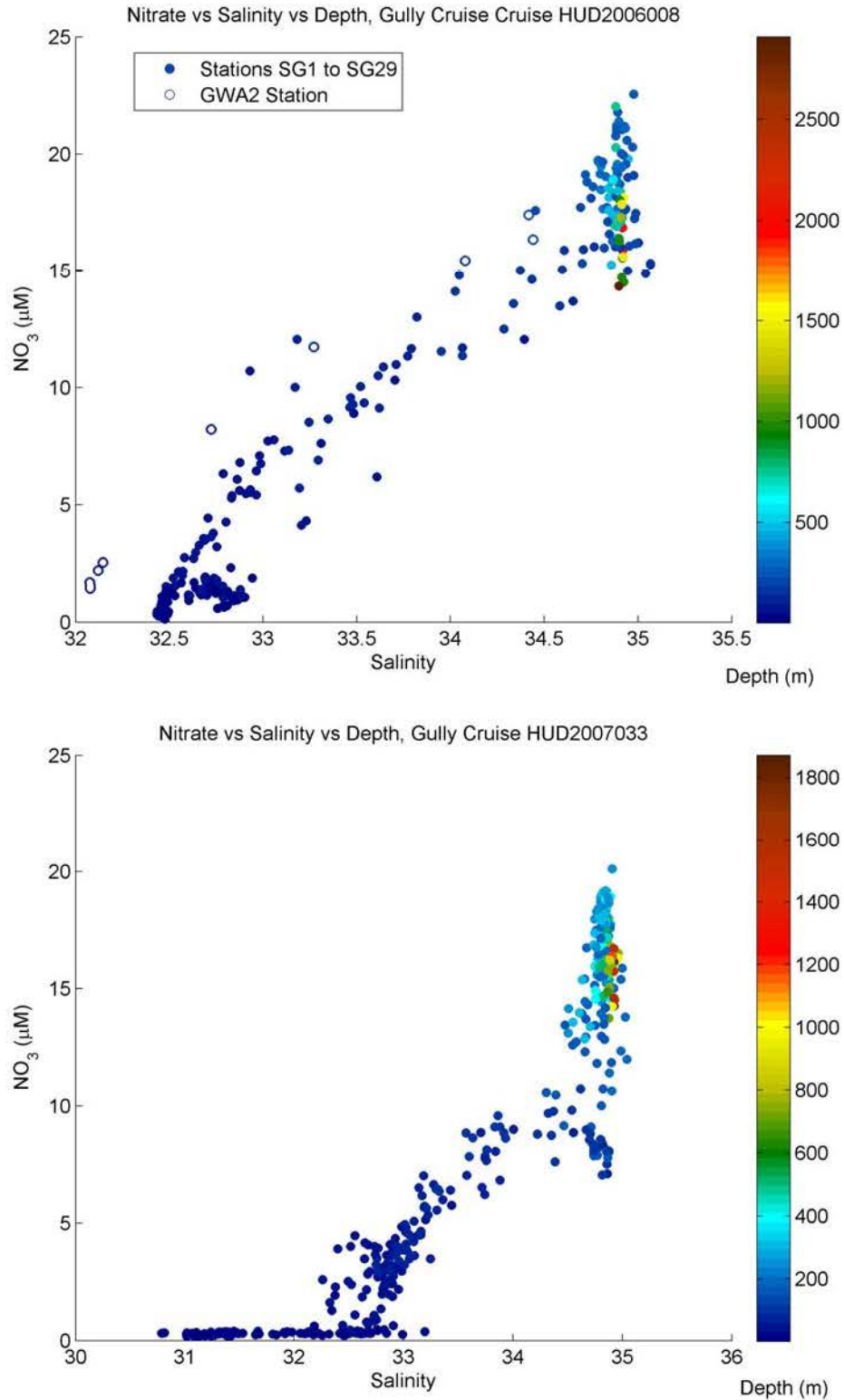


Figure A- 50: Composite plot of nitrate versus salinity data from HUD2006008 and HUD2007033 colour-coded by depth. The GWA2 station is a reference station at 44.2309N 59.5588W, 220 m water depth, which is occasionally sampled by the Atlantic Zone Monitoring Program (AZMP).

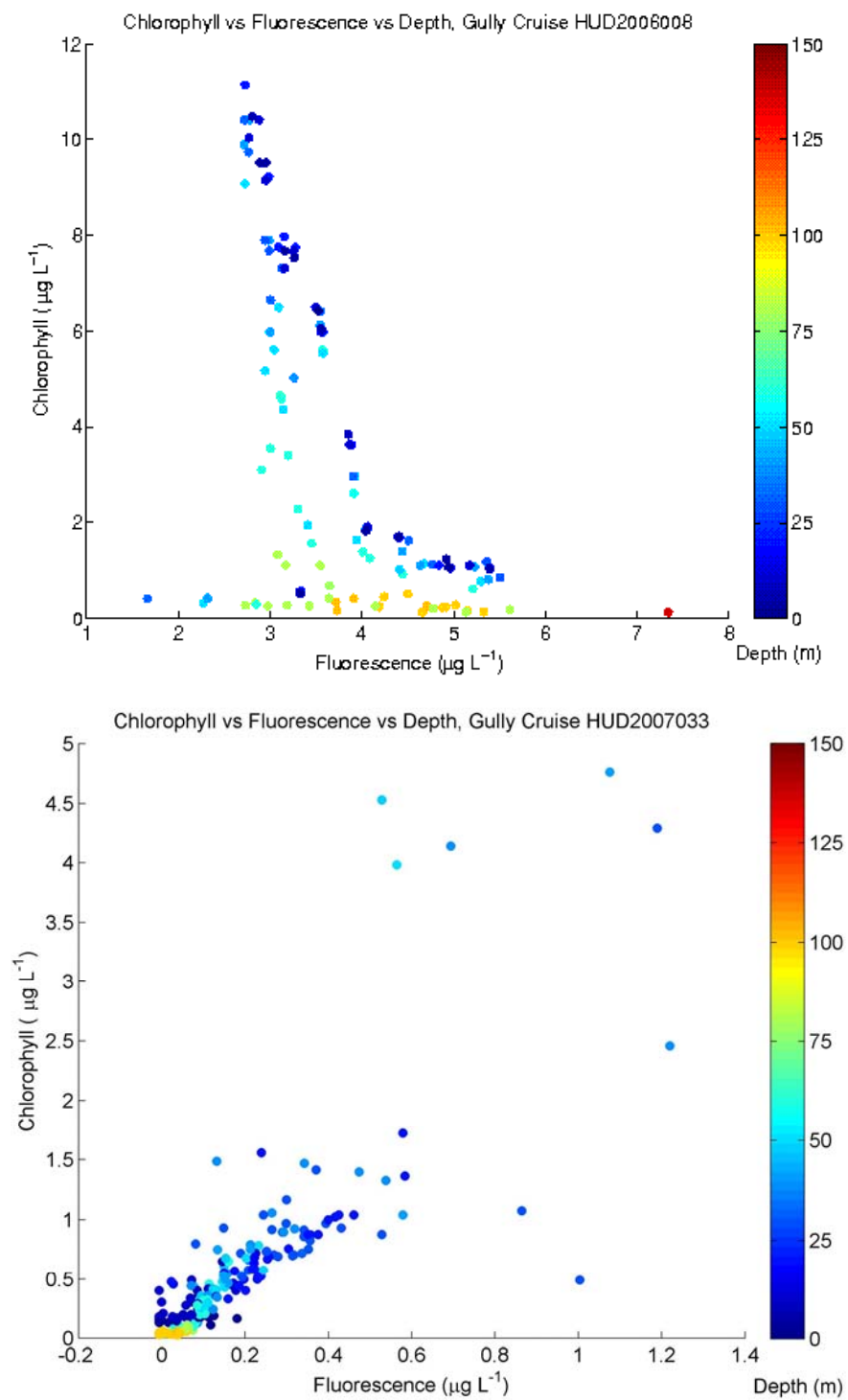


Figure A- 51: Composite plot of chlorophyll versus fluorescence data from HUD2006008 and HUD2007033 colour-coded by depth.

Appendix 4: Biological data from CTD stations, 2007

Biological data were from bottle samples collected during the CTD surveys conducted on the HUD2007-033 cruise from August 2-8, 2007 at sites SG1 through SG29 (**Figure 1**). CTD surveys were completed with Sea-Bird 911 CTD and 24-bottle rosette. Section plots were created for bacteria, *Synechococcus*, picoeukaryotes and nanophytoplankton (Figure A- 52 to Figure A- 57).

Bubble plots were also generated for all the biological data integrated from 0 to 100 m (Figure A- 58).

All plots were created using MATLAB R2008b.

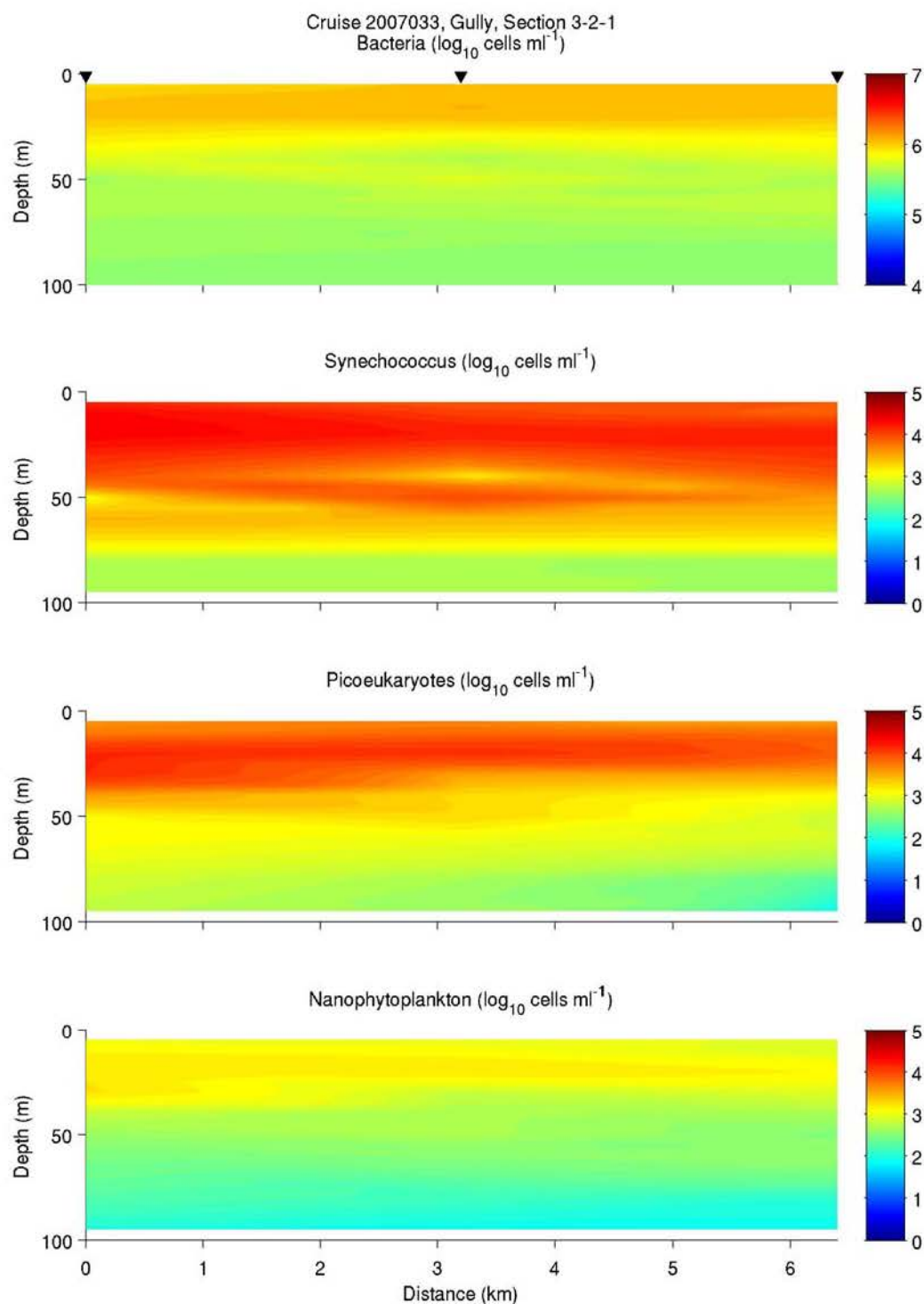


Figure A- 52: Section plots for bacteria, *Synechococcus*, picoeukaryotes and nanophytoplankton. Refer to Figure 1 for numbering of the CTD stations.

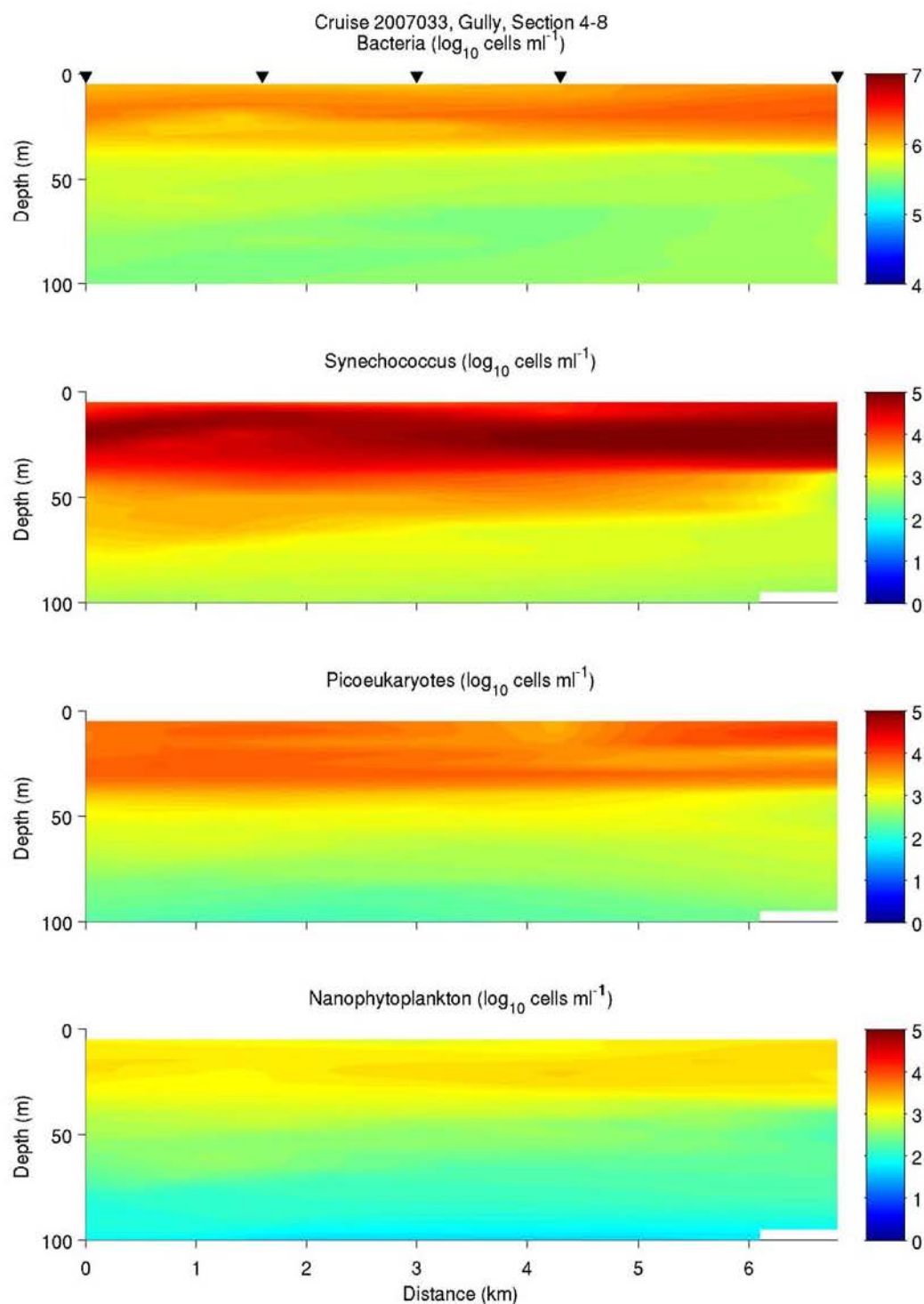


Figure A- 53: Section plots for bacteria, Synechococcus, Picoeukaryotes and Nanophytoplankton versus distance. Refer to Figure 1 for numbering of the CTD stations.

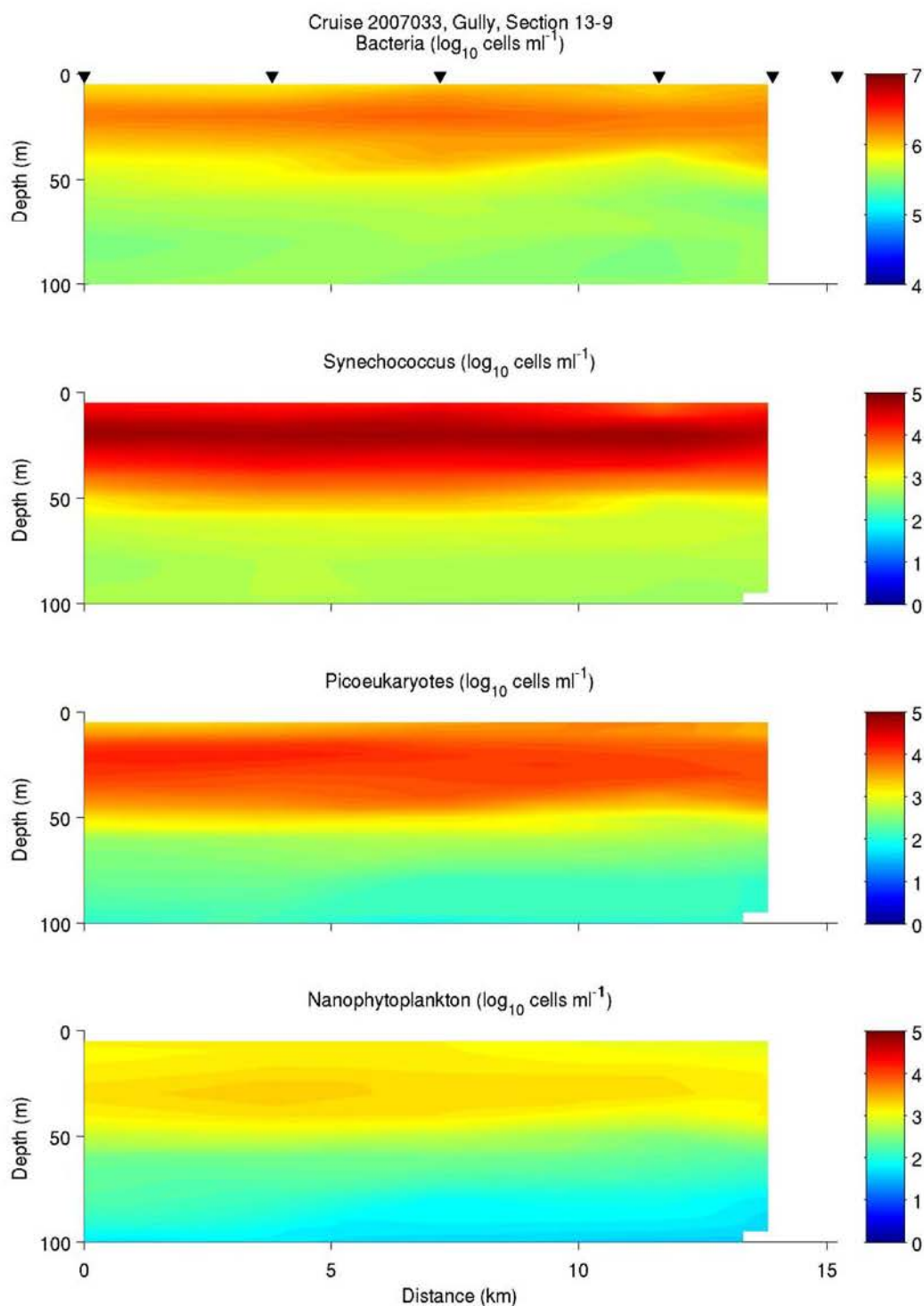


Figure A- 54: Section plots for bacteria, Synechococcus, Picoeukaryotes and Nanophytoplankton versus distance. Refer to Figure 1 for numbering of the CTD stations.

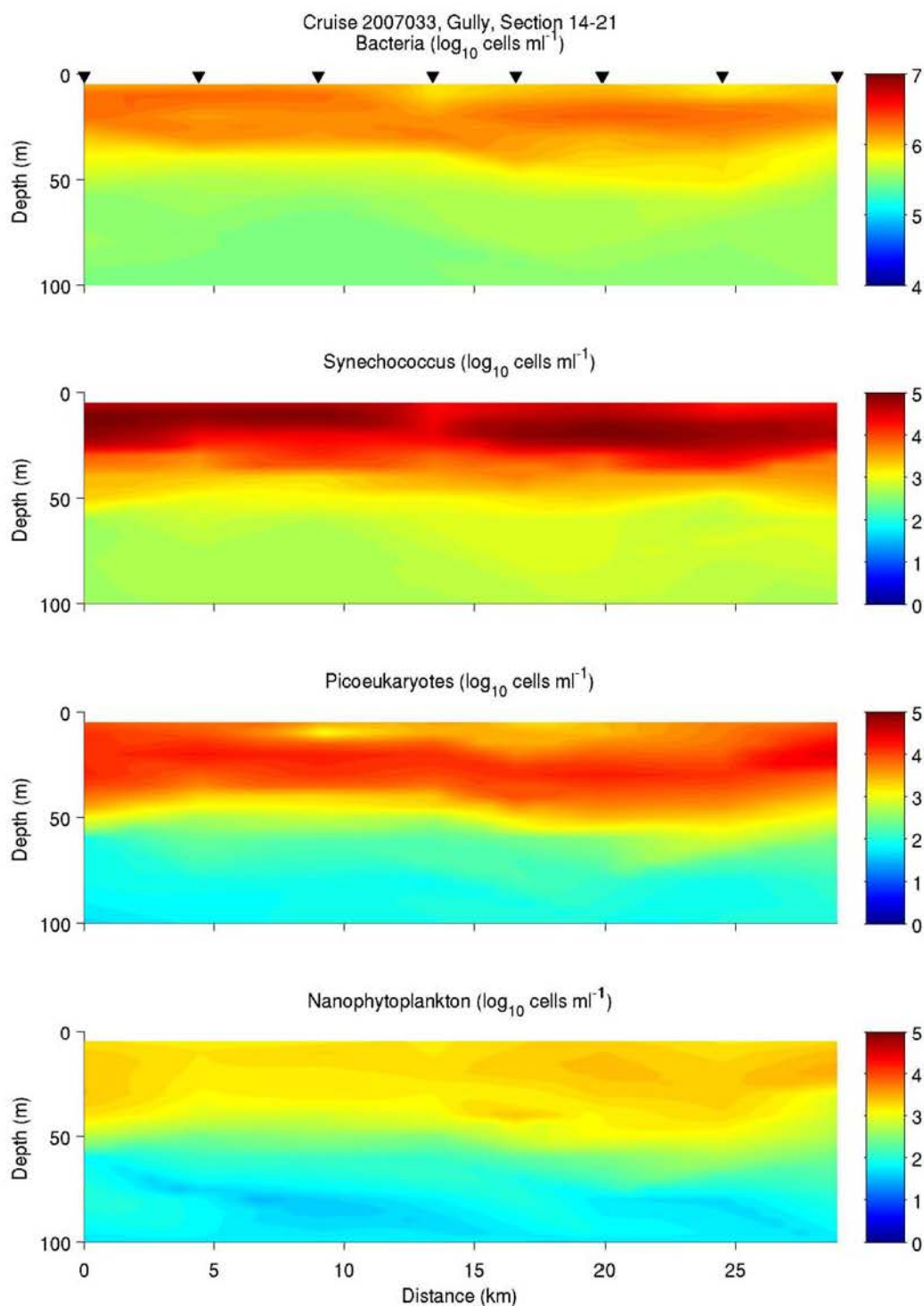


Figure A- 55: Section plots for bacteria, Synechococcus, Picoeukaryotes and Nanophytoplankton versus distance. Refer to Figure 1 for numbering of the CTD stations.

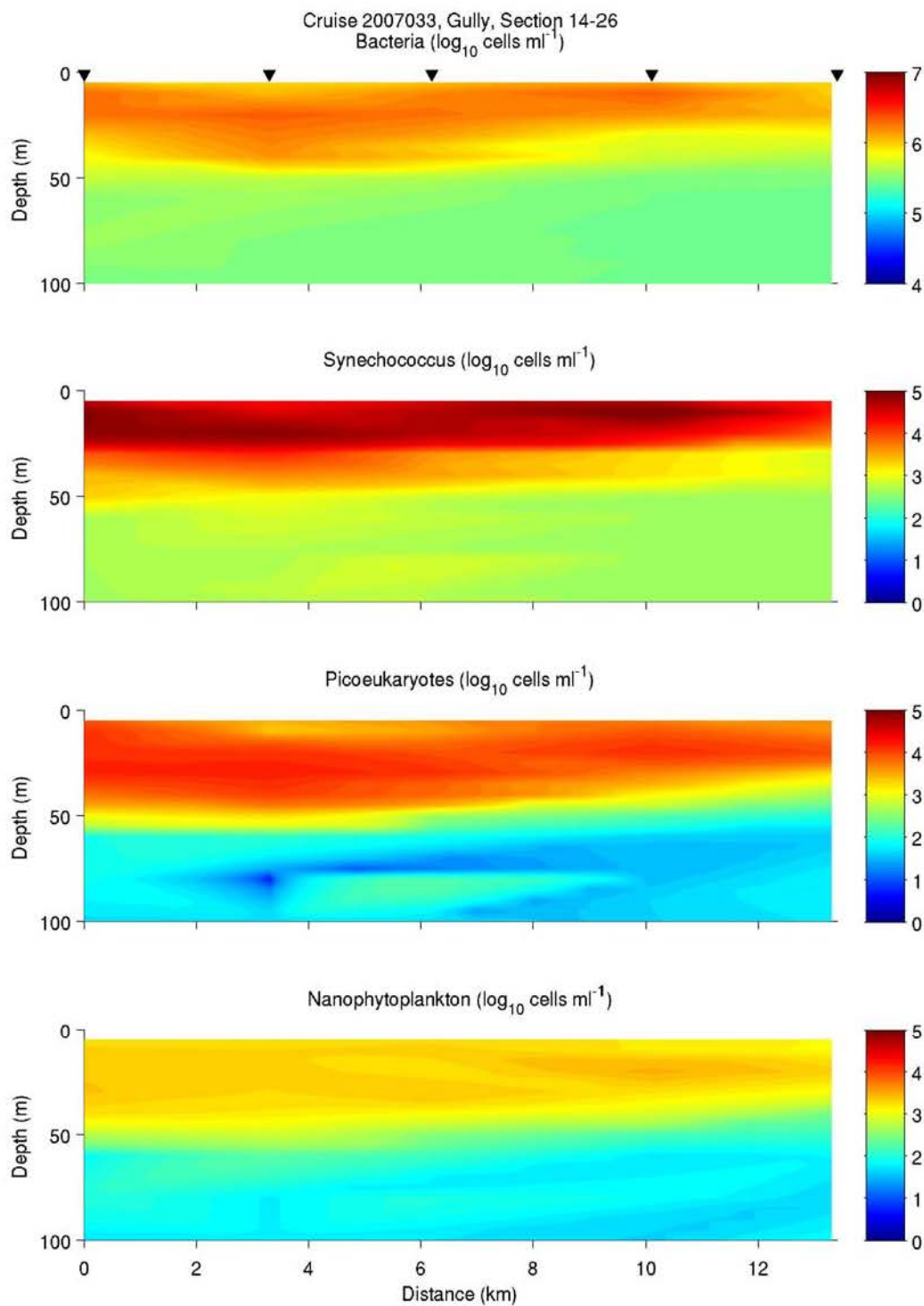


Figure A- 56: Section plots for bacteria, Synechococcus, Picoeukaryotes and Nanophytoplankton versus distance. Refer to Figure 1 for numbering of the CTD stations.

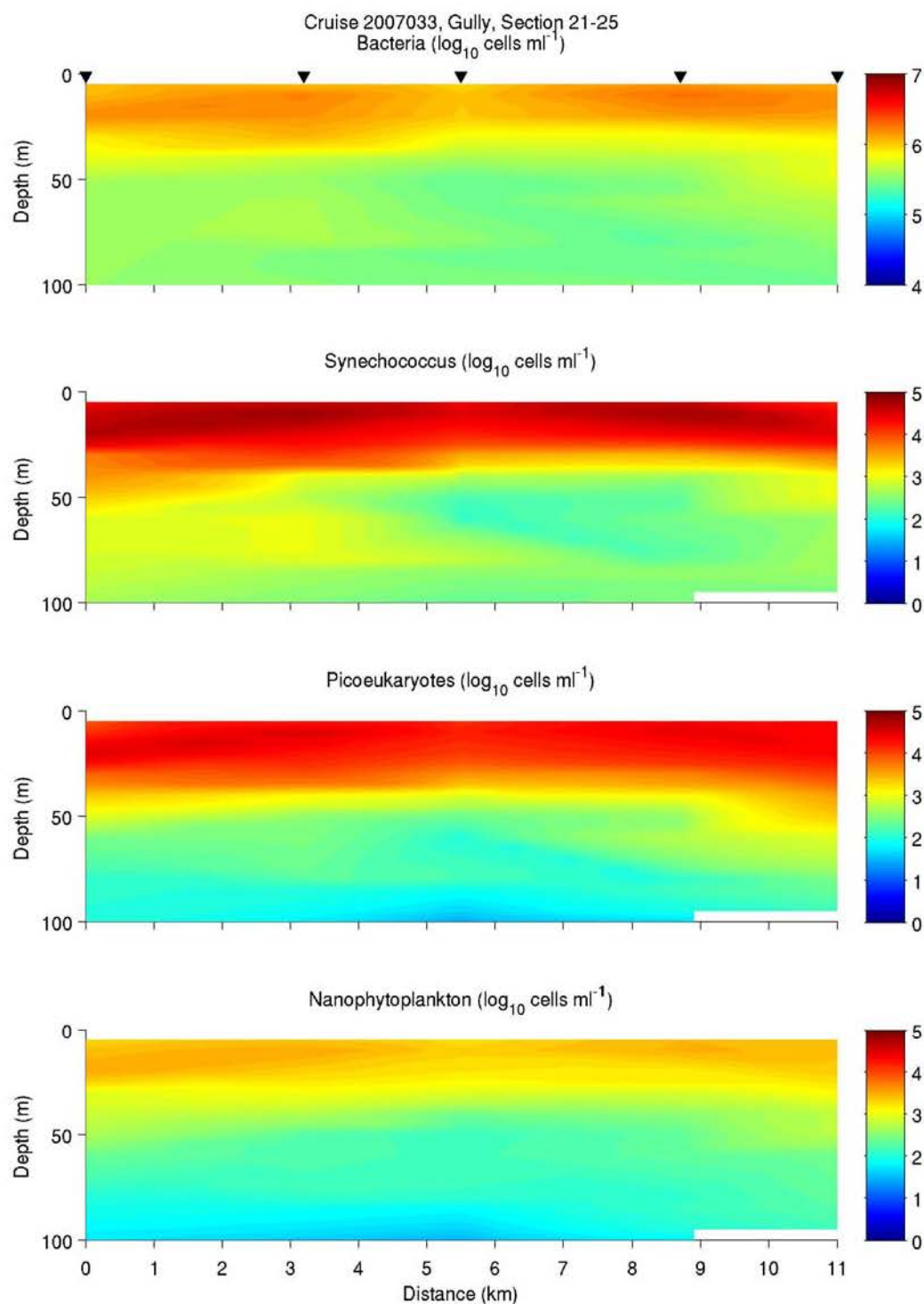


Figure A- 57: Section plots for bacteria, Synechococcus, Picoeukaryotes and Nanophytoplankton versus distance. Refer to Figure 1 for numbering of the CTD stations.

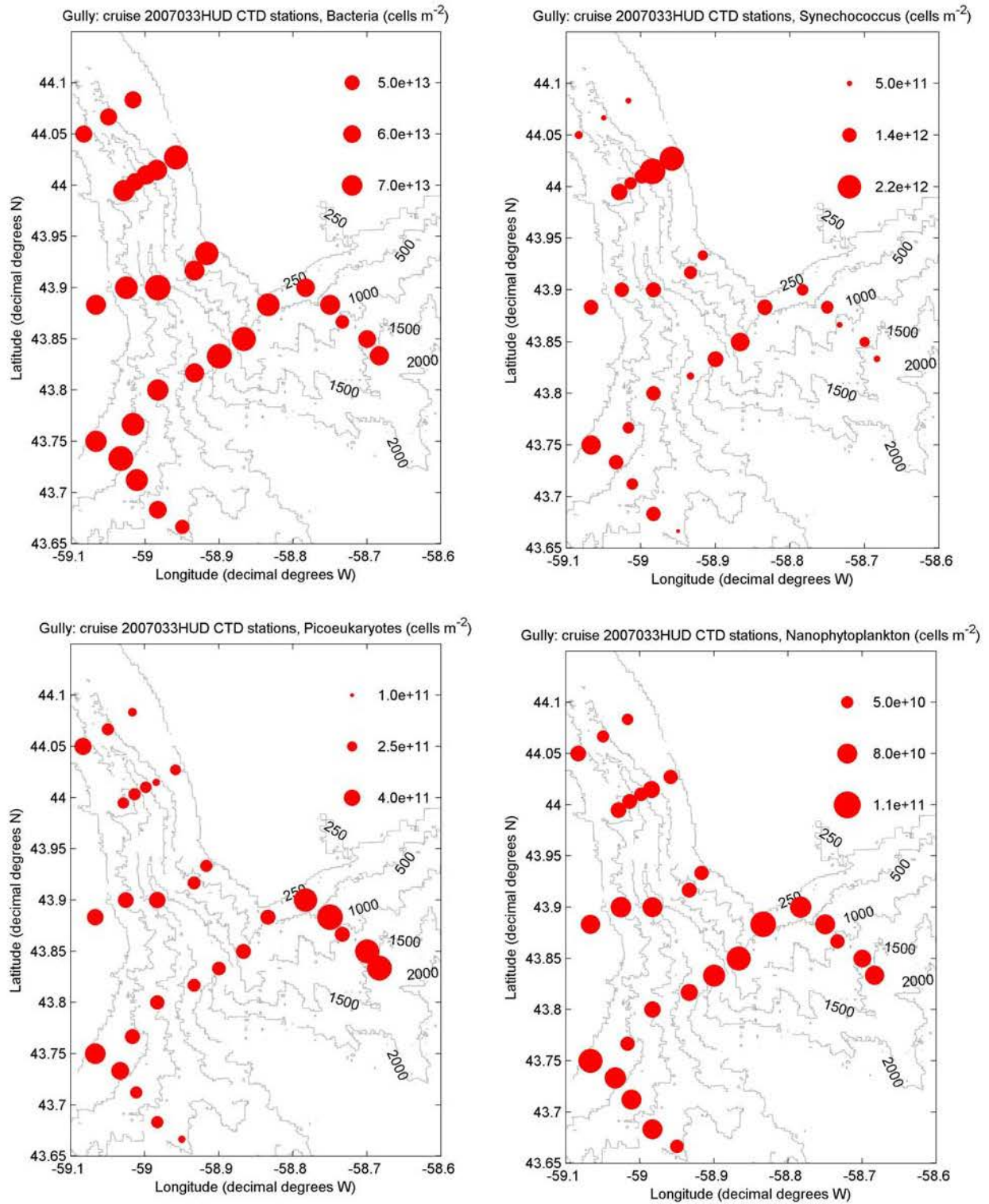


Figure A- 58: Bubble plots for bacteria, *Synechococcus*, Picoeukaryotes and Nanophytoplankton versus distance. Refer to the legend in the upper right of each panel for concentration values.

Appendix 5: Acoustic Doppler Current Profiler (ADCP) Moored Current Meter

Four moorings were deployed at the sites SG2 (mooring #1588), SG10 (mooring #1591), SG11 (mooring #1589), SG12 (mooring #1590), in Zone 1 of the Gully (**Figure 1**), each had an RDI ADCP current profiler (Appendix 1). The moorings were deployed April 23 and 24, 2006 and recovered on August 3, 2007. The deep central mooring at SG11 was missing the upper 200 m, which included the ADCP, when recovered; it went missing on 17 June, 2007. Also the two moorings on the canyon axis (#1588 and #1589) were frequently pulled deeper in the strong flows, with the top of mooring 1589 dipping nearly 500 m at times.

Figure A- 59 to Figure A- 66 are contour time series plots of currents, vertical shear and percentage of good pings. Figure A- 67 to Figure A- 74 are current time series plots for depth binned data, the percent of data return is given on each plot. Figure A- 75 to Figure A- 79 are stick plots of daily averaged U and V speed components.

All plots were created using MATLAB R2008b.

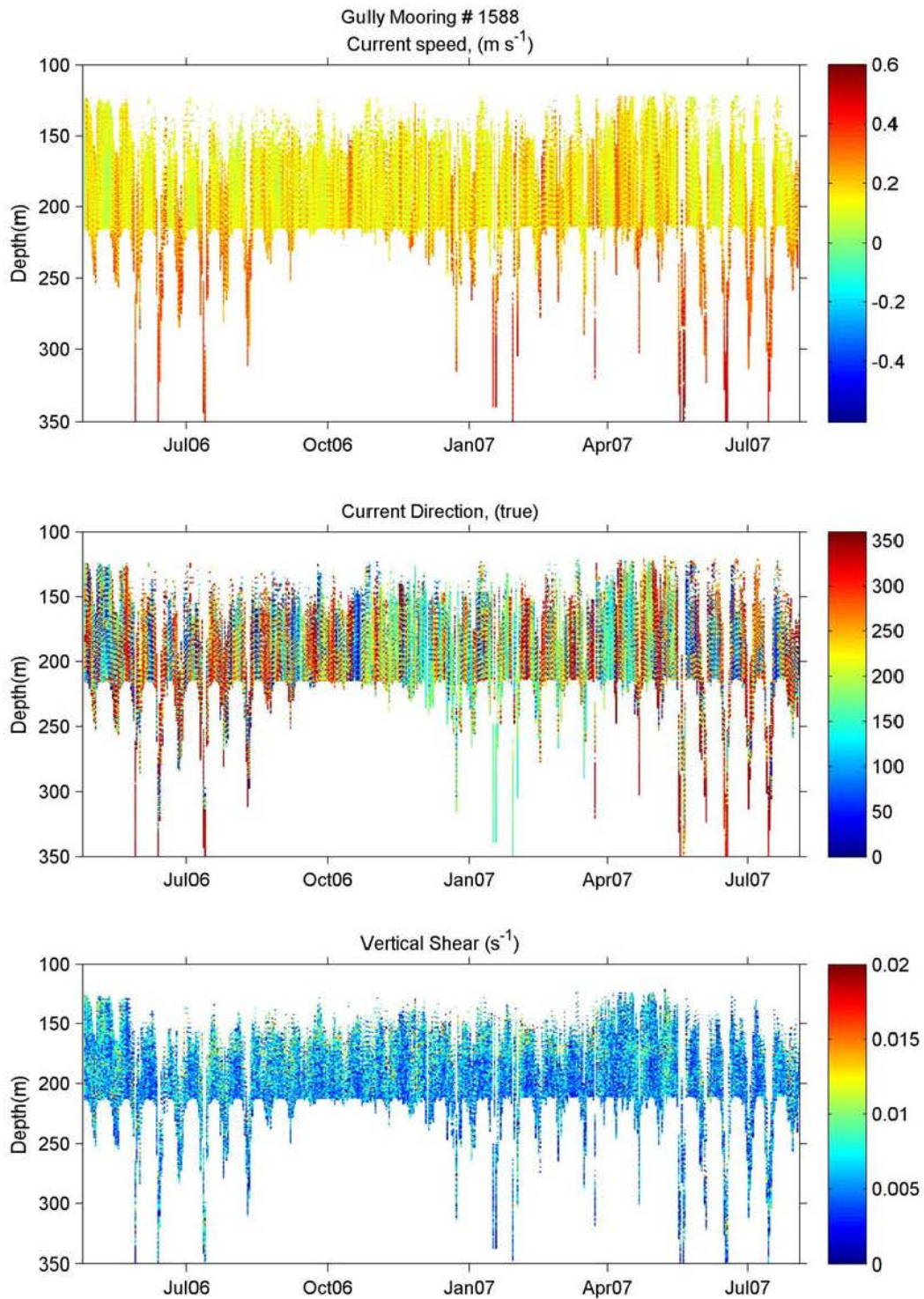


Figure A- 59: Time series of speed, direction and vertical shear from upward-looking ADCP on mooring 1588 (SG2). Changing depth bins with time are a result of mooring knockdown.

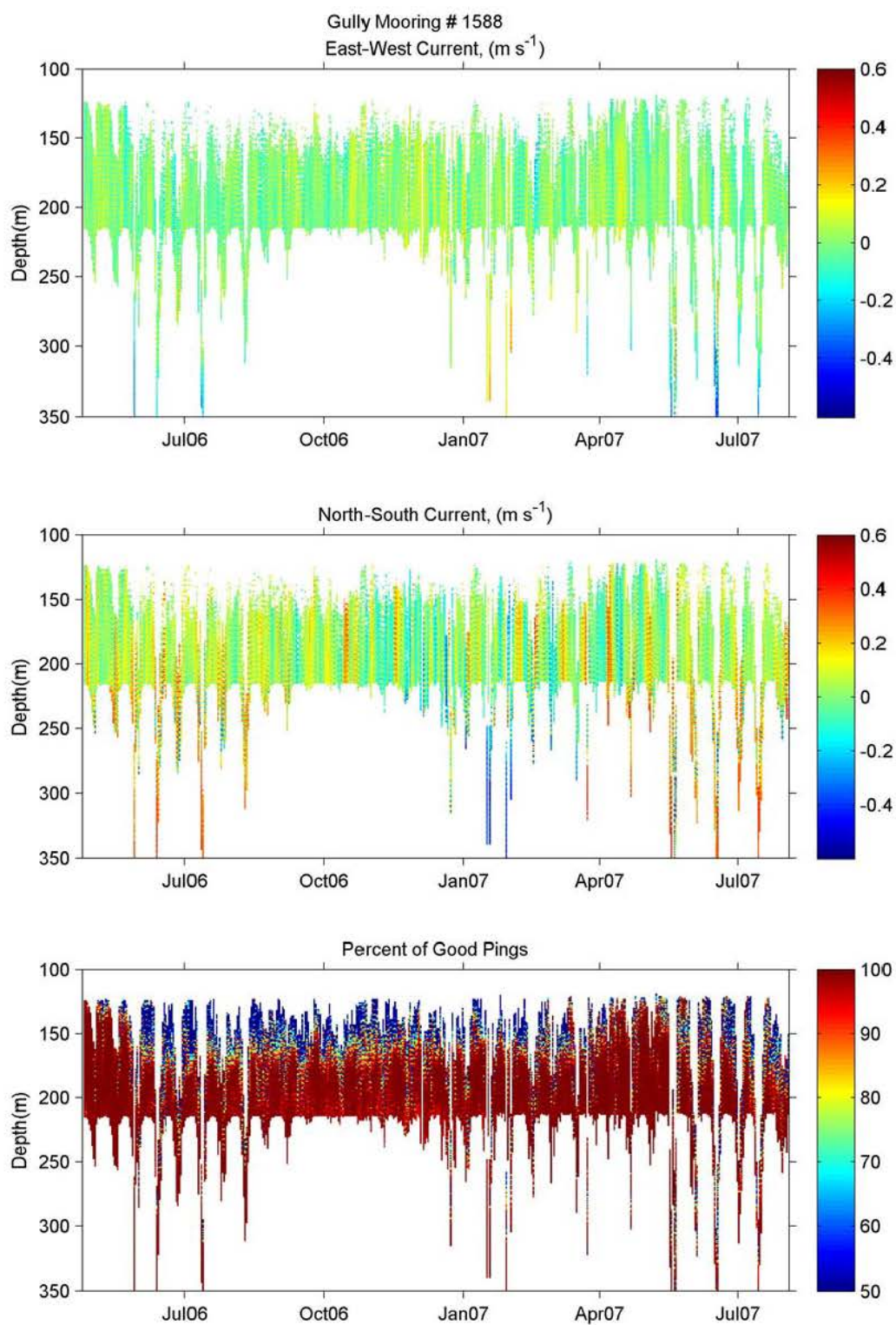


Figure A- 60: Time series of east-west and north-south speed components and percent good pings from upward-looking ADCP on mooring 1588 (SG2). Changing depth bins with time are a result of mooring knockdown.

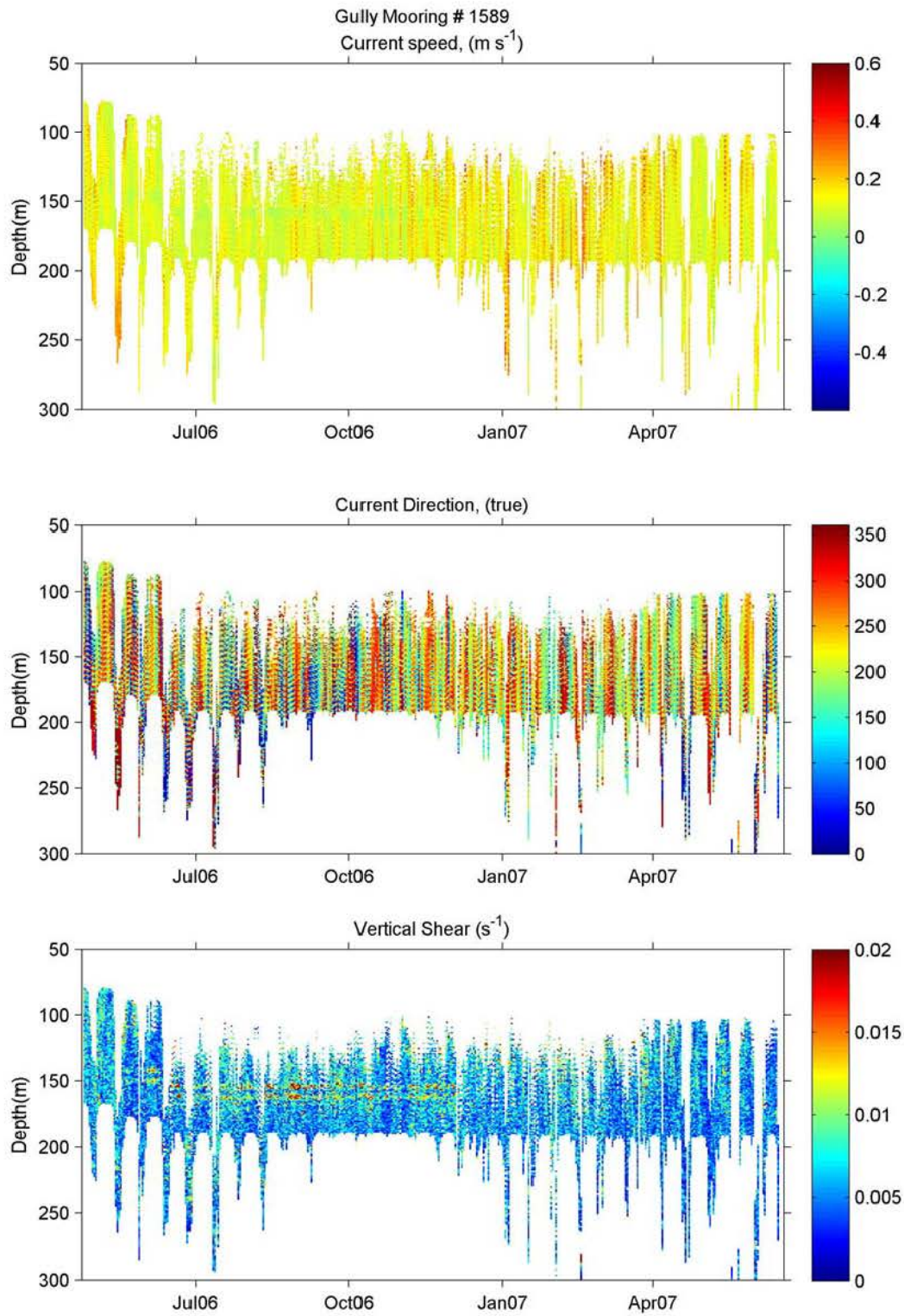


Figure A- 61: Time series of speed, direction and vertical shear from upward-looking ADCP on mooring 1589 (SG11). Changing depth bins with time are a result of mooring knockdown.

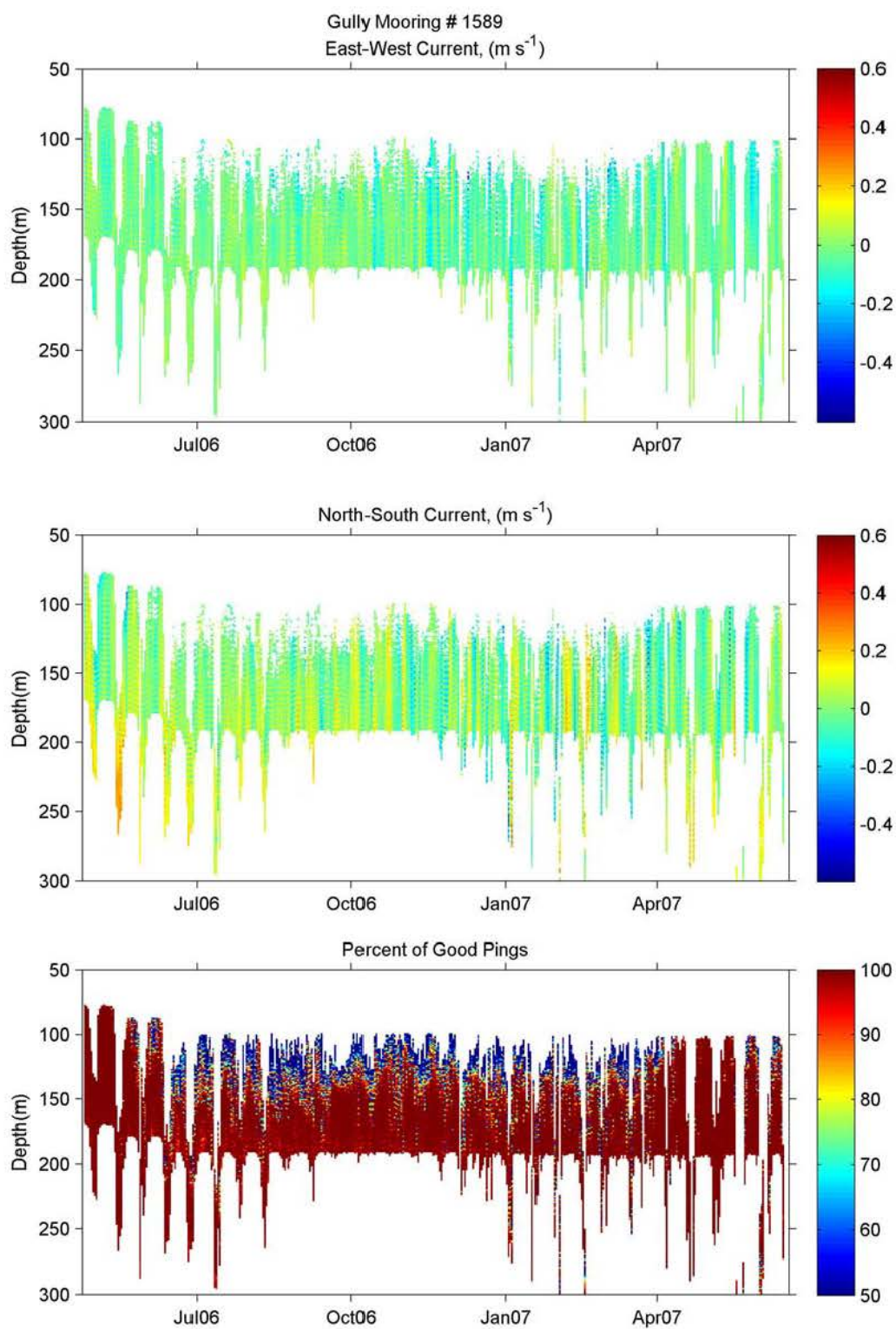


Figure A- 62: Time series of east-west and north-south speed components and percent good pings from upward-looking ADCP on mooring 1589 (SG11). Changing depth bins with time are a result of mooring knockdown.

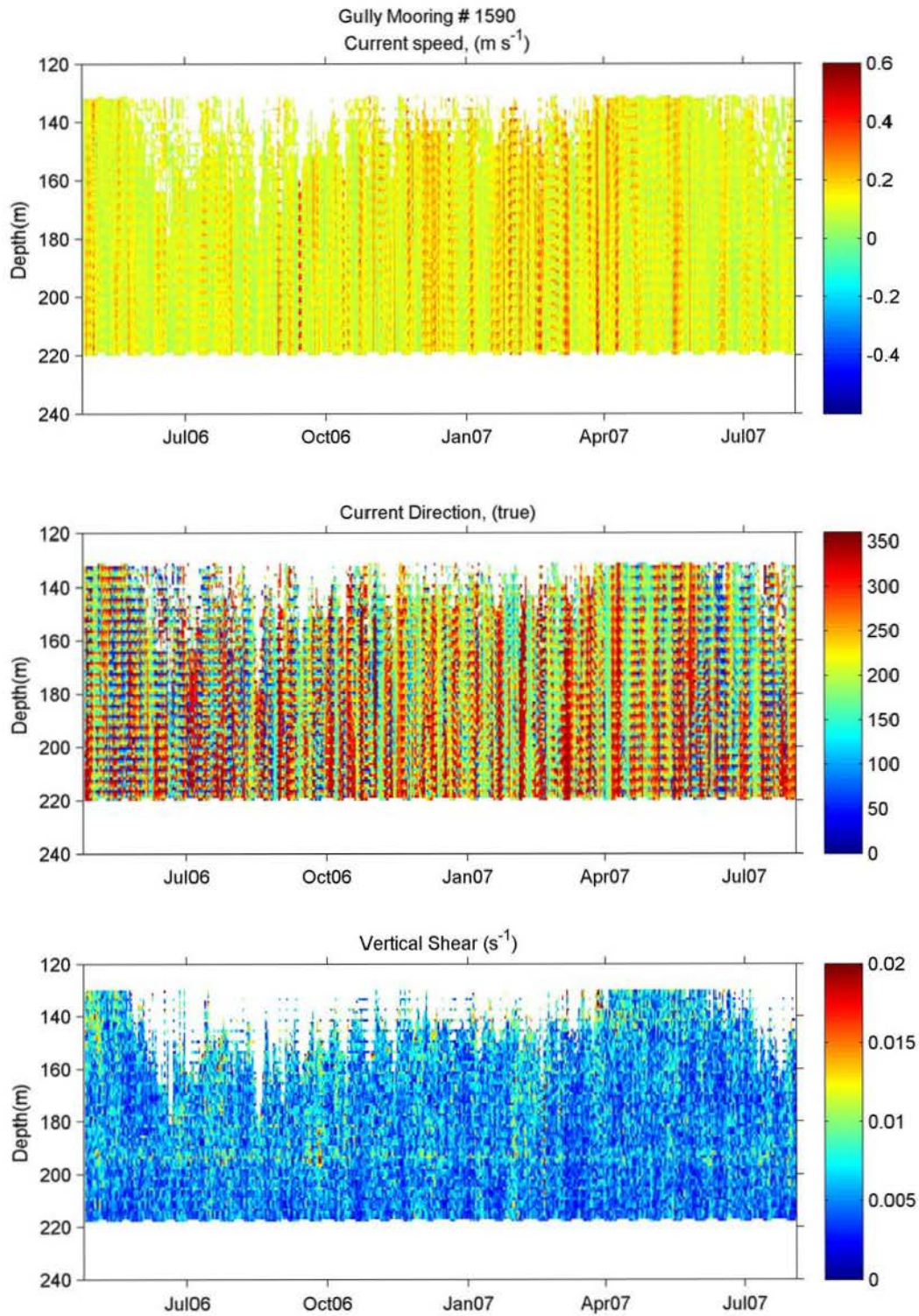


Figure A- 63: Time series of speed, direction and vertical shear from upward-looking ADCP on mooring 1590 (SG12). Changing depth bins with time are a result of mooring knockdown.

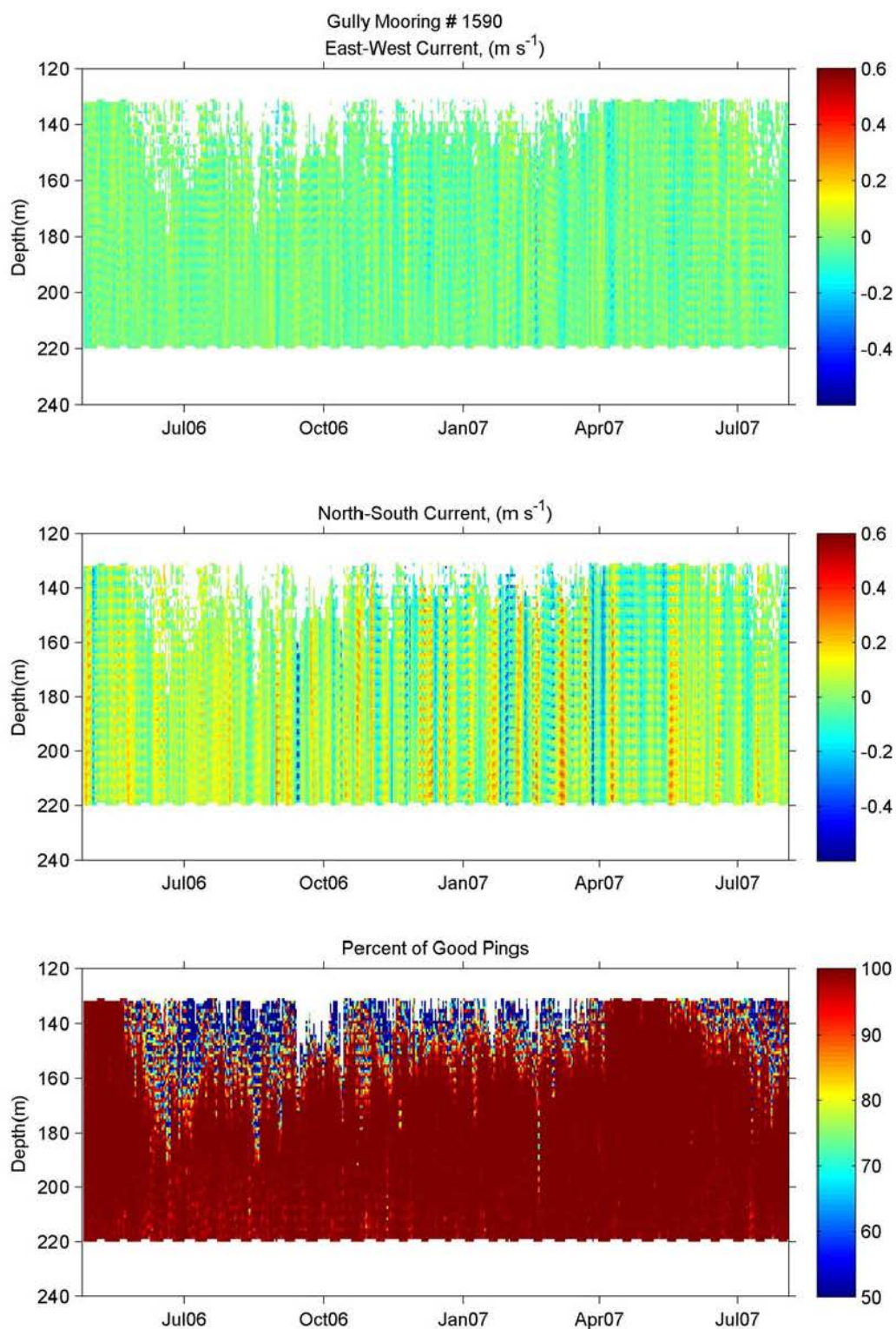


Figure A- 64: Time series of east-west and north-south speed components and percent good pings from upward-looking ADCP on mooring 1590 (SG12). Changing depth bins with time are a result of mooring knockdown.

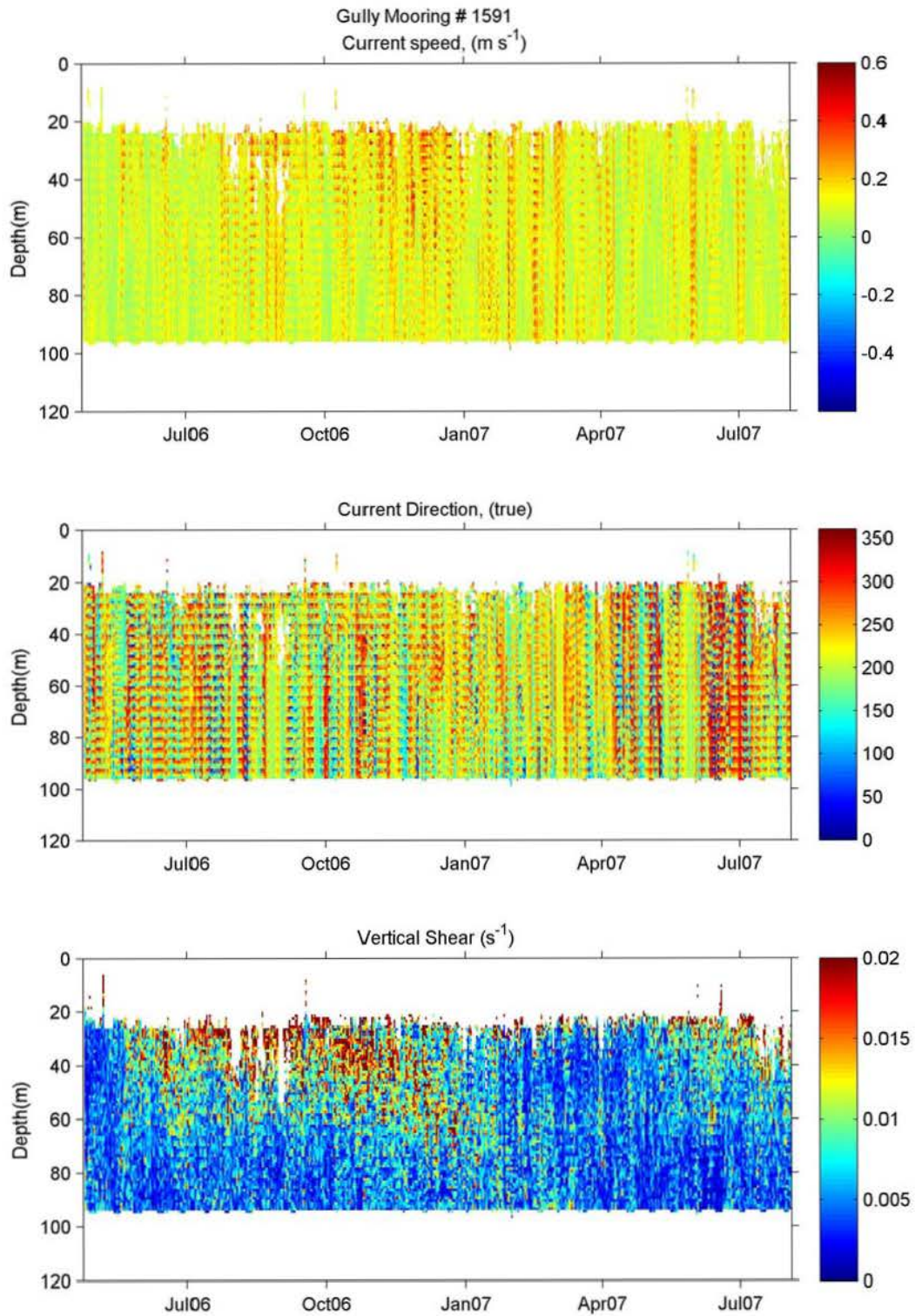


Figure A- 65: Time series of speed, direction and vertical shear from upward-looking ADCP on mooring 1591 (SG10). Changing depth bins with time are a result of mooring knockdown.

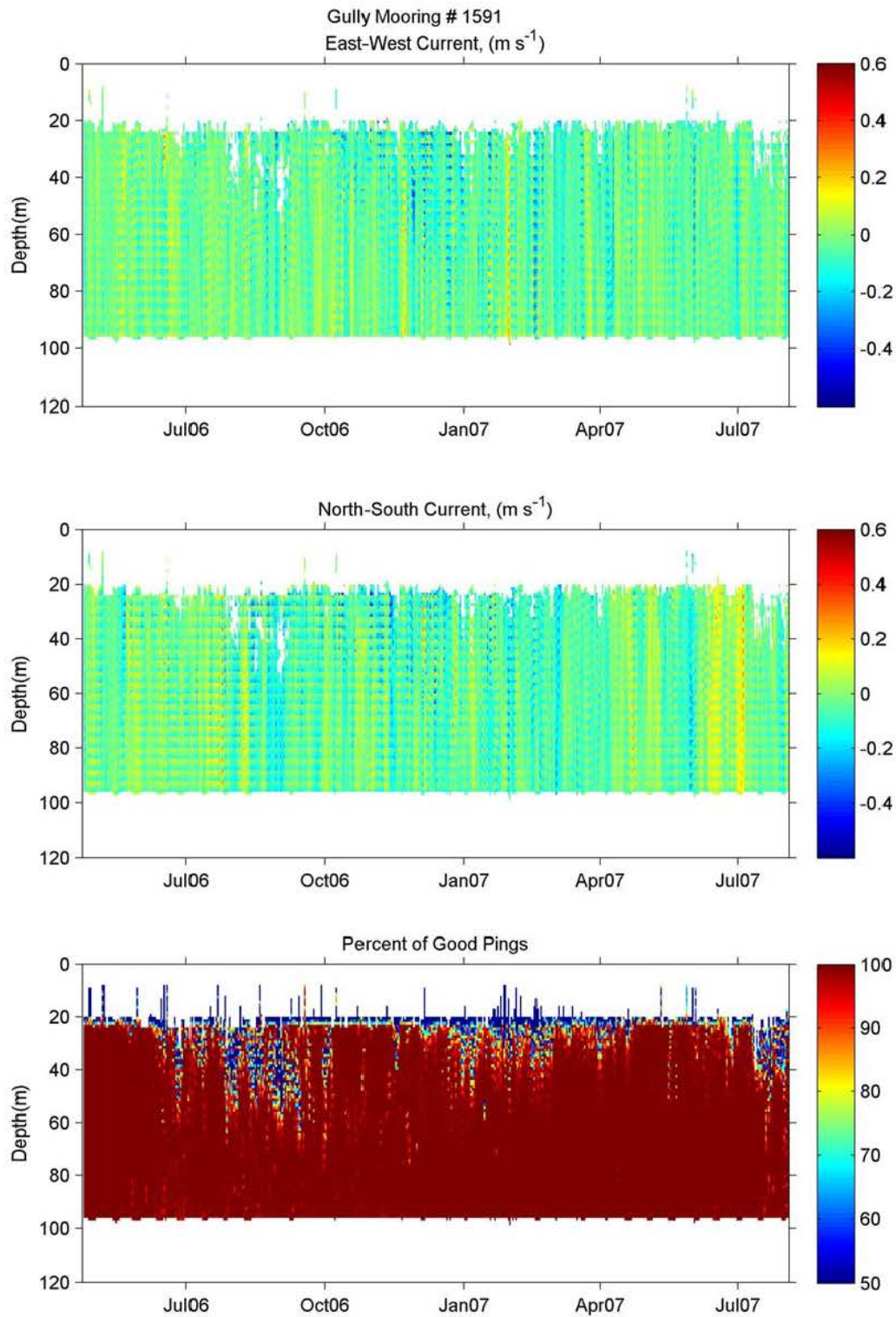


Figure A- 66: Time series of east-west and north-south speed components and percent good pings from upward-looking ADCP on mooring 1591 (SG10). Changing depth bins with time are a result of mooring knockdown.

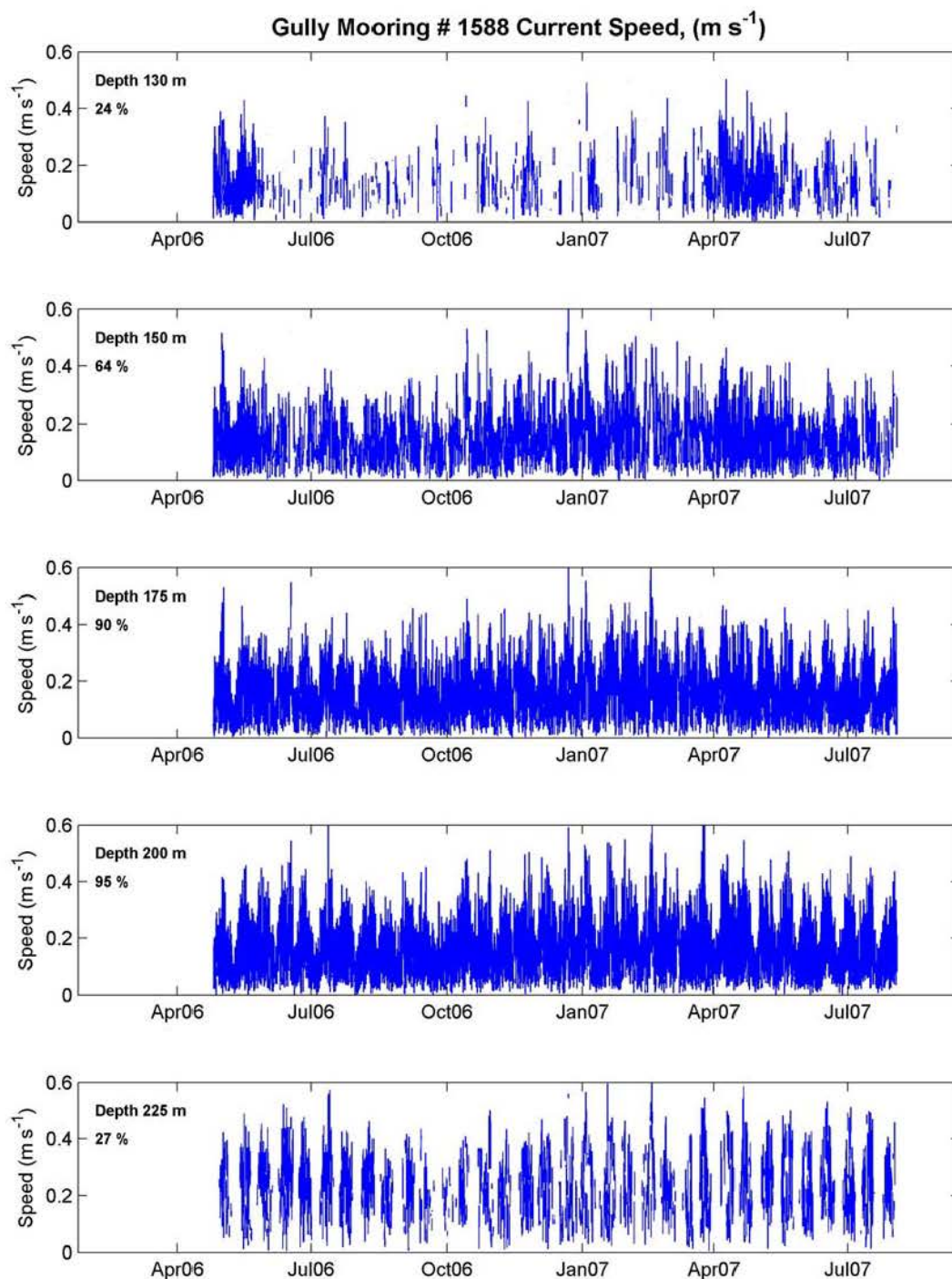


Figure A- 67: ADCP time series of current speed in 25-m averaged bins centered at the depths indicated in the panels. The percent of time with data available in the bin is indicated by the number below the depth bin.

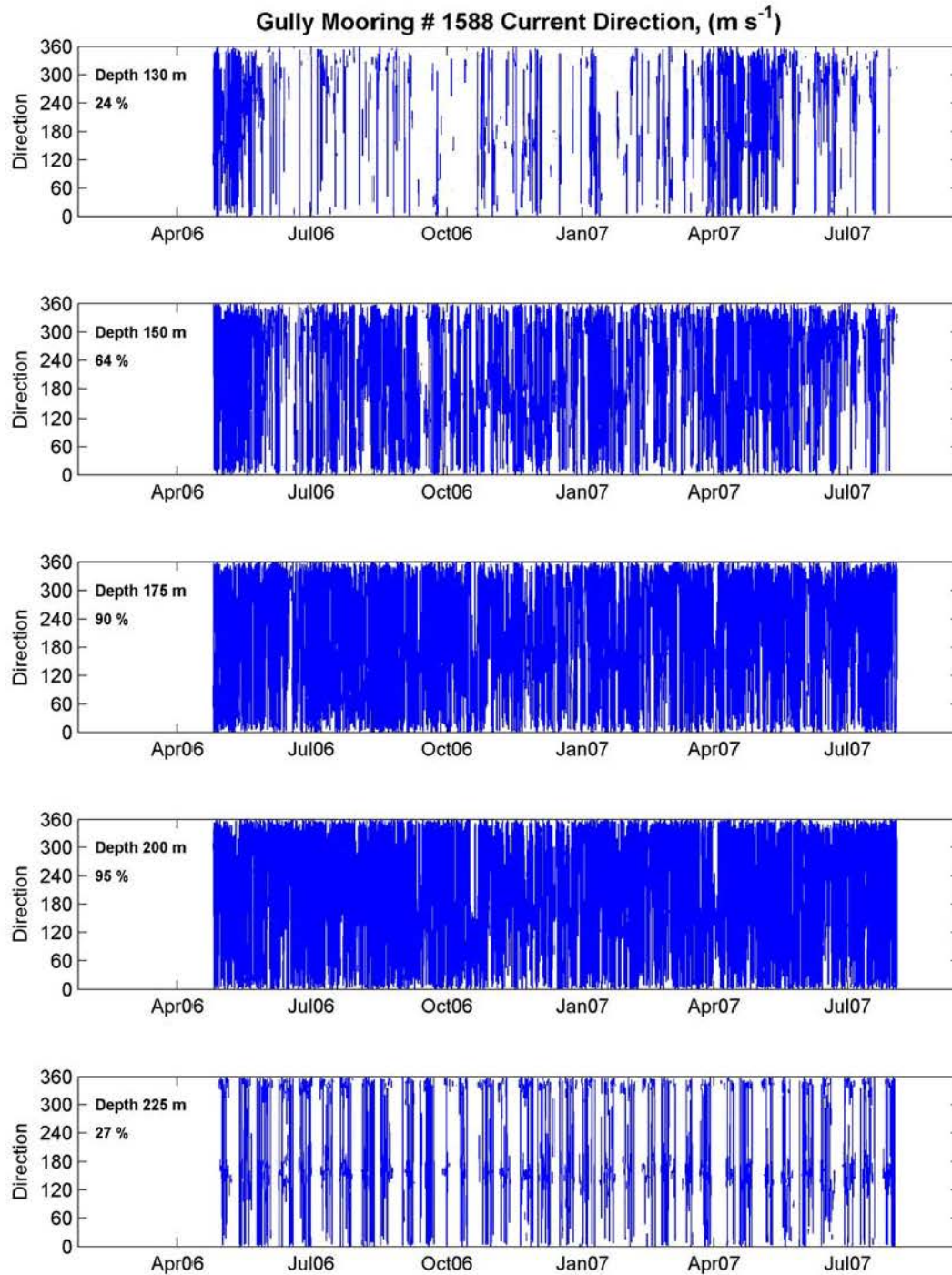


Figure A- 68: ADCP time series of current direction in 25-m averaged bins centered at the depths indicated in the panels. The percent of time with data available in the bin is indicated by the number below the depth bin.

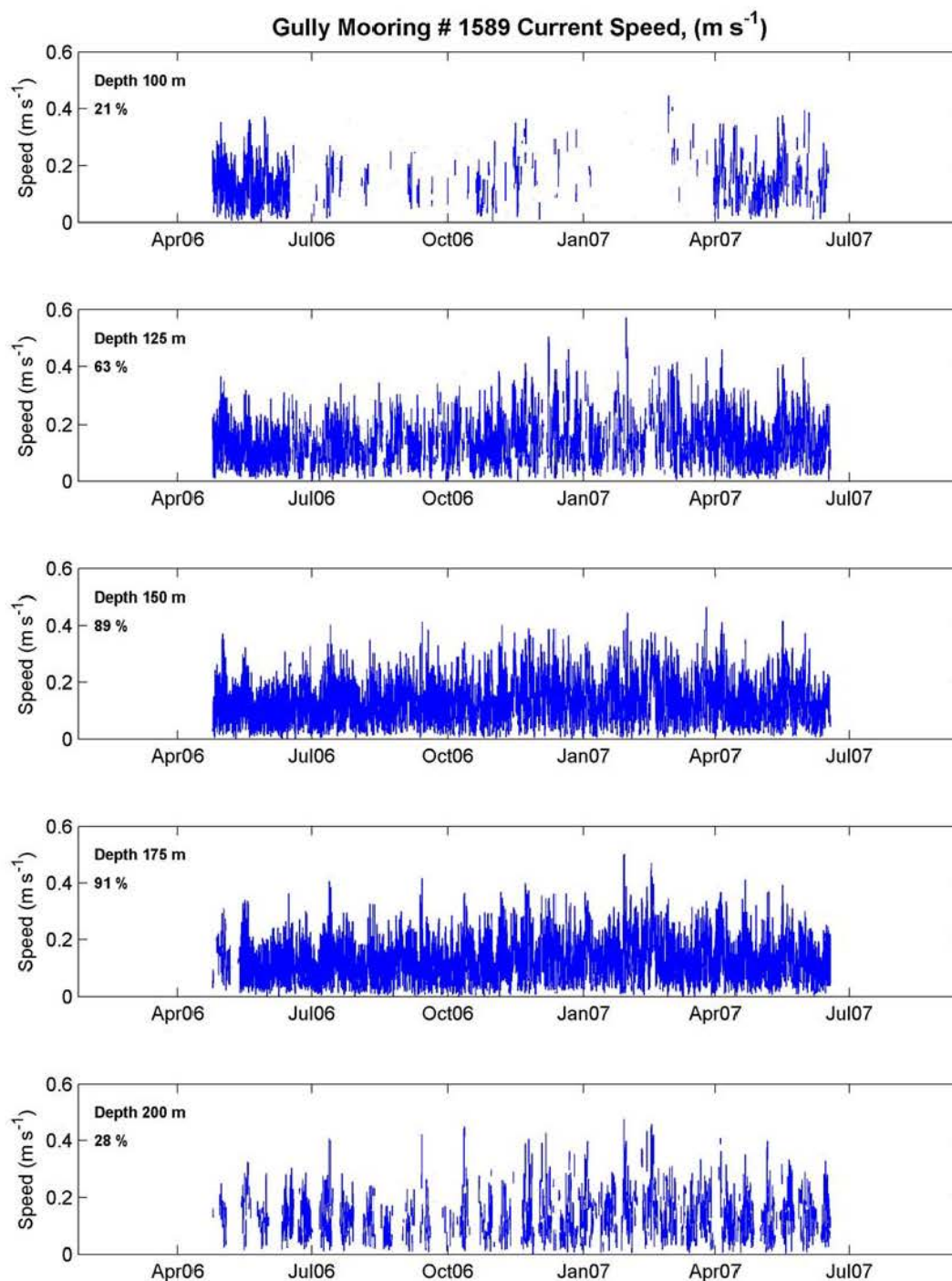


Figure A- 69: ADCP time series of current speed in 25-m averaged bins centered at the depths indicated in the panels. The percent of time with data available in the bin is indicated by the number below the depth bin.

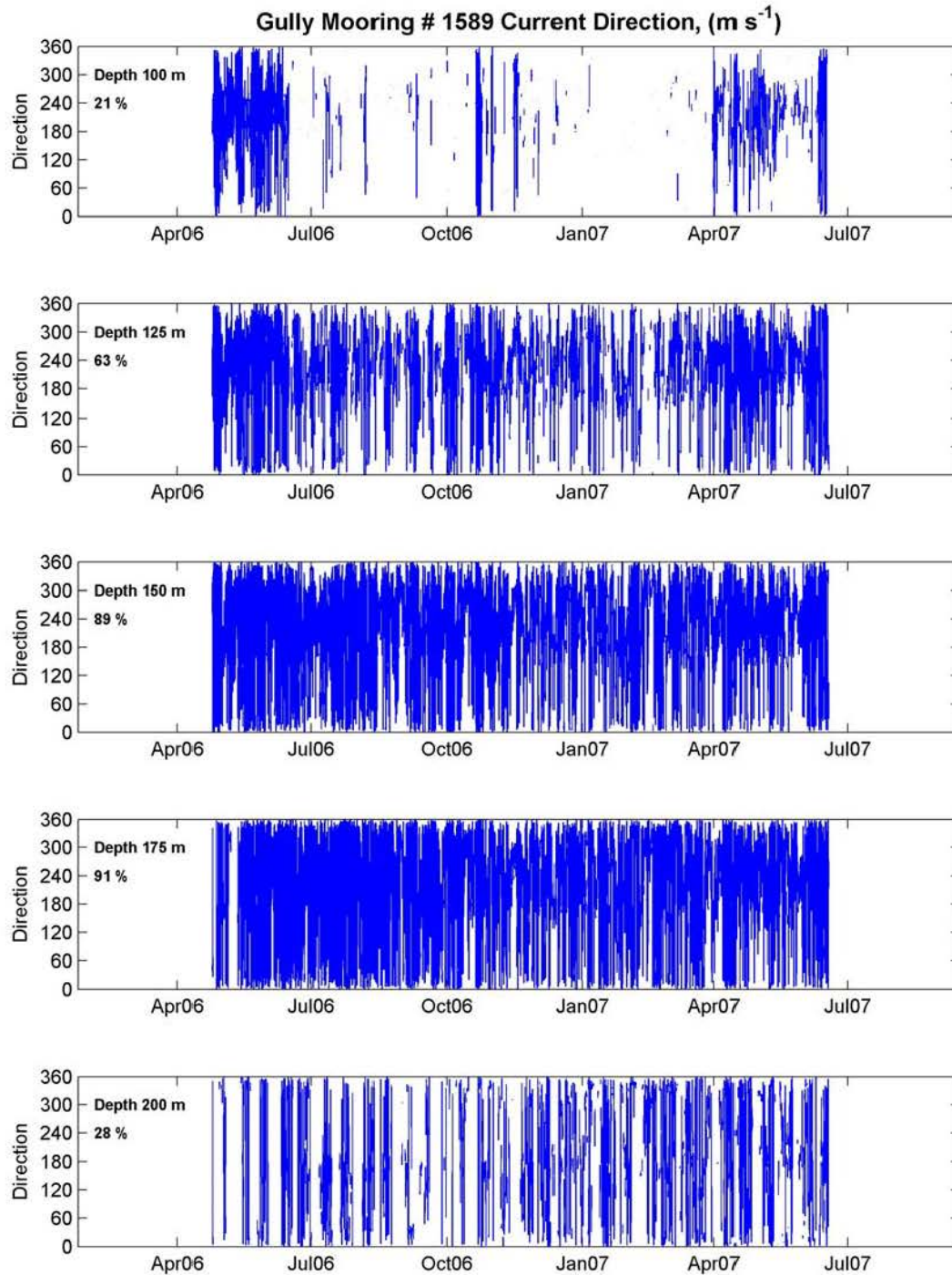


Figure A- 70: ADCP time series of current direction in 25-m averaged bins centered at the depths indicated in the panels. The percent of time with data available in the bin is indicated by the number below the depth bin.

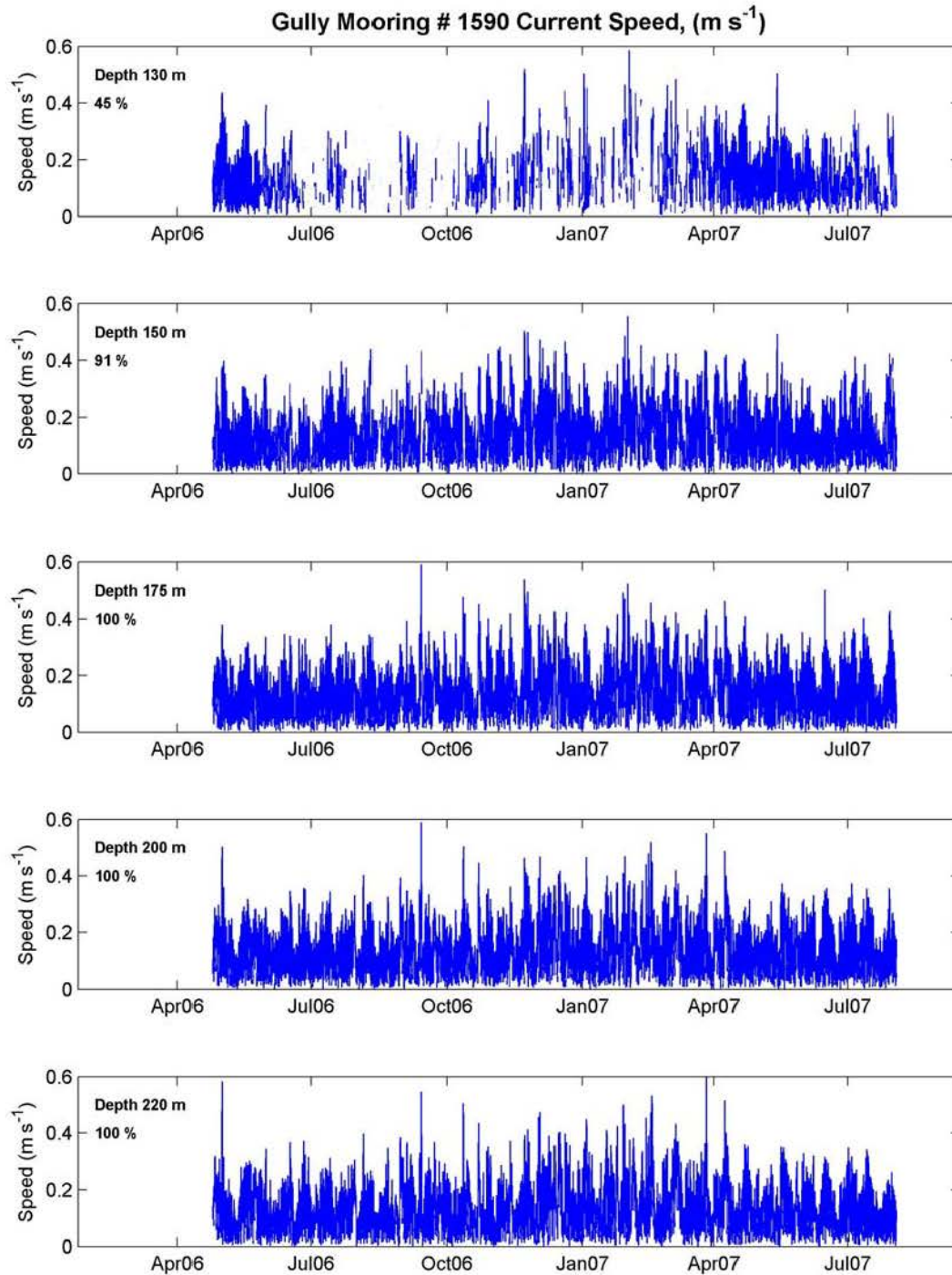


Figure A- 71: ADCP time series of current speed in 25-m averaged bins centered at the depths indicated in the panels. The percent of time with data available in the bin is indicated by the number below the depth bin.

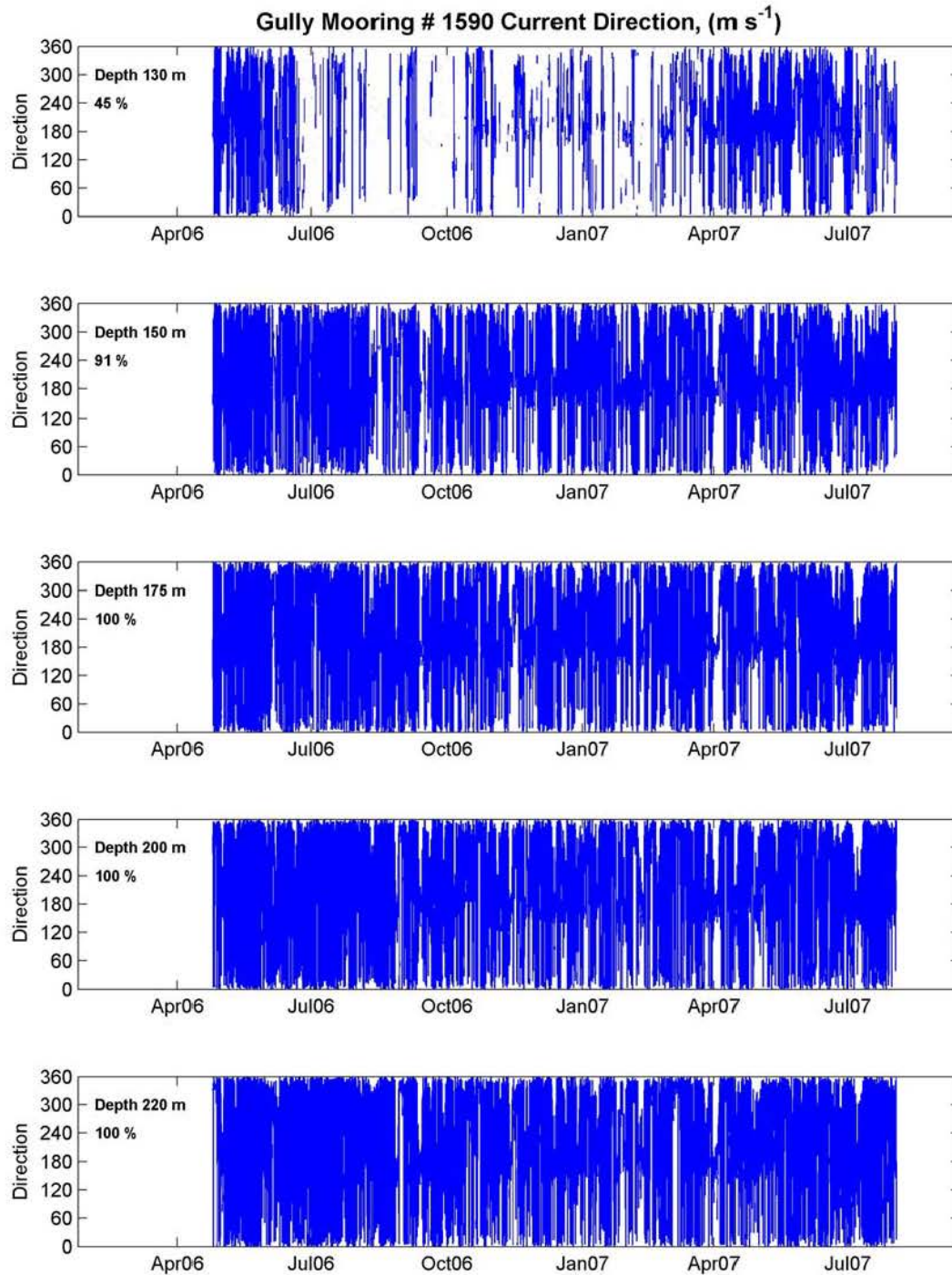


Figure A- 72: ADCP time series of current direction in 25-m averaged bins centered at the depths indicated in the panels. The percent of time with data available in the bin is indicated by the number below the depth bin.

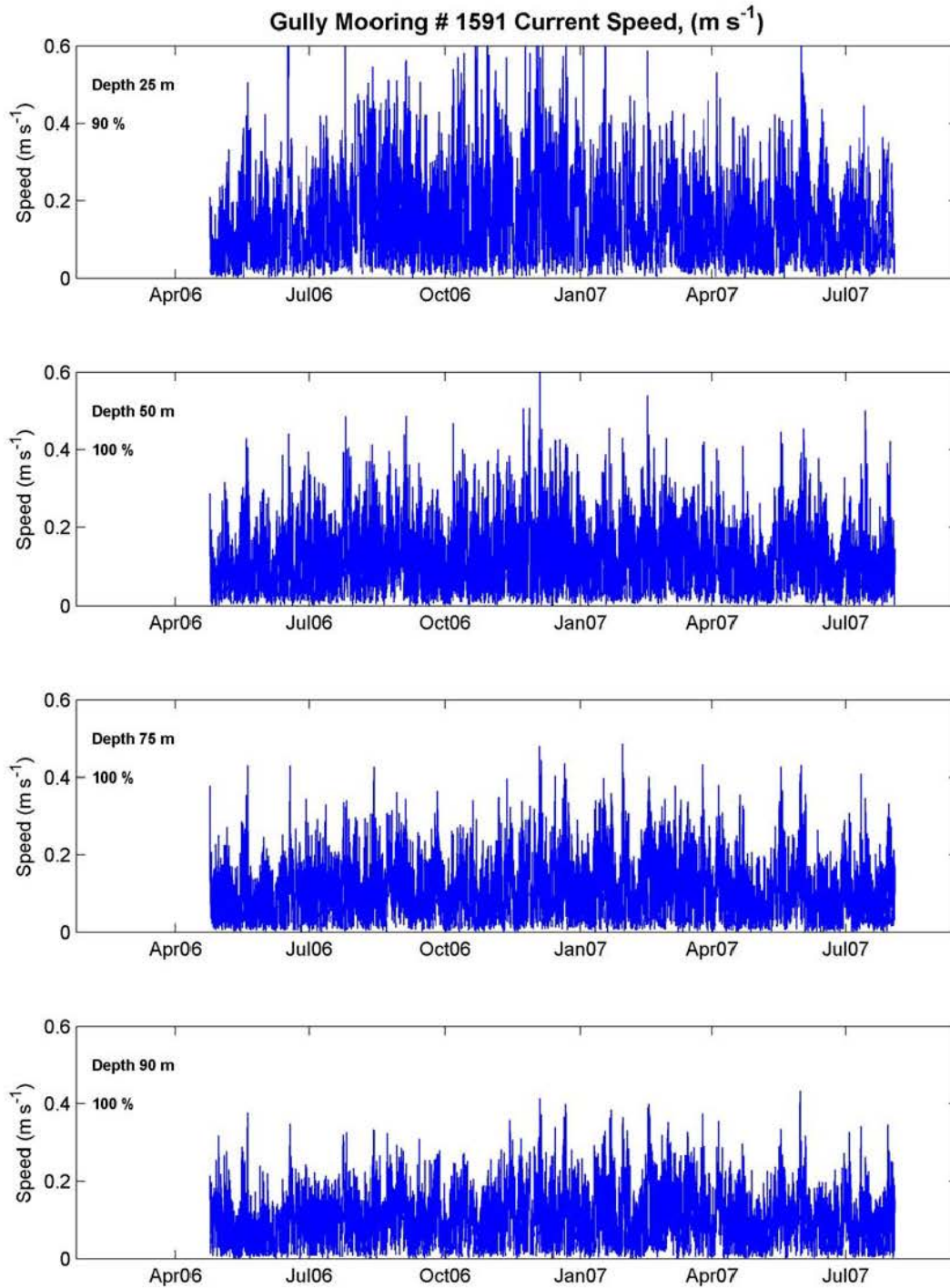


Figure A- 73: ADCP time series of current speed in 25-m averaged bins centered at the depths indicated in the panels. The percent of time with data available in the bin is indicated by the number below the depth bin.

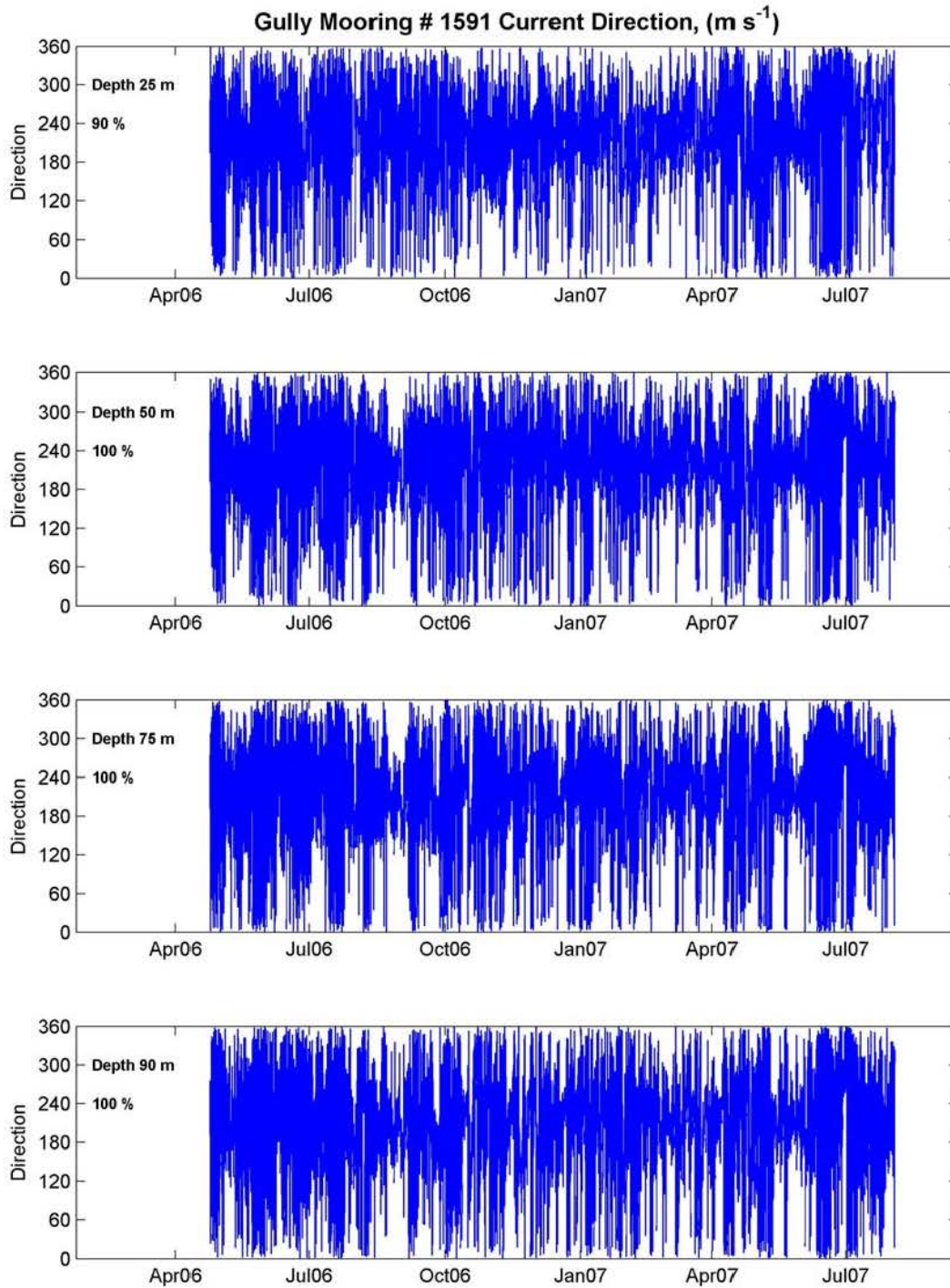


Figure A- 74: ADCP time series of current direction in 25-m averaged bins centered at the depths indicated in the panels. The percent of time with data available in the bin is indicated by the number below the depth bin.

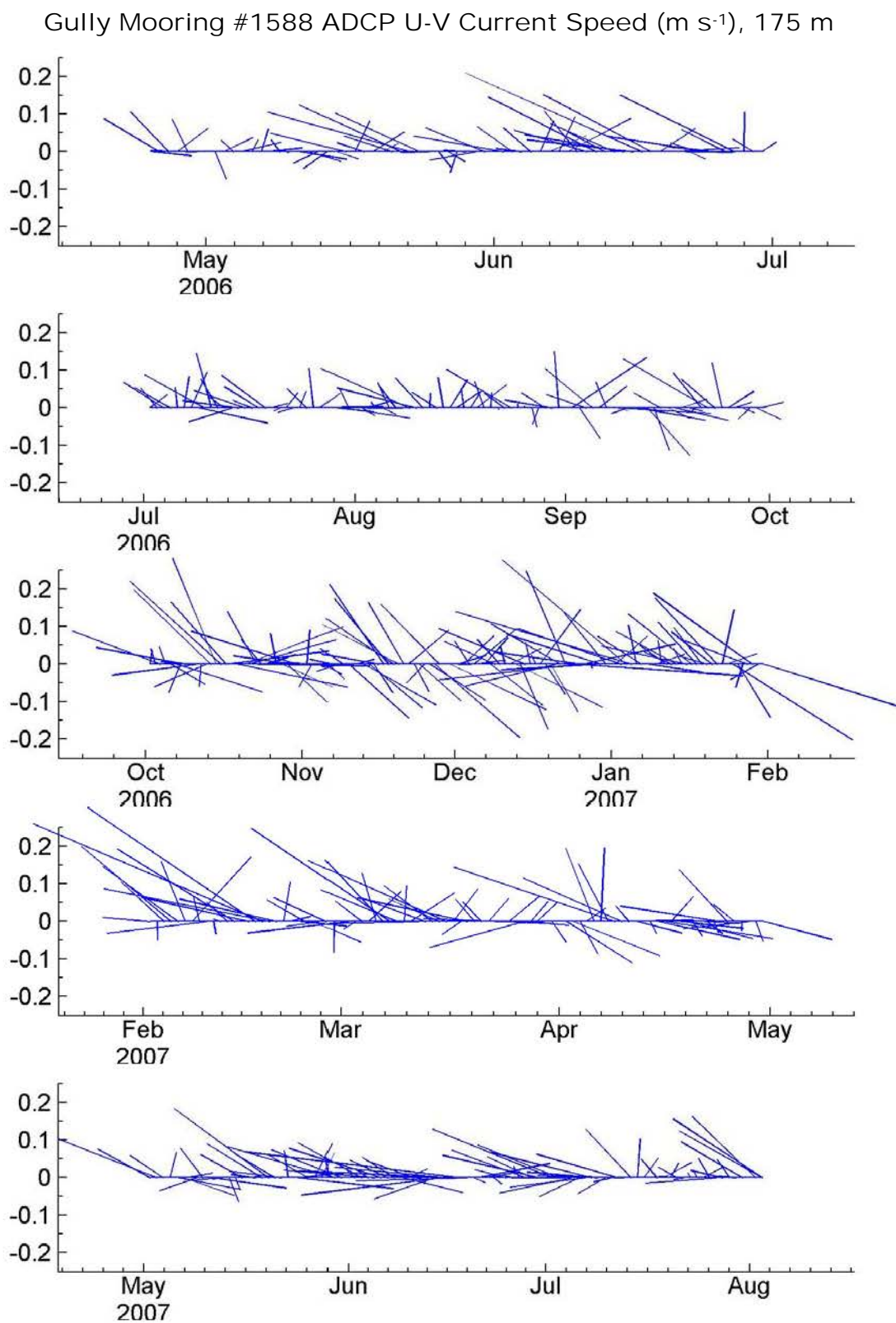


Figure A- 75: ADCP stick plot of current speed/direction at 175 m depth.

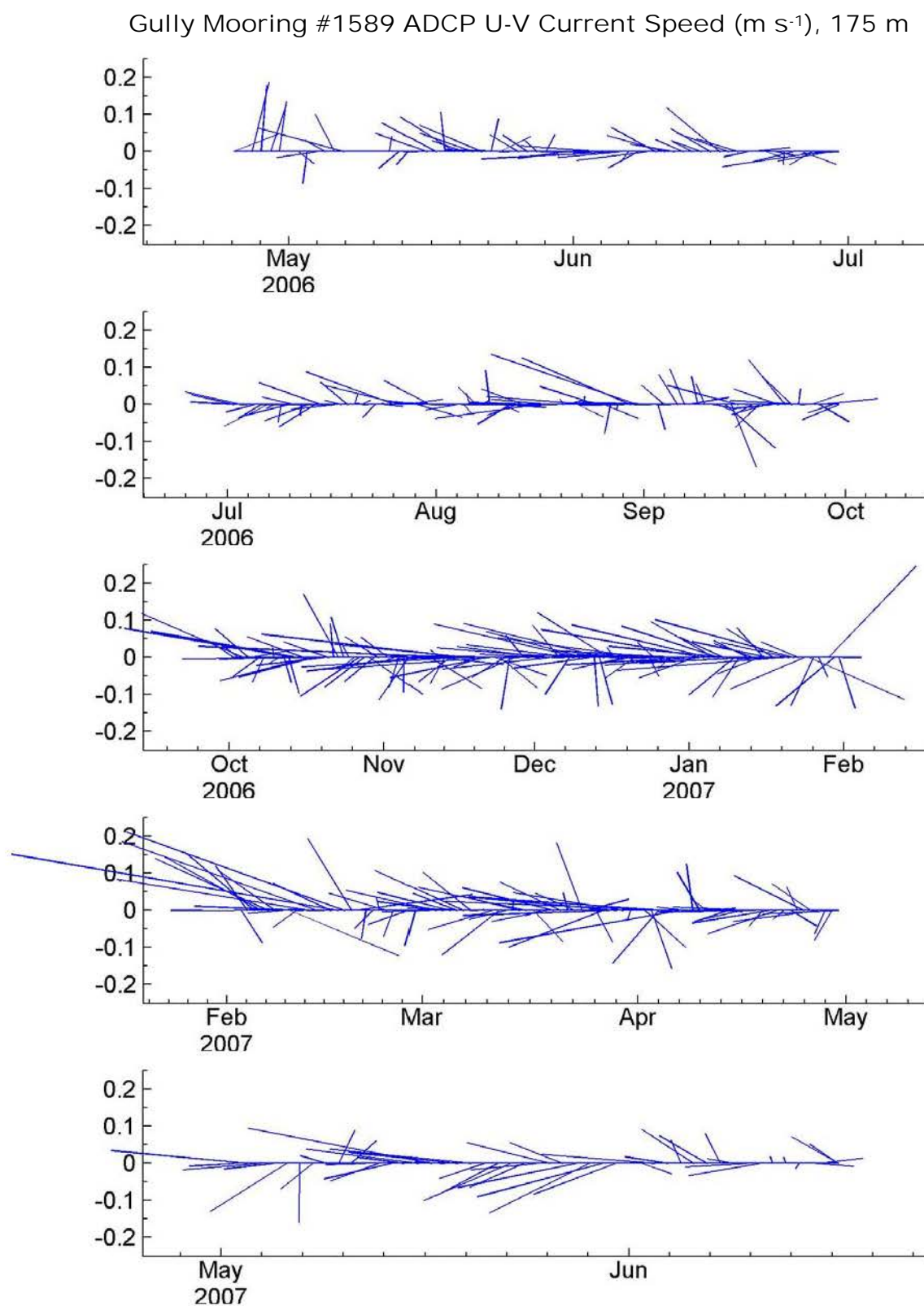


Figure A- 76: ADCP stick plot of current speed/direction at 175 m depth.

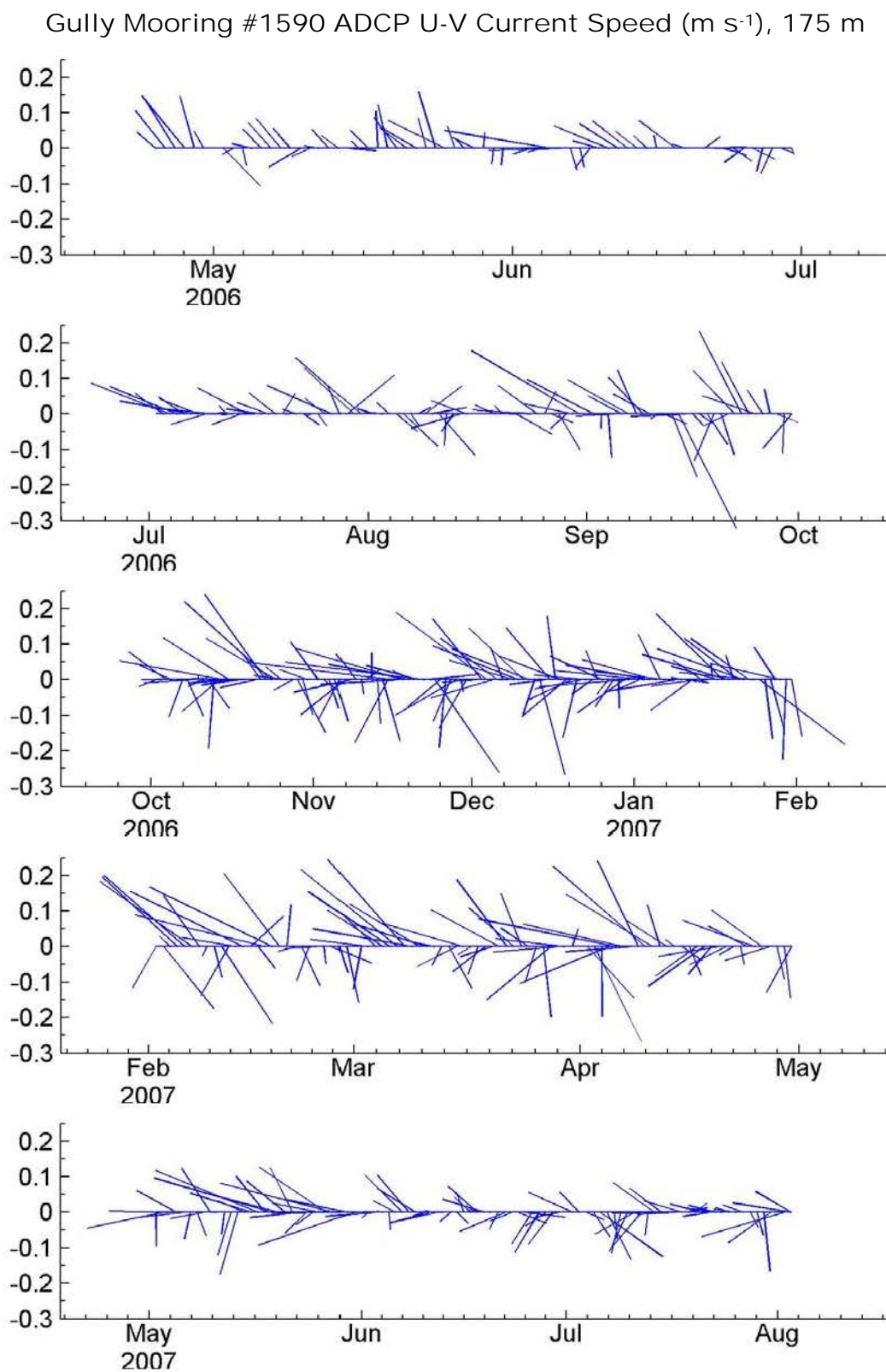


Figure A- 77: ADCP stick plot of current speed/direction at 175 m depth.

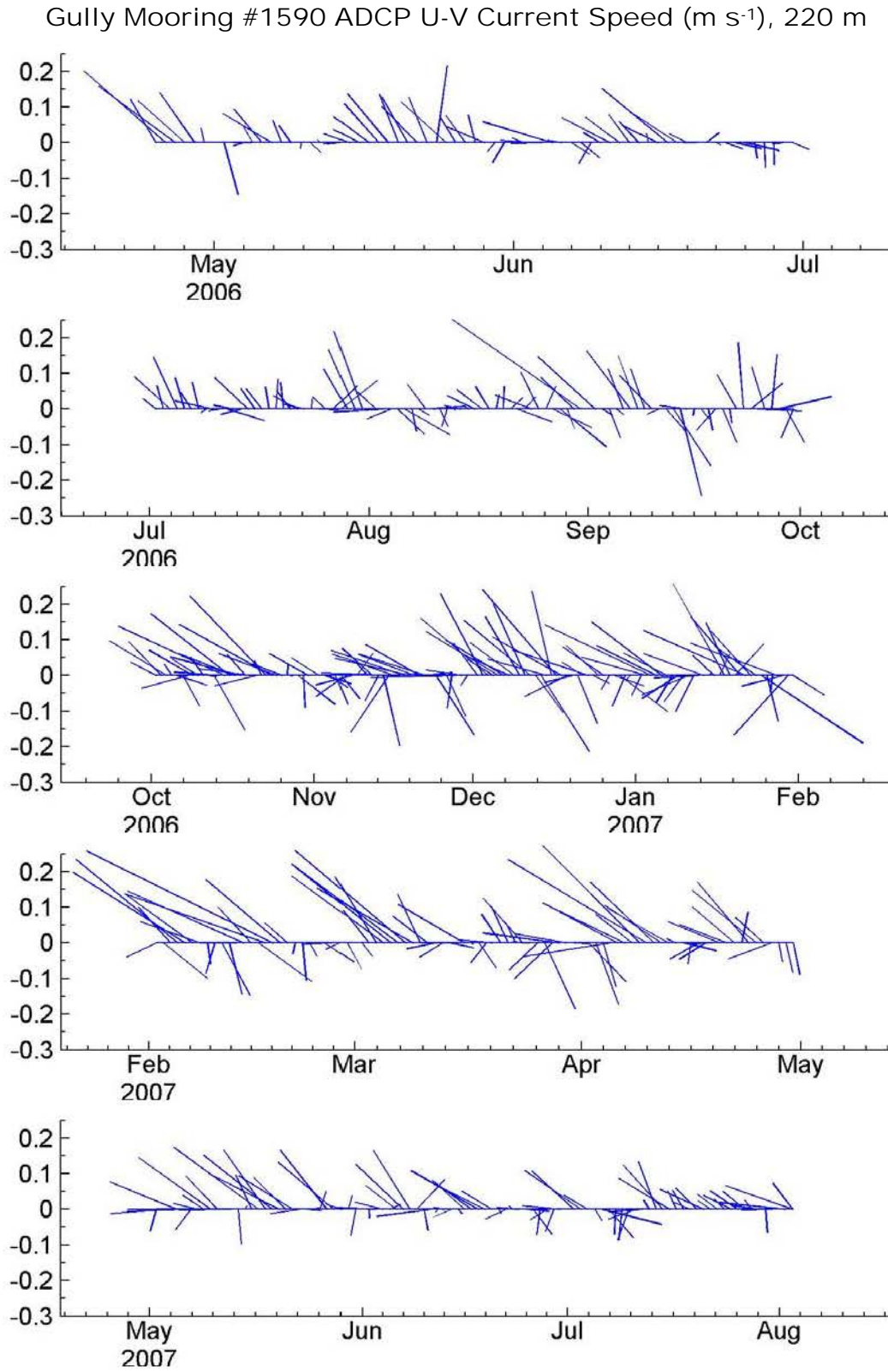
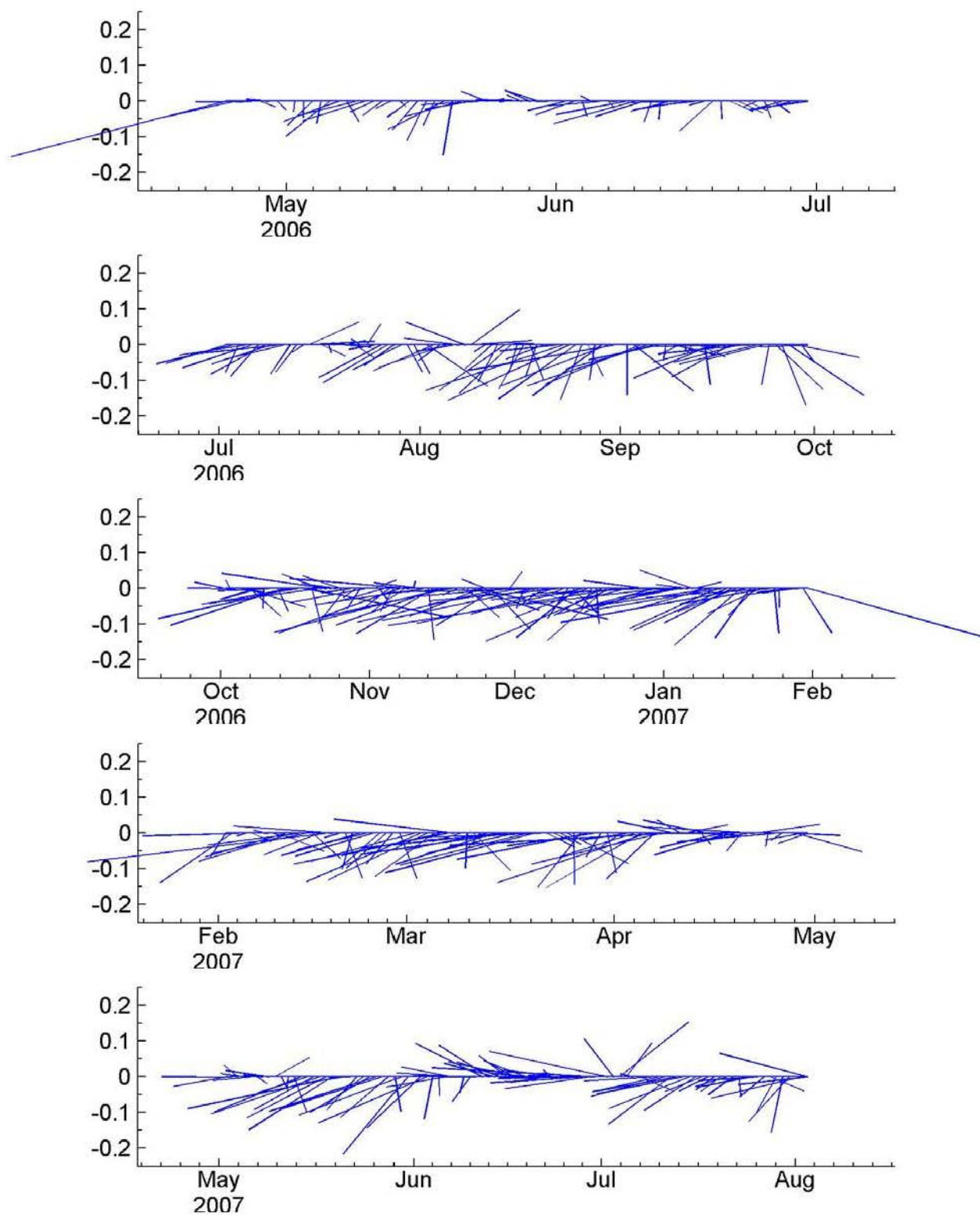


Figure A- 78: ADCP stick plot of current speed/direction at 220 m depth.

Gully Mooring #1591 ADCP U-V Current Speed (m s^{-1}), 75 m**Figure A- 79: ADCP stick plot of current speed/direction at 75 m depth.**

Appendix 6: RCM Single Point Moored Current Meter

Four moorings were deployed at the sites SG2 (mooring #1588), SG10 (mooring #1591), SG11 (mooring #1589), SG12 (mooring #1590), in Zone 1 of the Gully (**Figure 1**), which each had several Aanderaa RCM8 current meters (Appendix 1). The moorings were deployed April 23 and 24, 2006 and recovered on August 3, 2007. The deep central mooring at SG11 when recovered was missing the upper 200 m which did not include an RCM, it went missing on 17 June, 2007. Also the two moorings on the canyon axis (#1588 and #1589) underwent vertical displacements up to 500 m for mooring 1589.

Figures include pressure, temperature, salinity, and current time series plots for each RCM meter.

All plots were created using MATLAB R2008b.

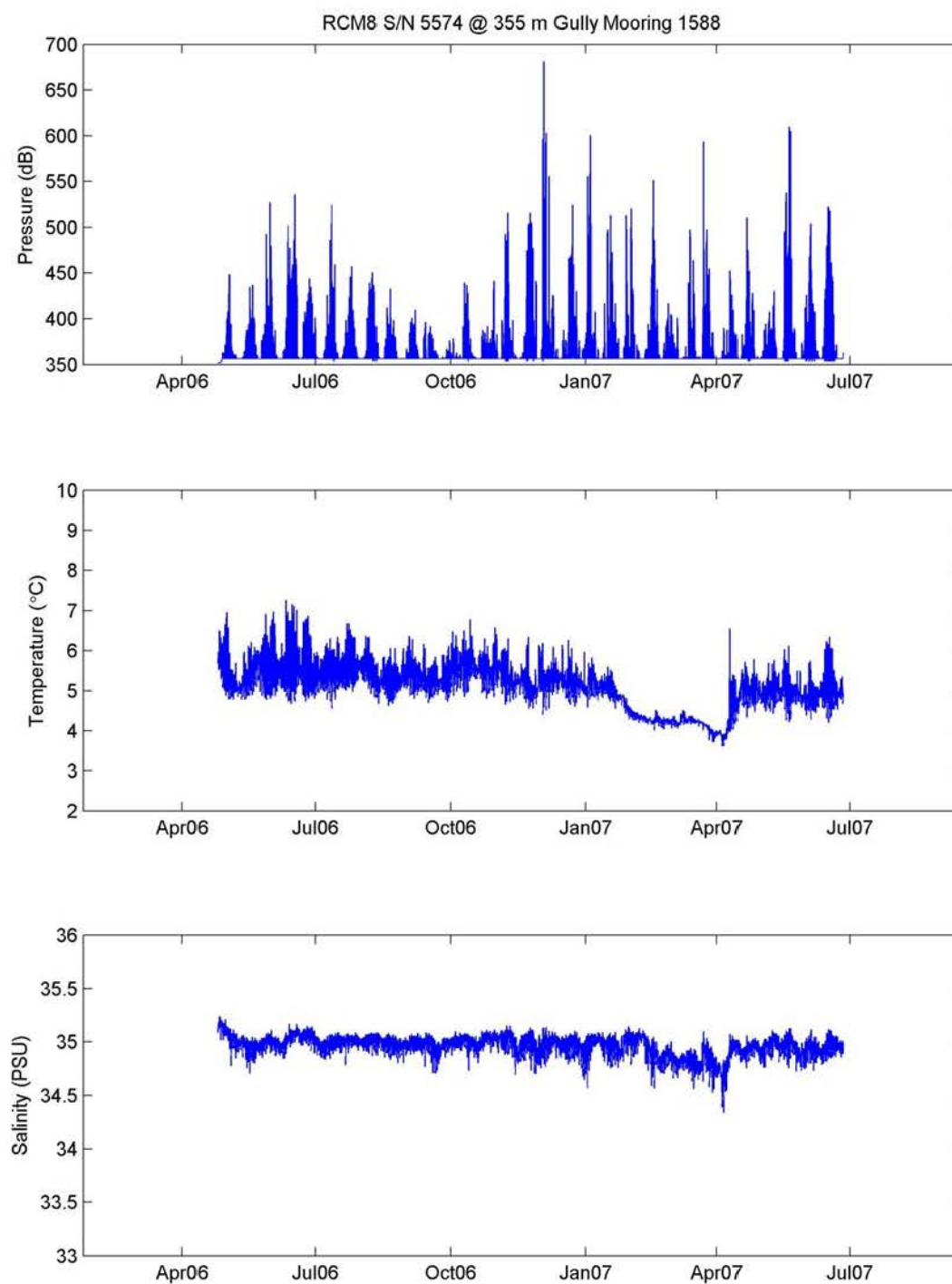


Figure A- 80: RCM-based pressure, temperature and salinity time series on mooring 1588 (SG2).

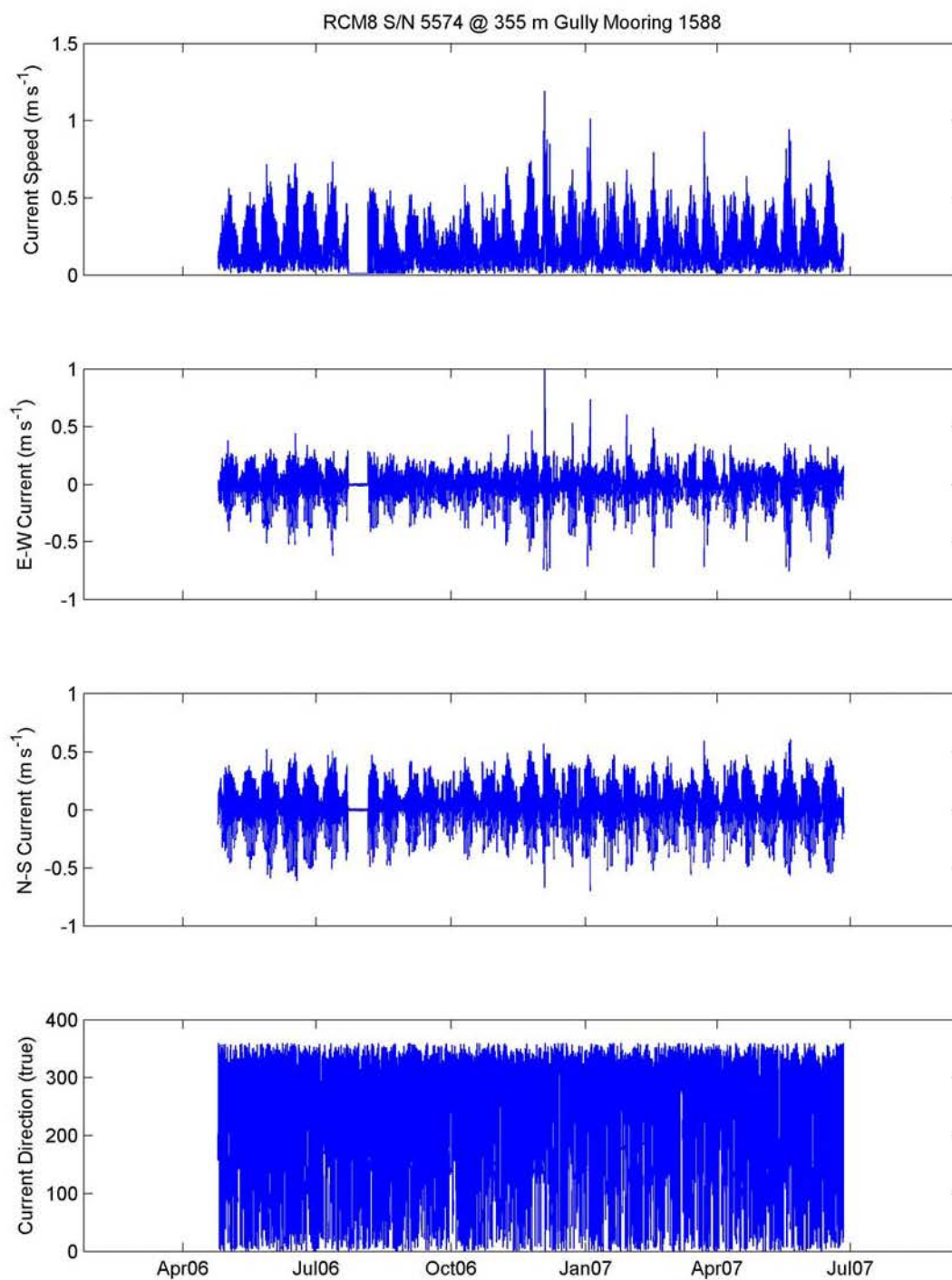


Figure A- 81: Current speed, east-west and north-south components, and current direction time series on mooring 1588 (SG2).

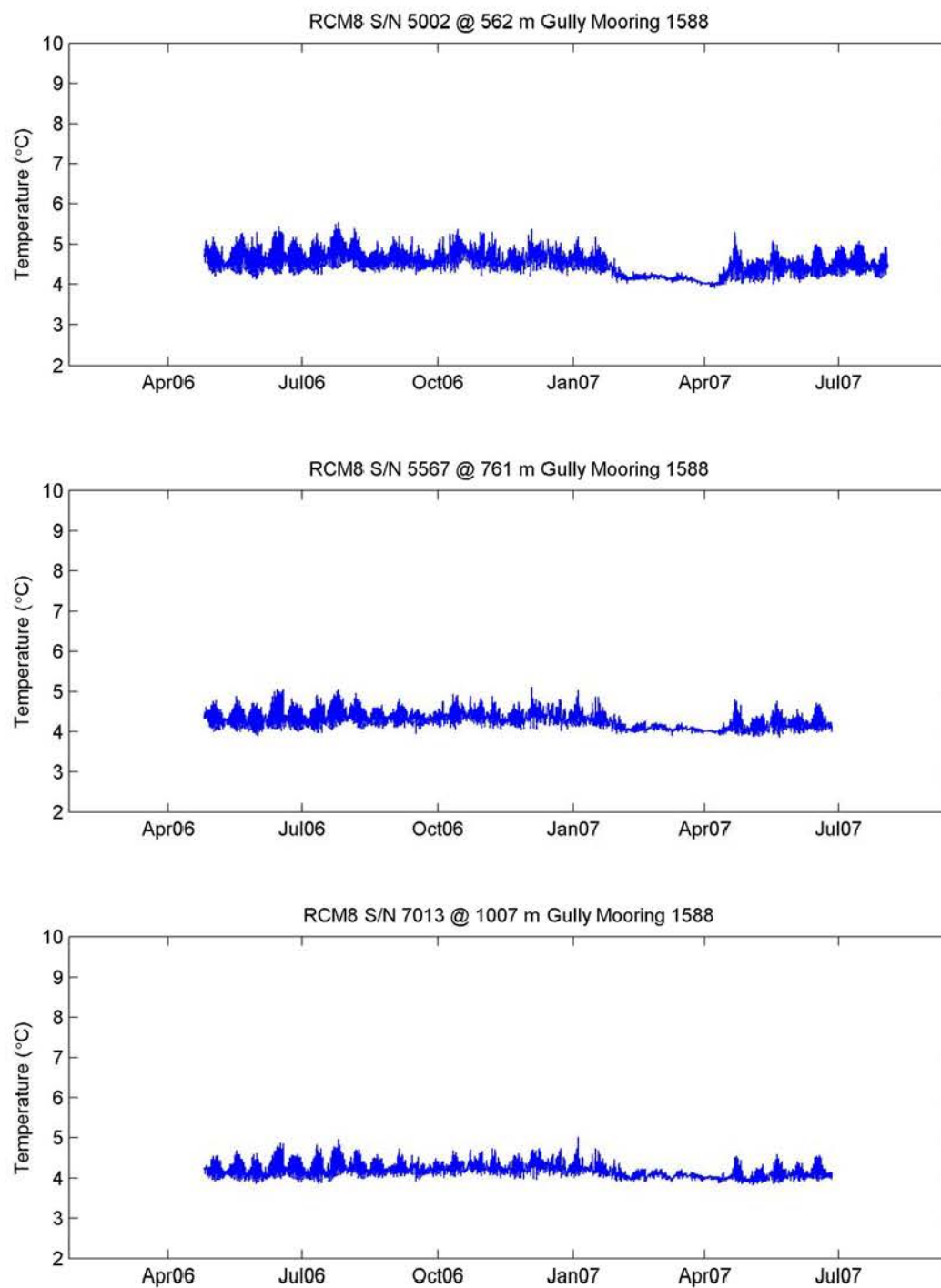


Figure A- 82: RCM-based temperature time series on mooring 1588 (SG2).

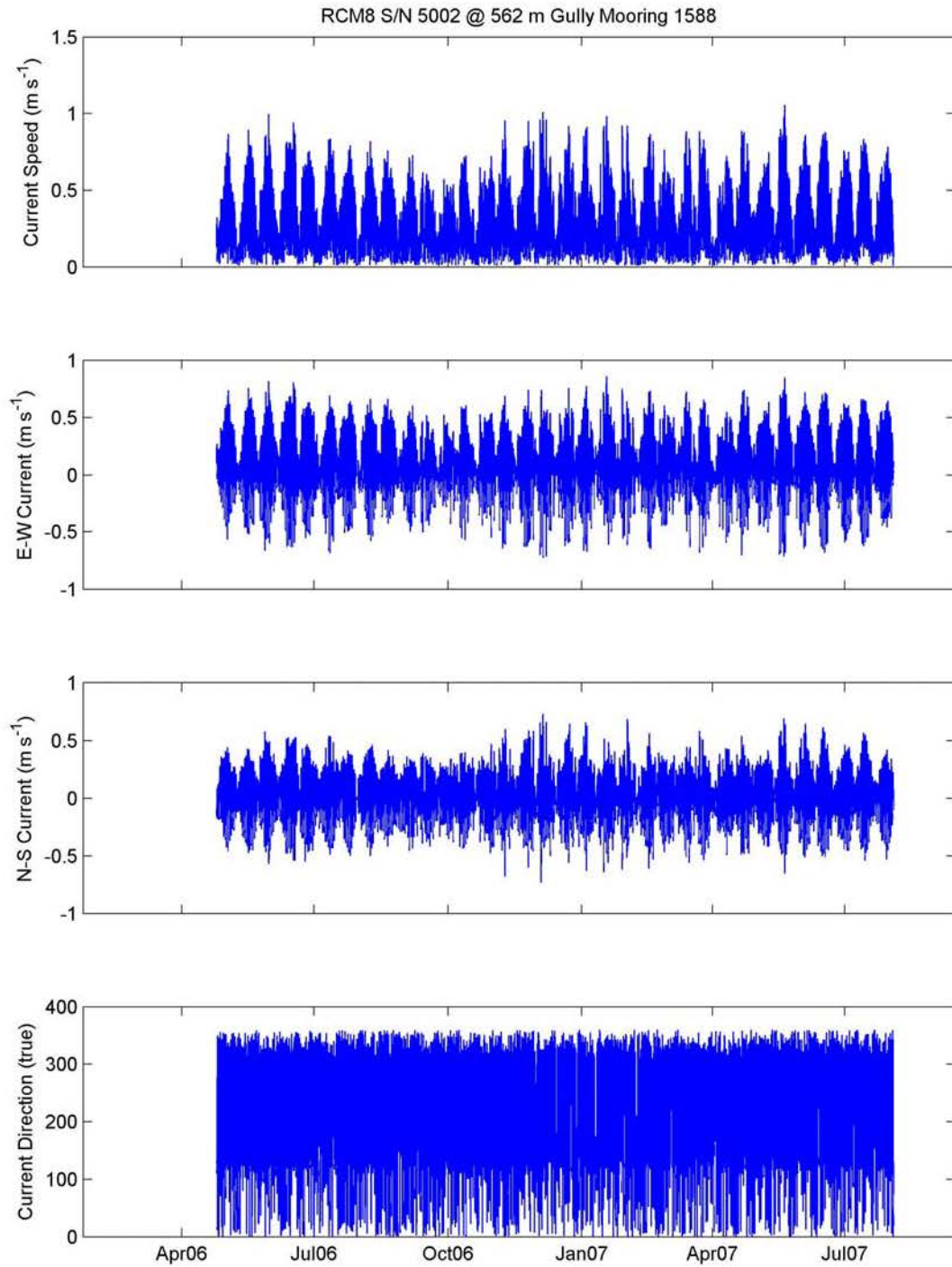


Figure A- 83: Current speed, east-west and north-south components, and current direction time series on mooring 1588 (SG2).

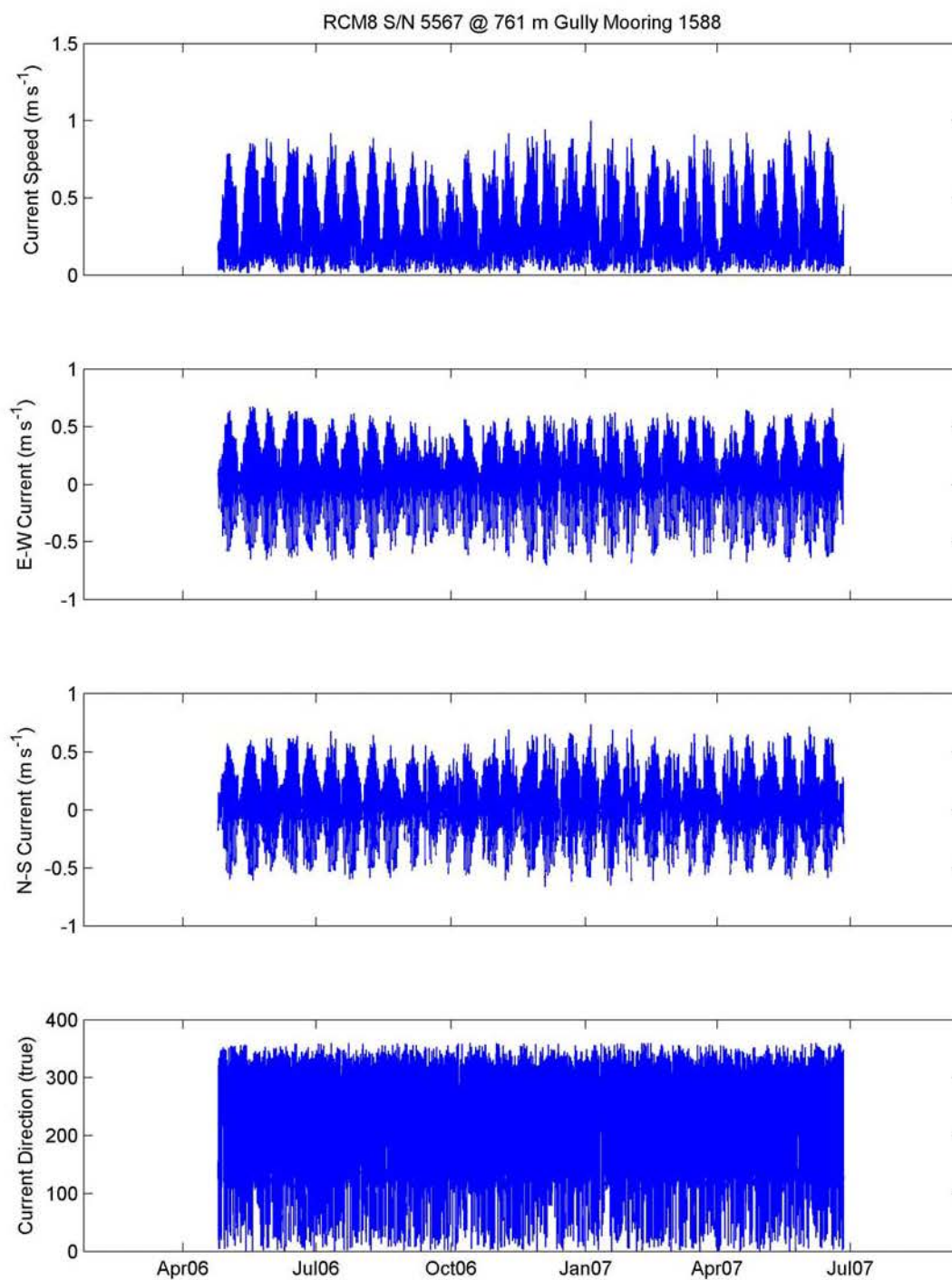


Figure A- 84: Current speed, east-west and north-south components, and current direction time series on mooring 1588 (SG2).

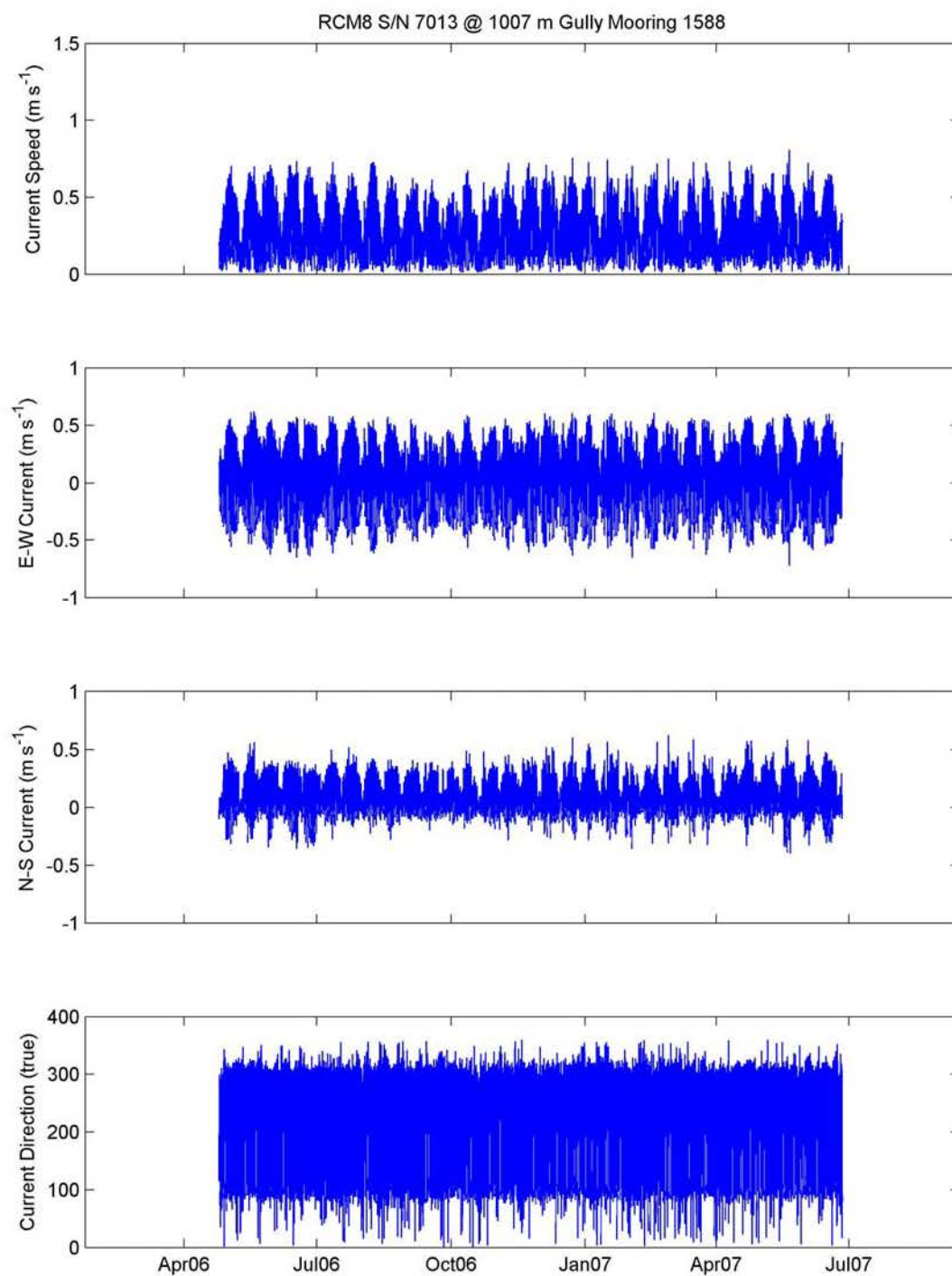


Figure A- 85: Current speed, east-west and north-south components, and current direction time series on mooring 1588 (SG2).

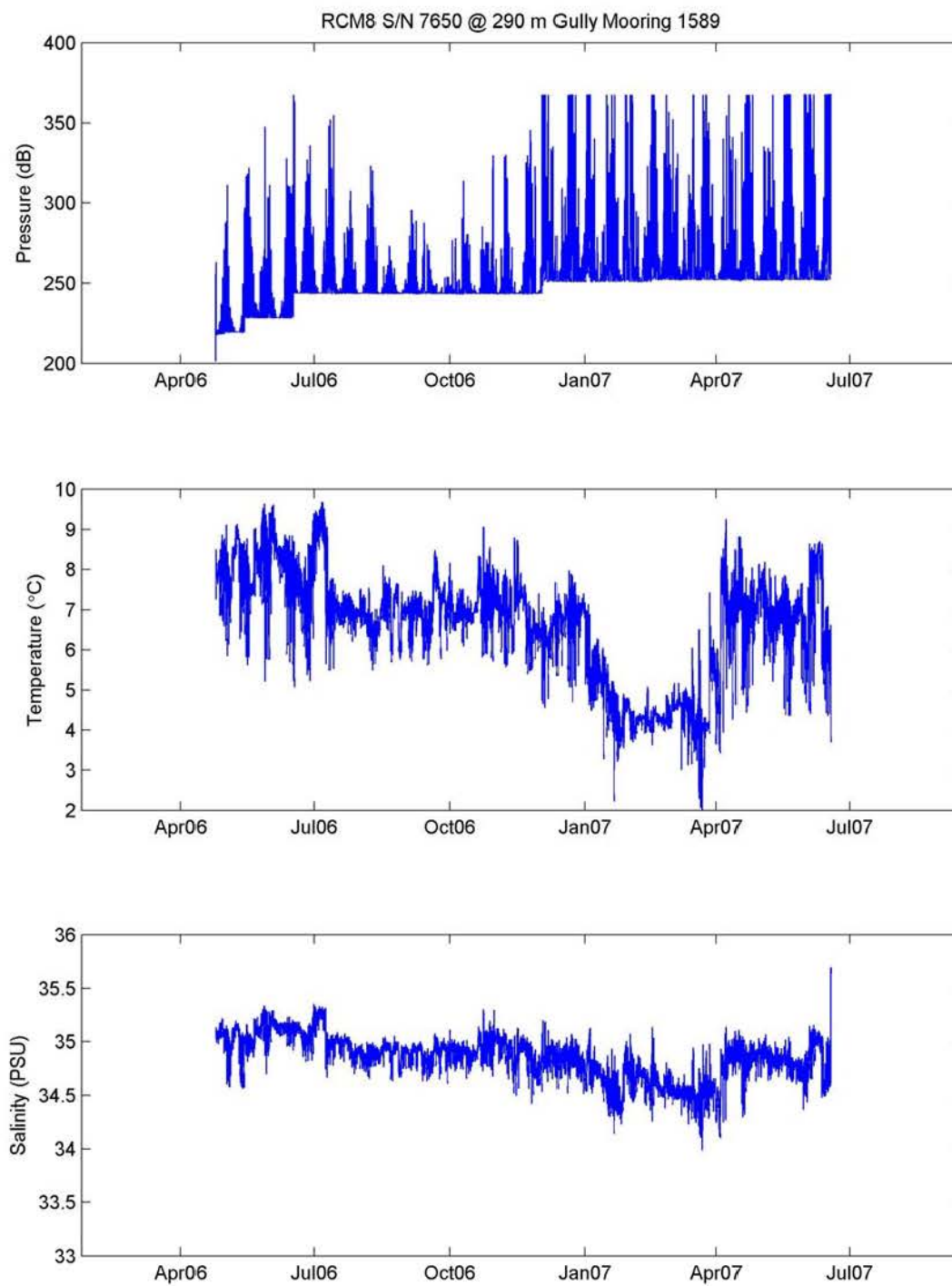


Figure A- 86: RCM-based pressure, temperature and salinity time series on mooring 1589 (SG11).

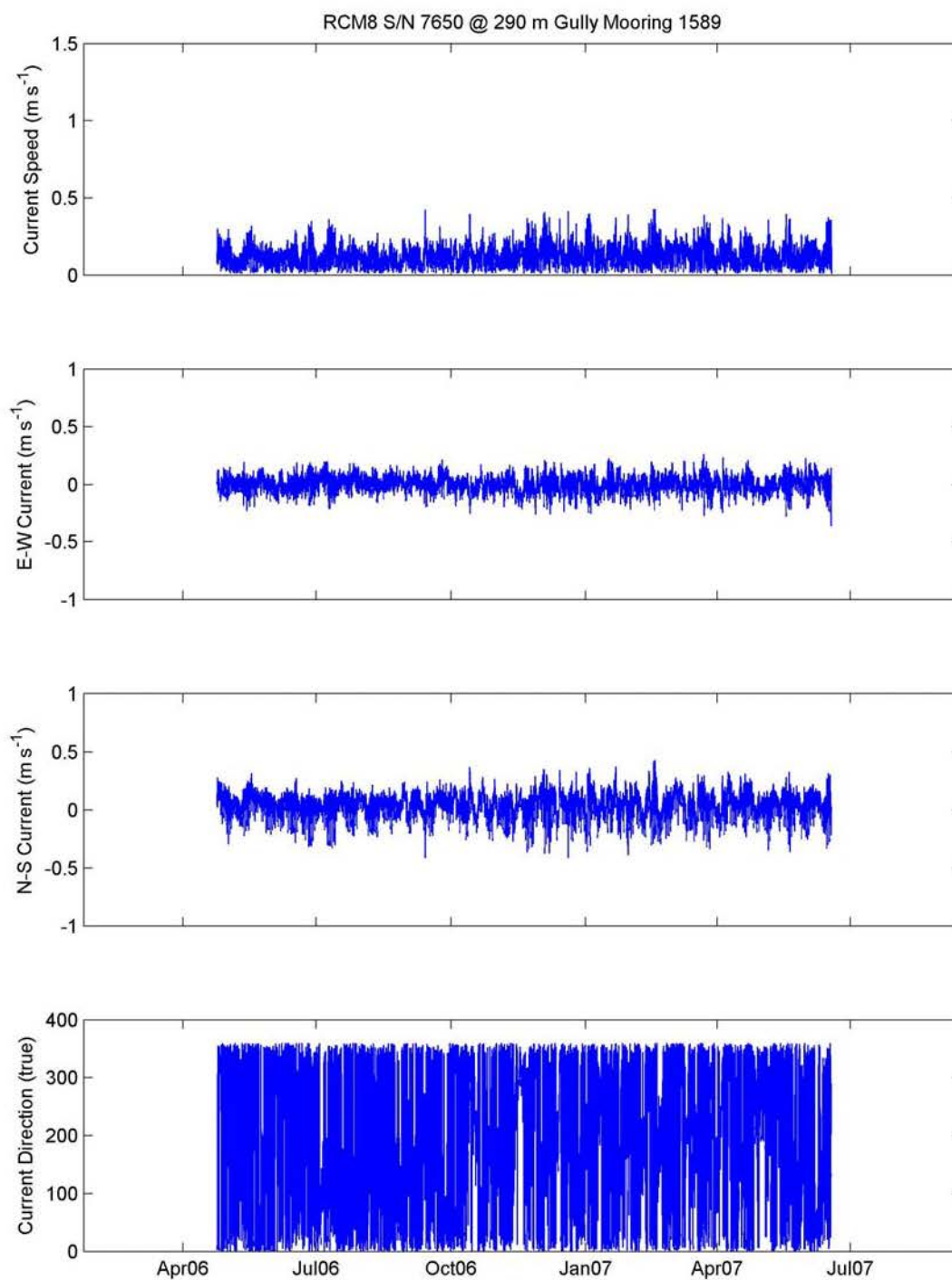
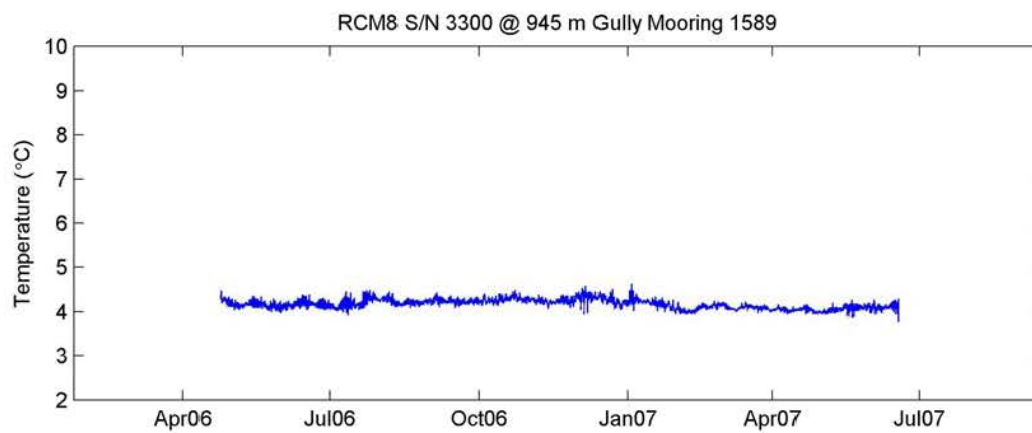
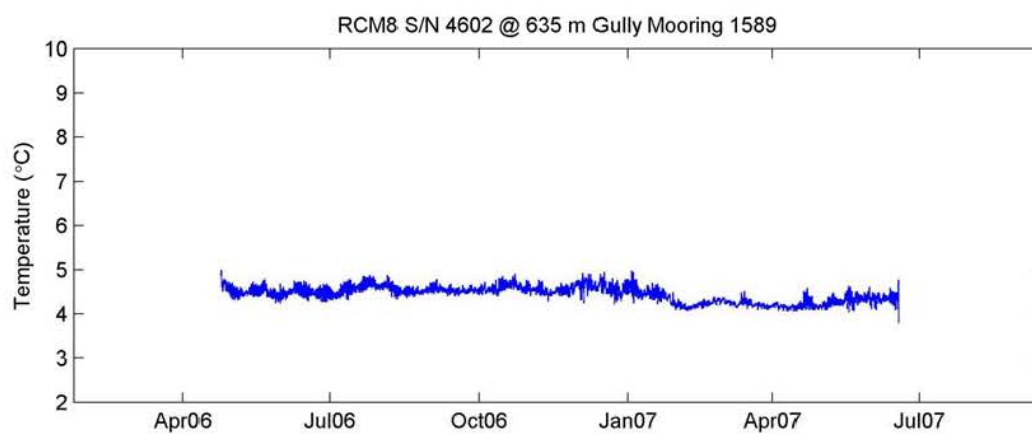
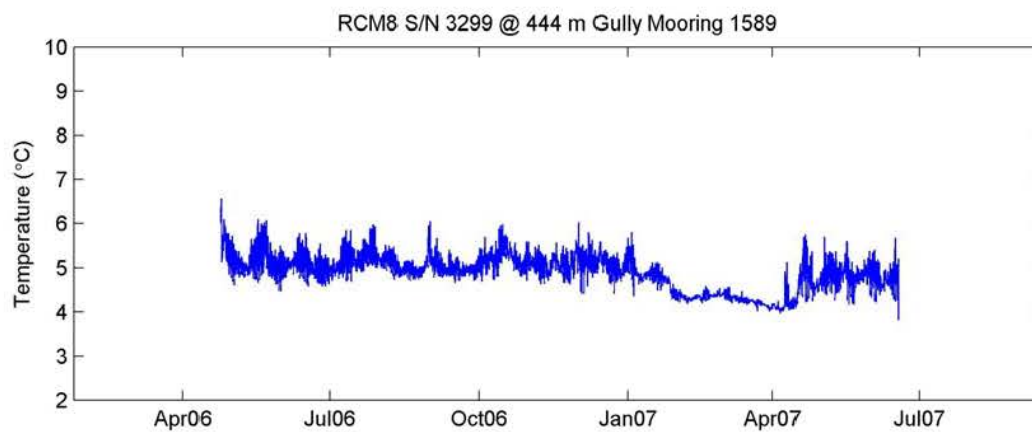


Figure A- 87: Current speed, east-west and north-south components, and current direction time series on mooring 1589 (SG11).



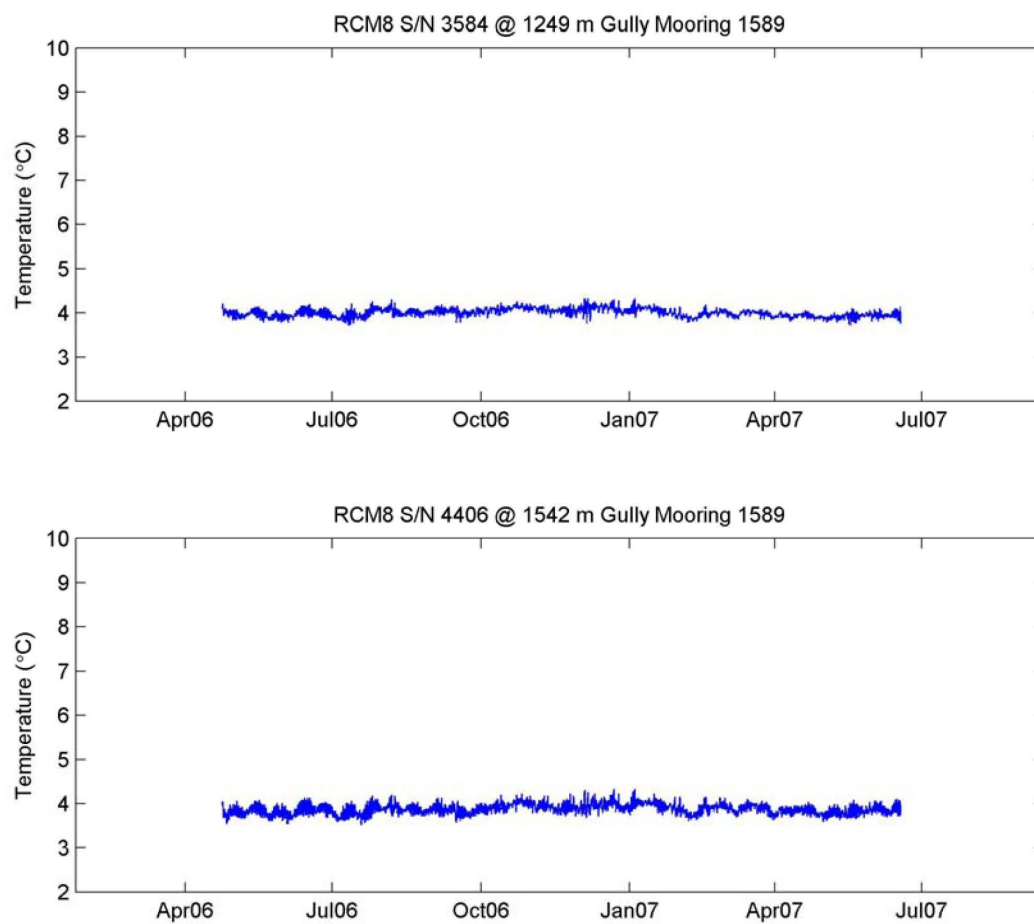


Figure A- 88: RCM-based temperature time series on mooring 1589 (SG11).

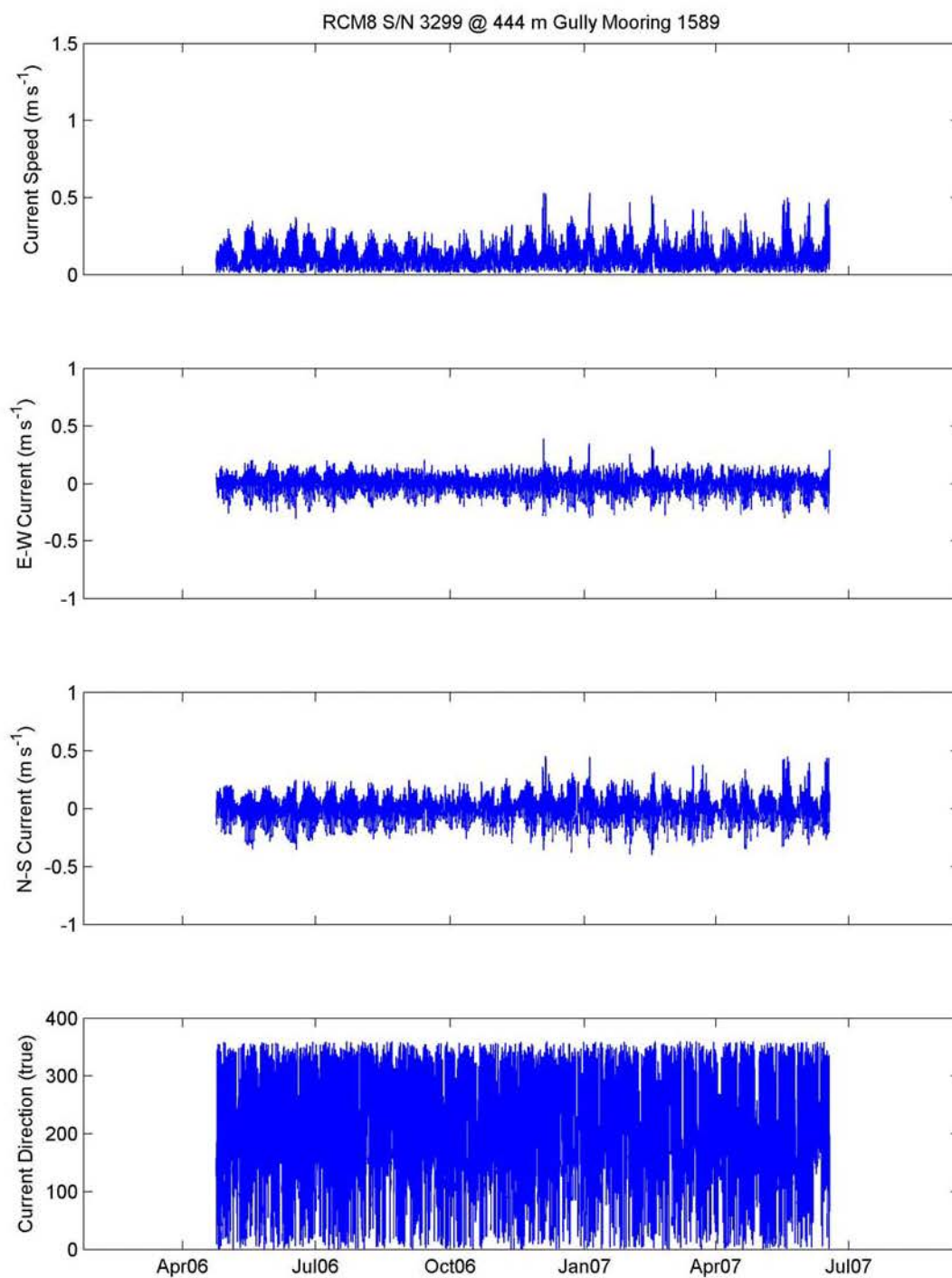


Figure A- 89: Current speed, east-west and north-south components, and current direction time series on mooring 1589 (SG11).

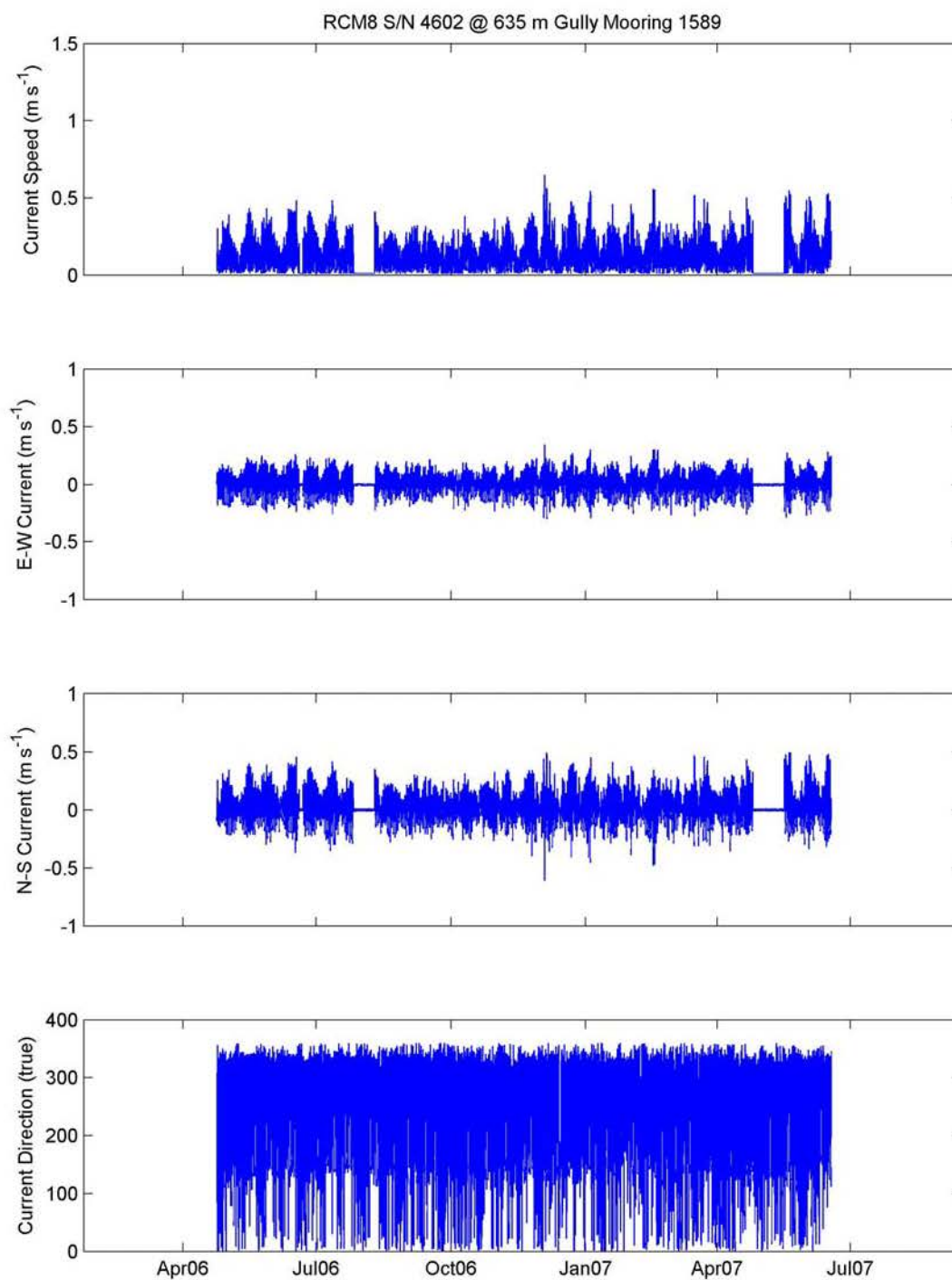


Figure A- 90: Current speed, east-west and north-south components, and current direction time series on mooring 1589 (SG11).

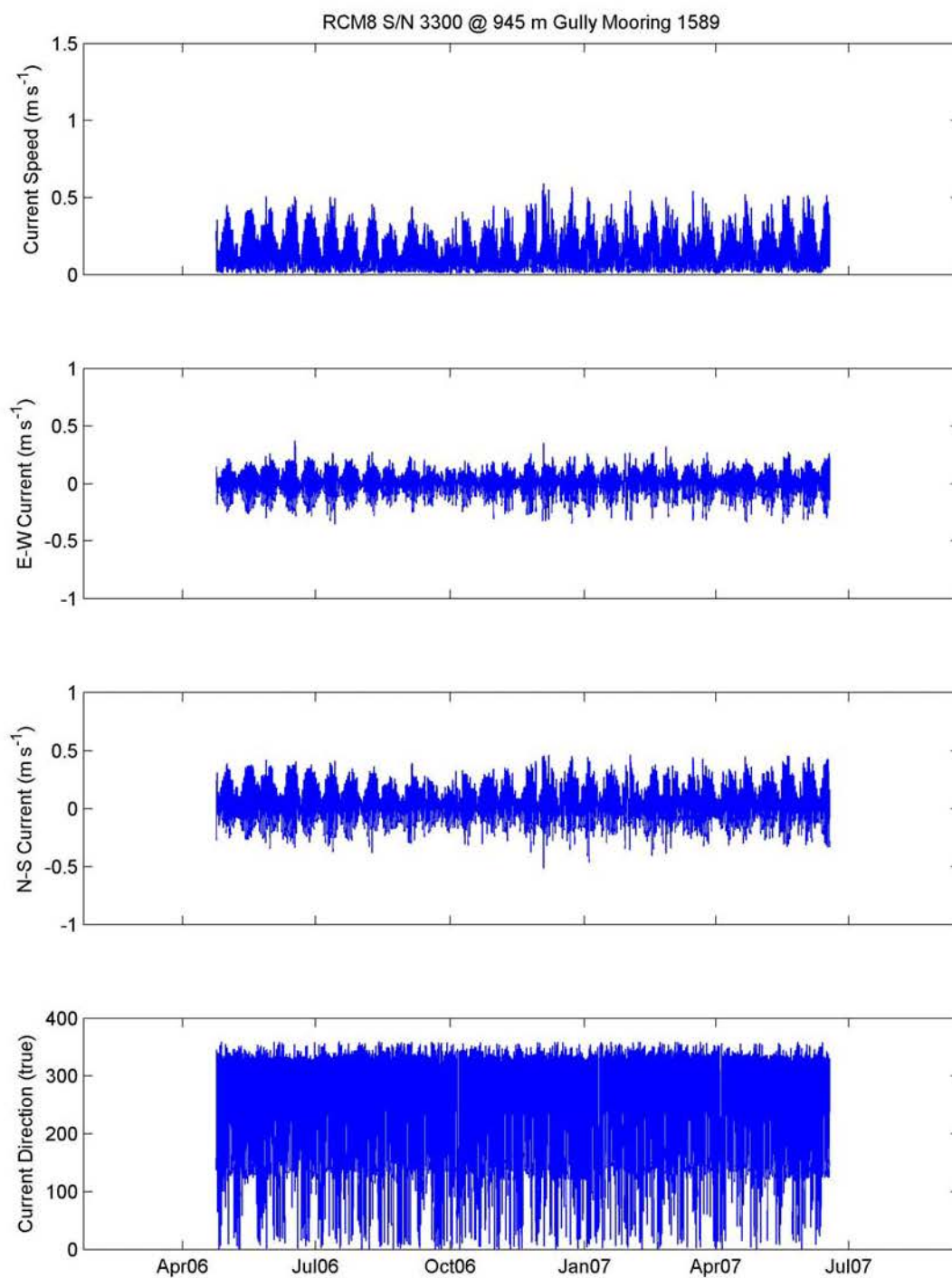


Figure A- 91: Current speed, east-west and north-south components, and current direction time series on mooring 1589 (SG11).

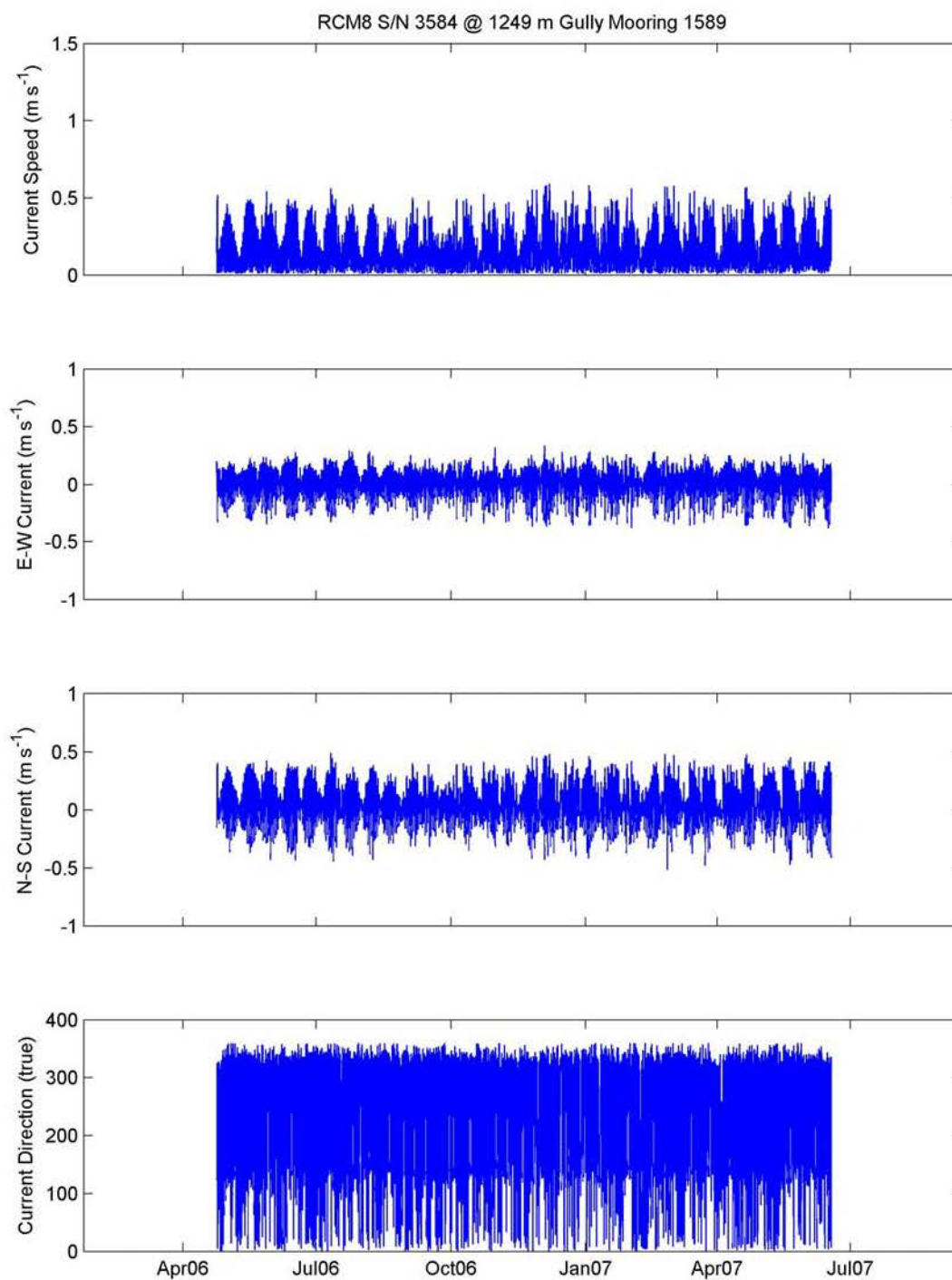


Figure A- 92: Current speed, east-west and north-south components, and current direction time series on mooring 1589 (SG11).

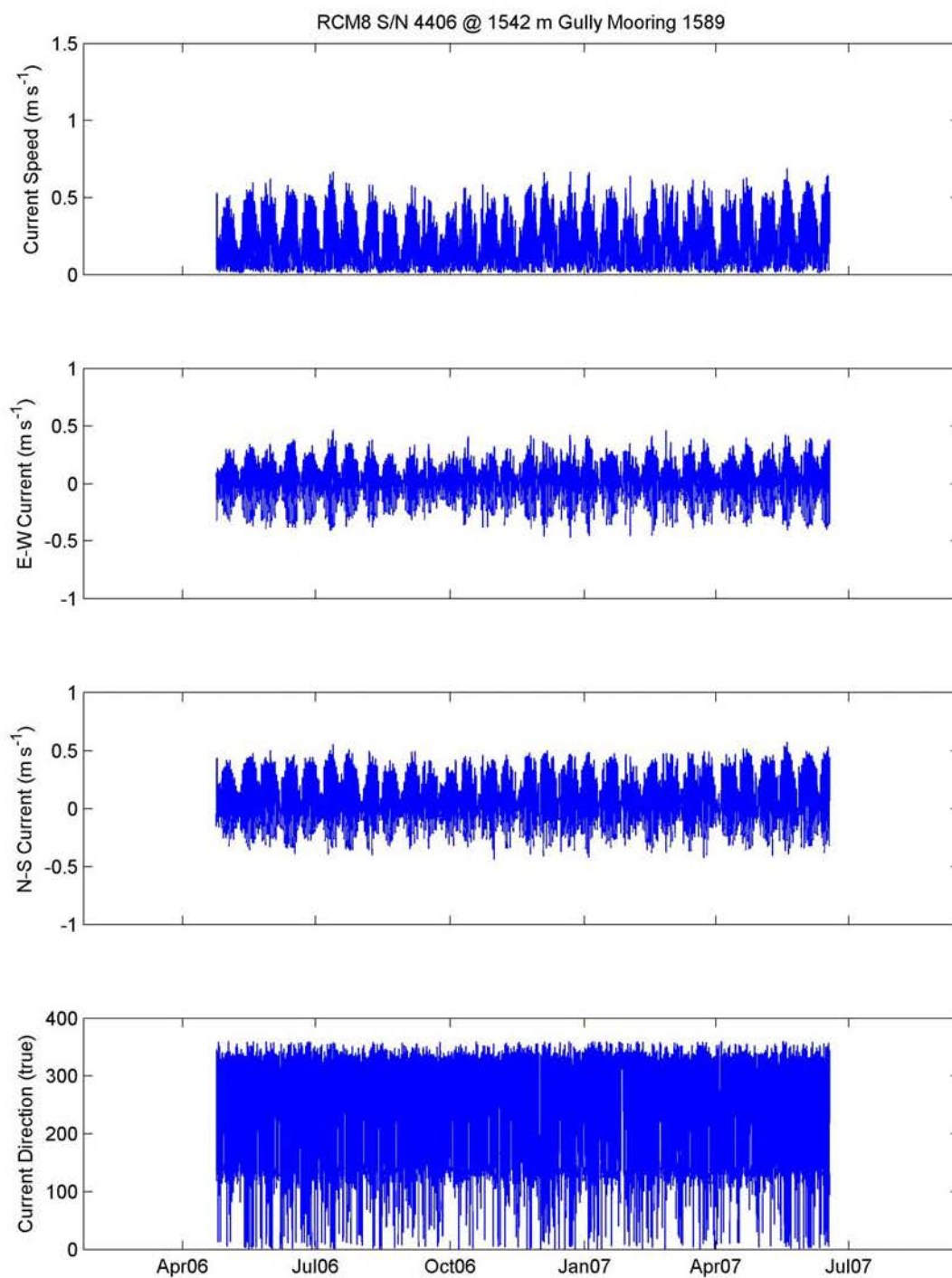


Figure A- 93: Current speed, east-west and north-south components, and current direction time series on mooring 1589 (SG11).

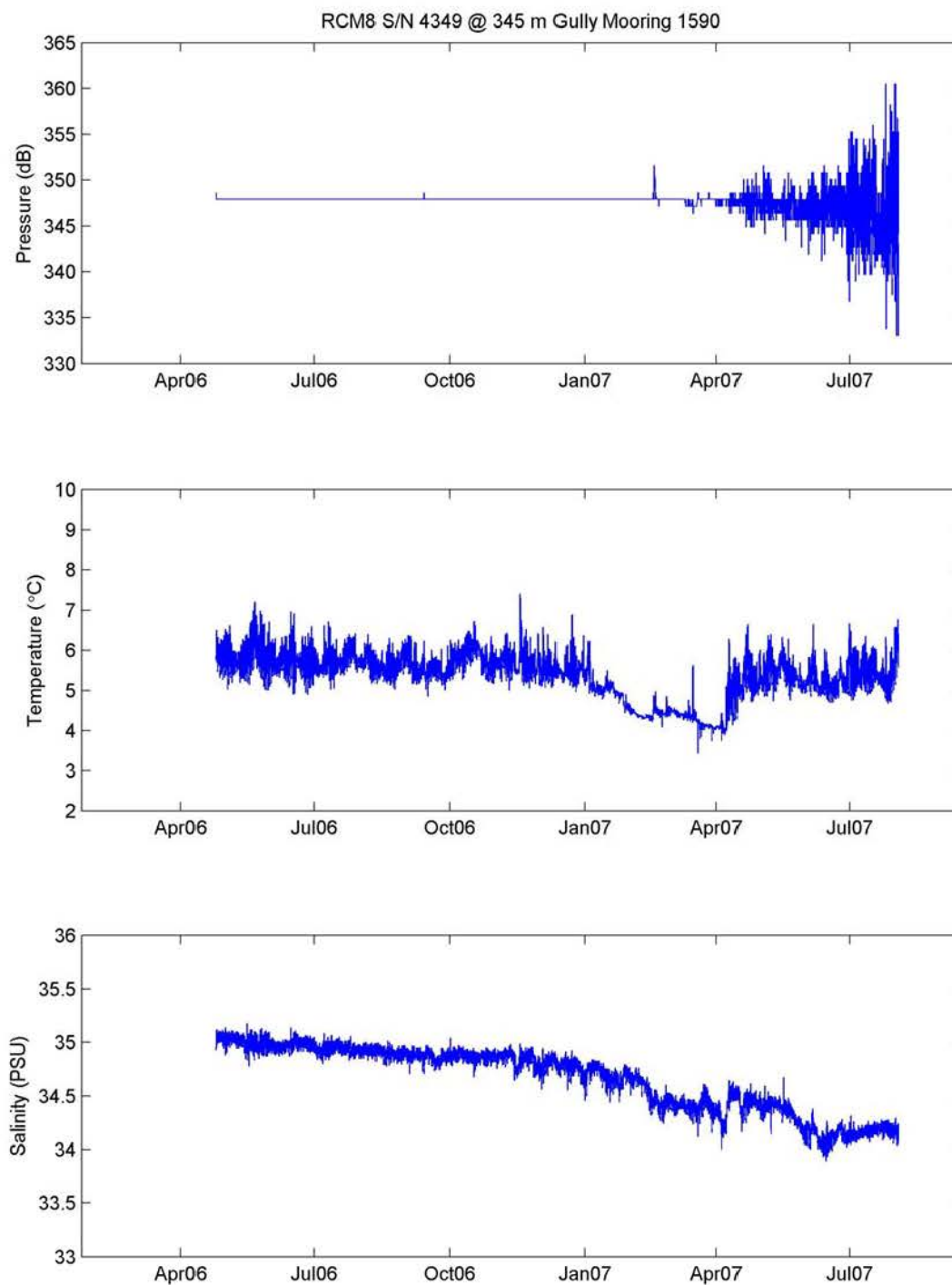


Figure A- 94: RCM-based pressure, temperature and salinity time series on mooring 1590 (SG12).

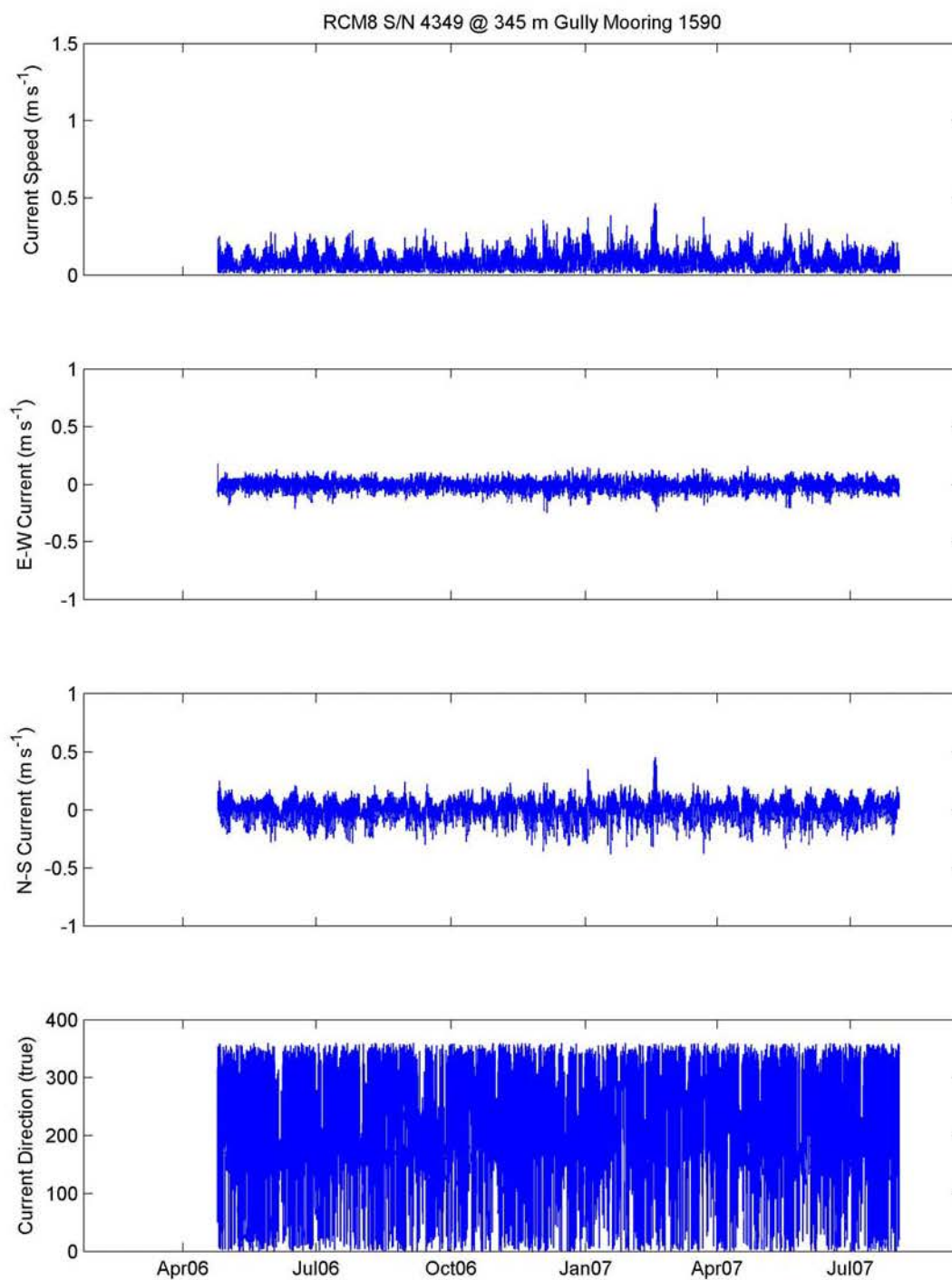


Figure A- 95: Current speed, east-west and north-south components, and current direction time series on mooring 1590 (SG12).

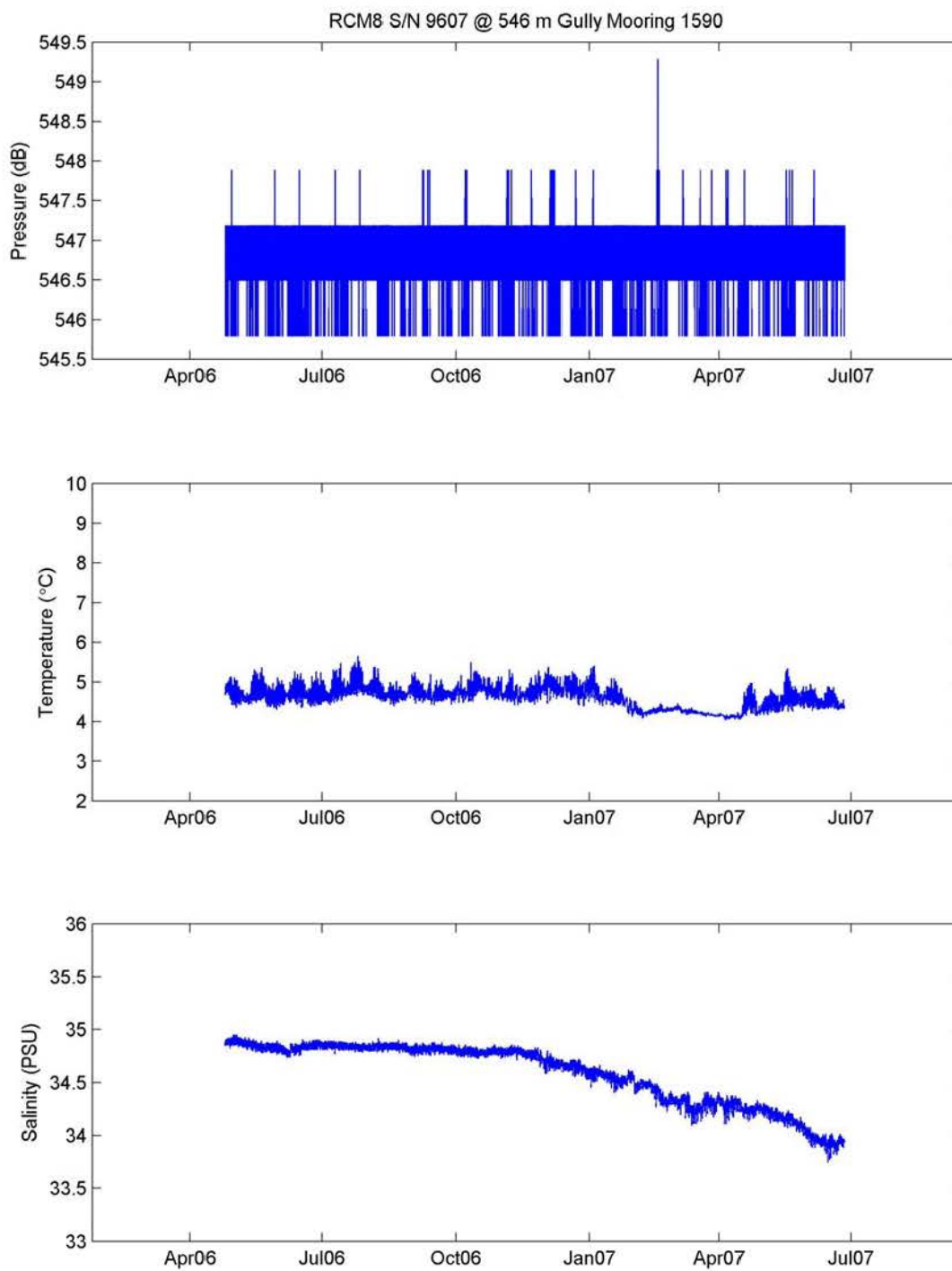


Figure A- 96: RCM-based pressure, temperature and salinity time series on mooring 1590 (SG12).

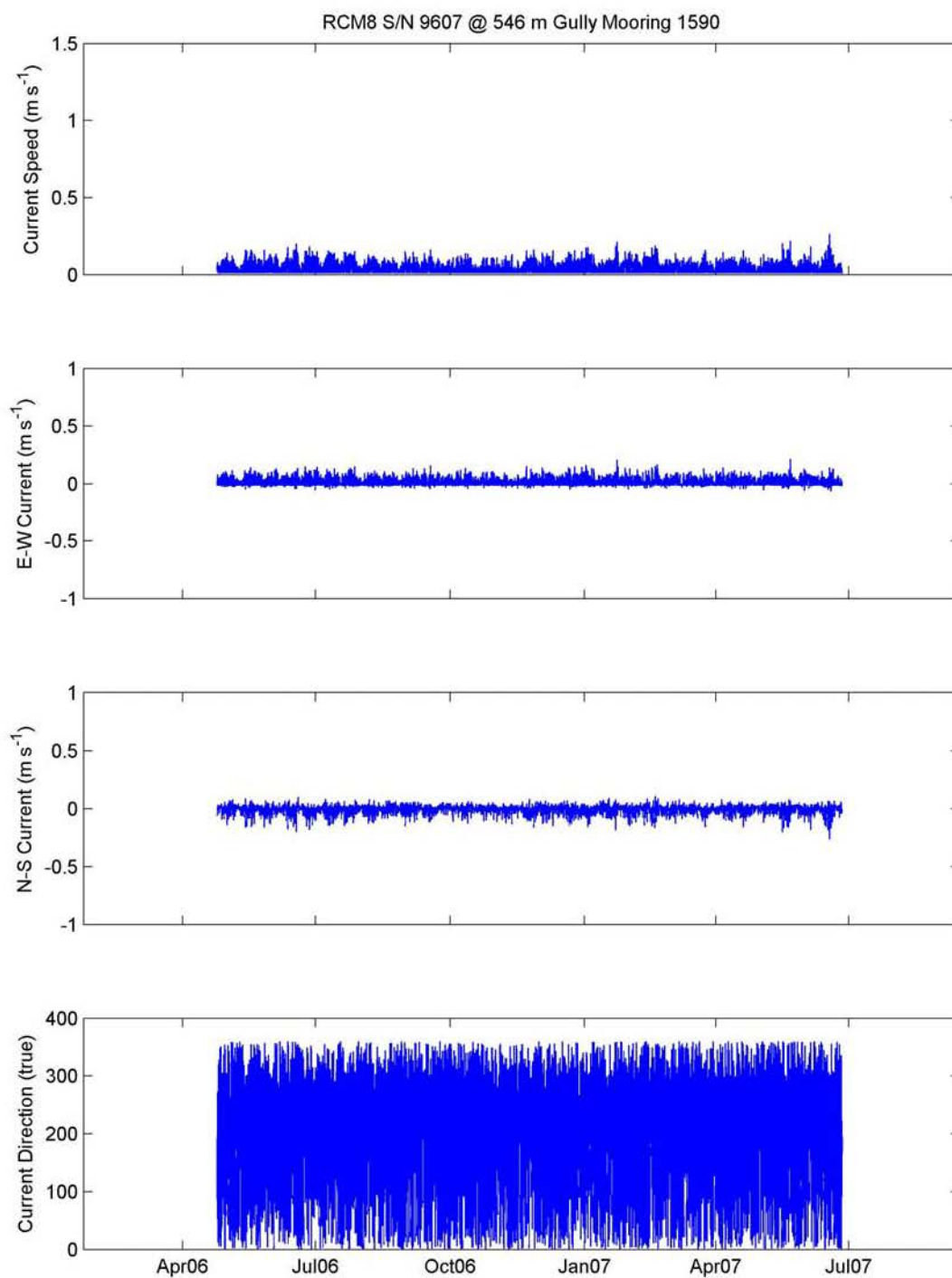


Figure A- 97: Current speed, east-west and north-south components, and current direction time series on mooring 1590 (SG12).

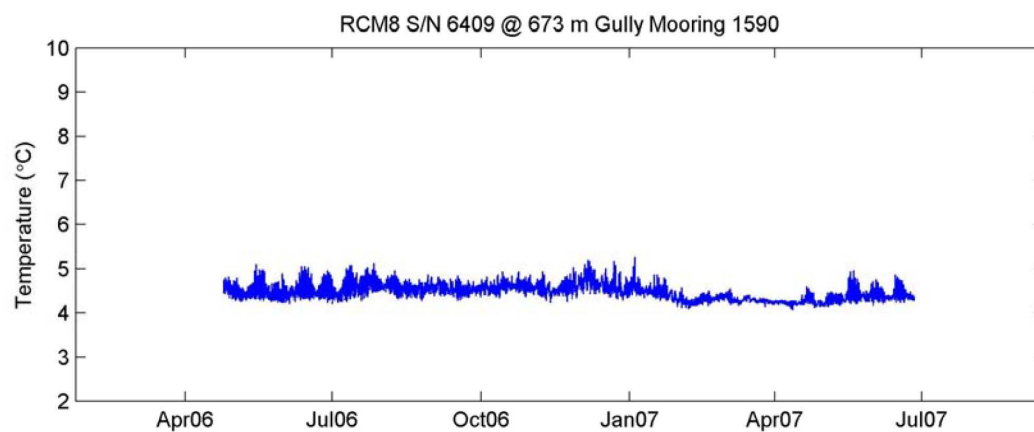


Figure A- 98: RCM-based temperature time series on mooring 1590 (SG12).

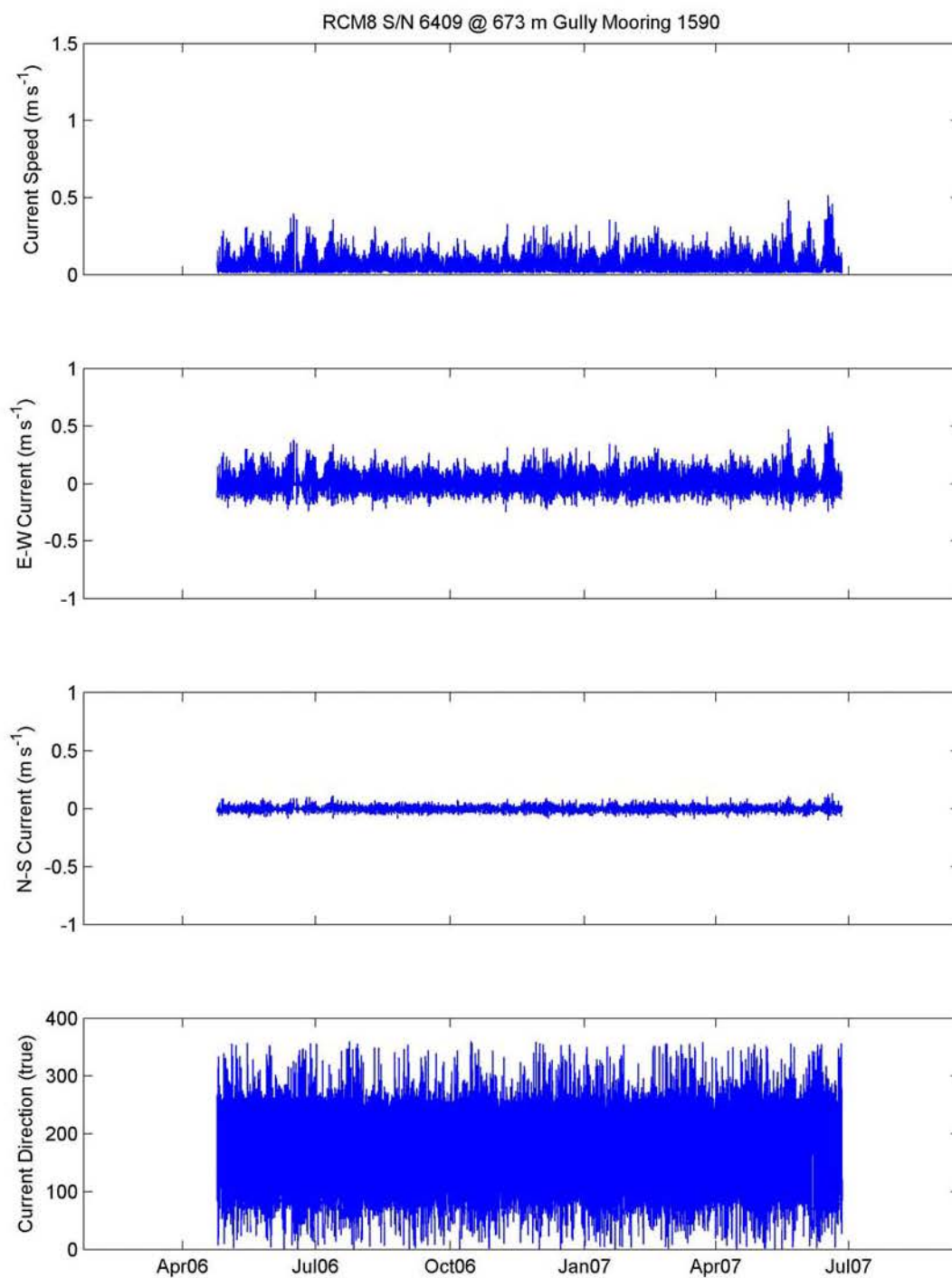


Figure A- 99: Current speed, east-west and north-south components, and current direction time series on mooring 1590 (SG12).

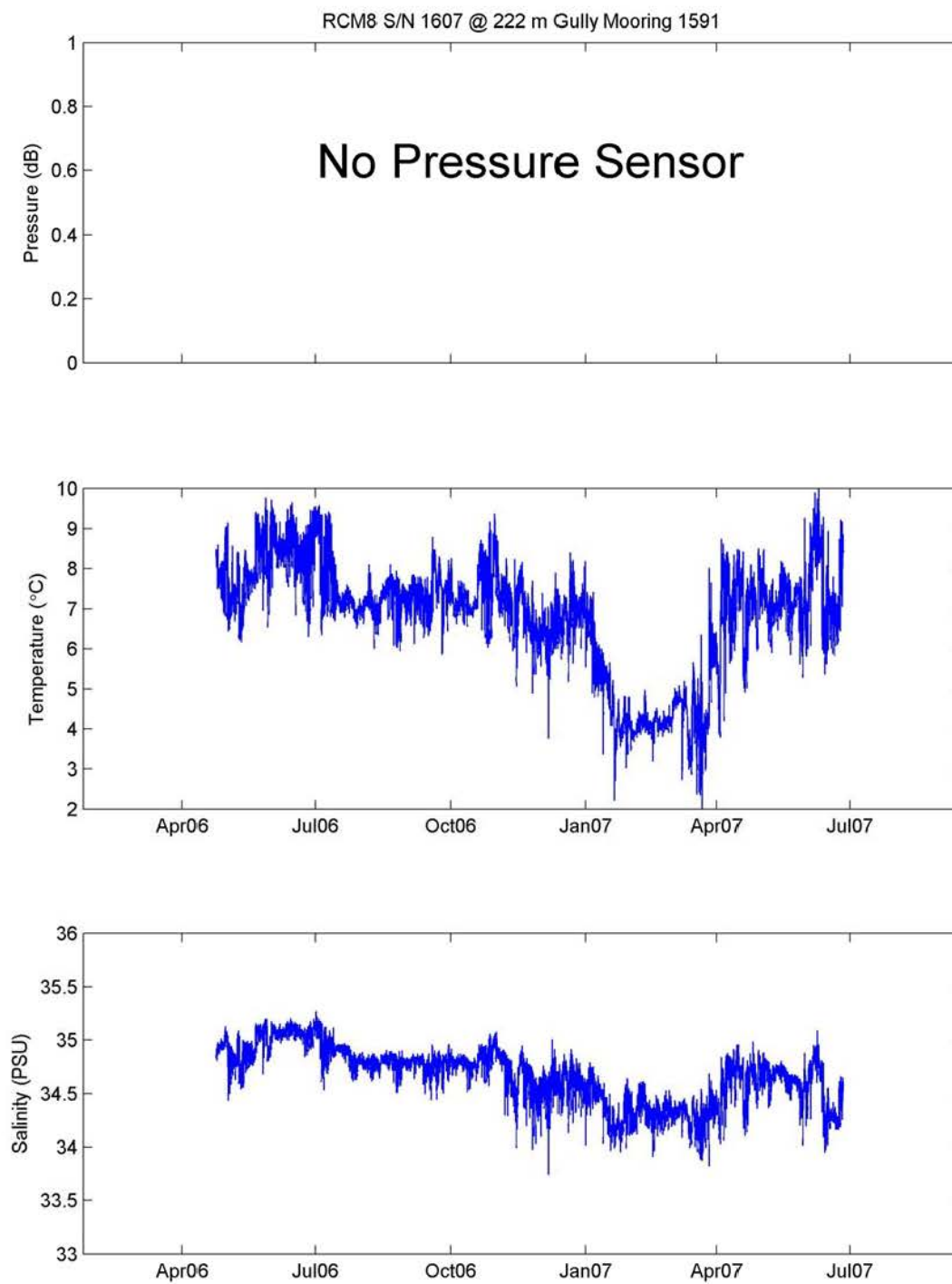


Figure A- 100: RCM-based temperature and salinity time series on mooring 1591 (SG10).

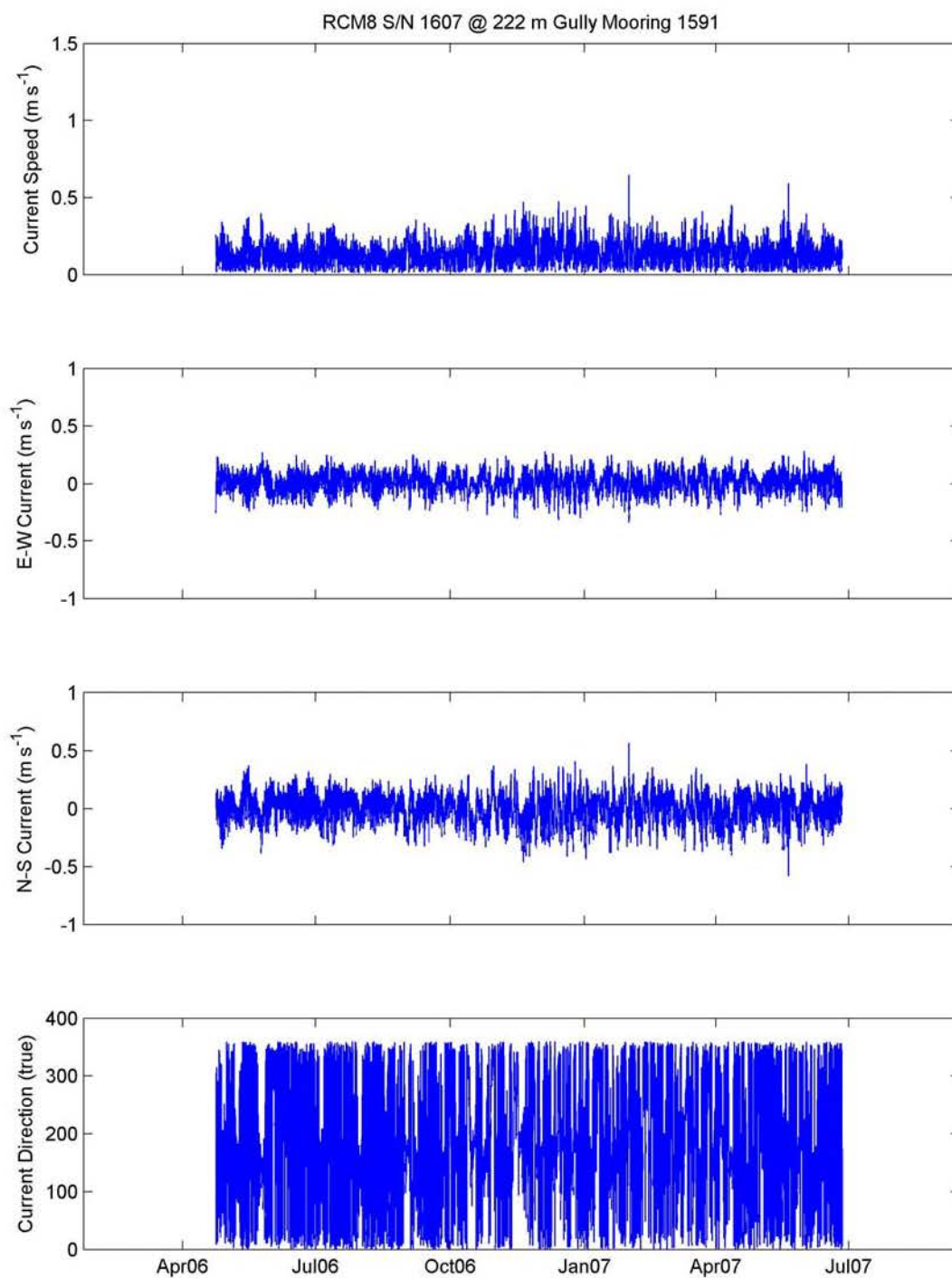


Figure A- 101: Current speed, east-west and north-south components, and current direction time series on mooring 1591 (SG10).

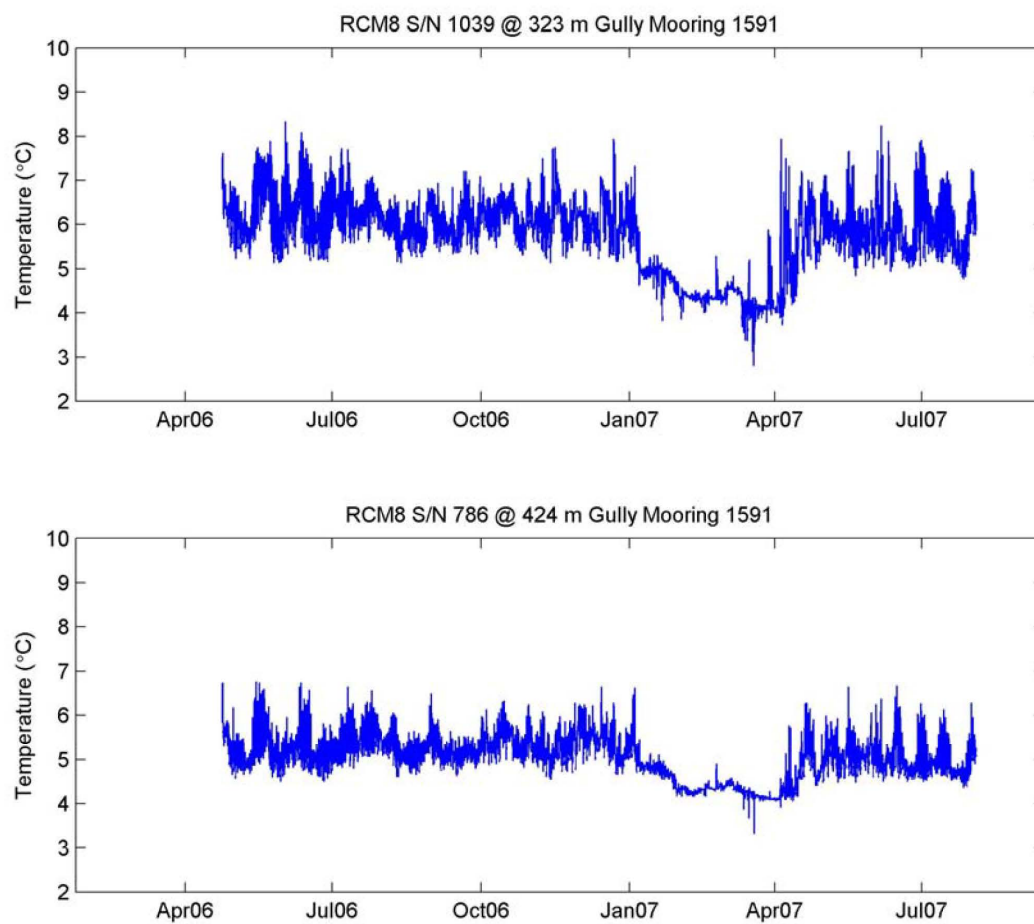


Figure A- 102: RCM-based temperature time series on mooring 1591 (SG10).

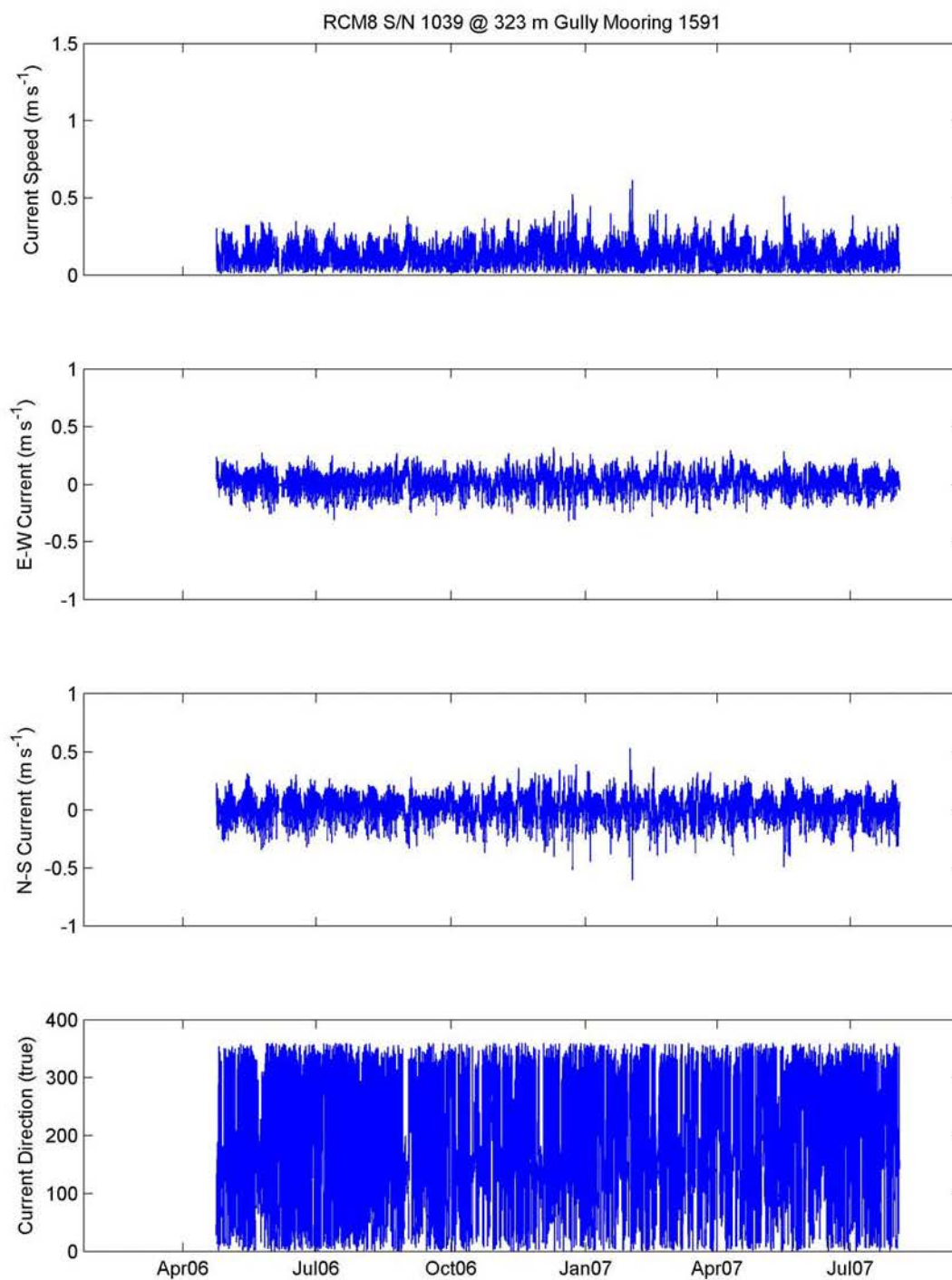


Figure A- 103: Current speed, east-west and north-south components, and current direction time series on mooring 1591 (SG10).

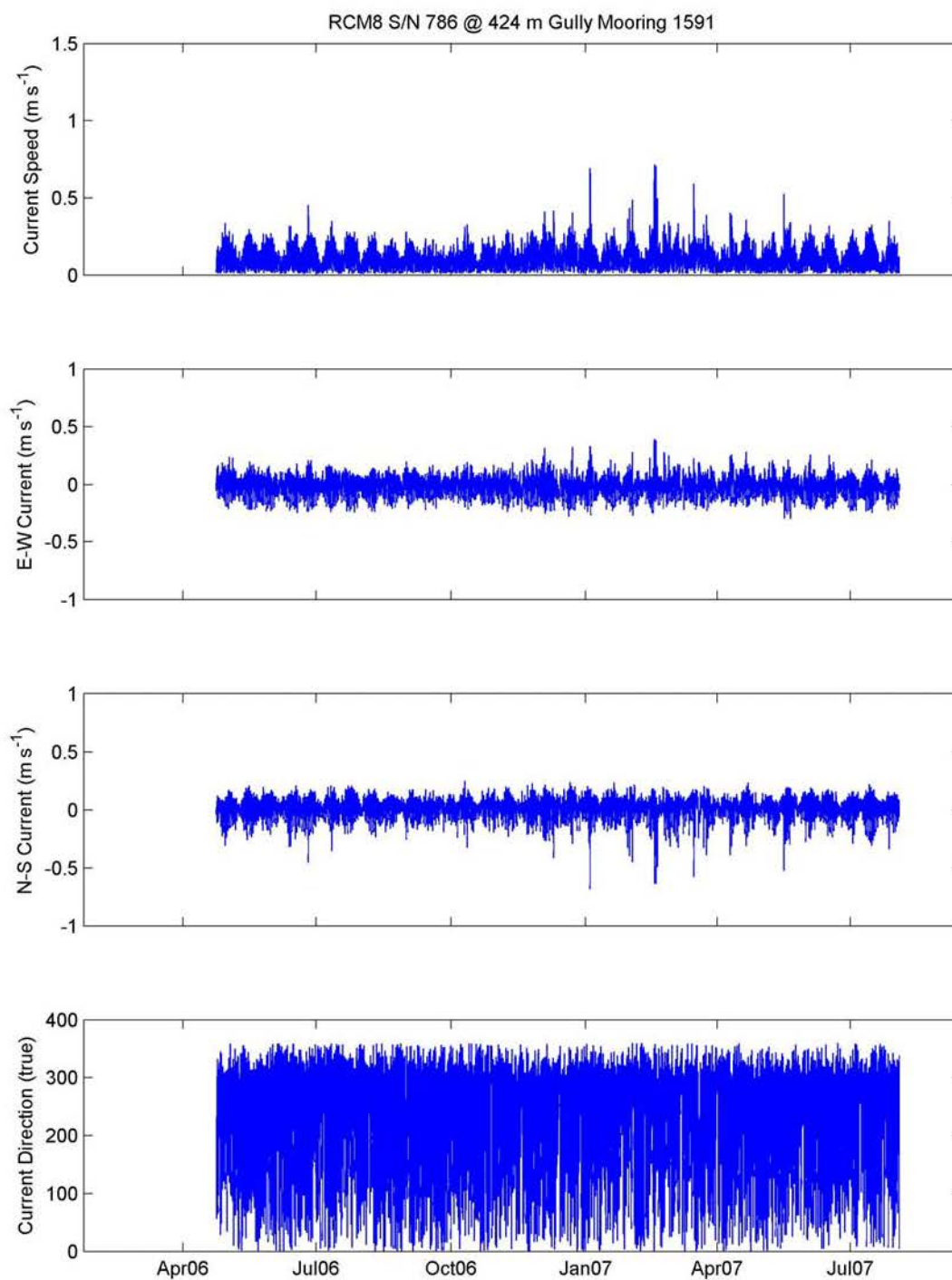


Figure A- 104: Current speed, east-west and north-south components, and current direction time series on mooring 1591 (SG10).

Appendix 7: Moored Temperature-Salinity Time Series

Four moorings were deployed at the sites SG2 (mooring #1588), SG10 (mooring #1591), SG11 (mooring #1589), SG12 (mooring #1590), in Zone 1 of the Gully (**Figure 1**). Each mooring consisted of Aanderaa RCM8 meters and Sea-Bird SBE37 Microcat sensors which measured both temperature and salinity, and Vemco Minilog temperature recorders (Appendix 1). The moorings were deployed April 23 and 24, 2006 and recovered on August 3, 2007. The deep central mooring at SG11 when recovered was missing the upper 200 m which included two Microcats; it went missing on 17 June, 2007. Also the two moorings on the canyon axis (#1588 and #1589) underwent vertical displacements, up to 500 m for mooring 1589.

Figure A- 106 to Figure A- 110 are Microcat time series plots of pressure, temperature and salinity. **Error! Reference source not found.** are Minilog temperature time series plots. **Error! Reference source not found.** to **Error! Reference source not found.** are temperature and salinity contour plots versus time for each mooring combining all instruments. **Error! Reference source not found.** to **Error! Reference source not found.** are daily averaged temperature and salinity scatter plots for both RCM meters and Microcat sensors. Colour bar shows time.

All plots were created using MATLAB R2008b.

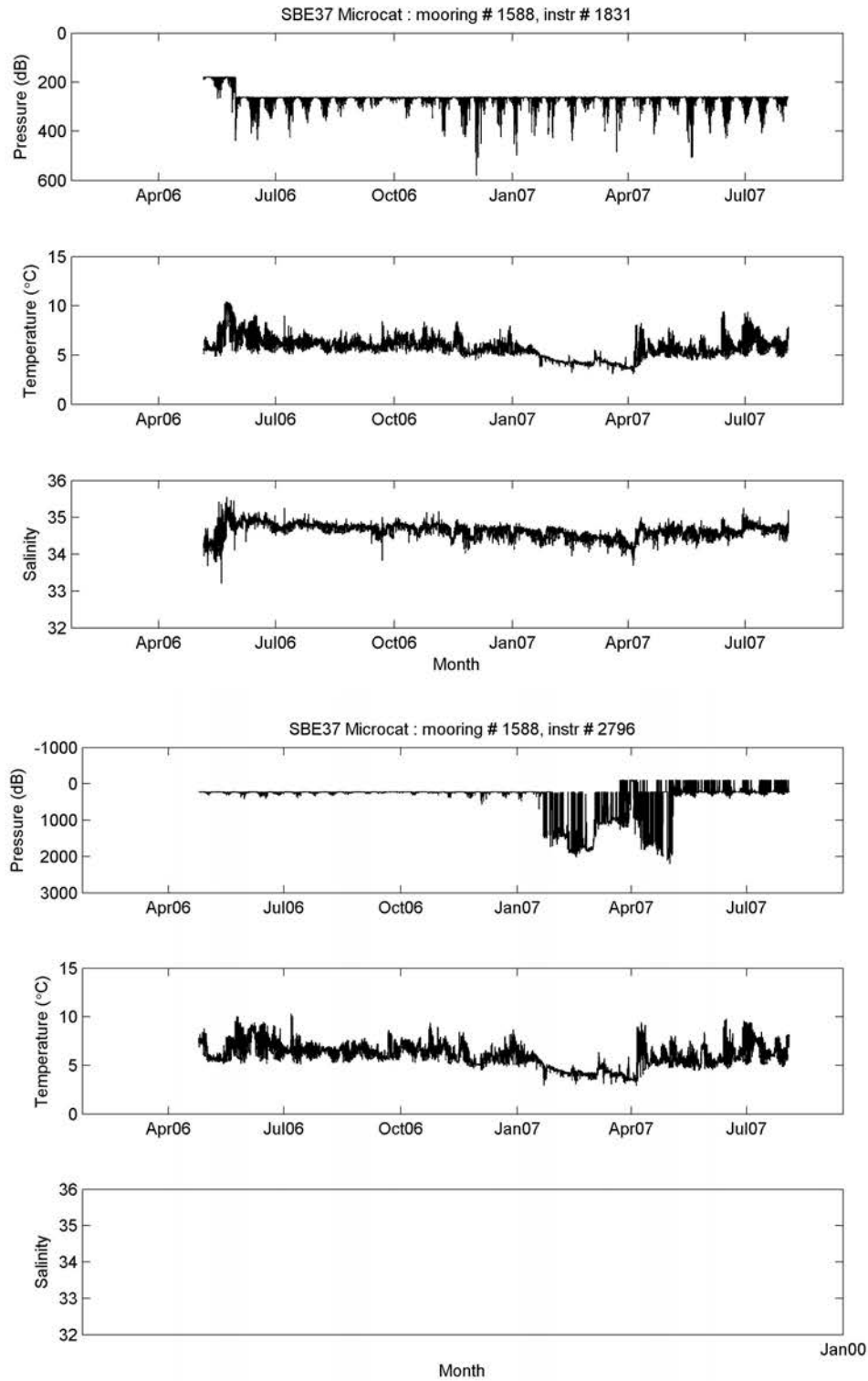


Figure A- 105: SBE37 Microcat pressure, temperature and salinity time series for mooring 1588. Refer to schematic in Appendix A for location of instruments on mooring. This instrument had a faulty conductivity sensor.

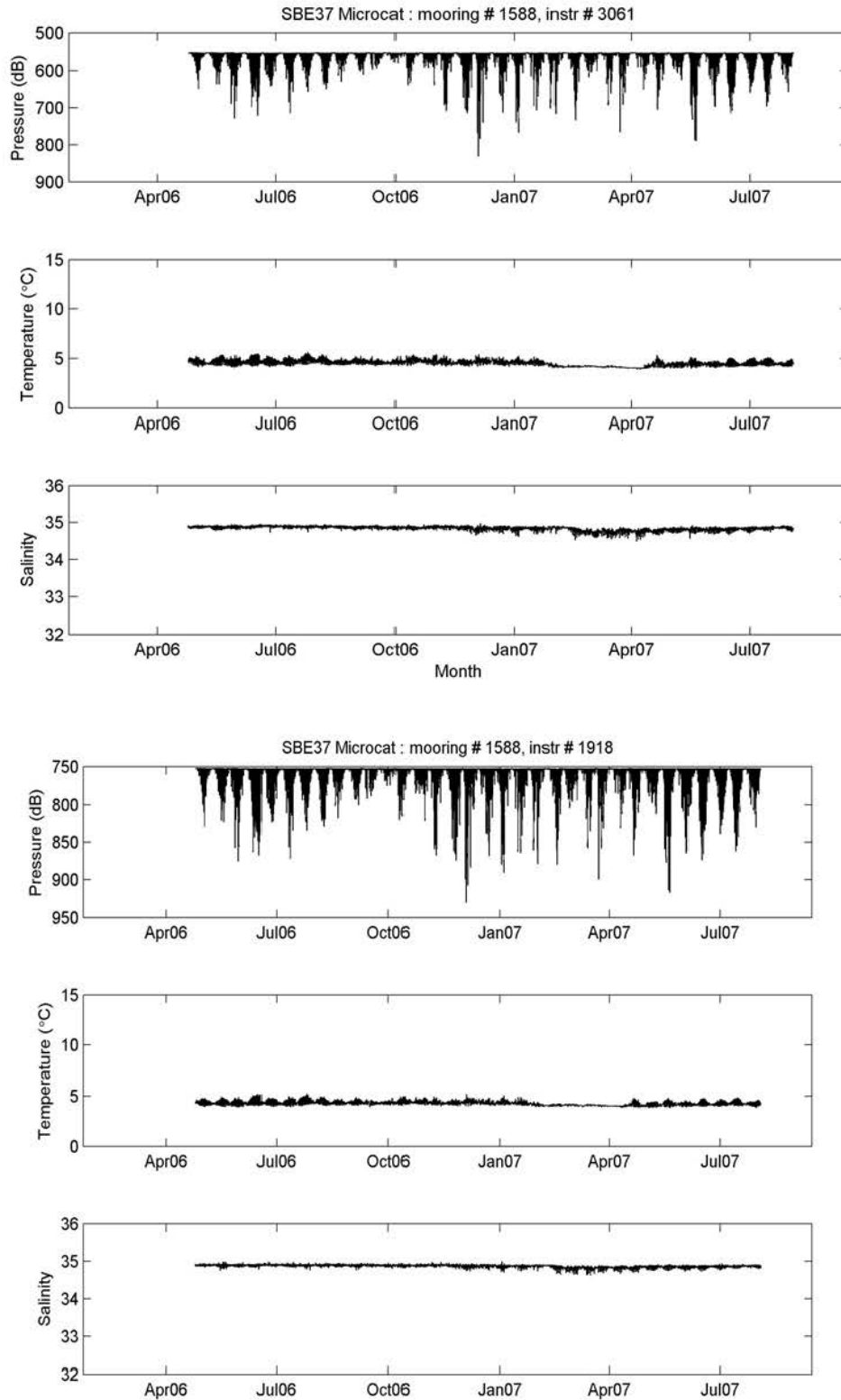


Figure A- 106: SBE37 Microcat pressure, temperature and salinity time series for mooring 1588. Refer to schematic in Appendix A for location of instruments on mooring. Instrument #2796 had faulty conductivity sensor.

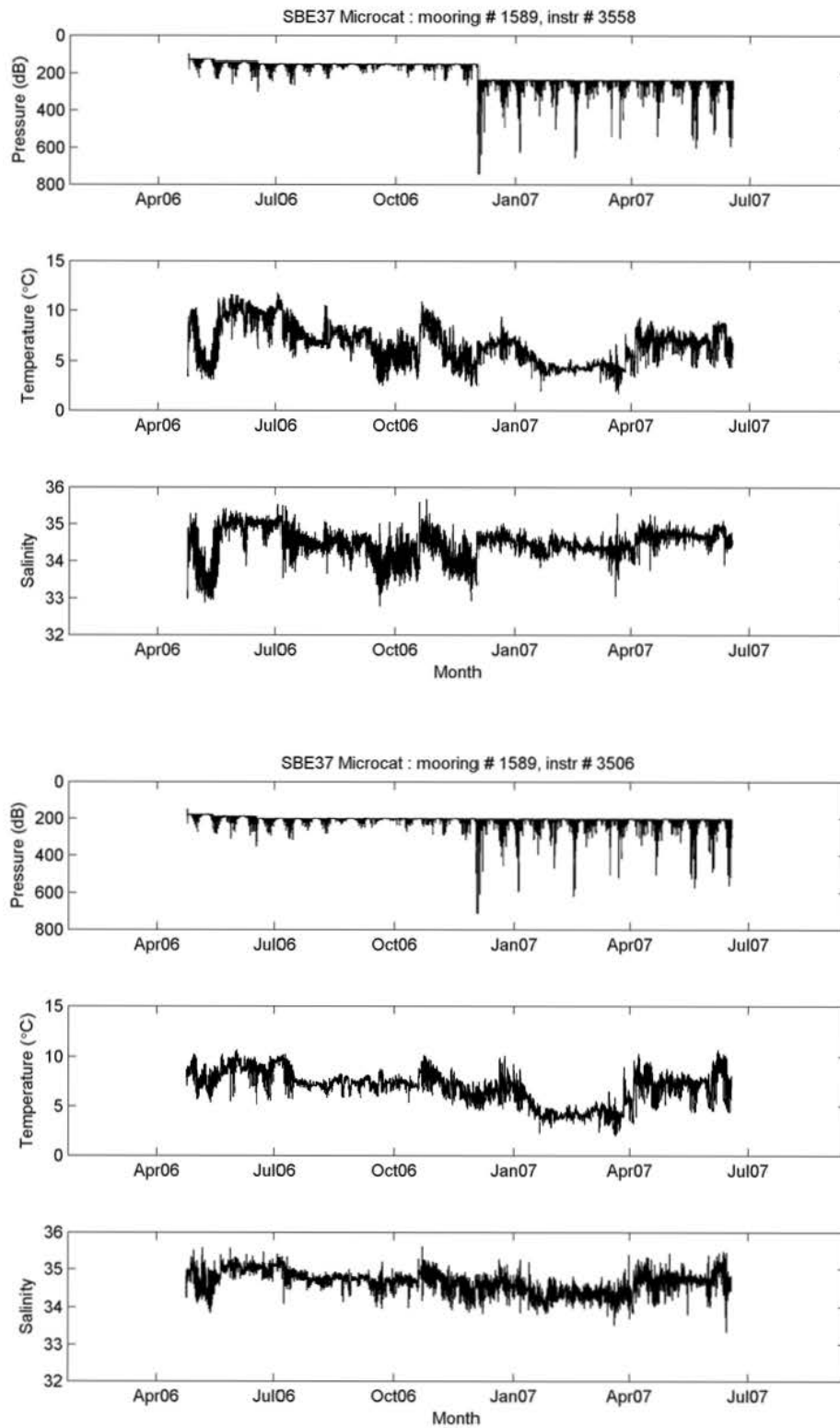


Figure A- 107: SBE37 Microcat pressure, temperature and salinity time series for mooring 1589. Refer to schematic in Appendix A for location of instruments on mooring.

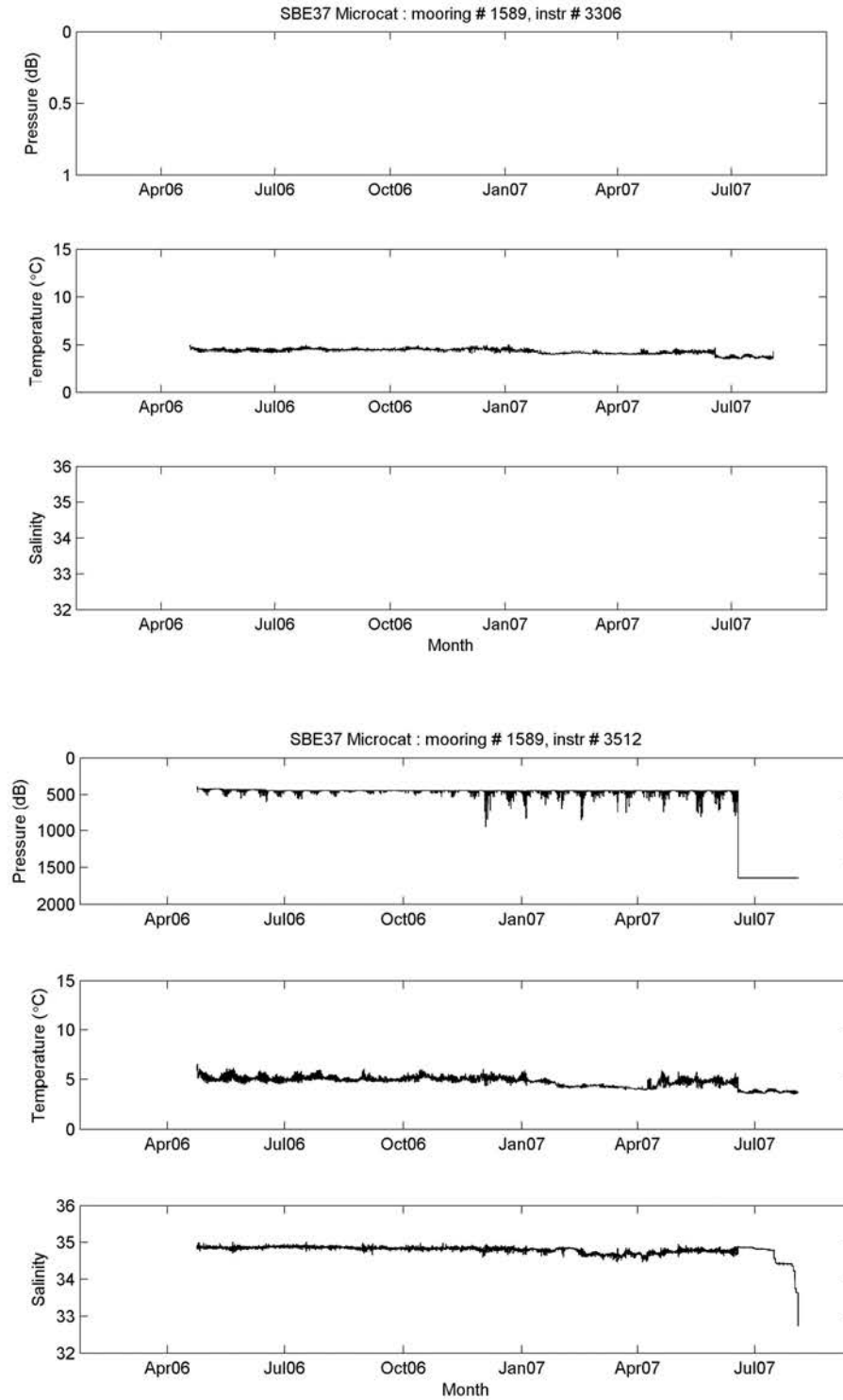


Figure A- 108: SBE37 Microcat pressure, temperature and salinity time series for mooring 1589. Refer to schematic in Appendix A for location of instruments on mooring. Instrument #3306 had faulty conductivity and pressure sensors.

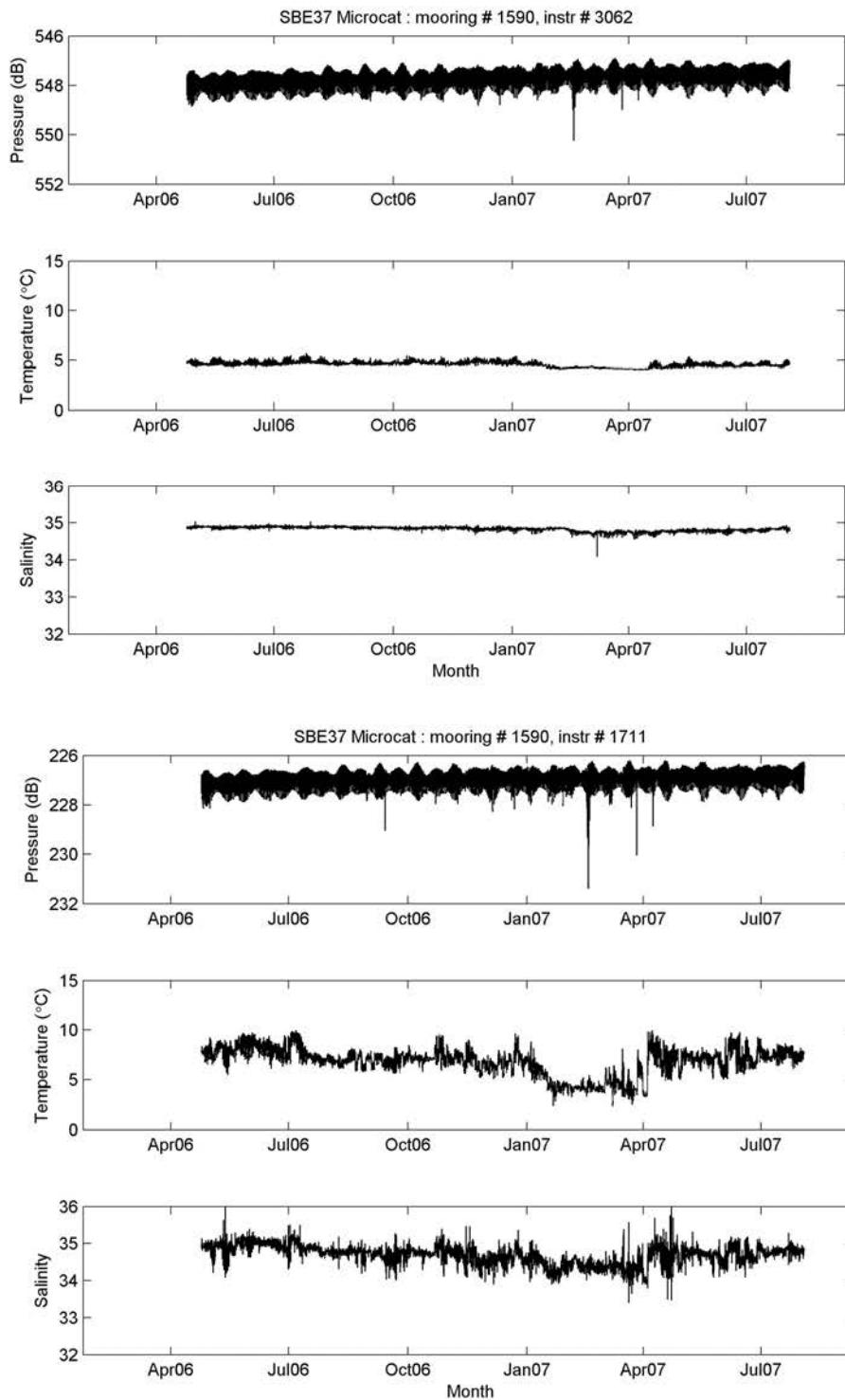


Figure A- 109: SBE37 Microcat pressure, temperature and salinity time series for mooring 1590. Refer to schematic in Appendix A for location of instruments on mooring.

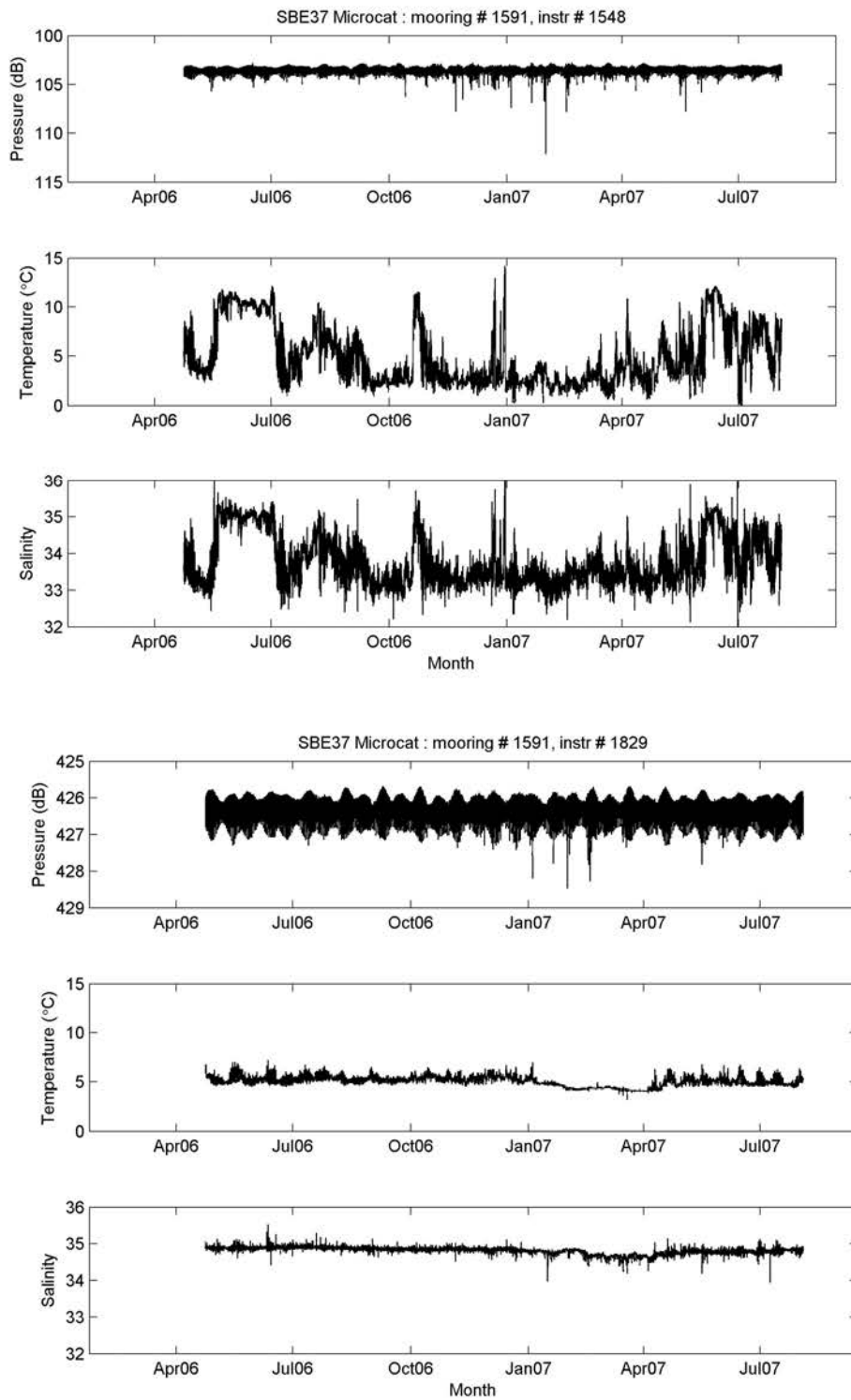


Figure A- 110: SBE37 Microcat pressure, temperature and salinity time series for mooring 1591. Refer to schematic in Appendix A for location of instruments on mooring.

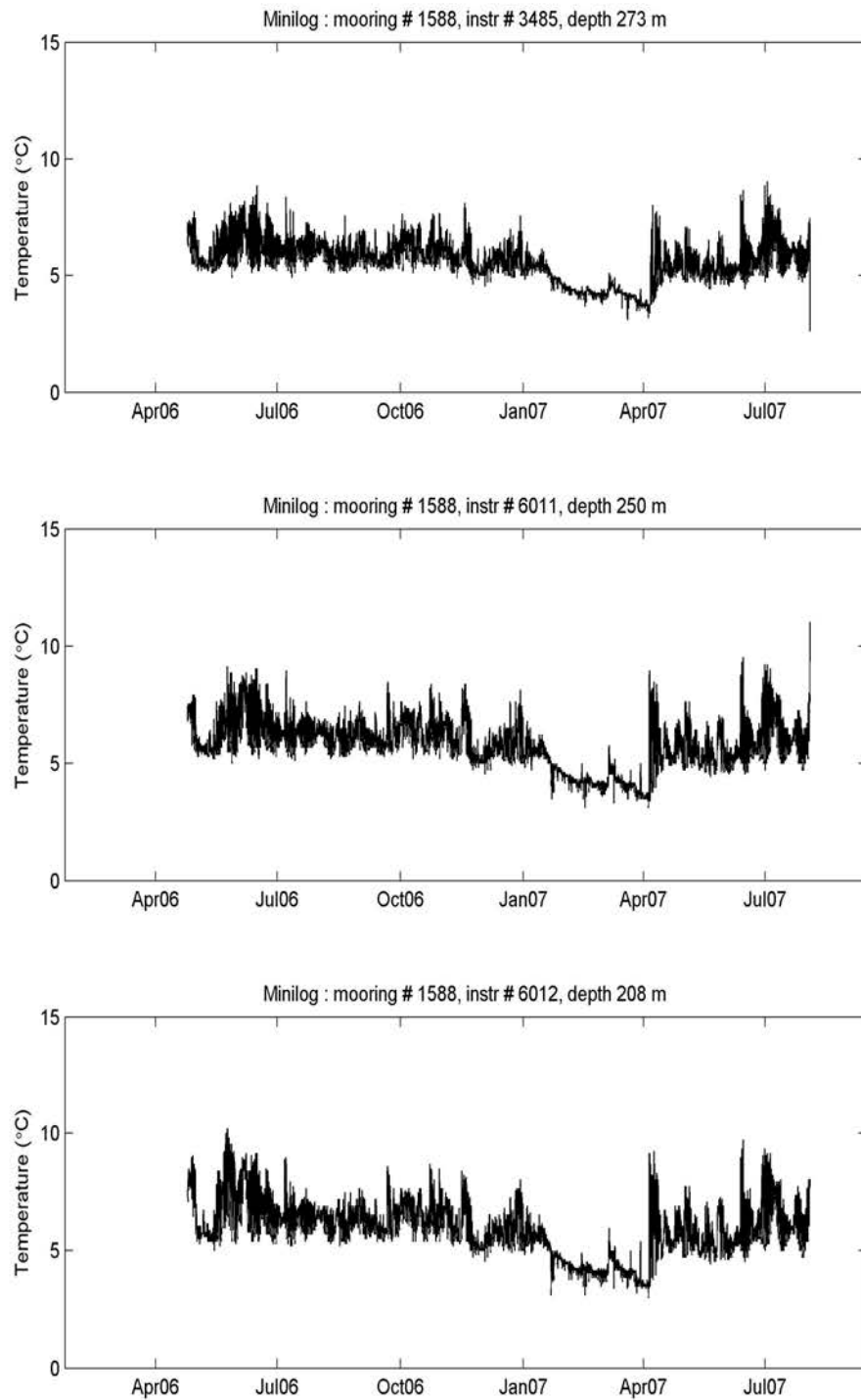


Figure A- 111: Minilog temperature time series for mooring 1588. Refer to schematic in Appendix A for location of instruments on mooring.

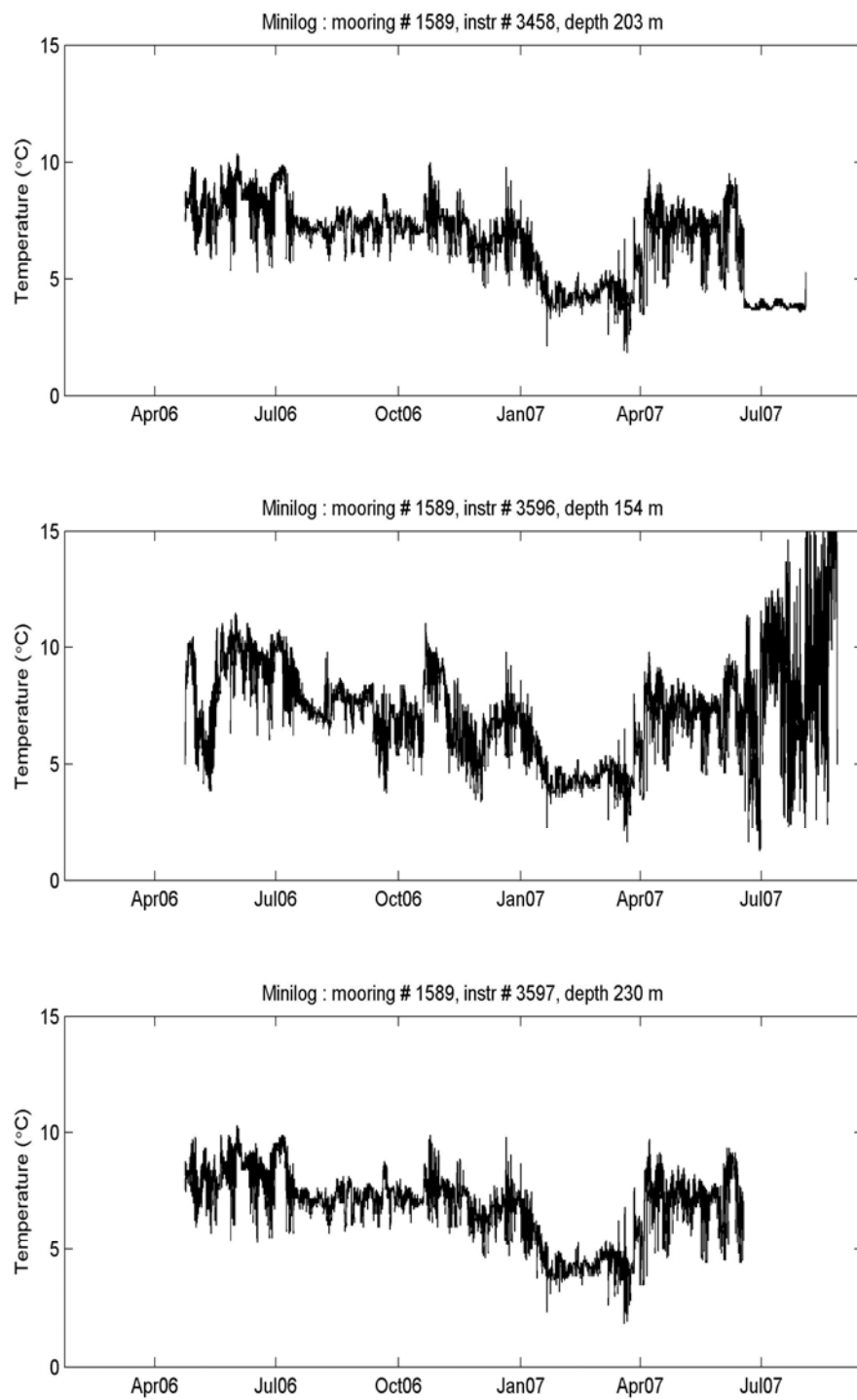


Figure A- 112: Minilog temperature time series for mooring 1589. Refer to schematic in Appendix A for location of instruments on mooring.

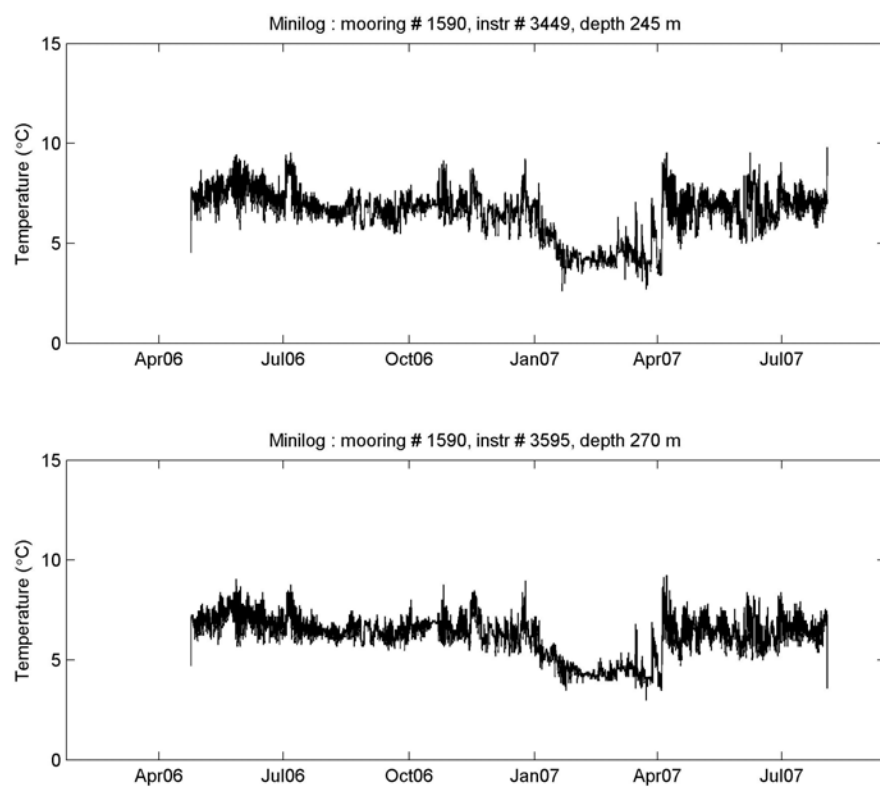


Figure A- 113: Minilog temperature time series for mooring 1590. Refer to schematic in Appendix A for location of instruments on mooring.

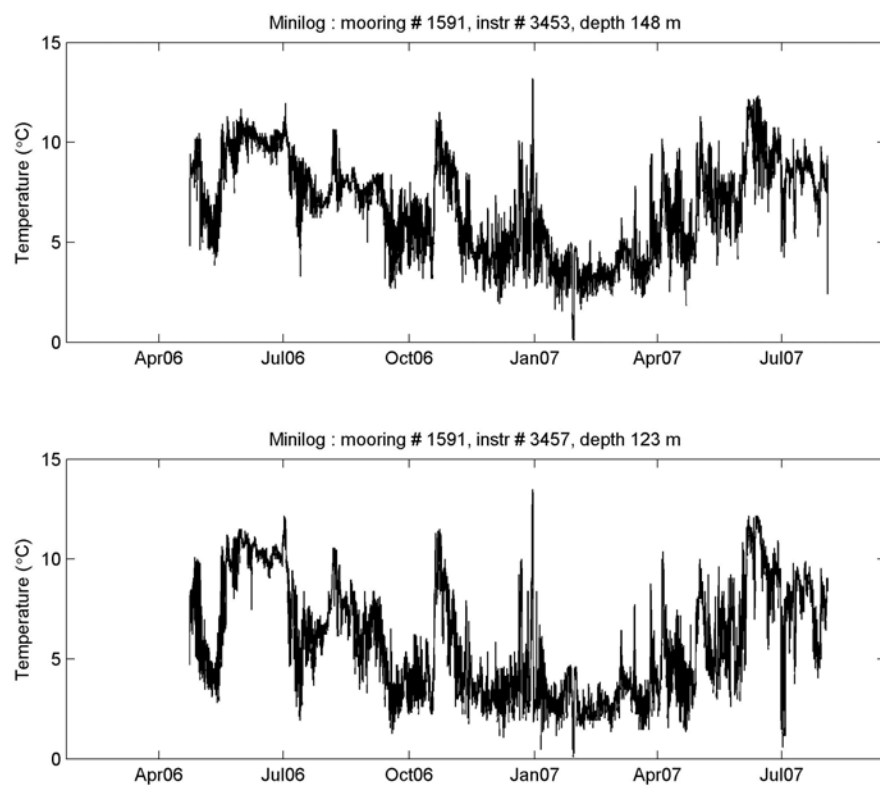


Figure A- 114: Minilog temperature time series for mooring 1591. Refer to schematic in Appendix A for location of instruments on mooring.

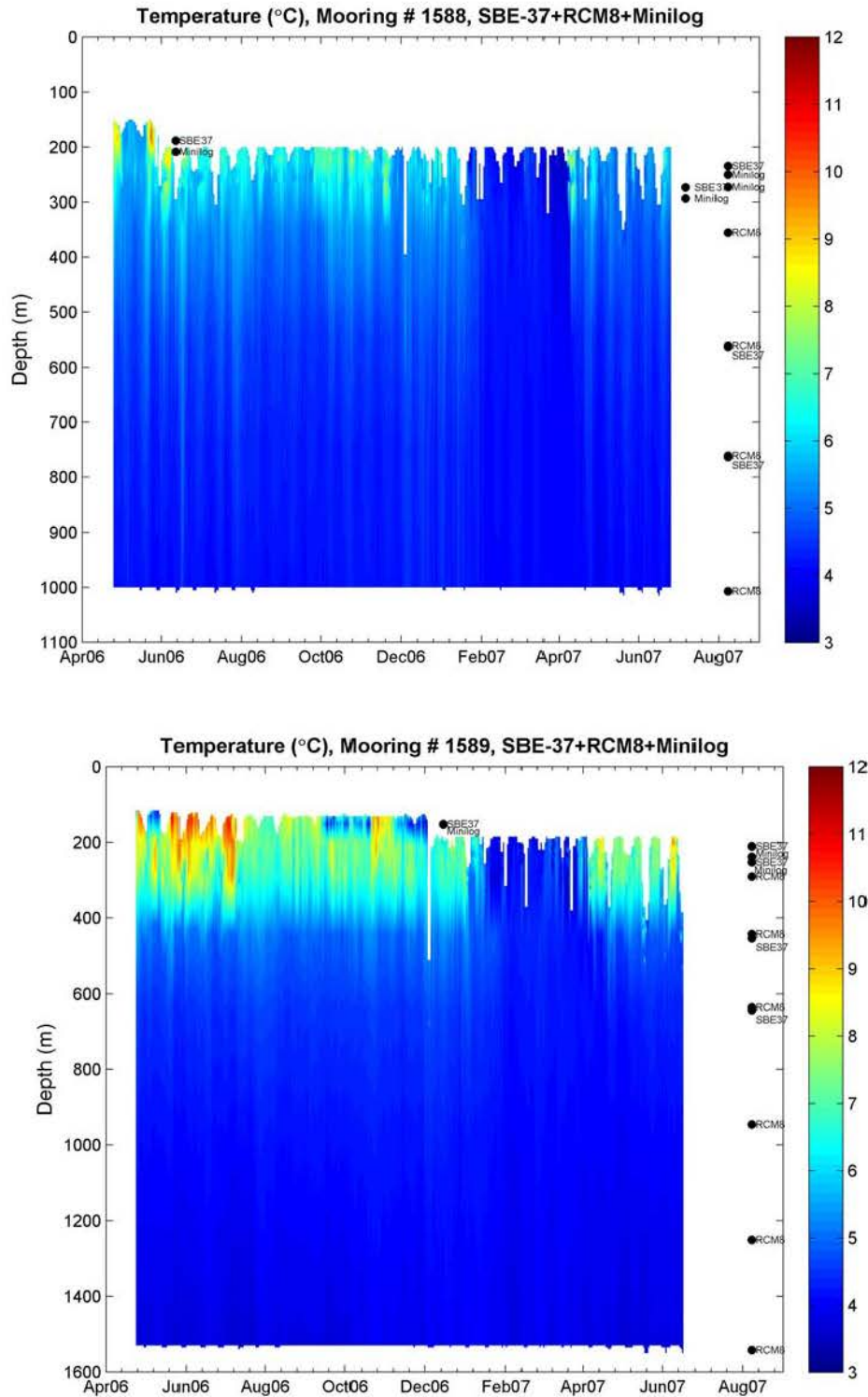


Figure A- 115: Combined Minilog, Microcat and RCM temperature time series for moorings 1588 and 1589. Refer to schematic in Appendix A for location of instruments on mooring. Dots indicate the positions of instruments on the moorings.

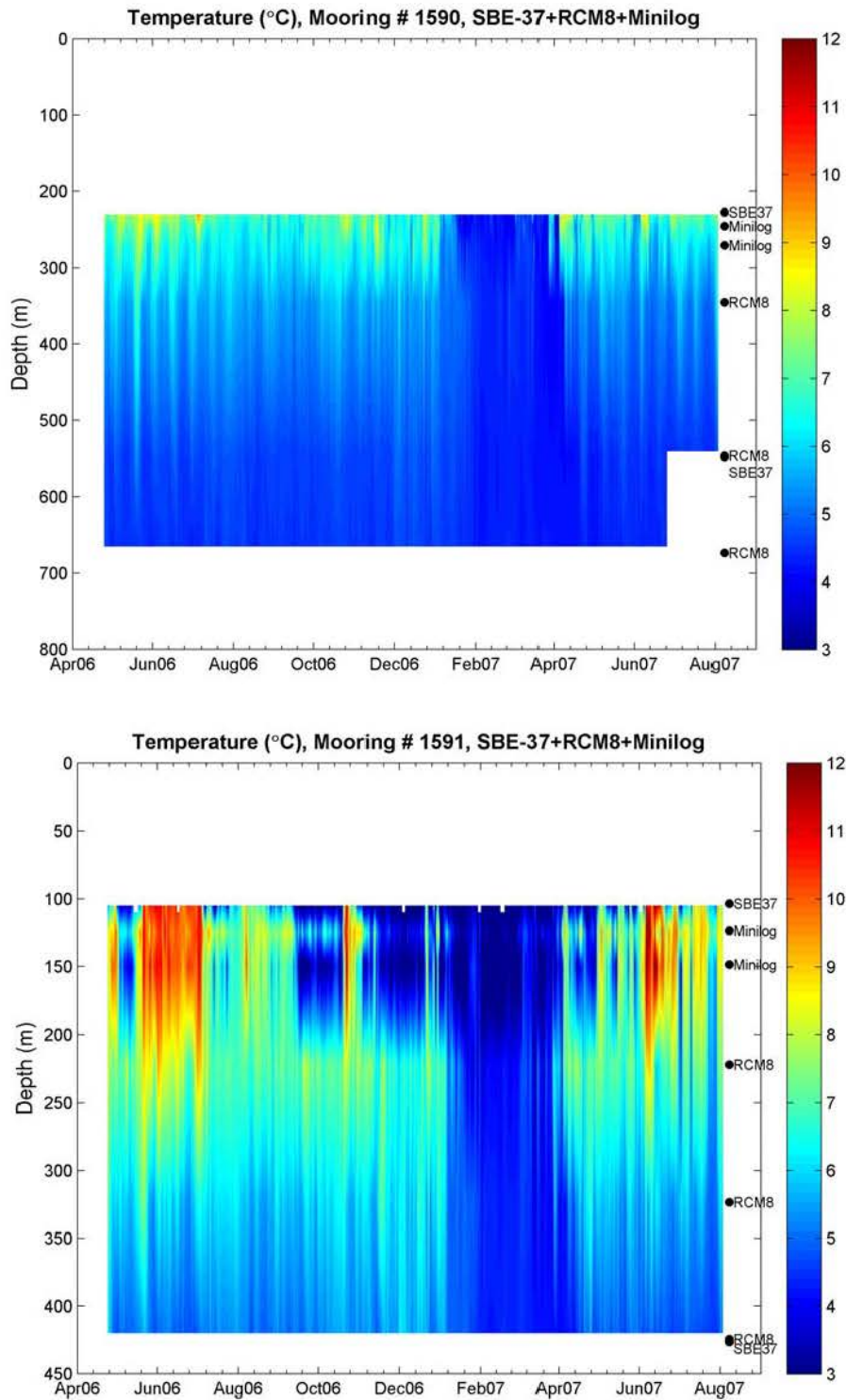


Figure A- 116: Combined Minilog, Microcat and RCM temperature time series for moorings 1590 and 1591. Refer to schematic in Appendix A for location of instruments on mooring.

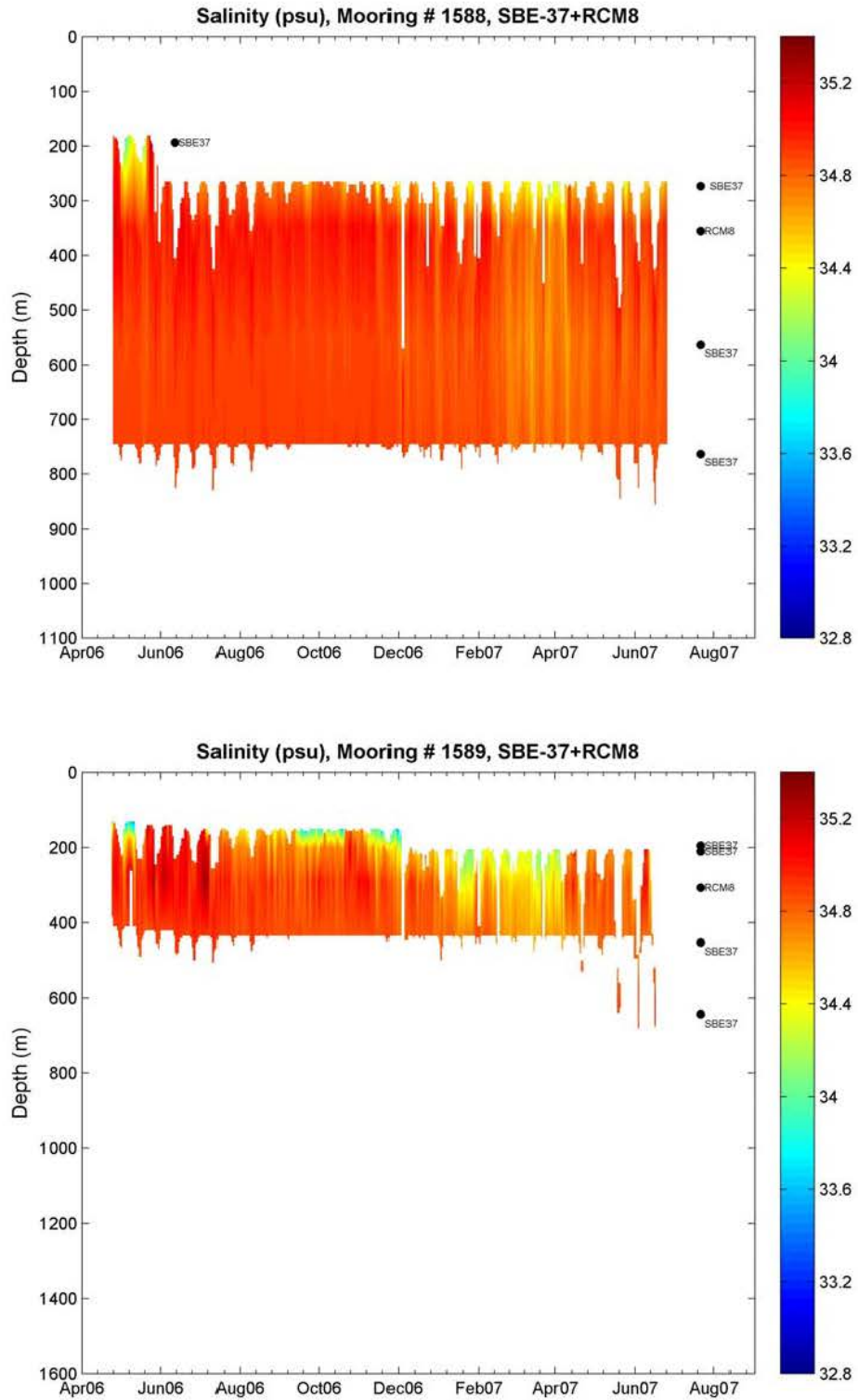


Figure A- 117: Combined, Microcat and RCM salinity time series for moorings 1588 and 1589. Refer to schematic in Appendix A for location of instruments on mooring.

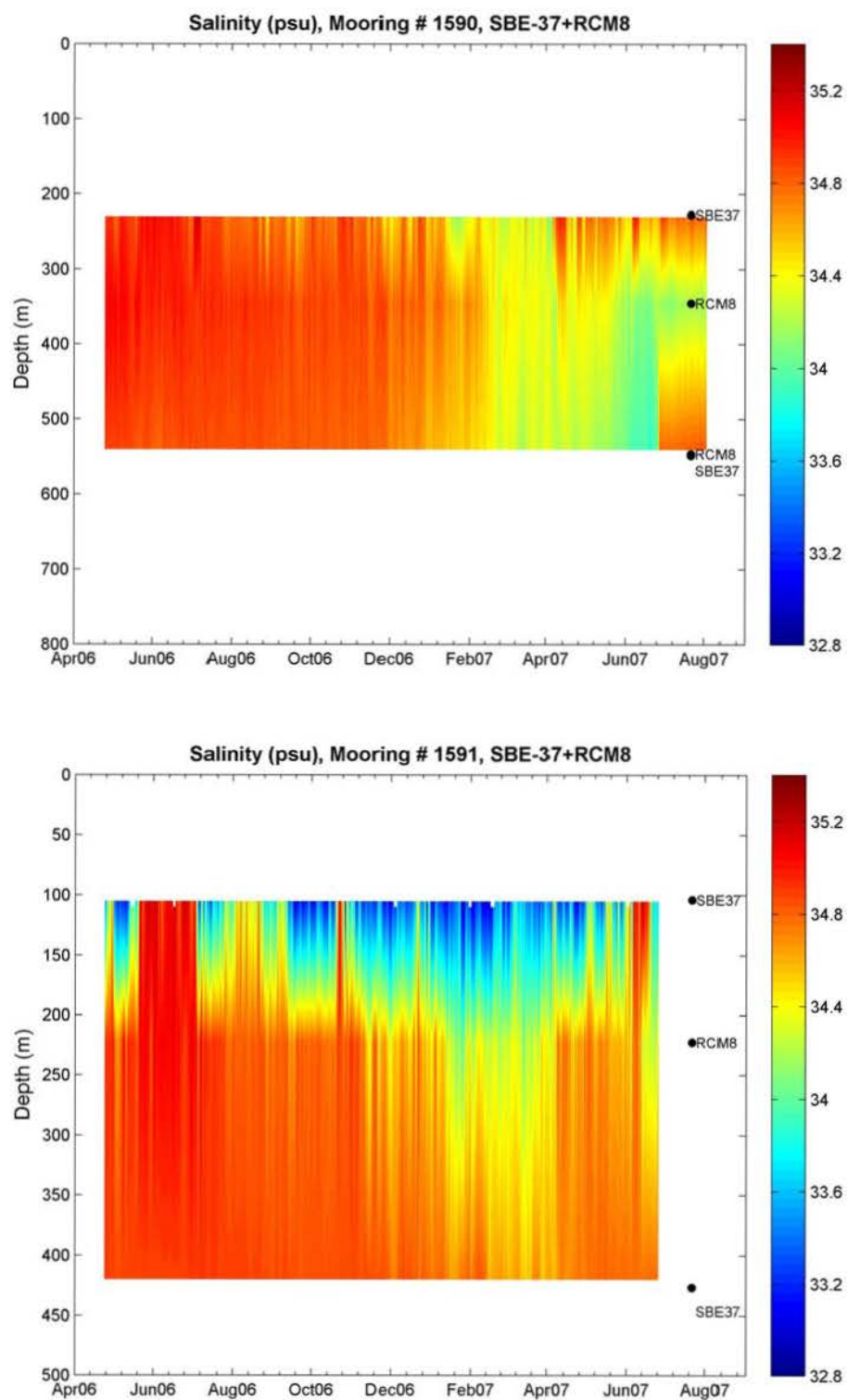


Figure A- 118: Combined, Microcat and RCM salinity time series for moorings 1590 and 1591. Refer to schematic in Appendix A for location of instruments on mooring.

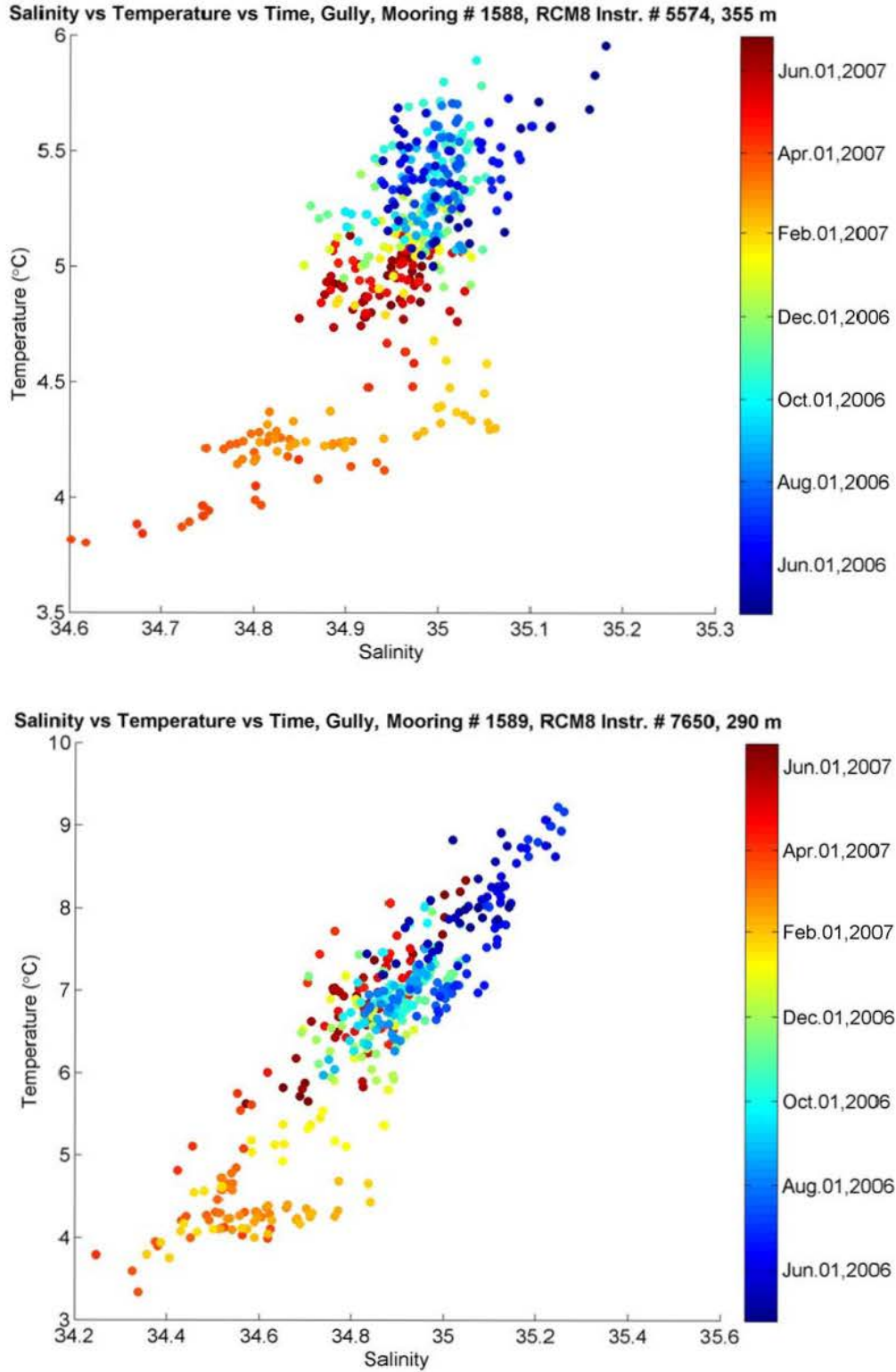


Figure A- 119: Temperature-salinity plots for moorings 1588 and 1589 colour-coded by time of sample.

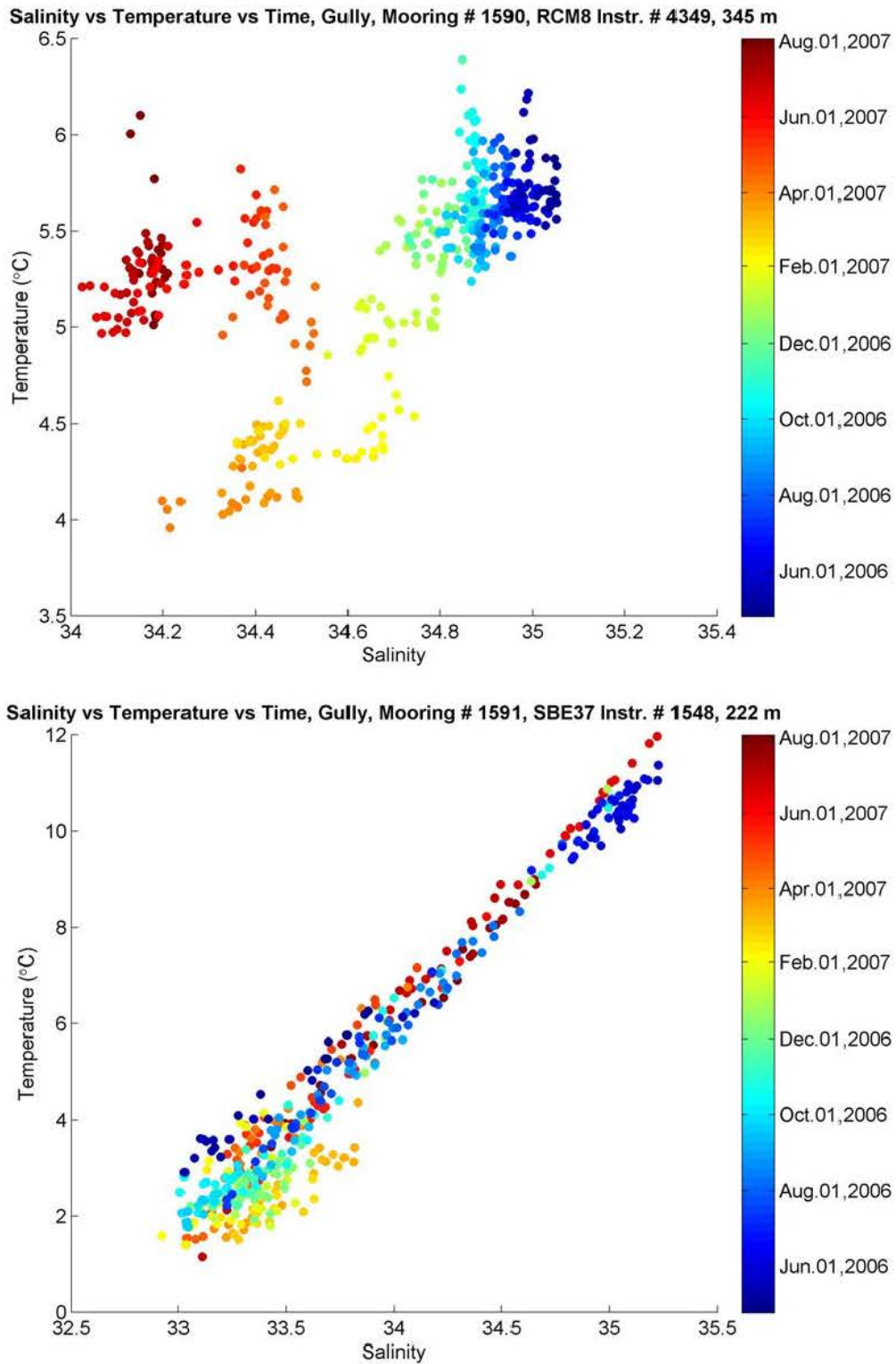


Figure A- 120: Temperature-salinity plots for moorings 1590 and 1591 colour-coded by time of sample.

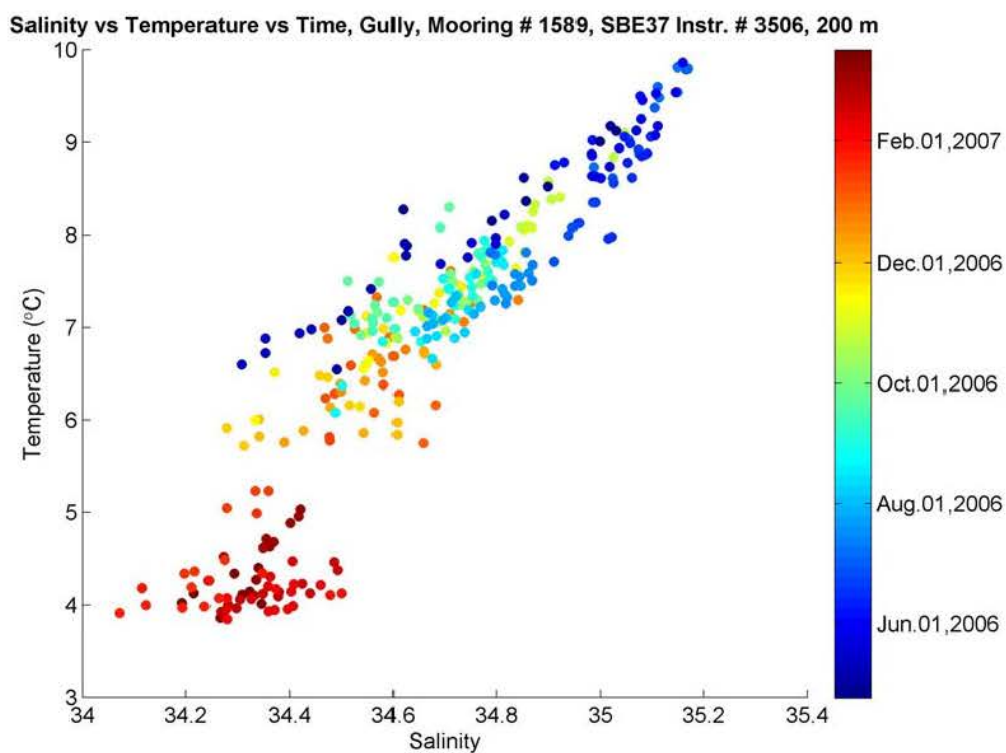
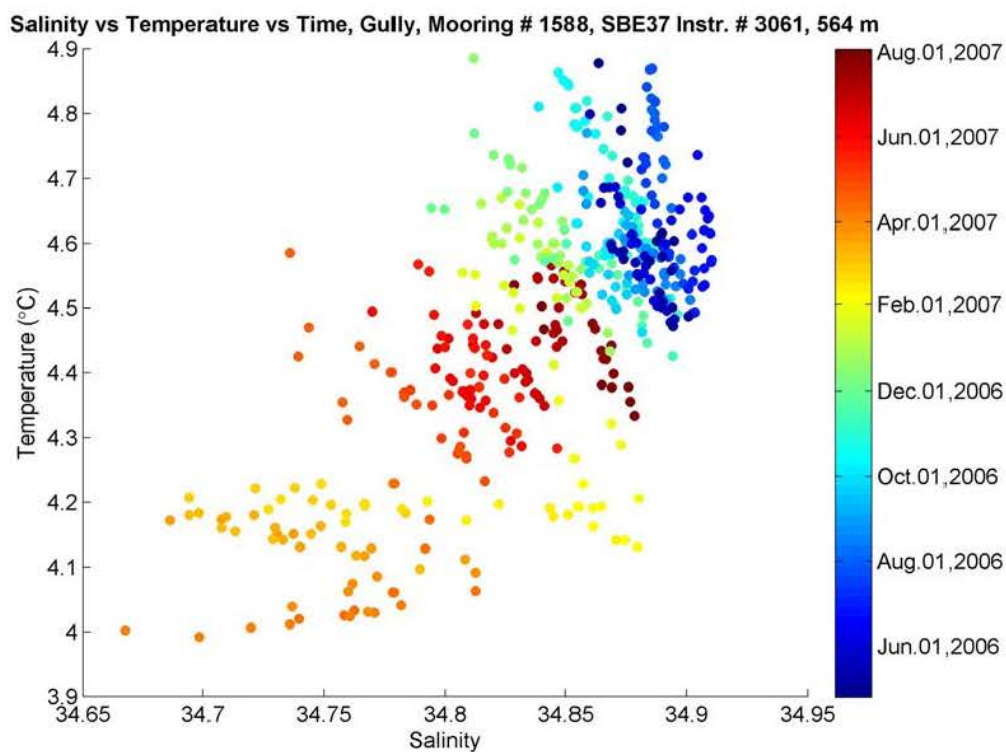


Figure A- 121: Temperature-salinity plots for moorings 1588 and 1589 colour-coded by time of sample.

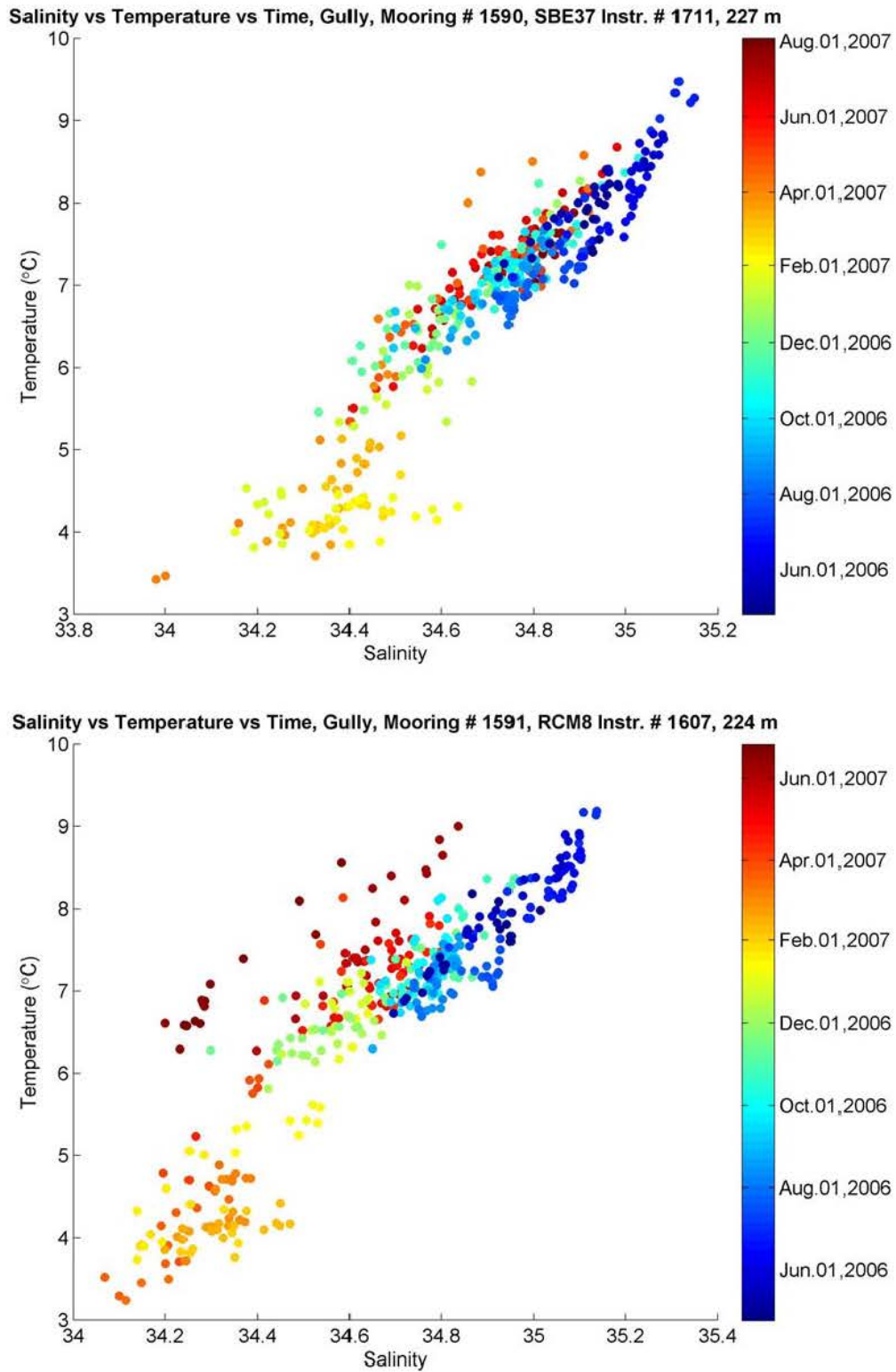


Figure A- 122: Temperature-salinity plots for moorings 1590 and 1591 colour-coded by time of sample.

Appendix 8: Current Meter Data Synthesis

Four moorings were deployed at the sites SG2 (mooring #1588), SG10 (mooring #1591), SG11 (mooring #1589), SG12 (mooring #1590), in Zone 1 of the Gully (**Figure 1**); each mooring had an RDI ADCP current profiler and several Aanderaa RCM8 current meters (Appendix 1). The moorings were deployed April 23 and 24, 2006 and recovered on August 3, 2007. The deep central mooring at SG11 when recovered was missing the upper 200 m which did not include an RCM, it went missing on 17 June, 2007. Also the two moorings on the canyon axis (#1588 and #1589) underwent vertical displacements, up to 500 m for mooring 1589.

This appendix provides a synthesis of the current data collected from the moored instrumentation. Plots include depth-averaged time series, waterfall plots of monthly averaged velocity for across and along-canyon components, monthly averaged time series of across and along-canyon components, summary tables, annual and monthly-averaged sections and current roses at selected depths.

All plots were created using MATLAB R2008b.

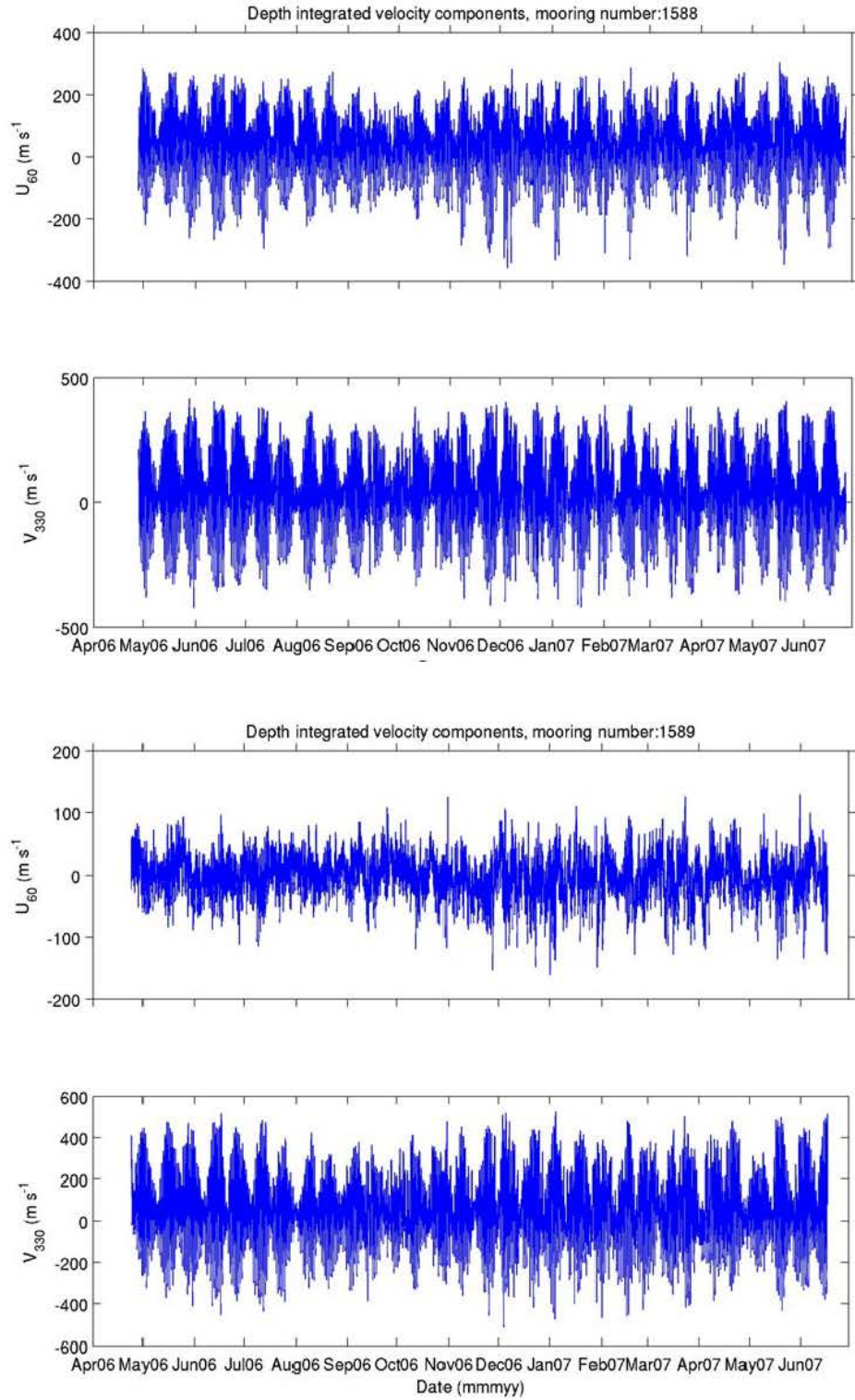


Figure A- 123: Depth-integrated velocity components (across-canyon U_{60} , along-canyon V_{330}) for moorings 1588 and 1589.

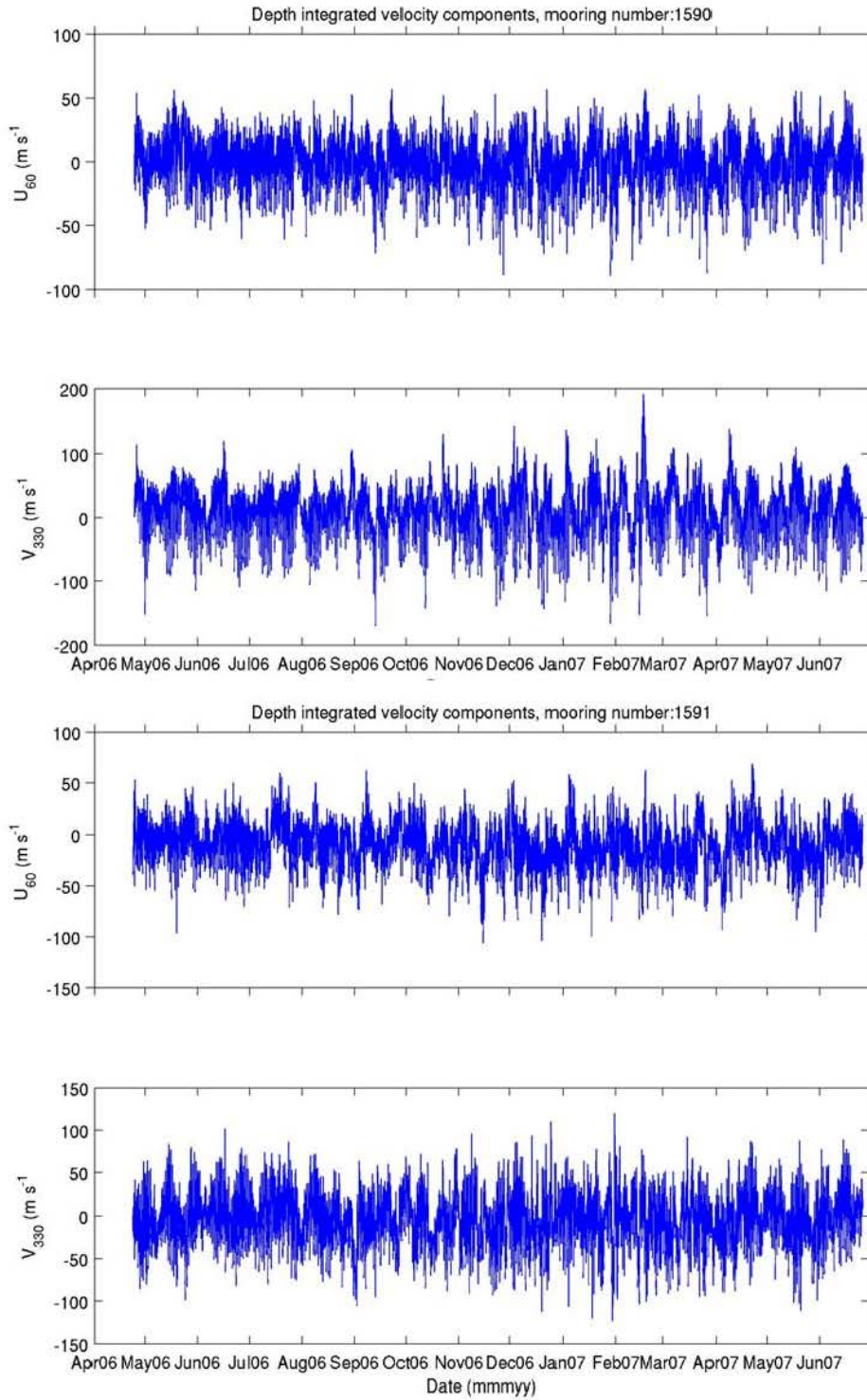


Figure A- 124: Depth-integrated velocity components (across-canyon U_{60} , along-canyon V_{330}) for moorings 1590 and 1591.

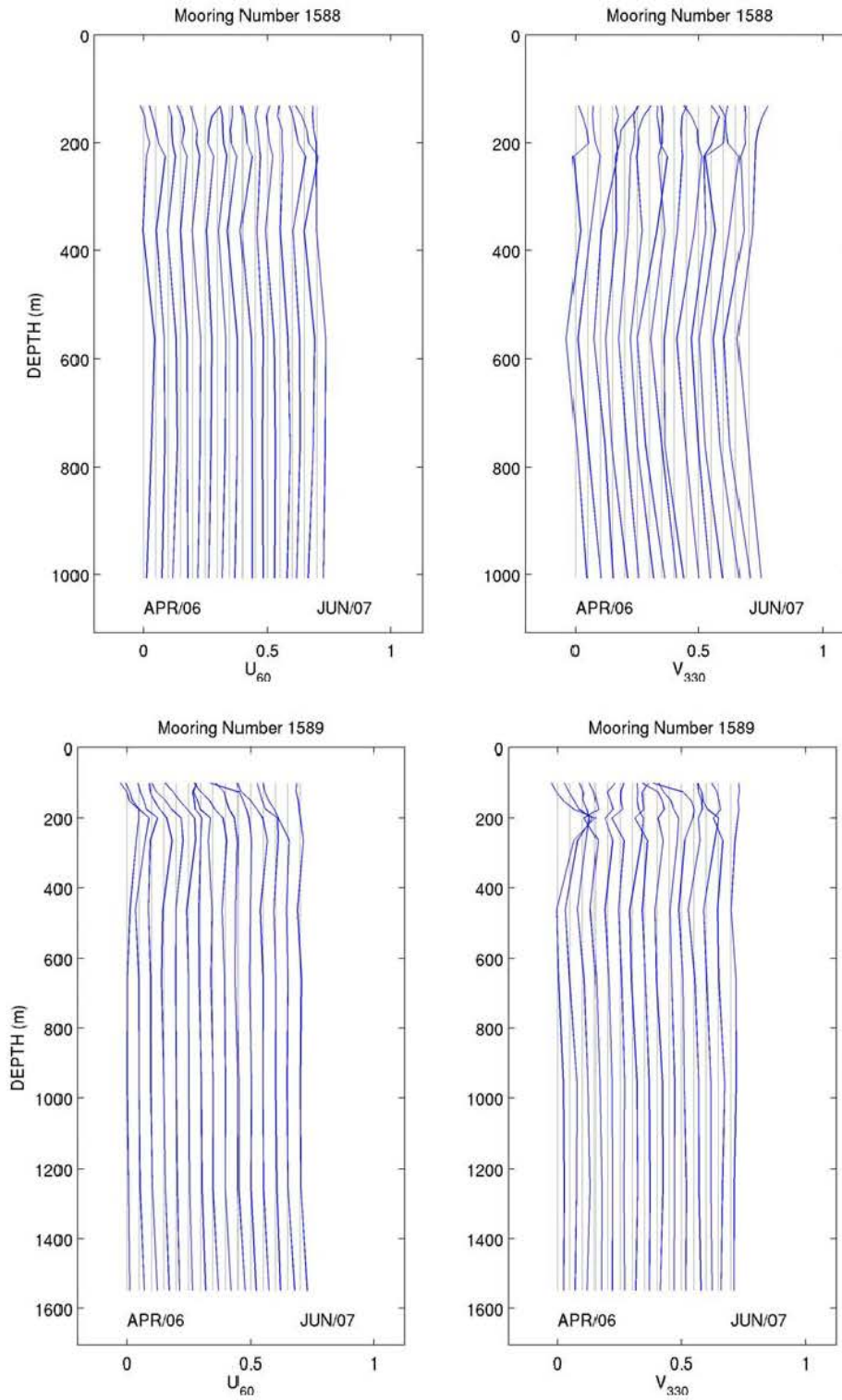


Figure A- 125: Waterfall plot of monthly vertical profiles (blue) of velocity components (across-canyon U_{60} , along-canyon V_{330} in m s^{-1}) for moorings 1588 and 1589. Gray vertical bars are for zero-reference.

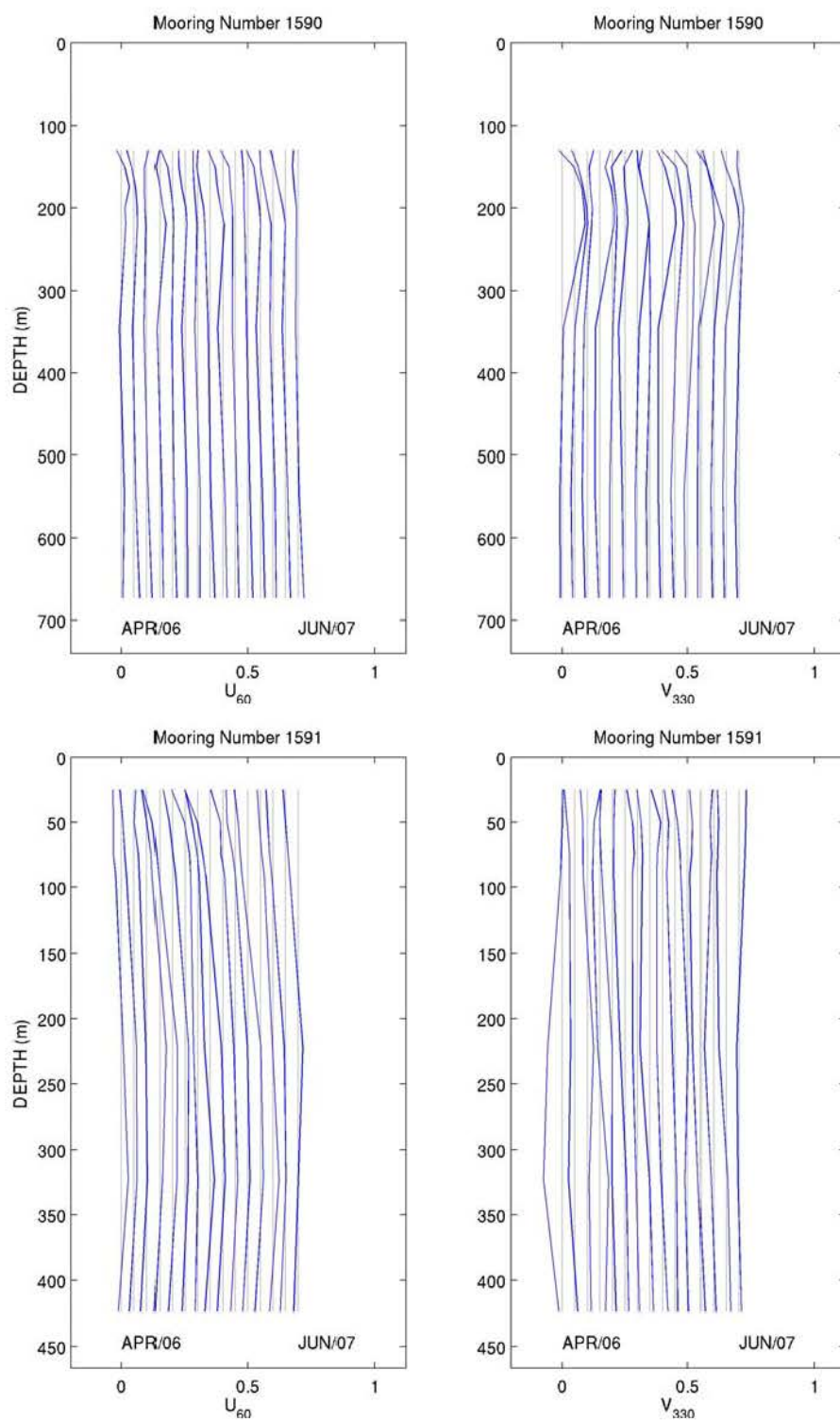


Figure A- 126: Waterfall plot of monthly vertical profiles (blue) of velocity components (across-canyon U_{60} , along-canyon V_{330} in m s^{-1}) for moorings 1590 and 1591. Gray vertical bars are for zero-reference.

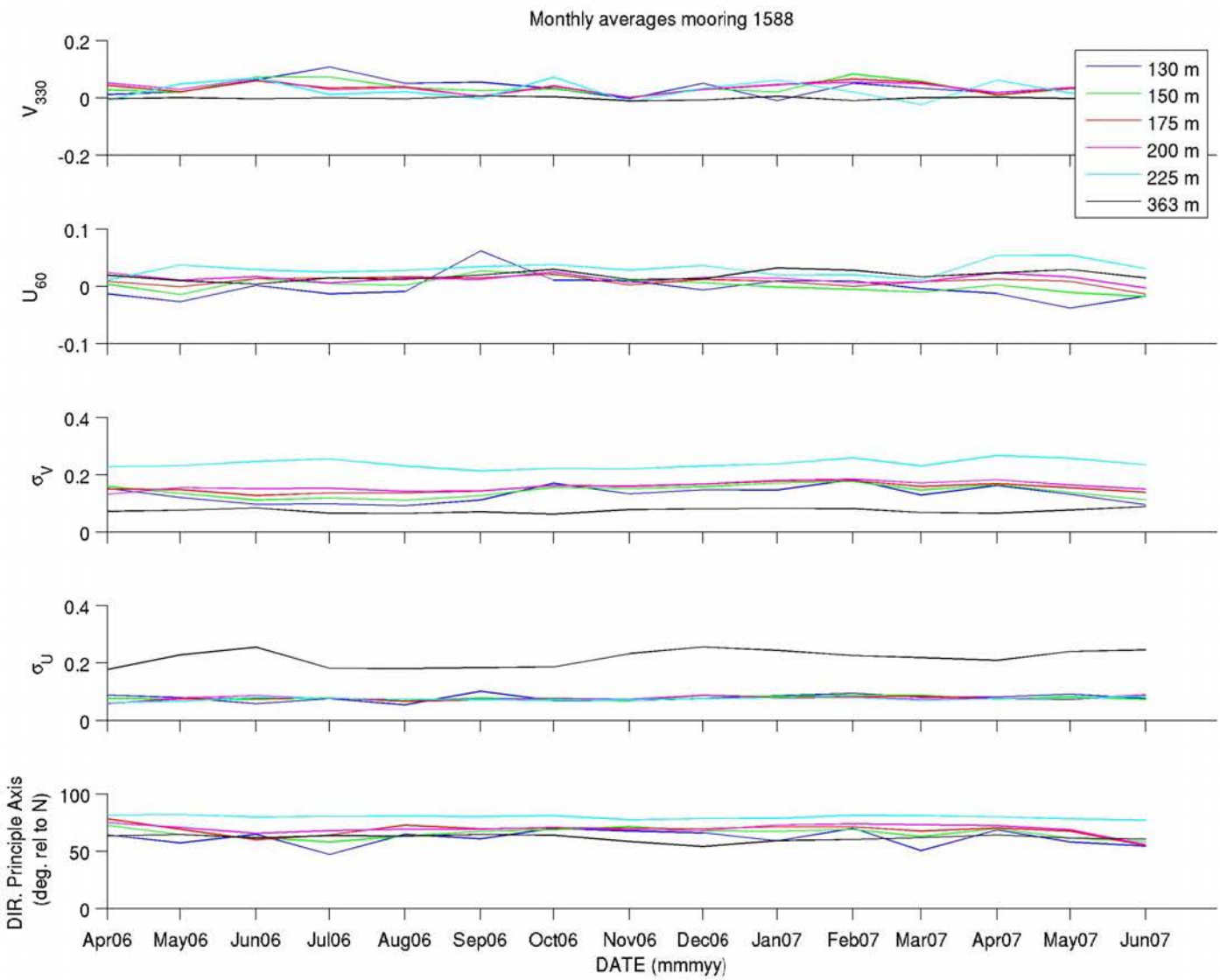


Figure A-127: Monthly averages and variances of velocity components (across-canyon U_{60} , along-canyon V_{330} in m s^{-1}) and direction of the principal axis of the flow for mooring 1588.

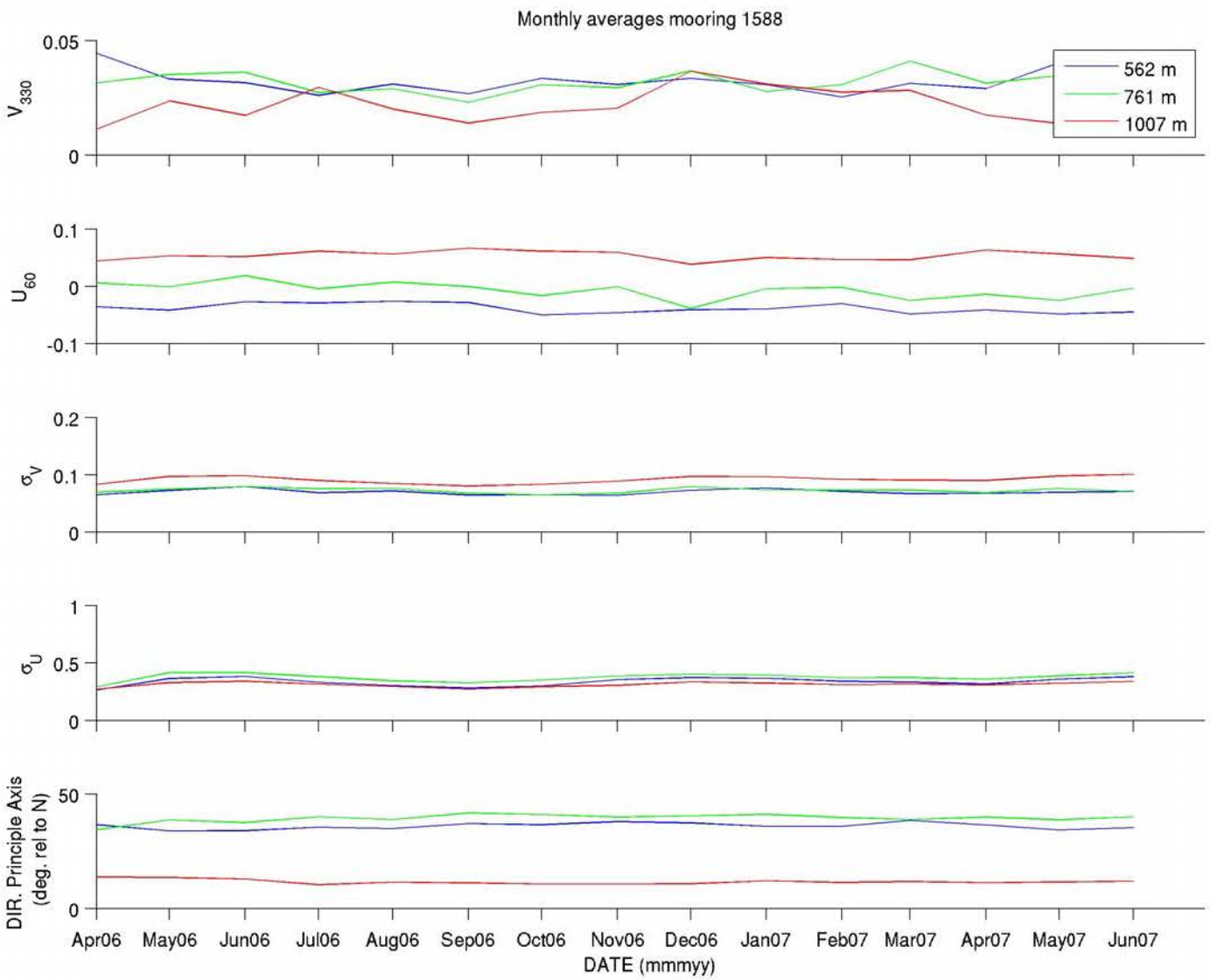


Figure A-128: Monthly averages and variances of velocity components (across-canyon U_{60} , along-canyon V_{330} in m s⁻¹) and direction of the principal axis of the flow for mooring 1588.

Table A- 1: Summary of monthly averages for temperature (T), salinity (S), speed, direction (Dir), principal axis, and variance across-canyon (σU_{60}) and along-canyon (σV_{150}) for mooring 1588.

Type	Year	Month	Depth m	T ° C	S psu	Speed m/s	Dir. rel.true	X Axis to E	σU_{60} m^2/s^2	σV_{150} m^2/s^2
ADCP	2006	4	130	NaN	NaN	0.02	-49	64	0.09	0.15
ADCP	2006	5	130	NaN	NaN	0.03	-53	57	0.08	0.12
ADCP	2006	6	130	NaN	NaN	0.06	1	65	0.06	0.10
ADCP	2006	7	130	NaN	NaN	0.11	-7	47	0.08	0.10
ADCP	2006	8	130	NaN	NaN	0.05	-11	65	0.05	0.09
ADCP	2006	9	130	NaN	NaN	0.08	49	61	0.10	0.11
ADCP	2006	10	130	NaN	NaN	0.03	19	70	0.07	0.17
ADCP	2006	11	130	NaN	NaN	0.01	104	68	0.07	0.13
ADCP	2006	12	130	NaN	NaN	0.05	-7	66	0.08	0.15
ADCP	2007	1	130	NaN	NaN	0.01	137	59	0.09	0.15
ADCP	2007	2	130	NaN	NaN	0.05	11	70	0.10	0.18
ADCP	2007	3	130	NaN	NaN	0.03	-8	51	0.08	0.13
ADCP	2007	4	130	NaN	NaN	0.02	-37	68	0.08	0.16
ADCP	2007	5	130	NaN	NaN	0.05	-50	58	0.09	0.13
ADCP	2007	6	130	NaN	NaN	0.08	-13	54	0.08	0.10
ADCP	2006	4	150	NaN	NaN	0.03	8	73	0.08	0.16
ADCP	2006	5	150	NaN	NaN	0.02	-38	64	0.08	0.13
ADCP	2006	6	150	NaN	NaN	0.07	10	62	0.07	0.11
ADCP	2006	7	150	NaN	NaN	0.07	3	58	0.08	0.12
ADCP	2006	8	150	NaN	NaN	0.04	3	63	0.07	0.11
ADCP	2006	9	150	NaN	NaN	0.04	47	67	0.08	0.13
ADCP	2006	10	150	NaN	NaN	0.04	33	69	0.07	0.16
ADCP	2006	11	150	NaN	NaN	0.01	75	72	0.07	0.15
ADCP	2006	12	150	NaN	NaN	0.03	11	68	0.09	0.16
ADCP	2007	1	150	NaN	NaN	0.02	-4	67	0.08	0.17
ADCP	2007	2	150	NaN	NaN	0.08	-4	69	0.09	0.18
ADCP	2007	3	150	NaN	NaN	0.06	-10	63	0.09	0.15
ADCP	2007	4	150	NaN	NaN	0.01	13	70	0.07	0.16
ADCP	2007	5	150	NaN	NaN	0.04	-17	61	0.08	0.14
ADCP	2007	6	150	NaN	NaN	0.06	-19	58	0.07	0.11

Type	Year	Month	Depth m	T ° C	S psu	Speed m/s	Dir. rel.true	X Axis to E	σ U60 m2/s2	σ V150 m2/s2
ADCP	2006	4	175	NaN	NaN	0.04	11	78	0.06	0.15
ADCP	2006	5	175	NaN	NaN	0.02	-3	69	0.08	0.15
ADCP	2006	6	175	NaN	NaN	0.06	13	60	0.08	0.13
ADCP	2006	7	175	NaN	NaN	0.04	23	64	0.08	0.14
ADCP	2006	8	175	NaN	NaN	0.04	22	73	0.07	0.14
ADCP	2006	9	175	NaN	NaN	0.02	73	70	0.07	0.14
ADCP	2006	10	175	NaN	NaN	0.04	28	70	0.08	0.16
ADCP	2006	11	175	NaN	NaN	0.00	56	70	0.07	0.16
ADCP	2006	12	175	NaN	NaN	0.03	23	70	0.09	0.17
ADCP	2007	1	175	NaN	NaN	0.05	11	71	0.08	0.18
ADCP	2007	2	175	NaN	NaN	0.07	0	71	0.08	0.18
ADCP	2007	3	175	NaN	NaN	0.06	8	67	0.08	0.16
ADCP	2007	4	175	NaN	NaN	0.02	51	70	0.08	0.17
ADCP	2007	5	175	NaN	NaN	0.03	15	68	0.07	0.16
ADCP	2007	6	175	NaN	NaN	0.04	-20	55	0.09	0.14
ADCP	2006	4	200	NaN	NaN	0.06	25	75	0.06	0.13
ADCP	2006	5	200	NaN	NaN	0.03	19	71	0.08	0.16
ADCP	2006	6	200	NaN	NaN	0.07	14	66	0.09	0.15
ADCP	2006	7	200	NaN	NaN	0.03	11	68	0.08	0.15
ADCP	2006	8	200	NaN	NaN	0.04	22	69	0.07	0.14
ADCP	2006	9	200	NaN	NaN	0.01	67	69	0.07	0.14
ADCP	2006	10	200	NaN	NaN	0.05	30	71	0.08	0.16
ADCP	2006	11	200	NaN	NaN	0.01	85	69	0.07	0.16
ADCP	2006	12	200	NaN	NaN	0.03	28	68	0.09	0.17
ADCP	2007	1	200	NaN	NaN	0.05	17	73	0.08	0.18
ADCP	2007	2	200	NaN	NaN	0.06	7	74	0.08	0.19
ADCP	2007	3	200	NaN	NaN	0.05	9	73	0.07	0.17
ADCP	2007	4	200	NaN	NaN	0.03	53	72	0.08	0.18
ADCP	2007	5	200	NaN	NaN	0.04	25	69	0.08	0.16
ADCP	2007	6	200	NaN	NaN	0.03	-6	56	0.09	0.15
ADCP	2006	4	225	NaN	NaN	0.01	130	82	0.06	0.23

Type	Year	Month	Depth m	T ° C	S psu	Speed m/s	Dir. rel.true	X Axis to E	σ U60 m ² /s ²	σ V150 m ² /s ²
ADCP	2006	5	225	NaN	NaN	0.06	38	82	0.07	0.23
ADCP	2006	6	225	NaN	NaN	0.07	23	80	0.08	0.25
ADCP	2006	7	225	NaN	NaN	0.03	66	80	0.08	0.26
ADCP	2006	8	225	NaN	NaN	0.04	52	81	0.07	0.23
ADCP	2006	9	225	NaN	NaN	0.03	95	80	0.07	0.21
ADCP	2006	10	225	NaN	NaN	0.08	28	81	0.07	0.22
ADCP	2006	11	225	NaN	NaN	0.03	118	78	0.07	0.22
ADCP	2006	12	225	NaN	NaN	0.05	48	79	0.08	0.23
ADCP	2007	1	225	NaN	NaN	0.07	18	79	0.08	0.24
ADCP	2007	2	225	NaN	NaN	0.03	44	81	0.08	0.26
ADCP	2007	3	225	NaN	NaN	0.03	156	81	0.07	0.23
ADCP	2007	4	225	NaN	NaN	0.08	41	80	0.08	0.27
ADCP	2007	5	225	NaN	NaN	0.06	73	78	0.08	0.26
ADCP	2007	6	225	NaN	NaN	0.03	74	77	0.08	0.24
R 5574	2006	4	363	8.3	34.9	0.02	100	63	0.07	0.18
R 5574	2006	5	363	6.8	34.6	0.01	85	65	0.08	0.23
R 5574	2006	6	363	6.5	34.9	0.01	135	62	0.08	0.26
R 5574	2006	7	363	6.2	34.8	0.01	90	64	0.07	0.18
R 5574	2006	8	363	6	34.7	0.01	107	63	0.07	0.18
R 5574	2006	9	363	5.9	34.7	0.02	74	64	0.07	0.18
R 5574	2006	10	363	6.3	34.7	0.03	83	64	0.06	0.19
R 5574	2006	11	363	5.9	34.6	0.02	131	58	0.08	0.23
R 5574	2006	12	363	5.6	34.6	0.02	124	54	0.08	0.26
R 5574	2007	1	363	5.2	34.6	0.03	81	59	0.08	0.24
R 5574	2007	2	363	4.3	34.5	0.03	109	60	0.08	0.23
R 5574	2007	3	363	4.2	34.4	0.02	89	62	0.07	0.22
R 5574	2007	4	363	5.2	34.5	0.02	84	64	0.07	0.21
R 5574	2007	5	363	5.4	34.6	0.03	95	61	0.08	0.24
R 5574	2007	6	363	5.5	34.6	0.01	98	61	0.09	0.25
R 5002	2006	4	562	8.2	34.8	0.06	-39	37	0.07	0.26
R 5002	2006	5	562	6.8	34.6	0.05	-52	34	0.07	0.37

Type	Year	Month	Depth m	T ° C	S psu	Speed m/s	Dir. rel.true	X Axis to E	σ_{U60} m ² /s ²	σ_{V150} m ² /s ²
R 5002	2006	6	562	6.5	34.9	0.04	-41	34	0.08	0.38
R 5002	2006	7	562	6.2	34.8	0.04	-48	36	0.07	0.33
R 5002	2006	8	562	6	34.7	0.04	-41	35	0.07	0.30
R 5002	2006	9	562	5.9	34.7	0.04	-47	37	0.06	0.28
R 5002	2006	10	562	6.3	34.7	0.06	-56	37	0.07	0.30
R 5002	2006	11	562	5.9	34.6	0.06	-56	38	0.06	0.36
R 5002	2006	12	562	5.6	34.6	0.05	-51	37	0.07	0.37
R 5002	2007	1	562	5.2	34.6	0.05	-53	36	0.08	0.37
R 5002	2007	2	562	4.3	34.5	0.04	-50	36	0.07	0.34
R 5002	2007	3	562	4.2	34.4	0.06	-57	38	0.07	0.33
R 5002	2007	4	562	5.2	34.5	0.05	-55	36	0.07	0.32
R 5002	2007	5	562	5.4	34.6	0.06	-50	34	0.07	0.36
R 5002	2007	6	562	5.6	34.6	0.06	-52	35	0.07	0.38
R 5567	2006	4	761	8.3	34.9	0.03	11	34	0.07	0.29
R 5567	2006	5	761	6.8	34.6	0.04	-2	39	0.08	0.42
R 5567	2006	6	761	6.5	34.9	0.04	27	38	0.08	0.42
R 5567	2006	7	761	6.2	34.8	0.03	-9	40	0.08	0.38
R 5567	2006	8	761	6	34.7	0.03	14	39	0.08	0.34
R 5567	2006	9	761	5.9	34.7	0.02	-1	42	0.07	0.33
R 5567	2006	10	761	6.3	34.7	0.04	-28	41	0.07	0.35
R 5567	2006	11	761	5.9	34.6	0.03	-2	40	0.07	0.39
R 5567	2006	12	761	5.6	34.6	0.05	-46	40	0.08	0.40
R 5567	2007	1	761	5.2	34.6	0.03	-9	41	0.07	0.40
R 5567	2007	2	761	4.3	34.5	0.03	-4	40	0.07	0.37
R 5567	2007	3	761	4.2	34.4	0.05	-31	39	0.07	0.37
R 5567	2007	4	761	5.2	34.5	0.03	-24	40	0.07	0.36
R 5567	2007	5	761	5.4	34.6	0.04	-35	39	0.08	0.39
R 5567	2007	6	761	5.5	34.6	0.03	-6	40	0.07	0.41
R 7013	2006	4	1007	8.2	34.8	0.05	76	14	0.08	0.27
R 7013	2006	5	1007	6.8	34.6	0.06	66	14	0.10	0.33
R 7013	2006	6	1007	6.5	34.9	0.06	72	13	0.10	0.34

Type	Year	Month	Depth m	T ° C	S psu	Speed m/s	Dir. rel.true	X Axis to E	σ_{U60} m ² /s ²	σ_{V150} m ² /s ²
R 7013	2006	7	1007	6.2	34.8	0.07	64	10	0.09	0.32
R 7013	2006	8	1007	6	34.7	0.06	70	11	0.09	0.30
R 7013	2006	9	1007	5.9	34.7	0.07	78	11	0.08	0.27
R 7013	2006	10	1007	6.3	34.7	0.06	73	11	0.08	0.29
R 7013	2006	11	1007	5.9	34.6	0.06	71	11	0.09	0.31
R 7013	2006	12	1007	5.6	34.6	0.05	46	11	0.10	0.34
R 7013	2007	1	1007	5.2	34.6	0.06	58	12	0.10	0.33
R 7013	2007	2	1007	4.3	34.5	0.05	59	11	0.09	0.31
R 7013	2007	3	1007	4.2	34.4	0.05	59	12	0.09	0.32
R 7013	2007	4	1007	5.2	34.5	0.07	75	11	0.09	0.31
R 7013	2007	5	1007	5.4	34.6	0.06	76	12	0.10	0.32
R 7013	2007	6	1007	5.5	34.6	0.06	62	12	0.10	0.34

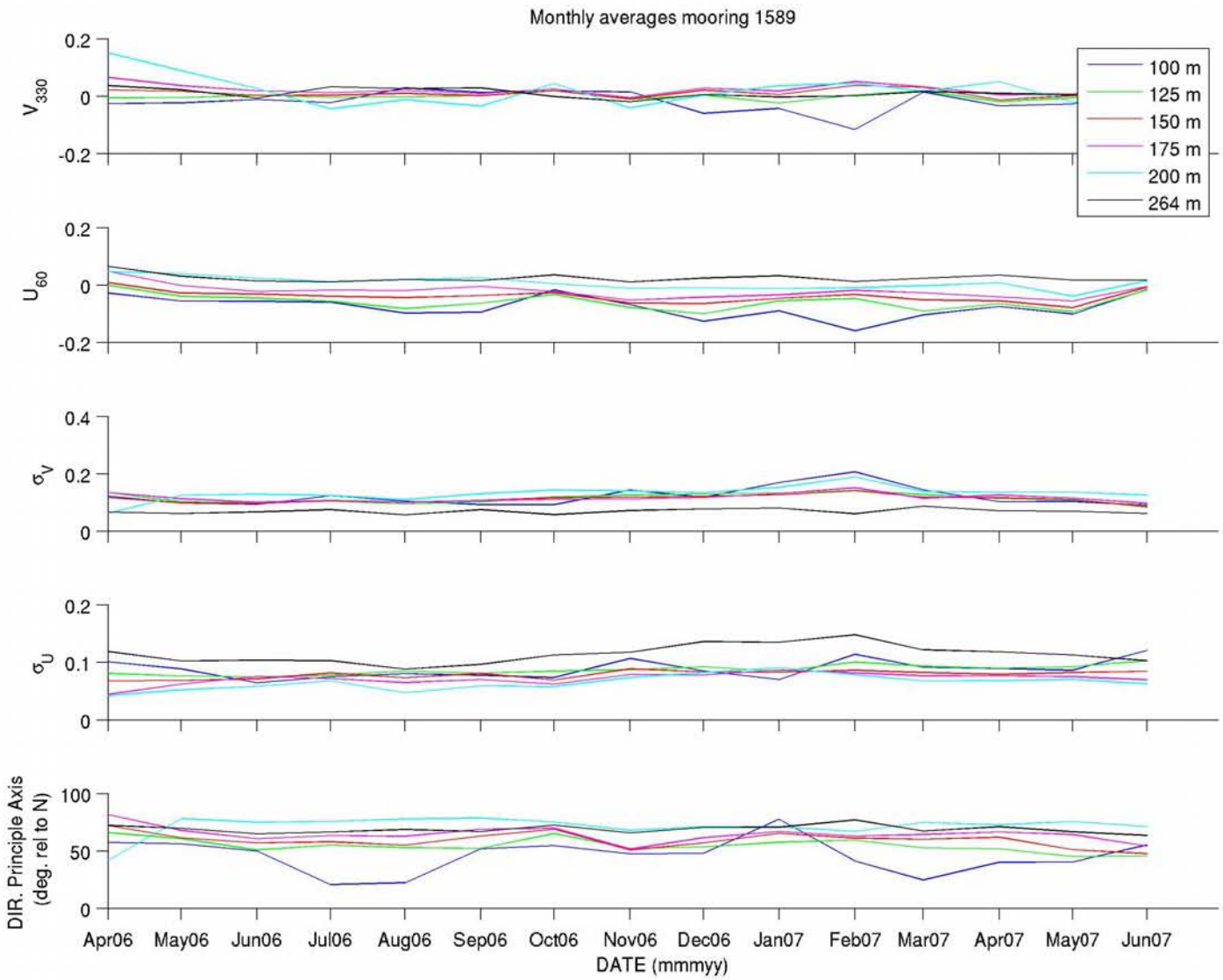


Figure A- 129: Monthly averages and variances of velocity components (across-canyon U_{60} , along-canyon V_{330} in m s^{-1}) and direction of the principal axis of the flow for mooring 1589.

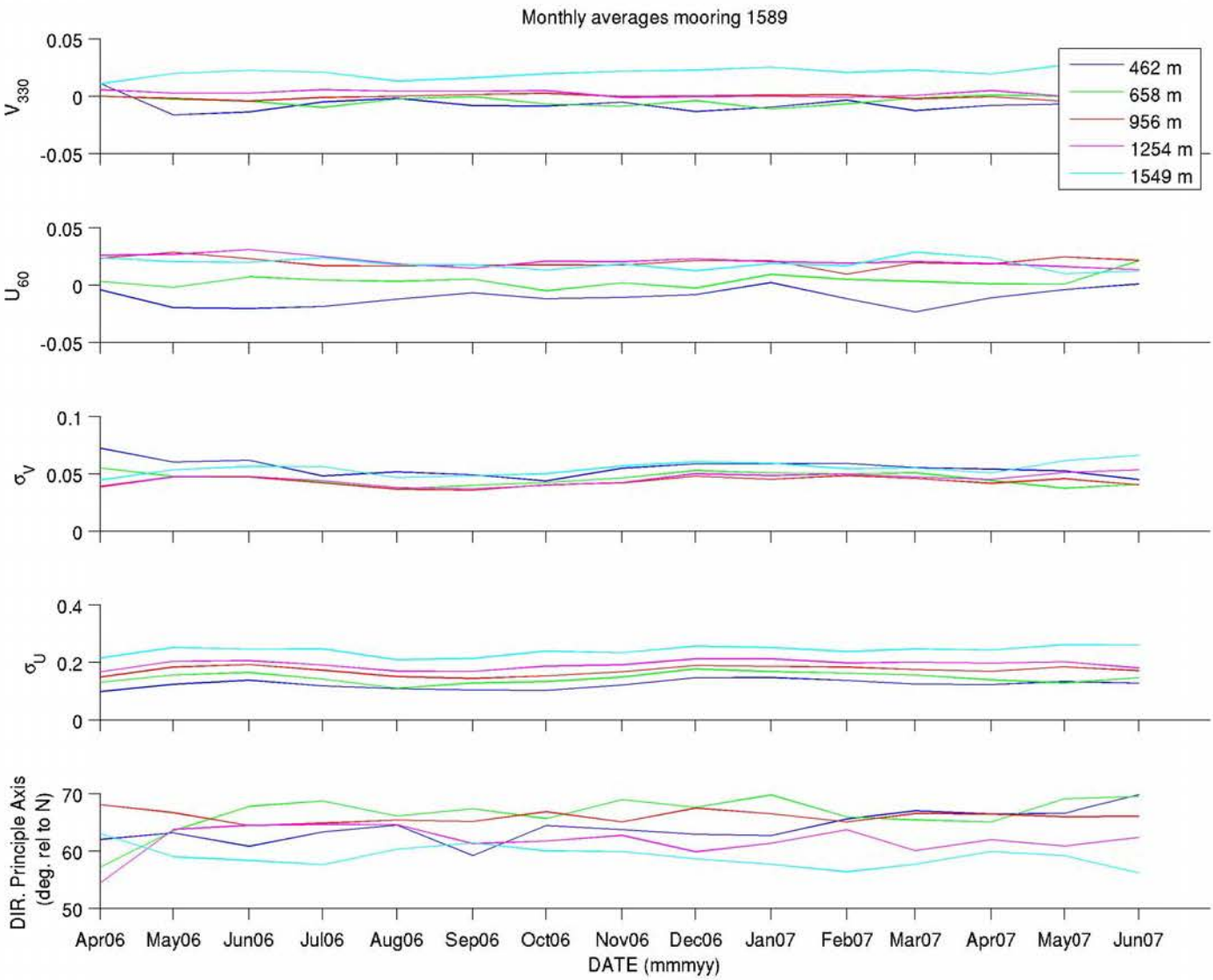


Figure A-130: Monthly averages and variances of velocity components (across-canyon U_{60} , along-canyon V_{330} in m s^{-1}) and direction of the principal axis of the flow for mooring 1589.

Table A- 2 : Summary of monthly averages for temperature (T), salinity (S), speed, direction (Dir), principal axis, and variance across-canyon (σU_{60}) and along-canyon (σV_{150}) for mooring 1589.

Type	Year	Month	Depth m	T ° C	S psu	Speed m/s	Dir. rel.true	X Axis to E	σU_{60} m ² /s ²	ΣV_{150} m ² /s ²
ADCP	2006	4	100	NaN	NaN	0.04	227	57	0.10	0.12
ADCP	2006	5	100	NaN	NaN	0.06	247	56	0.09	0.10
ADCP	2006	6	100	NaN	NaN	0.06	258	50	0.07	0.09
ADCP	2006	7	100	NaN	NaN	0.06	249	21	0.08	0.12
ADCP	2006	8	100	NaN	NaN	0.10	-74	22	0.08	0.10
ADCP	2006	9	100	NaN	NaN	0.10	-82	52	0.08	0.09
ADCP	2006	10	100	NaN	NaN	0.03	-42	55	0.07	0.09
ADCP	2006	11	100	NaN	NaN	0.07	-78	47	0.11	0.14
ADCP	2006	12	100	NaN	NaN	0.14	245	48	0.09	0.12
ADCP	2007	1	100	NaN	NaN	0.1	245	78	0.07	0.17
ADCP	2007	2	100	NaN	NaN	0.20	234	41	0.11	0.21
ADCP	2007	3	100	NaN	NaN	0.11	-82	25	0.09	0.14
ADCP	2007	4	100	NaN	NaN	0.08	246	40	0.09	0.10
ADCP	2007	5	100	NaN	NaN	0.11	255	40	0.09	0.10
ADCP	2007	6	100	NaN	NaN	0.04	-26	55	0.12	0.09
ADCP	2006	4	125	NaN	NaN	0.01	189	66	0.08	0.14
ADCP	2006	5	125	NaN	NaN	0.04	263	61	0.08	0.10
ADCP	2006	6	125	NaN	NaN	0.05	-86	51	0.08	0.10
ADCP	2006	7	125	NaN	NaN	0.06	266	55	0.08	0.11
ADCP	2006	8	125	NaN	NaN	0.08	268	53	0.09	0.10
ADCP	2006	9	125	NaN	NaN	0.06	-88	52	0.08	0.10
ADCP	2006	10	125	NaN	NaN	0.04	-58	65	0.09	0.12
ADCP	2006	11	125	NaN	NaN	0.08	262	52	0.09	0.13
ADCP	2006	12	125	NaN	NaN	0.10	-88	53	0.09	0.13
ADCP	2007	1	125	NaN	NaN	0.06	246	58	0.08	0.13
ADCP	2007	2	125	NaN	NaN	0.05	-85	60	0.10	0.14
ADCP	2007	3	125	NaN	NaN	0.09	-79	53	0.09	0.13
ADCP	2007	4	125	NaN	NaN	0.07	254	52	0.09	0.11
ADCP	2007	5	125	NaN	NaN	0.09	266	45	0.09	0.11
ADCP	2007	6	125	NaN	NaN	0.04	-26	45	0.10	0.09

Type	Year	Month	Depth m	T ° C	S psu	Speed m/s	Dir. rel.true	X Axis to E	σ U60 m2/s2	σ V150 m2/s2
ADCP	2006	4	150	NaN	NaN	0.02	21	72	0.07	0.12
ADCP	2006	5	150	NaN	NaN	0.03	-60	61	0.07	0.10
ADCP	2006	6	150	NaN	NaN	0.03	-85	57	0.07	0.10
ADCP	2006	7	150	NaN	NaN	0.04	-85	58	0.08	0.11
ADCP	2006	8	150	NaN	NaN	0.05	-77	55	0.07	0.1
ADCP	2006	9	150	NaN	NaN	0.04	-87	63	0.08	0.11
ADCP	2006	10	150	NaN	NaN	0.03	-55	69	0.07	0.12
ADCP	2006	11	150	NaN	NaN	0.06	262	51	0.09	0.12
ADCP	2006	12	150	NaN	NaN	0.07	-72	57	0.08	0.12
ADCP	2007	1	150	NaN	NaN	0.05	-82	65	0.08	0.13
ADCP	2007	2	150	NaN	NaN	0.05	-41	61	0.09	0.14
ADCP	2007	3	150	NaN	NaN	0.06	-59	60	0.08	0.12
ADCP	2007	4	150	NaN	NaN	0.06	256	62	0.08	0.12
ADCP	2007	5	150	NaN	NaN	0.08	-89	51	0.08	0.11
ADCP	2007	6	150	NaN	NaN	0.03	-15	48	0.08	0.09
ADCP	2006	4	175	NaN	NaN	0.08	36	82	0.04	0.13
ADCP	2006	5	175	NaN	NaN	0.04	-3	68	0.06	0.11
ADCP	2006	6	175	NaN	NaN	0.03	-51	61	0.08	0.10
ADCP	2006	7	175	NaN	NaN	0.02	-54	63	0.07	0.11
ADCP	2006	8	175	NaN	NaN	0.03	-43	63	0.07	0.1
ADCP	2006	9	175	NaN	NaN	0.01	-32	69	0.07	0.11
ADCP	2006	10	175	NaN	NaN	0.03	-43	70	0.06	0.11
ADCP	2006	11	175	NaN	NaN	0.05	265	52	0.08	0.11
ADCP	2006	12	175	NaN	NaN	0.05	-57	62	0.08	0.12
ADCP	2007	1	175	NaN	NaN	0.04	-63	67	0.09	0.13
ADCP	2007	2	175	NaN	NaN	0.05	-20	63	0.08	0.15
ADCP	2007	3	175	NaN	NaN	0.04	-39	64	0.08	0.12
ADCP	2007	4	175	NaN	NaN	0.04	-83	67	0.08	0.13
ADCP	2007	5	175	NaN	NaN	0.06	-82	64	0.08	0.12
ADCP	2007	6	175	NaN	NaN	0.03	-9	54	0.07	0.10
ADCP	2006	4	200	NaN	NaN	0.16	17	42	0.04	0.06

Type	Year	Month	Depth m	T ° C	S psu	Speed m/s	Dir. rel.true	X Axis to E	σ U60 m2/s2	σ V150 m2/s2
ADCP	2006	5	200	NaN	NaN	0.10	24	78	0.05	0.13
ADCP	2006	6	200	NaN	NaN	0.04	41	75	0.06	0.13
ADCP	2006	7	200	NaN	NaN	0.05	166	76	0.07	0.12
ADCP	2006	8	200	NaN	NaN	0.02	121	78	0.05	0.11
ADCP	2006	9	200	NaN	NaN	0.04	144	79	0.06	0.13
ADCP	2006	10	200	NaN	NaN	0.04	5	75	0.06	0.14
ADCP	2006	11	200	NaN	NaN	0.04	195	68	0.07	0.14
ADCP	2006	12	200	NaN	NaN	0.01	-69	71	0.08	0.14
ADCP	2007	1	200	NaN	NaN	0.04	-20	71	0.09	0.15
ADCP	2007	2	200	NaN	NaN	0.05	-11	67	0.08	0.19
ADCP	2007	3	200	NaN	NaN	0.02	-10	75	0.07	0.14
ADCP	2007	4	200	NaN	NaN	0.05	9	73	0.07	0.14
ADCP	2007	5	200	NaN	NaN	0.05	242	76	0.07	0.14
ADCP	2007	6	200	NaN	NaN	0.02	83	71	0.06	0.13
R 7650	2006	4	264	7.9	35.1	0.08	60	72	0.07	0.12
R 7650	2006	5	264	8	35	0.04	53	70	0.06	0.10
R 7650	2006	6	264	7.8	35.1	0.02	115	65	0.07	0.10
R 7650	2006	7	264	7.4	35	0.04	18	67	0.08	0.10
R 7650	2006	8	264	6.8	34.9	0.03	35	69	0.06	0.09
R 7650	2006	9	264	7	34.9	0.03	28	67	0.08	0.10
R 7650	2006	10	264	7	34.9	0.04	92	73	0.06	0.11
R 7650	2006	11	264	6.9	34.9	0.02	152	66	0.07	0.12
R 7650	2006	12	264	6.5	34.8	0.03	77	71	0.08	0.14
R 7650	2007	1	264	4.8	34.6	0.03	94	71	0.08	0.14
R 7650	2007	2	264	4.2	34.6	0.01	83	77	0.06	0.15
R 7650	2007	3	264	4.5	34.5	0.03	56	67	0.09	0.12
R 7650	2007	4	264	6.8	34.8	0.04	74	71	0.07	0.12
R 7650	2007	5	264	6.7	34.8	0.02	74	67	0.07	0.11
R 7650	2007	6	264	5.8	35.1	0.02	53	64	0.06	0.10
R 3299	2006	4	462	NaN	NaN	0.01	-20	62	0.07	0.10
R 3299	2006	5	462	NaN	NaN	0.03	-130	63	0.06	0.12

Type	Year	Month	Depth m	T ° C	S psu	Speed m/s	Dir. rel.true	X Axis to E	σ_{U60} m ² /s ²	σ_{V150} m ² /s ²
R 3299	2006	6	462	NaN	NaN	0.03	-124	61	0.06	0.14
R 3299	2006	7	462	NaN	NaN	0.02	-105	63	0.05	0.12
R 3299	2006	8	462	NaN	NaN	0.01	-98	65	0.05	0.11
R 3299	2006	9	462	NaN	NaN	0.01	-140	59	0.05	0.10
R 3299	2006	10	462	NaN	NaN	0.02	-126	64	0.04	0.10
R 3299	2006	11	462	NaN	NaN	0.01	-116	64	0.06	0.12
R 3299	2006	12	462	NaN	NaN	0.02	-147	63	0.06	0.15
R 3299	2007	1	462	NaN	NaN	0.01	168	63	0.06	0.15
R 3299	2007	2	462	NaN	NaN	0.01	-106	66	0.06	0.14
R 3299	2007	3	462	NaN	NaN	0.03	-118	67	0.06	0.12
R 3299	2007	4	462	NaN	NaN	0.01	-126	66	0.05	0.12
R 3299	2007	5	462	NaN	NaN	0.01	-148	67	0.05	0.13
R 3299	2007	6	462	NaN	NaN	0.01	176	70	0.05	0.13
R 4602	2006	4	658	NaN	NaN	0.00	84	57	0.06	0.13
R 4602	2006	5	658	NaN	NaN	0.00	-142	63	0.05	0.16
R 4602	2006	6	658	NaN	NaN	0.01	121	68	0.05	0.16
R 4602	2006	7	658	NaN	NaN	0.01	157	69	0.04	0.14
R 4602	2006	8	658	NaN	NaN	0.00	127	66	0.04	0.11
R 4602	2006	9	658	NaN	NaN	0.01	93	67	0.04	0.13
R 4602	2006	10	658	NaN	NaN	0.01	-143	66	0.04	0.13
R 4602	2006	11	658	NaN	NaN	0.01	168	69	0.05	0.15
R 4602	2006	12	658	NaN	NaN	0.01	-146	68	0.05	0.18
R 4602	2007	1	658	NaN	NaN	0.02	141	70	0.05	0.17
R 4602	2007	2	658	NaN	NaN	0.01	143	66	0.05	0.16
R 4602	2007	3	658	NaN	NaN	0.00	117	65	0.05	0.16
R 4602	2007	4	658	NaN	NaN	0.00	49	65	0.04	0.14
R 4602	2007	5	658	NaN	NaN	0.00	100	69	0.04	0.13
R 4602	2007	6	658	NaN	NaN	0.02	76	70	0.04	0.15
R 3300	2006	4	956	NaN	NaN	0.02	90	68	0.04	0.15
R 3300	2006	5	956	NaN	NaN	0.03	94	67	0.05	0.18
R 3300	2006	6	956	NaN	NaN	0.02	101	64	0.05	0.19

Type	Year	Month	Depth m	T ° C	S psu	Speed m/s	Dir. rel.true	X Axis to E	σ_{U60} m2/s2	σ_{V150} m2/s2
R 3300	2006	7	956	NaN	NaN	0.02	94	65	0.04	0.17
R 3300	2006	8	956	NaN	NaN	0.02	90	65	0.04	0.15
R 3300	2006	9	956	NaN	NaN	0.02	85	65	0.04	0.14
R 3300	2006	10	956	NaN	NaN	0.02	82	67	0.04	0.15
R 3300	2006	11	956	NaN	NaN	0.02	91	65	0.04	0.17
R 3300	2006	12	956	NaN	NaN	0.02	89	67	0.05	0.19
R 3300	2007	1	956	NaN	NaN	0.02	87	66	0.05	0.19
R 3300	2007	2	956	NaN	NaN	0.01	82	65	0.05	0.18
R 3300	2007	3	956	NaN	NaN	0.02	97	67	0.05	0.18
R 3300	2007	4	956	NaN	NaN	0.02	92	66	0.04	0.17
R 3300	2007	5	956	NaN	NaN	0.03	100	66	0.05	0.19
R 3300	2007	6	956	NaN	NaN	0.02	90	66	0.04	0.17
R 3584	2006	4	1254	NaN	NaN	0.03	78	54	0.04	0.17
R 3584	2006	5	1254	NaN	NaN	0.03	84	64	0.05	0.20
R 3584	2006	6	1254	NaN	NaN	0.03	85	64	0.05	0.21
R 3584	2006	7	1254	NaN	NaN	0.03	77	65	0.04	0.19
R 3584	2006	8	1254	NaN	NaN	0.02	77	65	0.04	0.17
R 3584	2006	9	1254	NaN	NaN	0.02	74	61	0.04	0.17
R 3584	2006	10	1254	NaN	NaN	0.02	77	62	0.04	0.19
R 3584	2006	11	1254	NaN	NaN	0.02	93	63	0.04	0.19
R 3584	2006	12	1254	NaN	NaN	0.02	91	60	0.05	0.21
R 3584	2007	1	1254	NaN	NaN	0.02	90	61	0.05	0.21
R 3584	2007	2	1254	NaN	NaN	0.02	92	64	0.05	0.20
R 3584	2007	3	1254	NaN	NaN	0.02	88	60	0.05	0.20
R 3584	2007	4	1254	NaN	NaN	0.02	76	62	0.05	0.20
R 3584	2007	5	1254	NaN	NaN	0.02	90	61	0.05	0.20
R 3584	2007	6	1254	NaN	NaN	0.01	79	62	0.05	0.18
R 4406	2006	4	1549	NaN	NaN	0.03	65	63	0.05	0.22
R 4406	2006	5	1549	NaN	NaN	0.03	46	59	0.05	0.25
R 4406	2006	6	1549	NaN	NaN	0.03	41	58	0.06	0.25
R 4406	2006	7	1549	NaN	NaN	0.03	49	58	0.06	0.25

Type	Year	Month	Depth m	T ° C	S psu	Speed m/s	Dir. rel.true	X Axis to E	σ_{U60} m ² /s ²	σ_{V150} m ² /s ²
R 4406	2006	8	1549	NaN	NaN	0.02	53	60	0.05	0.21
R 4406	2006	9	1549	NaN	NaN	0.02	48	61	0.05	0.21
R 4406	2006	10	1549	NaN	NaN	0.02	34	60	0.05	0.24
R 4406	2006	11	1549	NaN	NaN	0.03	40	60	0.06	0.23
R 4406	2006	12	1549	NaN	NaN	0.03	29	59	0.06	0.26
R 4406	2007	1	1549	NaN	NaN	0.03	37	58	0.06	0.25
R 4406	2007	2	1549	NaN	NaN	0.03	39	56	0.05	0.24
R 4406	2007	3	1549	NaN	NaN	0.04	52	58	0.06	0.25
R 4406	2007	4	1549	NaN	NaN	0.03	51	60	0.05	0.24
R 4406	2007	5	1549	NaN	NaN	0.03	20	59	0.06	0.26
R 4406	2007	6	1549	NaN	NaN	0.03	24	56	0.07	0.26

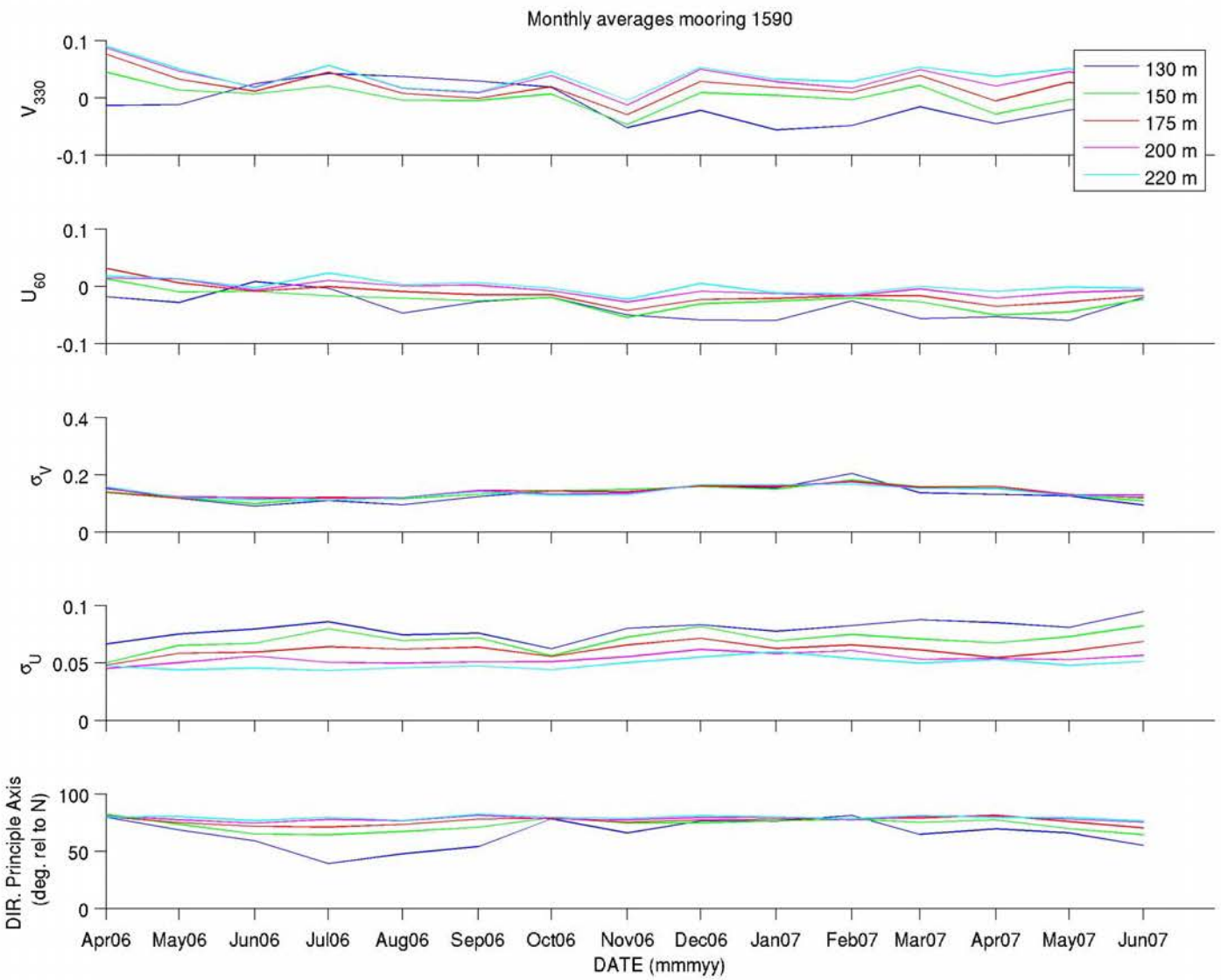


Figure A-131: Monthly averages and variances of velocity components (across-canyon U_{60} , along-canyon V_{330} in m s^{-1}) and direction of the principal axis of the flow for mooring 1590.

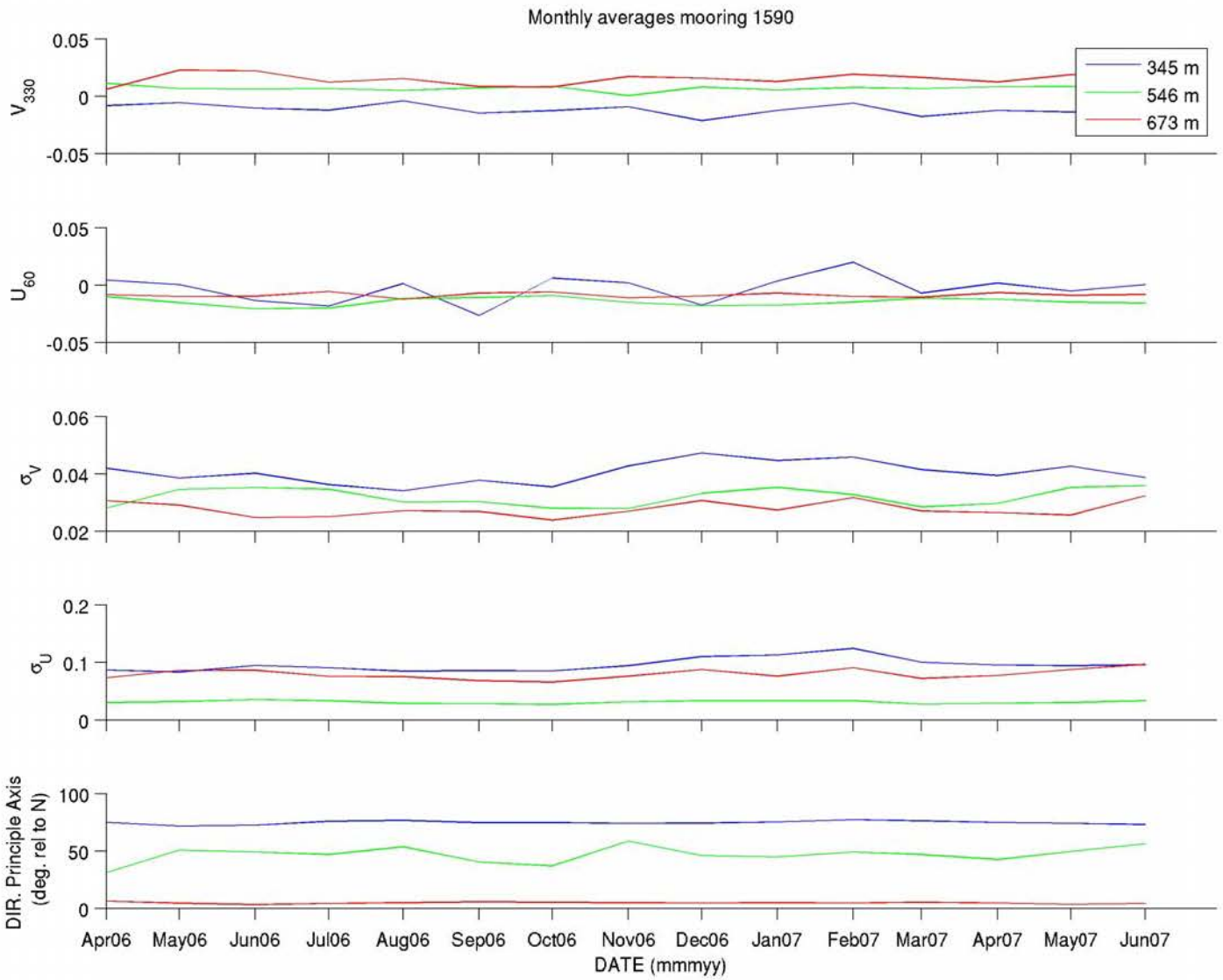


Figure A-132: Monthly averages and variances of velocity components (across-canyon U_{60} , along-canyon V_{330} in m s^{-1}) and direction of the principal axis of the flow for mooring 1590.

Table A- 3 : Summary of monthly averages for temperature (T), salinity (S), speed, direction (Dir), principal axis, and variance across-canyon (σU_{60}) and along-canyon (σV_{150}) for mooring 1590.

Type	Year	Month	Depth m	T ° C	S psu	Speed m/s	Dir. rel.true	X Axis to E	σU_{60} m ² /s ²	σV_{150} m ² /s ²
ADCP	2006	4	130	NaN	NaN	0.02	234	80	0.07	0.15
ADCP	2006	5	130	NaN	NaN	0.03	247	68	0.08	0.12
ADCP	2006	6	130	NaN	NaN	0.03	18	59	0.08	0.09
ADCP	2006	7	130	NaN	NaN	0.04	-5	39	0.09	0.11
ADCP	2006	8	130	NaN	NaN	0.06	-52	48	0.07	0.10
ADCP	2006	9	130	NaN	NaN	0.04	-43	54	0.08	0.12
ADCP	2006	10	130	NaN	NaN	0.03	-46	78	0.06	0.14
ADCP	2006	11	130	NaN	NaN	0.07	224	66	0.08	0.14
ADCP	2006	12	130	NaN	NaN	0.06	250	77	0.08	0.16
ADCP	2007	1	130	NaN	NaN	0.08	227	76	0.08	0.15
ADCP	2007	2	130	NaN	NaN	0.06	208	81	0.08	0.20
ADCP	2007	3	130	NaN	NaN	0.06	255	65	0.09	0.14
ADCP	2007	4	130	NaN	NaN	0.07	230	69	0.09	0.13
ADCP	2007	5	130	NaN	NaN	0.06	250	66	0.08	0.13
ADCP	2007	6	130	NaN	NaN	0.02	249	55	0.10	0.09
ADCP	2006	4	150	NaN	NaN	0.05	16	82	0.05	0.14
ADCP	2006	5	150	NaN	NaN	0.02	-37	74	0.07	0.12
ADCP	2006	6	150	NaN	NaN	0.01	-52	65	0.07	0.10
ADCP	2006	7	150	NaN	NaN	0.03	-39	64	0.08	0.12
ADCP	2006	8	150	NaN	NaN	0.02	259	67	0.07	0.12
ADCP	2006	9	150	NaN	NaN	0.03	260	71	0.07	0.13
ADCP	2006	10	150	NaN	NaN	0.02	-71	79	0.06	0.14
ADCP	2006	11	150	NaN	NaN	0.07	229	75	0.07	0.15
ADCP	2006	12	150	NaN	NaN	0.03	-74	75	0.08	0.16
ADCP	2007	1	150	NaN	NaN	0.03	-81	76	0.07	0.15
ADCP	2007	2	150	NaN	NaN	0.02	260	78	0.08	0.18
ADCP	2007	3	150	NaN	NaN	0.04	-52	75	0.07	0.16
ADCP	2007	4	150	NaN	NaN	0.06	241	77	0.07	0.15
ADCP	2007	5	150	NaN	NaN	0.05	266	70	0.07	0.13
ADCP	2007	6	150	NaN	NaN	0.02	249	64	0.08	0.11

Type	Year	Month	Depth m	T ° C	S psu	Speed m/s	Dir. rel.true	X Axis to E	σ U60 m2/s2	σ V150 m2/s2
ADCP	2006	4	175	NaN	NaN	0.08	22	80	0.05	0.14
ADCP	2006	5	175	NaN	NaN	0.03	10	75	0.06	0.12
ADCP	2006	6	175	NaN	NaN	0.01	-39	72	0.06	0.12
ADCP	2006	7	175	NaN	NaN	0.05	-1	71	0.06	0.12
ADCP	2006	8	175	NaN	NaN	0.01	-51	73	0.06	0.12
ADCP	2006	9	175	NaN	NaN	0.02	266	78	0.06	0.15
ADCP	2006	10	175	NaN	NaN	0.02	-38	79	0.06	0.14
ADCP	2006	11	175	NaN	NaN	0.05	235	75	0.07	0.14
ADCP	2006	12	175	NaN	NaN	0.04	-39	77	0.07	0.16
ADCP	2007	1	175	NaN	NaN	0.03	-50	78	0.06	0.16
ADCP	2007	2	175	NaN	NaN	0.02	-61	79	0.07	0.18
ADCP	2007	3	175	NaN	NaN	0.04	-23	79	0.06	0.16
ADCP	2007	4	175	NaN	NaN	0.04	262	81	0.06	0.16
ADCP	2007	5	175	NaN	NaN	0.04	-46	76	0.06	0.13
ADCP	2007	6	175	NaN	NaN	0.02	-74	70	0.07	0.12
ADCP	2006	4	200	NaN	NaN	0.09	9	81	0.05	0.15
ADCP	2006	5	200	NaN	NaN	0.05	15	77	0.05	0.12
ADCP	2006	6	200	NaN	NaN	0.02	-20	74	0.06	0.12
ADCP	2006	7	200	NaN	NaN	0.06	10	78	0.05	0.12
ADCP	2006	8	200	NaN	NaN	0.02	2	77	0.05	0.12
ADCP	2006	9	200	NaN	NaN	0.01	12	81	0.05	0.14
ADCP	2006	10	200	NaN	NaN	0.04	-12	78	0.05	0.13
ADCP	2006	11	200	NaN	NaN	0.03	245	77	0.06	0.14
ADCP	2006	12	200	NaN	NaN	0.05	-10	80	0.06	0.16
ADCP	2007	1	200	NaN	NaN	0.03	-25	80	0.06	0.16
ADCP	2007	2	200	NaN	NaN	0.02	-45	78	0.06	0.17
ADCP	2007	3	200	NaN	NaN	0.05	-5	81	0.05	0.15
ADCP	2007	4	200	NaN	NaN	0.03	-46	80	0.05	0.15
ADCP	2007	5	200	NaN	NaN	0.05	-13	78	0.05	0.13
ADCP	2007	6	200	NaN	NaN	0.02	-22	75	0.06	0.13
ADCP	2006	4	220	NaN	NaN	0.09	11	80	0.05	0.16

Type	Year	Month	Depth m	T ° C	S psu	Speed m/s	Dir. rel.true	X Axis to E	σU_{60} m ² /s ²	σV_{150} m ² /s ²
ADCP	2006	5	220	NaN	NaN	0.05	15	80	0.04	0.12
ADCP	2006	6	220	NaN	NaN	0.02	-9	77	0.05	0.11
ADCP	2006	7	220	NaN	NaN	0.06	22	80	0.04	0.11
ADCP	2006	8	220	NaN	NaN	0.02	10	77	0.05	0.12
ADCP	2006	9	220	NaN	NaN	0.01	31	82	0.05	0.14
ADCP	2006	10	220	NaN	NaN	0.05	-4	80	0.04	0.13
ADCP	2006	11	220	NaN	NaN	0.02	259	79	0.05	0.13
ADCP	2006	12	220	NaN	NaN	0.05	5	81	0.06	0.17
ADCP	2007	1	220	NaN	NaN	0.04	-20	80	0.06	0.17
ADCP	2007	2	220	NaN	NaN	0.03	-25	78	0.05	0.17
ADCP	2007	3	220	NaN	NaN	0.05	0	81	0.05	0.15
ADCP	2007	4	220	NaN	NaN	0.04	-13	79	0.05	0.15
ADCP	2007	5	220	NaN	NaN	0.05	-2	79	0.05	0.13
ADCP	2007	6	220	NaN	NaN	0.02	-9	76	0.05	0.12
R 4349	2006	4	345	7.7	34.9	0.01	153	75	0.04	0.09
R 4349	2006	5	345	8.1	34.9	0.01	177	72	0.04	0.08
R 4349	2006	6	345	8	35	0.02	-127	72	0.04	0.10
R 4349	2006	7	345	7.7	34.9	0.02	-124	76	0.04	0.09
R 4349	2006	8	345	6.9	34.7	0.00	162	77	0.03	0.09
R 4349	2006	9	345	6.9	34.7	0.03	-119	75	0.04	0.09
R 4349	2006	10	345	7.3	34.8	0.01	154	75	0.04	0.09
R 4349	2006	11	345	6.9	34.7	0.01	168	74	0.04	0.09
R 4349	2006	12	345	6.7	34.6	0.03	-141	74	0.05	0.11
R 4349	2007	1	345	5.2	34.4	0.01	164	75	0.05	0.11
R 4349	2007	2	345	4.2	34.4	0.02	107	77	0.05	0.12
R 4349	2007	3	345	4.6	34.4	0.02	-158	76	0.04	0.1
R 4349	2007	4	345	6.8	34.6	0.01	172	75	0.04	0.10
R 4349	2007	5	345	7.2	34.7	0.02	-159	74	0.04	0.09
R 4349	2007	6	345	7.2	34.7	0.01	179	73	0.04	0.10
R 9607	2006	4	546	7.7	34.9	0.02	-43	31	0.03	0.03
R 9607	2006	5	546	8.1	34.9	0.02	-67	51	0.04	0.03

Type	Year	Month	Depth m	T ° C	S psu	Speed m/s	Dir. rel.true	X Axis to E	σ_{U60} m2/s2	σ_{V150} m2/s2
R 9607	2006	6	546	8	35	0.02	-73	49	0.04	0.04
R 9607	2006	7	546	7.7	34.9	0.02	-72	47	0.04	0.03
R 9607	2006	8	546	6.9	34.7	0.01	-67	54	0.03	0.03
R 9607	2006	9	546	6.9	34.7	0.01	-57	40	0.03	0.03
R 9607	2006	10	546	7.3	34.8	0.01	-47	37	0.03	0.03
R 9607	2006	11	546	6.9	34.7	0.02	-88	59	0.03	0.03
R 9607	2006	12	546	6.7	34.6	0.02	-66	46	0.03	0.03
R 9607	2007	1	546	5.2	34.4	0.02	-72	45	0.04	0.03
R 9607	2007	2	546	4.2	34.4	0.02	-63	49	0.03	0.03
R 9607	2007	3	546	4.6	34.4	0.01	-60	47	0.03	0.03
R 9607	2007	4	546	6.8	34.6	0.02	-57	43	0.03	0.03
R 9607	2007	5	546	7.2	34.7	0.02	-61	50	0.04	0.03
R 9607	2007	6	546	7.1	34.7	0.02	-76	56	0.04	0.03
R 6409	2006	4	673	7.7	34.9	0.01	-55	6	0.03	0.07
R 6409	2006	5	673	8.1	34.9	0.03	-24	4	0.03	0.09
R 6409	2006	6	673	8	35	0.02	-24	3	0.03	0.09
R 6409	2006	7	673	7.7	34.9	0.01	-25	4	0.03	0.08
R 6409	2006	8	673	6.9	34.7	0.02	-39	5	0.03	0.08
R 6409	2006	9	673	6.9	34.7	0.01	-39	6	0.03	0.07
R 6409	2006	10	673	7.3	34.8	0.01	-37	5	0.02	0.07
R 6409	2006	11	673	6.9	34.7	0.02	-33	5	0.03	0.08
R 6409	2006	12	673	6.7	34.6	0.02	-32	5	0.03	0.09
R 6409	2007	1	673	5.2	34.4	0.02	-29	5	0.03	0.08
R 6409	2007	2	673	4.2	34.4	0.02	-28	5	0.03	0.09
R 6409	2007	3	673	4.6	34.4	0.02	-33	5	0.03	0.07
R 6409	2007	4	673	6.8	34.6	0.01	-28	5	0.03	0.08
R 6409	2007	5	673	7.2	34.7	0.02	-26	3	0.03	0.09
R 6409	2007	6	673	7.1	34.7	0.02	-20	4	0.03	0.10

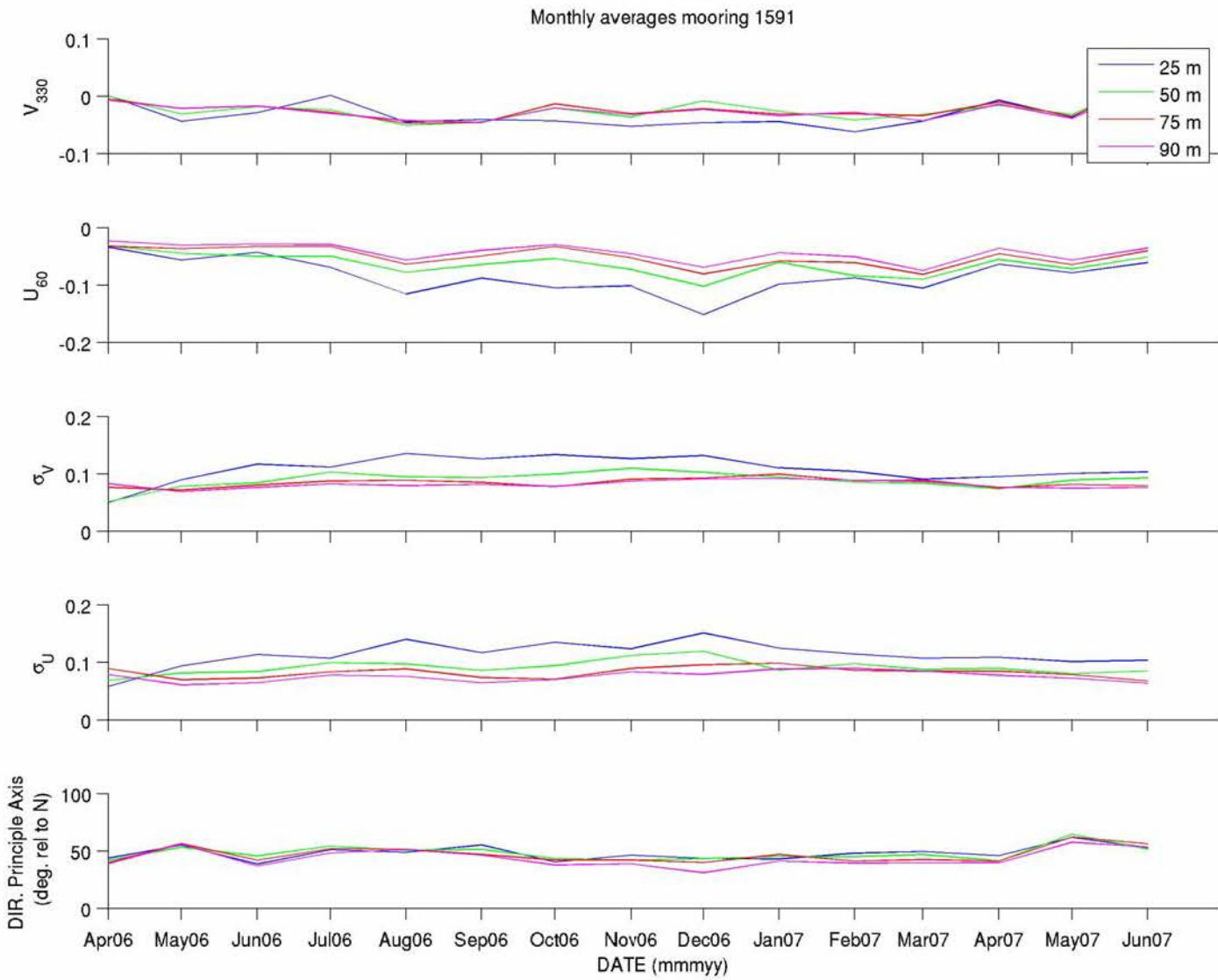


Figure A-133: Monthly averages and variances of velocity components (across-canyon U_{60} , along-canyon V_{330} in m s^{-1}) and direction of the principal axis of the flow for mooring 1591.

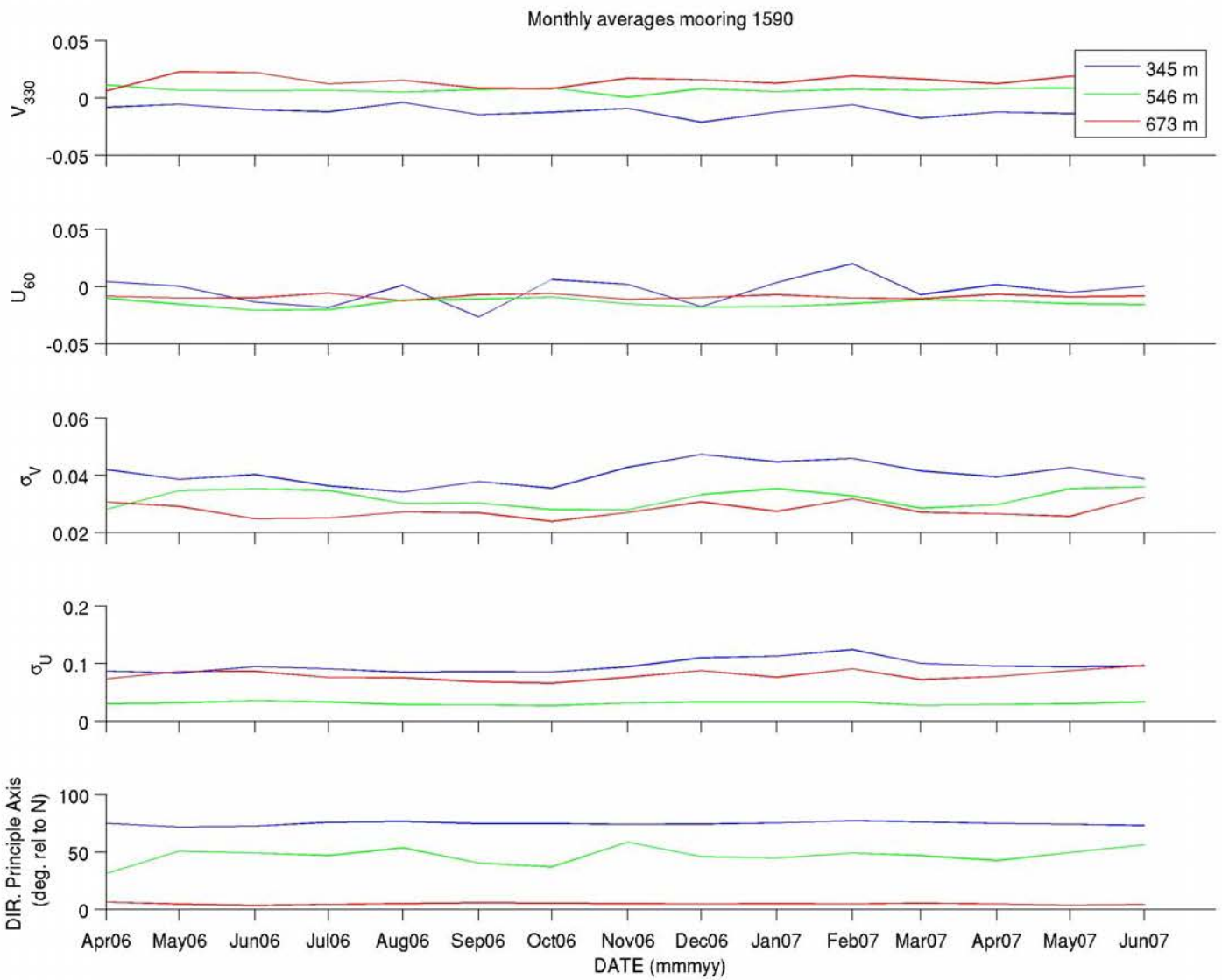


Figure A-134: Monthly averages and variances of velocity components (across-canyon U_{60} , along-canyon U_{330} in m s^{-1}) and direction of the principal axis of the flow for mooring 1591.

Table A- 4 : Summary of monthly averages for temperature (T), salinity (S), speed, direction (Dir), principal axis, and variance across-canyon ($\sigma U60$) and along-canyon ($\sigma V150$) for mooring 1591.

Type	Year	Month	Depth m	T ° C	S psu	Speed m/s	Dir. rel.true	X Axis to E	$\sigma U60$ m ² /s ²	$\sigma V150$ m ² /s ²
ADCP	2006	4	25	NaN	NaN	0.03	-88	44	0.06	0.05
ADCP	2006	5	25	NaN	NaN	0.07	232	55	0.09	0.09
ADCP	2006	6	25	NaN	NaN	0.05	236	39	0.11	0.12
ADCP	2006	7	25	NaN	NaN	0.07	-89	51	0.11	0.11
ADCP	2006	8	25	NaN	NaN	0.12	249	49	0.14	0.14
ADCP	2006	9	25	NaN	NaN	0.10	245	55	0.12	0.13
ADCP	2006	10	25	NaN	NaN	0.11	248	40	0.14	0.13
ADCP	2006	11	25	NaN	NaN	0.11	243	46	0.12	0.13
ADCP	2006	12	25	NaN	NaN	0.16	253	44	0.15	0.13
ADCP	2007	1	25	NaN	NaN	0.11	246	43	0.13	0.11
ADCP	2007	2	25	NaN	NaN	0.11	235	48	0.12	0.10
ADCP	2007	3	25	NaN	NaN	0.11	248	49	0.11	0.09
ADCP	2007	4	25	NaN	NaN	0.06	264	46	0.11	0.10
ADCP	2007	5	25	NaN	NaN	0.09	245	62	0.10	0.10
ADCP	2007	6	25	NaN	NaN	0.07	-65	53	0.10	0.10
ADCP	2006	4	50	NaN	NaN	0.03	270	42	0.07	0.05
ADCP	2006	5	50	NaN	NaN	0.06	235	53	0.08	0.08
ADCP	2006	6	50	NaN	NaN	0.05	250	46	0.08	0.08
ADCP	2006	7	50	NaN	NaN	0.06	244	54	0.1	0.10
ADCP	2006	8	50	NaN	NaN	0.09	237	50	0.10	0.10
ADCP	2006	9	50	NaN	NaN	0.08	235	51	0.09	0.09
ADCP	2006	10	50	NaN	NaN	0.06	249	44	0.09	0.10
ADCP	2006	11	50	NaN	NaN	0.08	243	42	0.11	0.11
ADCP	2006	12	50	NaN	NaN	0.10	265	43	0.12	0.10
ADCP	2007	1	50	NaN	NaN	0.07	246	45	0.09	0.09
ADCP	2007	2	50	NaN	NaN	0.09	244	45	0.10	0.09
ADCP	2007	3	50	NaN	NaN	0.10	250	47	0.09	0.08
ADCP	2007	4	50	NaN	NaN	0.06	254	41	0.09	0.07
ADCP	2007	5	50	NaN	NaN	0.08	246	65	0.08	0.09
ADCP	2007	6	50	NaN	NaN	0.06	-63	52	0.09	0.09

Type	Year	Month	Depth m	T ° C	S psu	Speed m/s	Dir. rel.true	X Axis to E	σ U60 m2/s2	σ V150 m2/s2
ADCP	2006	4	75	NaN	NaN	0.03	262	40	0.09	0.08
ADCP	2006	5	75	NaN	NaN	0.04	240	56	0.07	0.07
ADCP	2006	6	75	NaN	NaN	0.04	242	42	0.07	0.08
ADCP	2006	7	75	NaN	NaN	0.04	230	52	0.08	0.09
ADCP	2006	8	75	NaN	NaN	0.08	233	51	0.09	0.09
ADCP	2006	9	75	NaN	NaN	0.07	227	47	0.07	0.09
ADCP	2006	10	75	NaN	NaN	0.04	248	42	0.07	0.08
ADCP	2006	11	75	NaN	NaN	0.06	240	42	0.09	0.09
ADCP	2006	12	75	NaN	NaN	0.08	255	40	0.10	0.09
ADCP	2007	1	75	NaN	NaN	0.07	242	47	0.10	0.1
ADCP	2007	2	75	NaN	NaN	0.07	243	41	0.09	0.09
ADCP	2007	3	75	NaN	NaN	0.09	247	43	0.09	0.09
ADCP	2007	4	75	NaN	NaN	0.05	258	41	0.09	0.08
ADCP	2007	5	75	NaN	NaN	0.07	242	62	0.08	0.08
ADCP	2007	6	75	NaN	NaN	0.05	-60	56	0.07	0.08
ADCP	2006	4	90	NaN	NaN	0.02	253	39	0.08	0.08
ADCP	2006	5	90	NaN	NaN	0.04	235	56	0.06	0.07
ADCP	2006	6	90	NaN	NaN	0.03	239	37	0.07	0.08
ADCP	2006	7	90	NaN	NaN	0.04	224	48	0.08	0.08
ADCP	2006	8	90	NaN	NaN	0.07	233	51	0.08	0.08
ADCP	2006	9	90	NaN	NaN	0.06	221	46	0.07	0.08
ADCP	2006	10	90	NaN	NaN	0.04	235	38	0.07	0.08
ADCP	2006	11	90	NaN	NaN	0.06	235	39	0.08	0.09
ADCP	2006	12	90	NaN	NaN	0.07	251	31	0.08	0.09
ADCP	2007	1	90	NaN	NaN	0.06	232	41	0.09	0.09
ADCP	2007	2	90	NaN	NaN	0.06	241	39	0.09	0.09
ADCP	2007	3	90	NaN	NaN	0.09	240	40	0.09	0.09
ADCP	2007	4	90	NaN	NaN	0.04	248	40	0.08	0.08
ADCP	2007	5	90	NaN	NaN	0.07	236	58	0.07	0.08
ADCP	2007	6	90	NaN	NaN	0.04	-60	54	0.06	0.08
R 1607	2006	4	222	5.5	33.7	0.06	-83	57	0.1	0.1

Type	Year	Month	Depth m	T ° C	S psu	Speed m/s	Dir. rel.true	X Axis to E	σ_{U60} m2/s2	σ_{V150} m2/s2
R 1607	2006	5	222	6.6	34	0.02	-60	60	0.08	0.12
R 1607	2006	6	222	10.3	35	0.03	97	58	0.09	0.10
R 1607	2006	7	222	5.2	33.8	0.03	-21	64	0.08	0.12
R 1607	2006	8	222	6.1	34	0.02	-4	61	0.07	0.09
R 1607	2006	9	222	3.4	33.4	0.02	-57	63	0.08	0.12
R 1607	2006	10	222	4.5	33.7	0.03	-131	68	0.07	0.14
R 1607	2006	11	222	2.8	33.3	0.05	-120	66	0.08	0.14
R 1607	2006	12	222	3.5	33.6	0.03	-106	66	0.09	0.15
R 1607	2007	1	222	2.7	33.3	0.01	-120	66	0.08	0.15
R 1607	2007	2	222	2.1	33.3	0.00	164	68	0.09	0.13
R 1607	2007	3	222	2.8	33.5	0.03	-88	64	0.08	0.14
R 1607	2007	4	222	3.4	33.4	0.04	-94	66	0.08	0.13
R 1607	2007	5	222	4.7	33.7	0.03	-100	68	0.08	0.13
R 1607	2007	6	222	8.9	34.6	0.02	-27	59	0.08	0.12
R 1039	2006	4	323	5.5	33.7	0.08	-70	65	0.07	0.11
R 1039	2006	5	323	6.6	34	0.03	-66	62	0.07	0.13
R 1039	2006	6	323	10.3	35	0.01	57	61	0.07	0.13
R 1039	2006	7	323	5.1	33.8	0.04	75	53	0.07	0.11
R 1039	2006	8	323	6.1	34	0.02	-9	55	0.07	0.12
R 1039	2006	9	323	3.4	33.4	0.01	26	52	0.07	0.12
R 1039	2006	10	323	4.5	33.7	0.01	-90	60	0.06	0.13
R 1039	2006	11	323	2.8	33.3	0.02	-8	62	0.07	0.14
R 1039	2006	12	323	3.4	33.6	0.01	-35	56	0.08	0.15
R 1039	2007	1	323	2.7	33.3	0.01	32	62	0.07	0.14
R 1039	2007	2	323	2.1	33.3	0.01	-58	65	0.07	0.14
R 1039	2007	3	323	2.8	33.5	0.02	-43	61	0.07	0.14
R 1039	2007	4	323	3.4	33.4	0.03	-25	61	0.07	0.13
R 1039	2007	5	323	4.7	33.7	0.01	70	63	0.06	0.13
R 1039	2007	6	323	8.7	34.5	0.01	-90	57	0.06	0.11
R 786	2006	4	424	5.5	33.7	0.02	-130	43	0.04	0.11
R 786	2006	5	424	6.6	34	0.02	150	43	0.05	0.11

Type	Year	Month	Depth m	T ° C	S psu	Speed m/s	Dir. rel.true	X Axis to E	σ U60 m ² /s ²	σ V150 m ² /s ²
R 786	2006	6	424	10.3	35	0.03	149	52	0.05	0.11
R 786	2006	7	424	5.1	33.8	0.03	132	49	0.05	0.10
R 786	2006	8	424	6.1	34	0.02	140	43	0.04	0.09
R 786	2006	9	424	3.4	33.4	0.02	132	42	0.04	0.09
R 786	2006	10	424	4.5	33.7	0.01	146	43	0.04	0.10
R 786	2006	11	424	2.8	33.3	0.03	150	42	0.05	0.11
R 786	2006	12	424	3.4	33.6	0.03	137	44	0.05	0.13
R 786	2007	1	424	2.7	33.3	0.02	153	53	0.05	0.13
R 786	2007	2	424	2.1	33.3	0.02	173	56	0.06	0.15
R 786	2007	3	424	2.8	33.5	0.03	146	50	0.05	0.12
R 786	2007	4	424	3.4	33.4	0.02	150	43	0.04	0.11
R 786	2007	5	424	4.7	33.7	0.03	143	49	0.05	0.11
R 786	2007	6	424	8.7	34.5	0.02	153	43	0.04	0.10

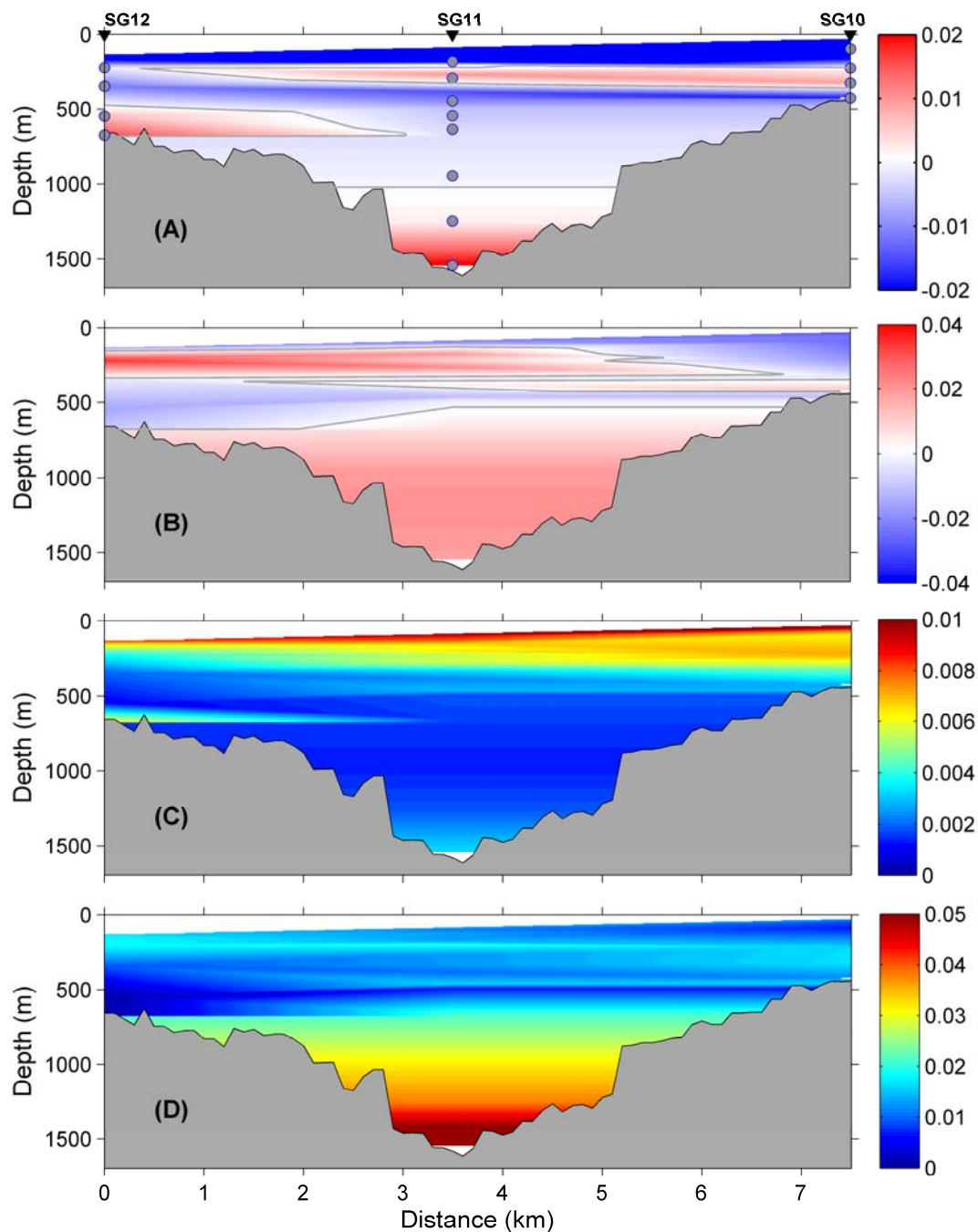


Figure A- 135: Average estimates from SG10, SG11 and SG12 moorings for the (A) across-canyon speed (m s^{-1} , positive northeast), (B) along-canyon speed (m s^{-1} , positive northwest), (C) across-canyon variance of speed ($\text{m}^2 \text{s}^{-2}$) and (D) along-canyon variance ($\text{m}^2 \text{s}^{-2}$). Grey lines in the top two panels represent the 0 m s^{-1} contour.

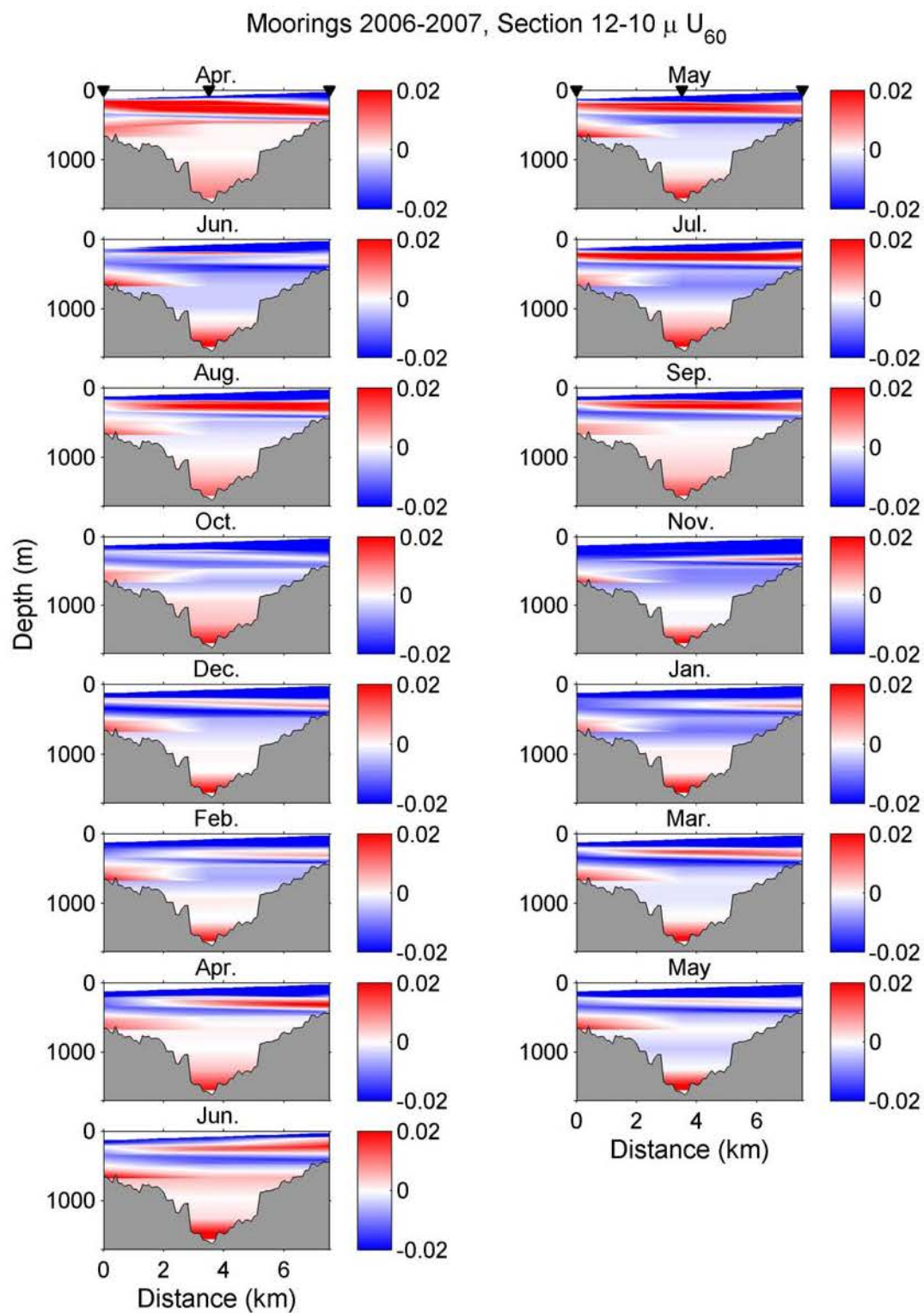


Figure A- 136: Monthly average estimates from SG10, SG11 and SG12 moorings for the across-canyon speed (m s^{-1} , positive northeast).

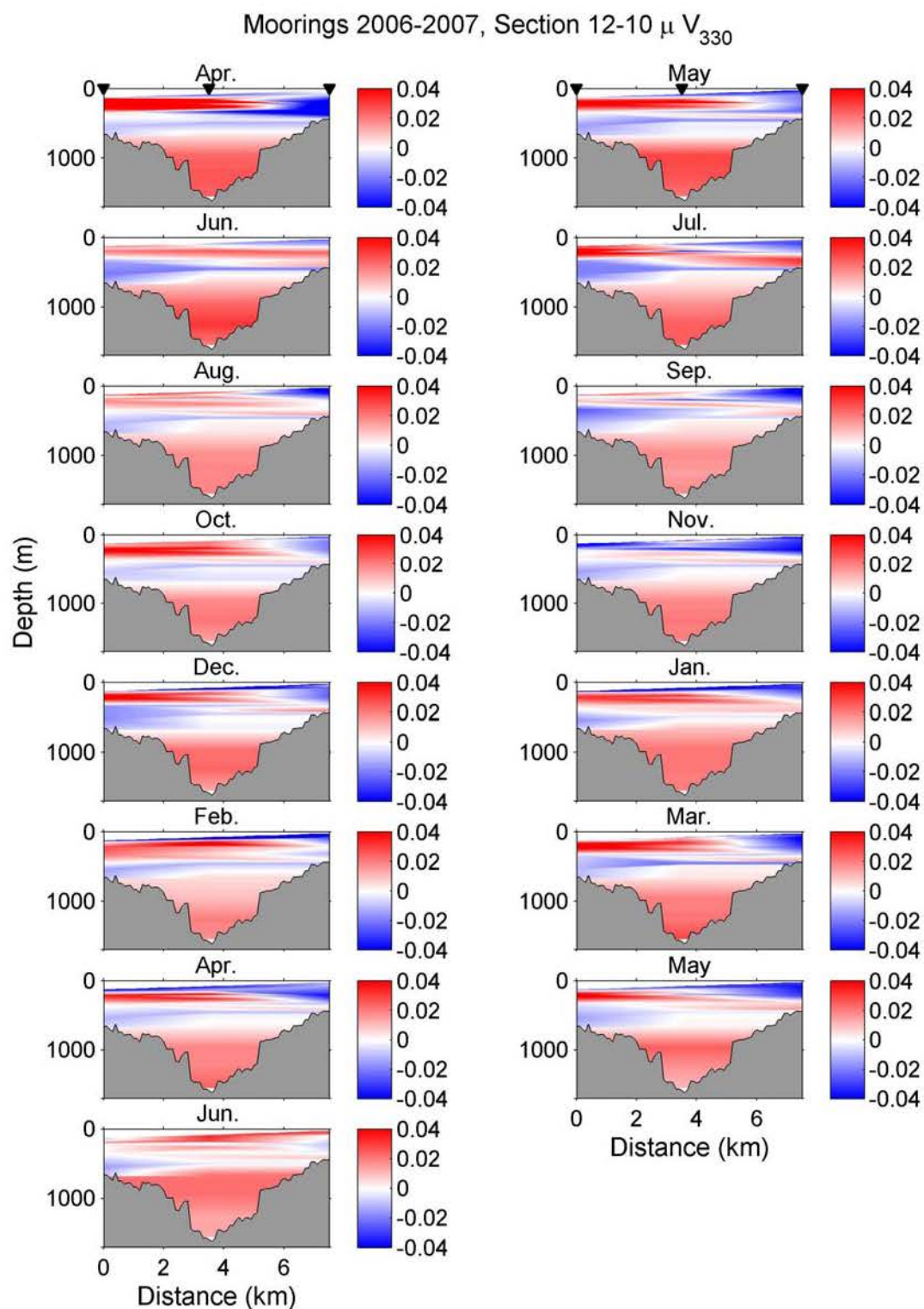


Figure A- 137: Monthly average estimates from SG10, SG11 and SG12 moorings for the along-canyon speed (m s^{-1} , positive northwest)

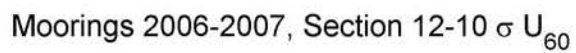


Figure A- 138: Monthly average estimates from SG10, SG11 and SG12 moorings for the across-canyon variance of speed ($\text{m}^2 \text{s}^{-2}$).

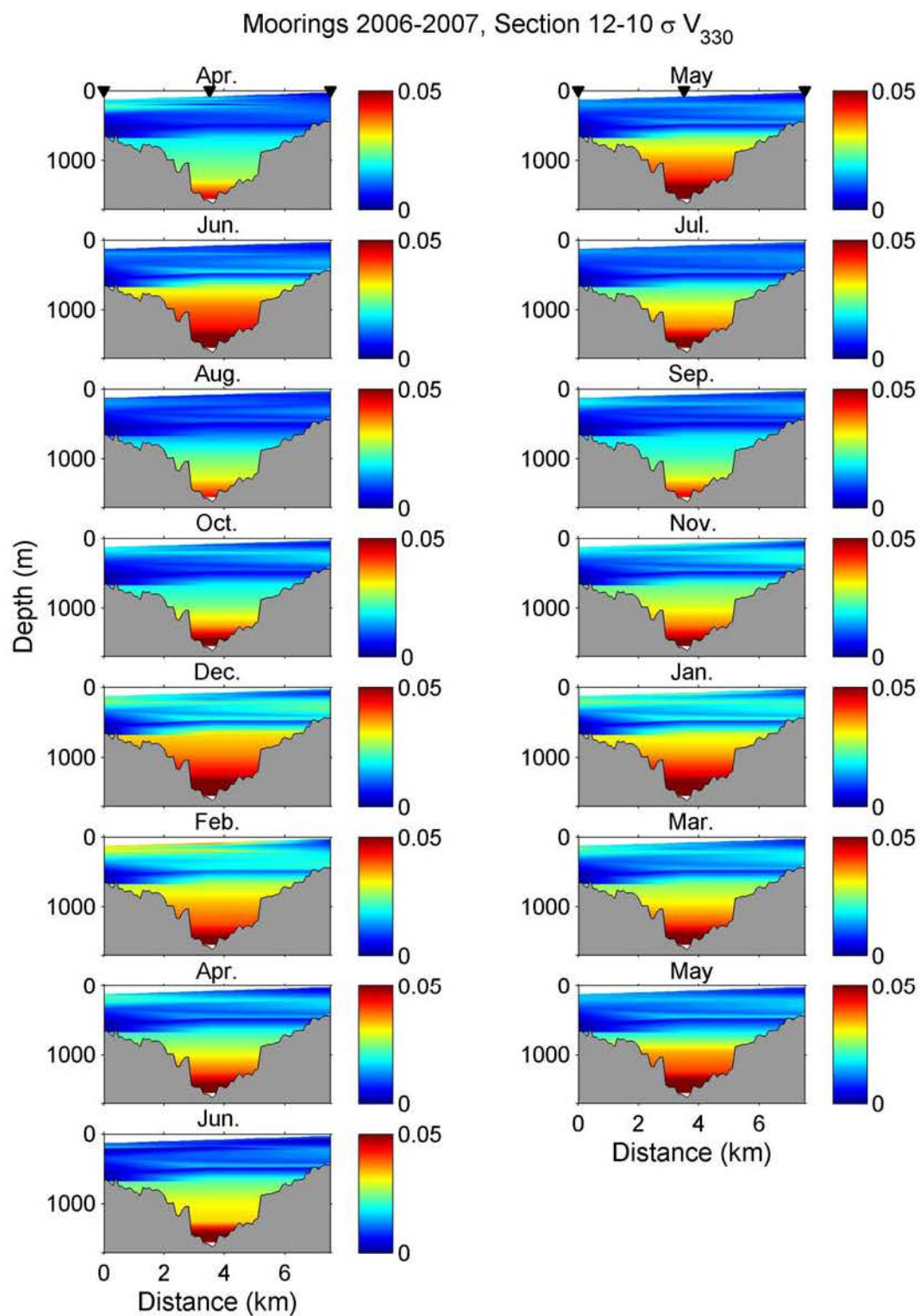


Figure A- 139: Monthly average estimates from SG10, SG11 and SG12 moorings for the along-canyon variance ($\text{m}^2 \text{s}^{-2}$).

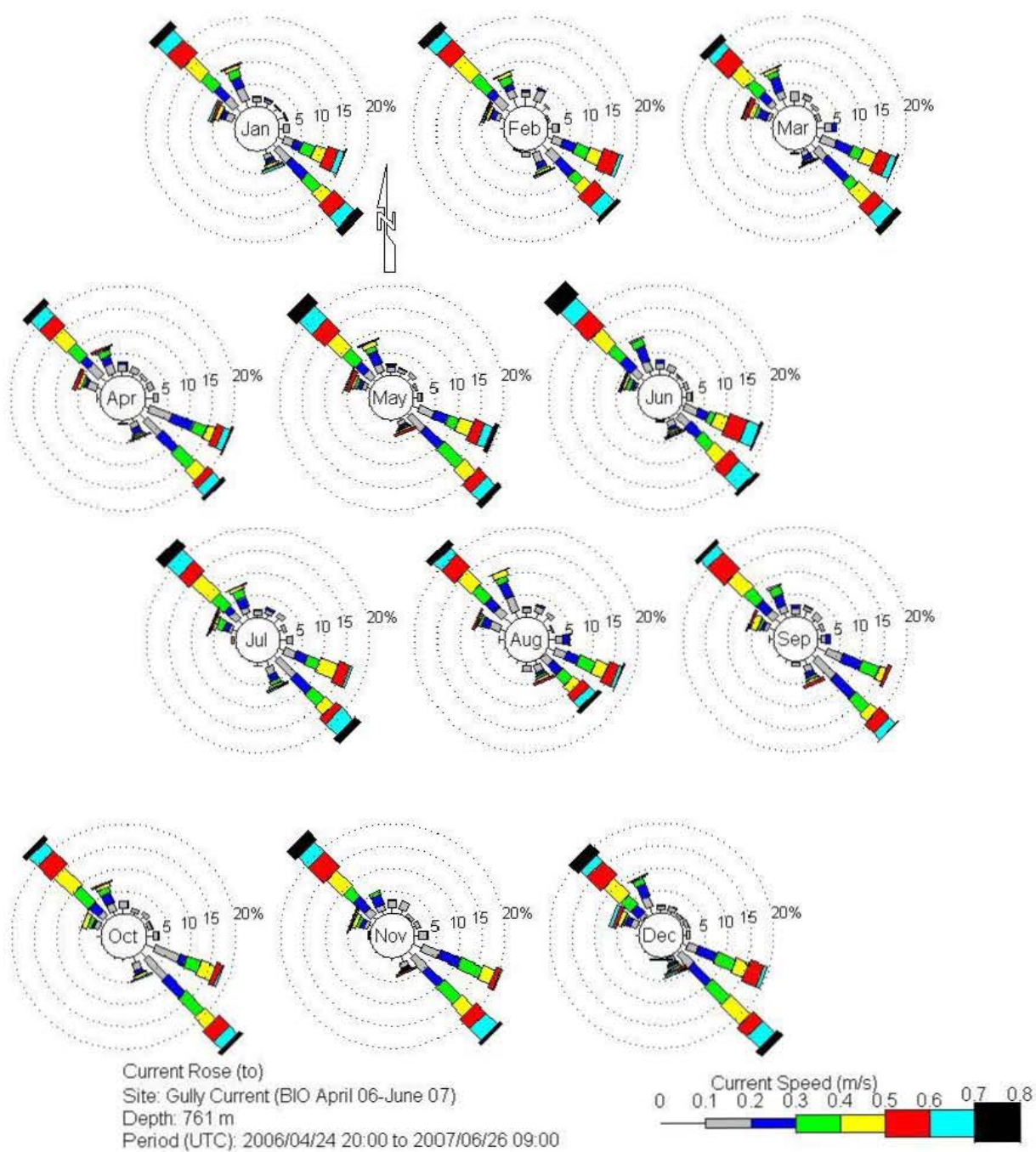
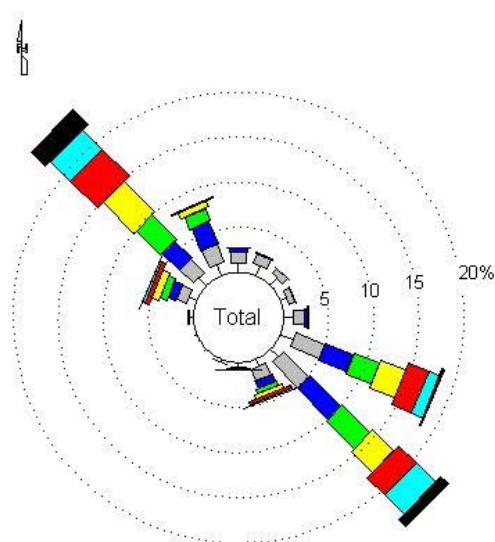


Figure A- 140: Monthly average current rose plots RCM8 Mooring 1588.



Current Rose (to)

Site: Gully Current (BIO April 06-June 07)

Depth: 761 m

Period (UTC): 2006/04/24 20:00 to 2007/06/26 09:00

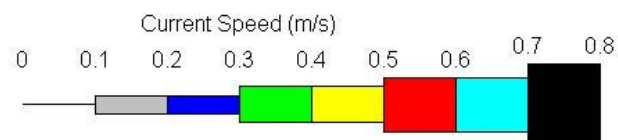


Figure A- 141: Annual average current rose plots RCM8 Mooring 1588.

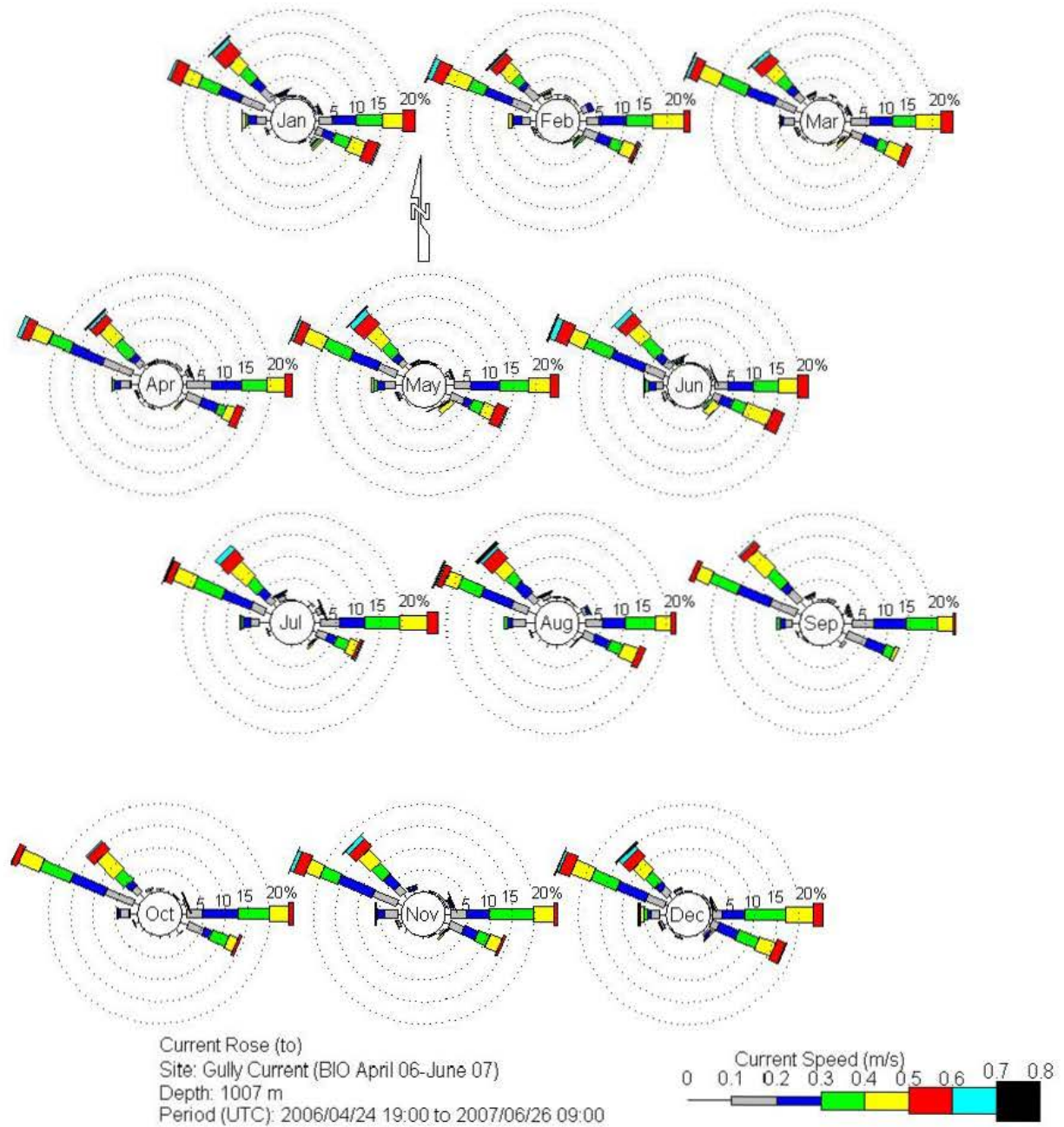
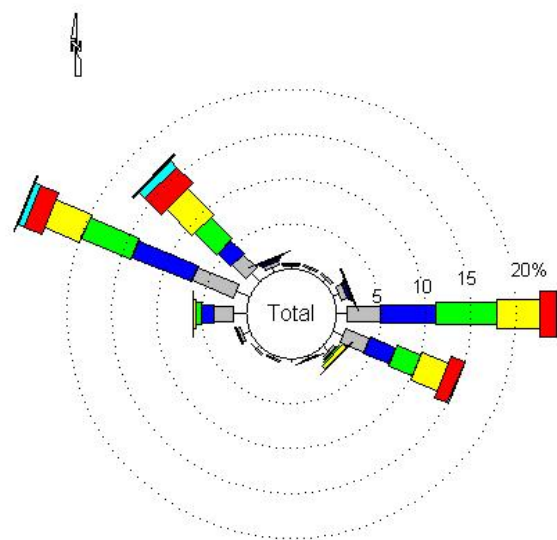


Figure A- 142: Monthly average current rose plots RCM8 Mooring 1588.



Current Rose (to)

Site: Gully Current (BIO April 06-June 07)

Depth: 1007 m

Period (UTC): 2006/04/24 19:00 to 2007/06/26 09:00

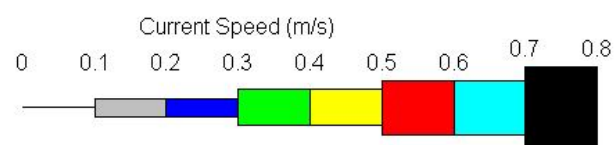


Figure A- 143: Annual average current rose plots RCM8 Mooring 1588.

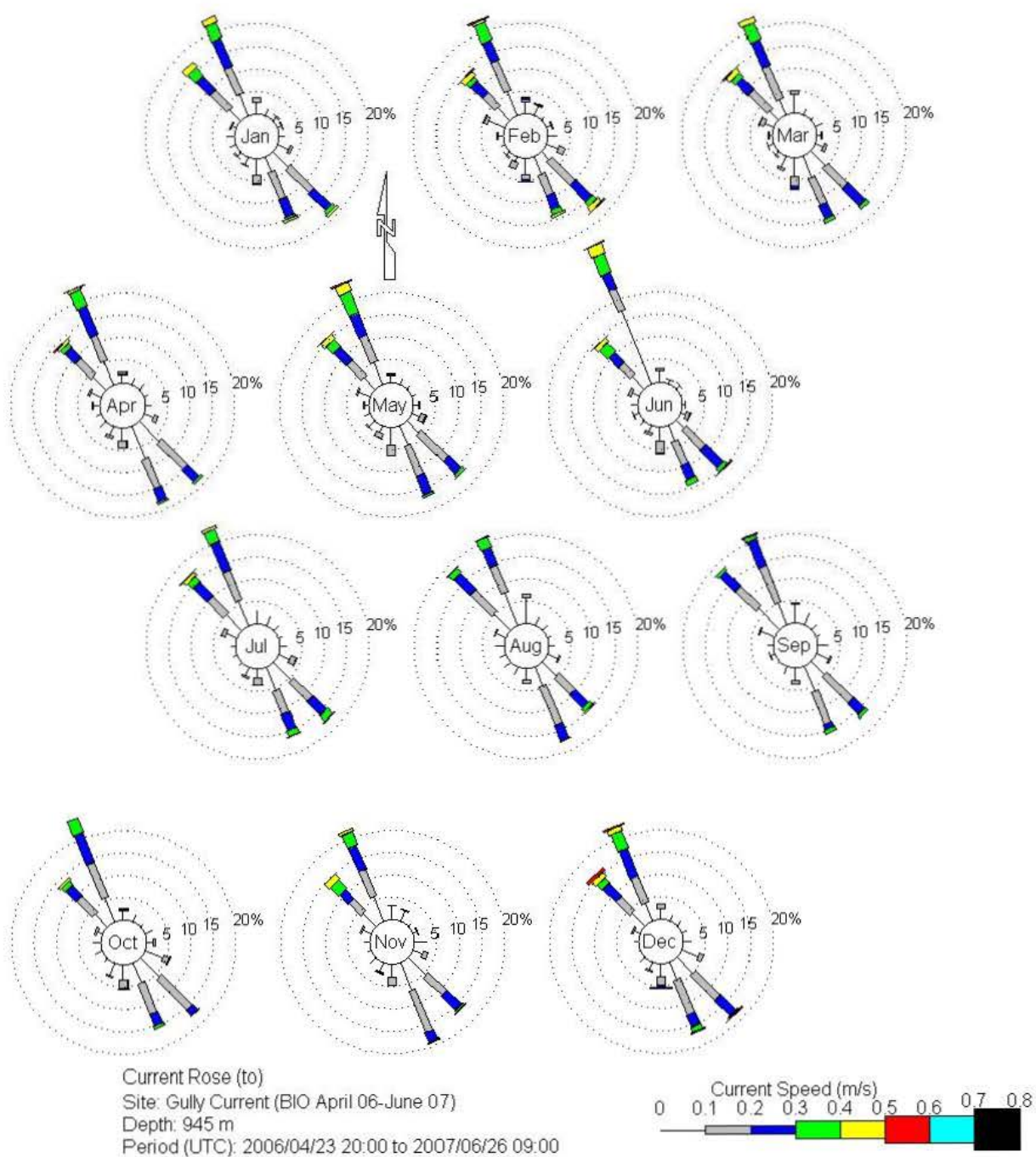


Figure A- 144: Monthly average current rose plots RCM8 Mooring 1589.

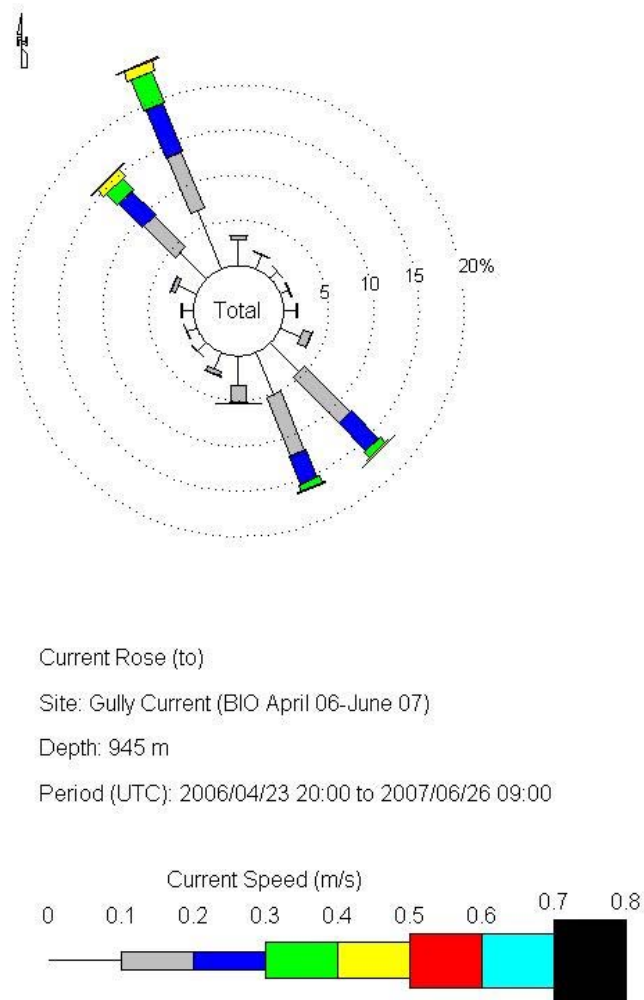


Figure A- 145: Annual average current rose plots RCM8 Mooring 1589.

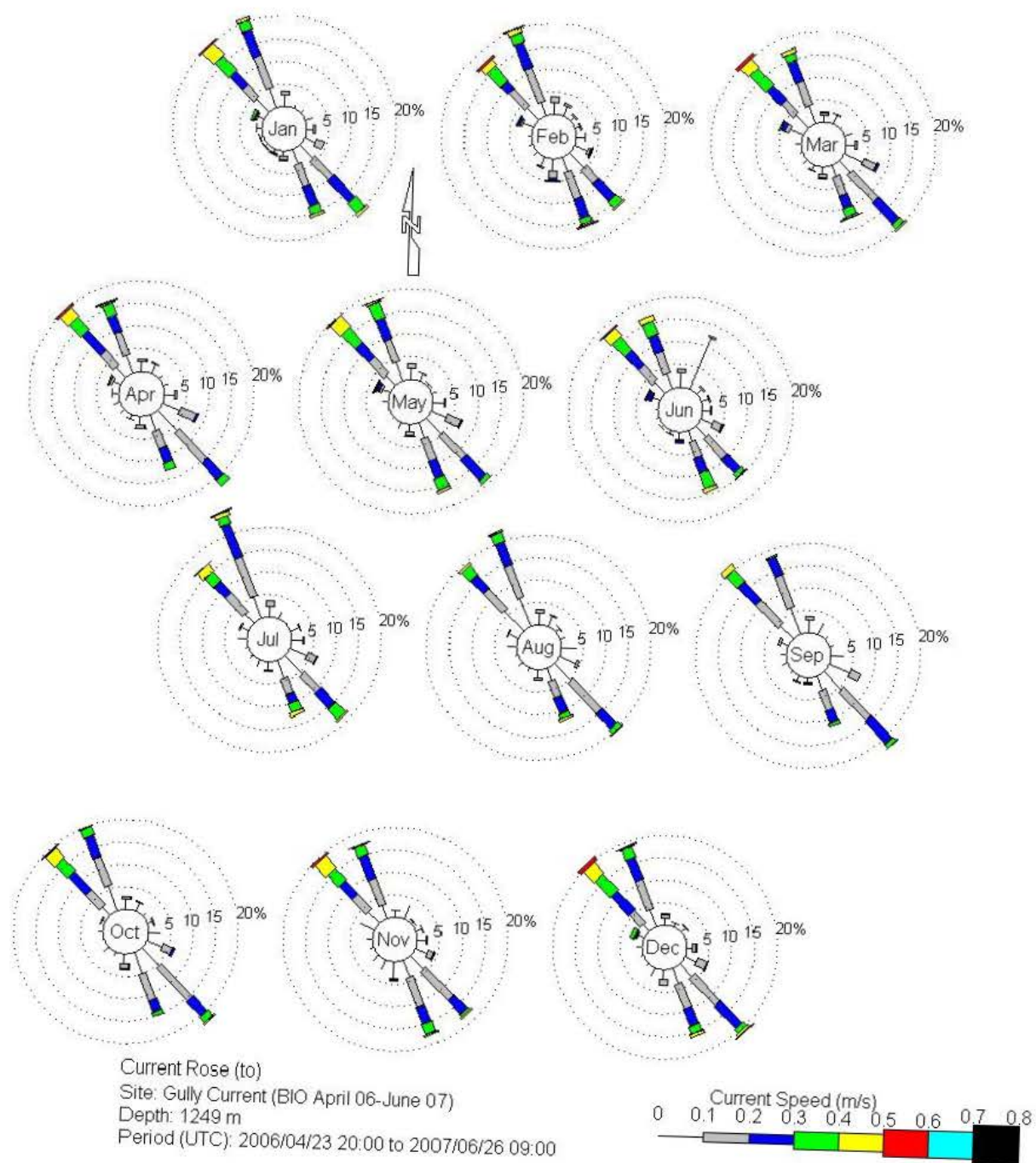


Figure A- 146: Monthly average current rose plots RCM8 Mooring 1589.

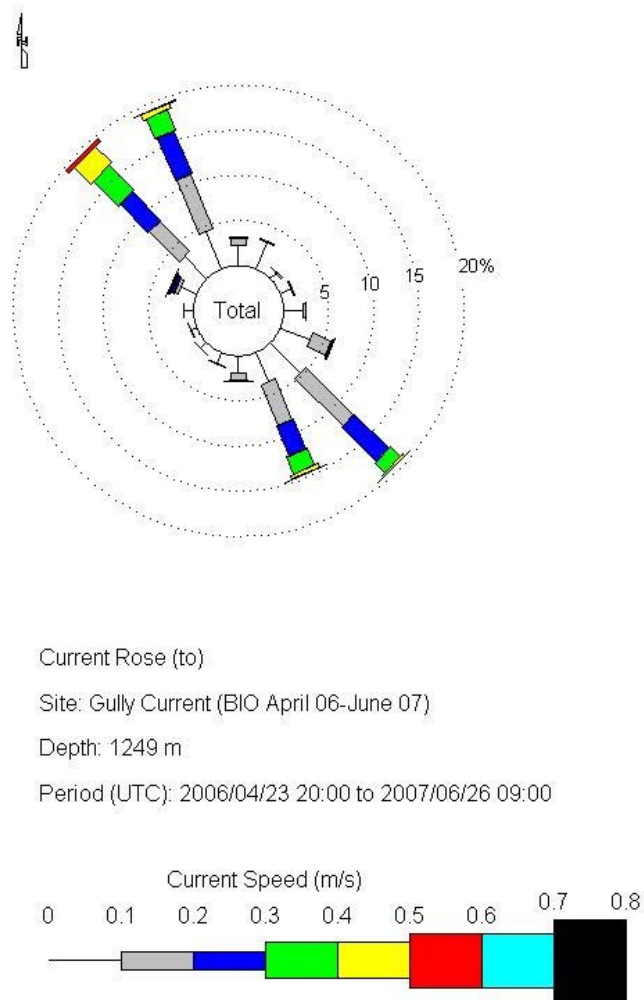


Figure A- 147: Annual average current rose plots RCM8 Mooring 1589.

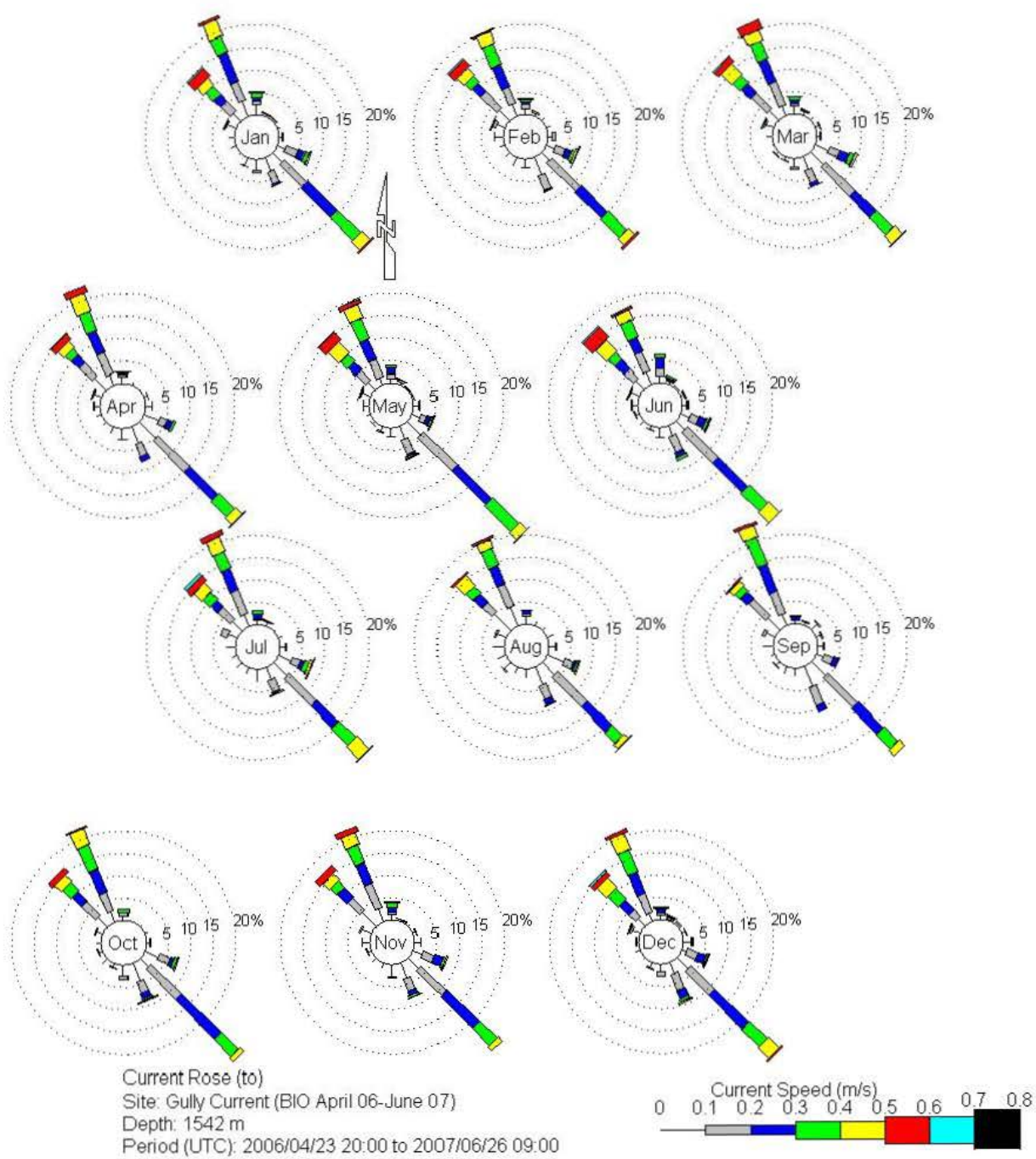
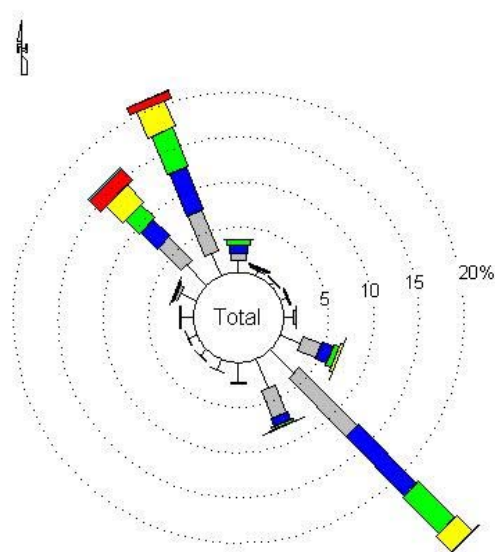


Figure A- 148: Monthly average current rose plots RCM8 Mooring 1589.



Current Rose (to)

Site: Gully Current (BIO April 06-June 07)

Depth: 1542 m

Period (UTC): 2006/04/23 20:00 to 2007/06/26 09:00

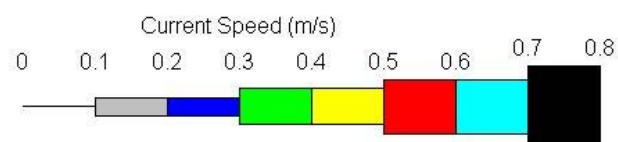


Figure A- 149: Annual average current rose plots RCM8 Mooring 1589.

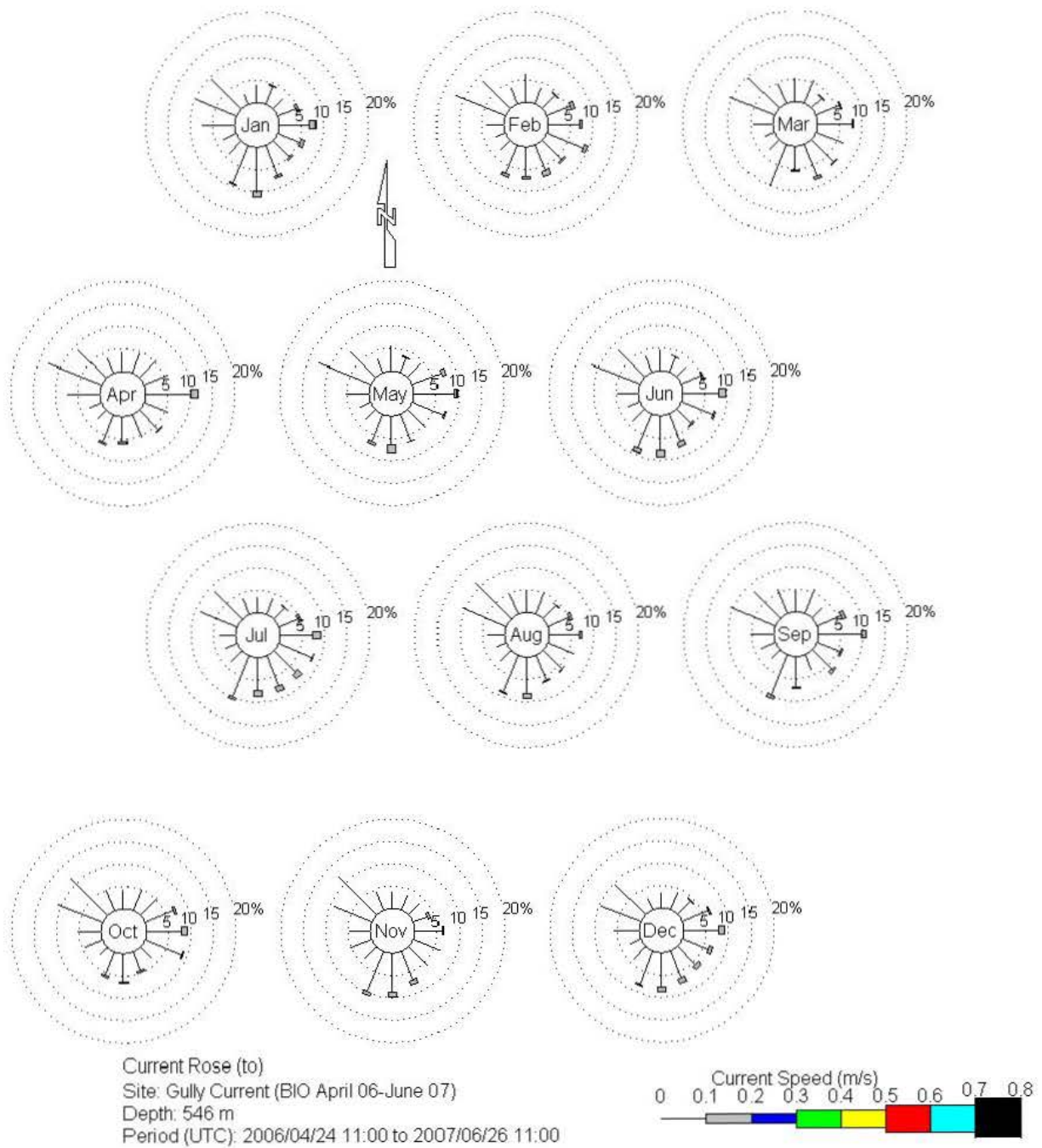
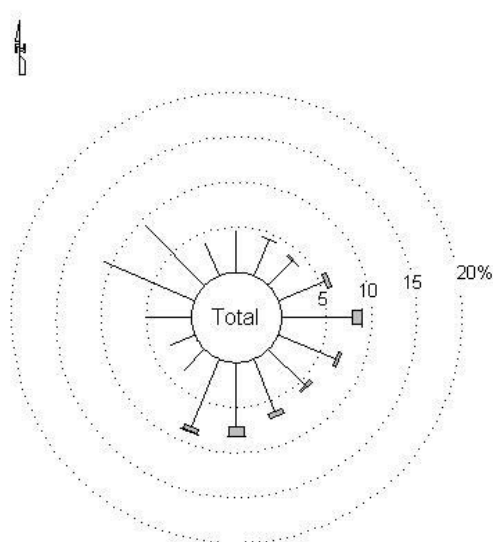


Figure A- 150: Monthly average current rose plots RCM8 Mooring 1590.



Current Rose (to)

Site: Gully Current (BIO April 06-June 07)

Depth: 546 m

Period (UTC): 2006/04/24 11:00 to 2007/06/26 11:00

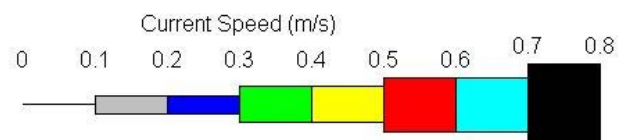


Figure A- 151: Annual average current rose plots RCM8 Mooring 1590.

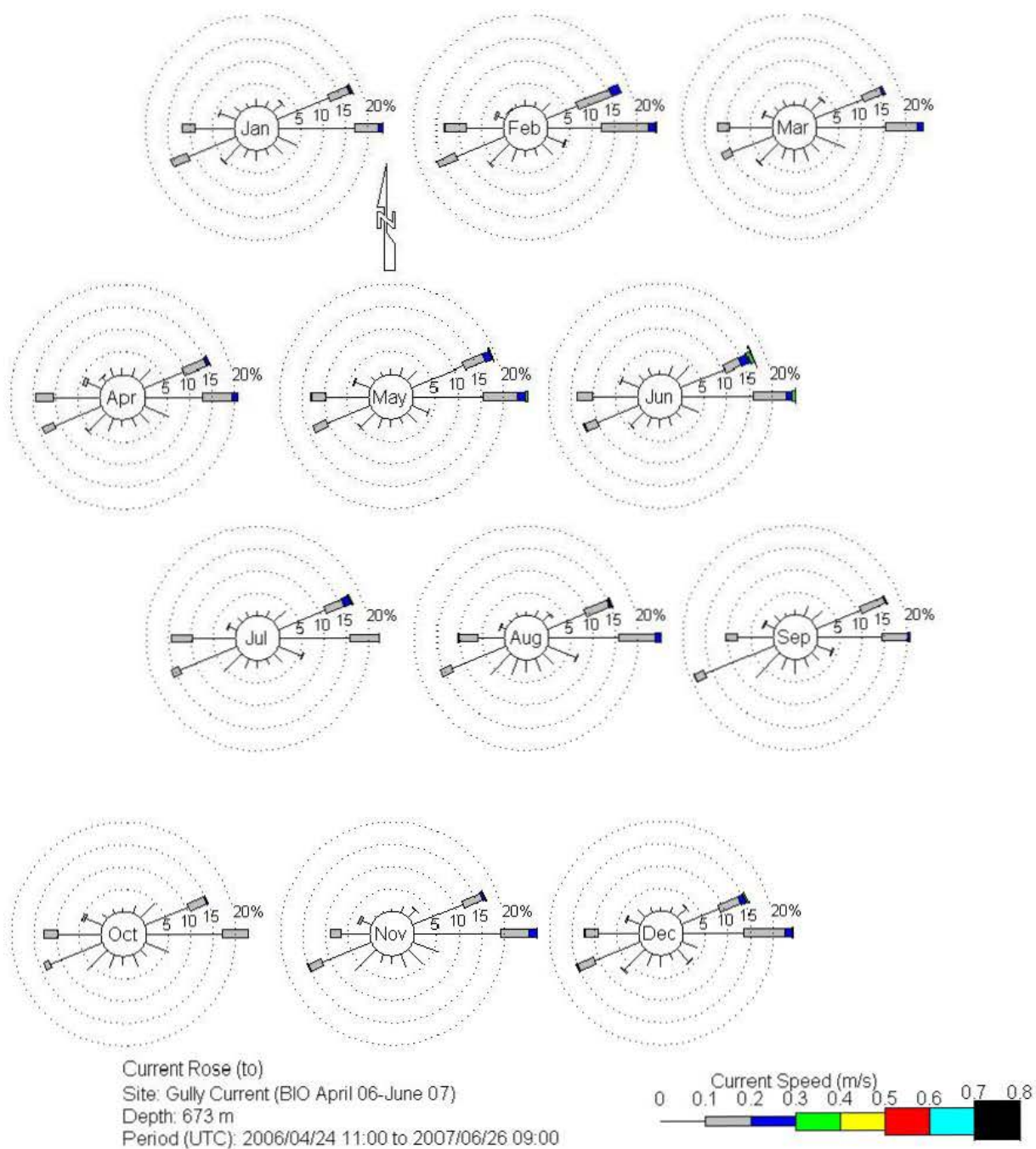
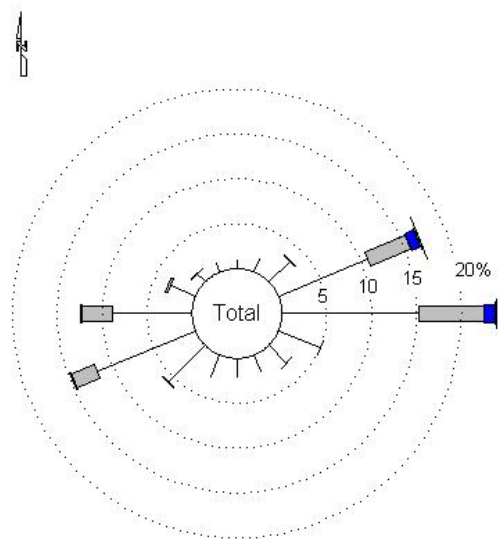


Figure A- 152: Monthly average current rose plots RCM8 Mooring 1590.



Current Rose (to)

Site: Gully Current (BIO April 06-June 07)

Depth: 673 m

Period (UTC): 2006/04/24 11:00 to 2007/06/26 09:00

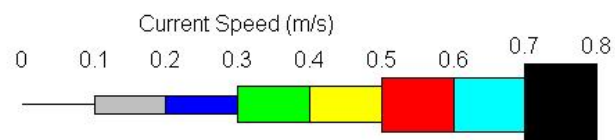


Figure A- 153: Annual average current rose plots RCM8 Mooring 1590.

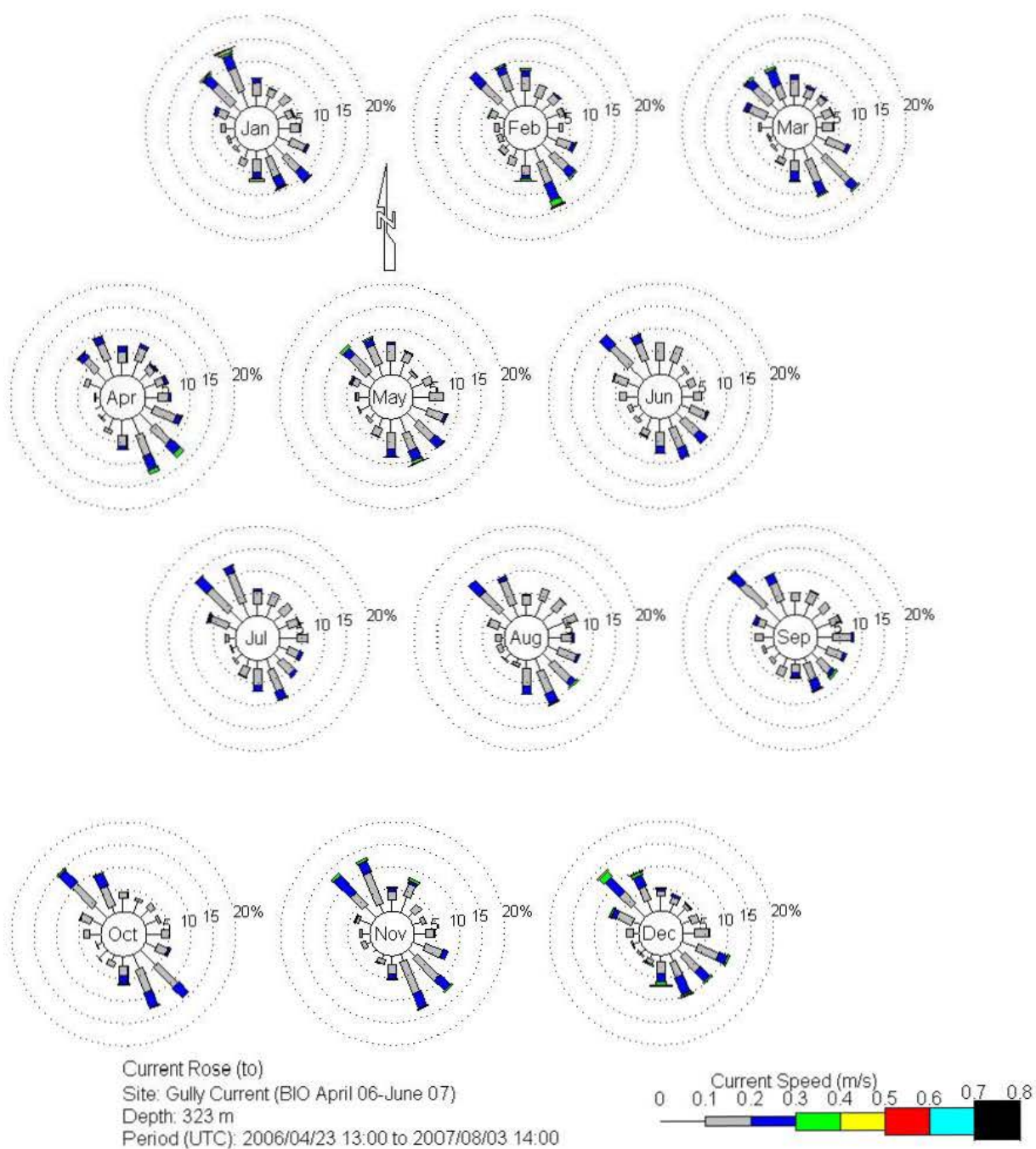
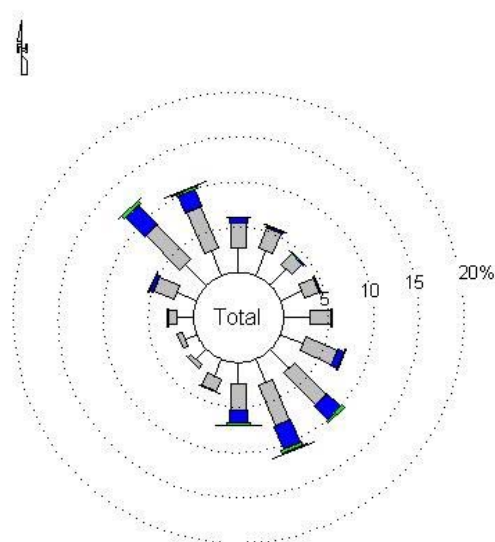


Figure A- 154: Monthly average current rose plots RCM8 Mooring 1591.



Current Rose (to)

Site: Gully Current (BIO April 06-June 07)

Depth: 323 m

Period (UTC): 2006/04/23 13:00 to 2007/08/03 14:00

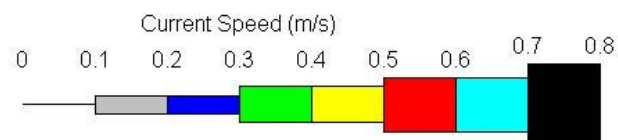


Figure A- 155: Annual average current rose plots RCM8 Mooring 1591.

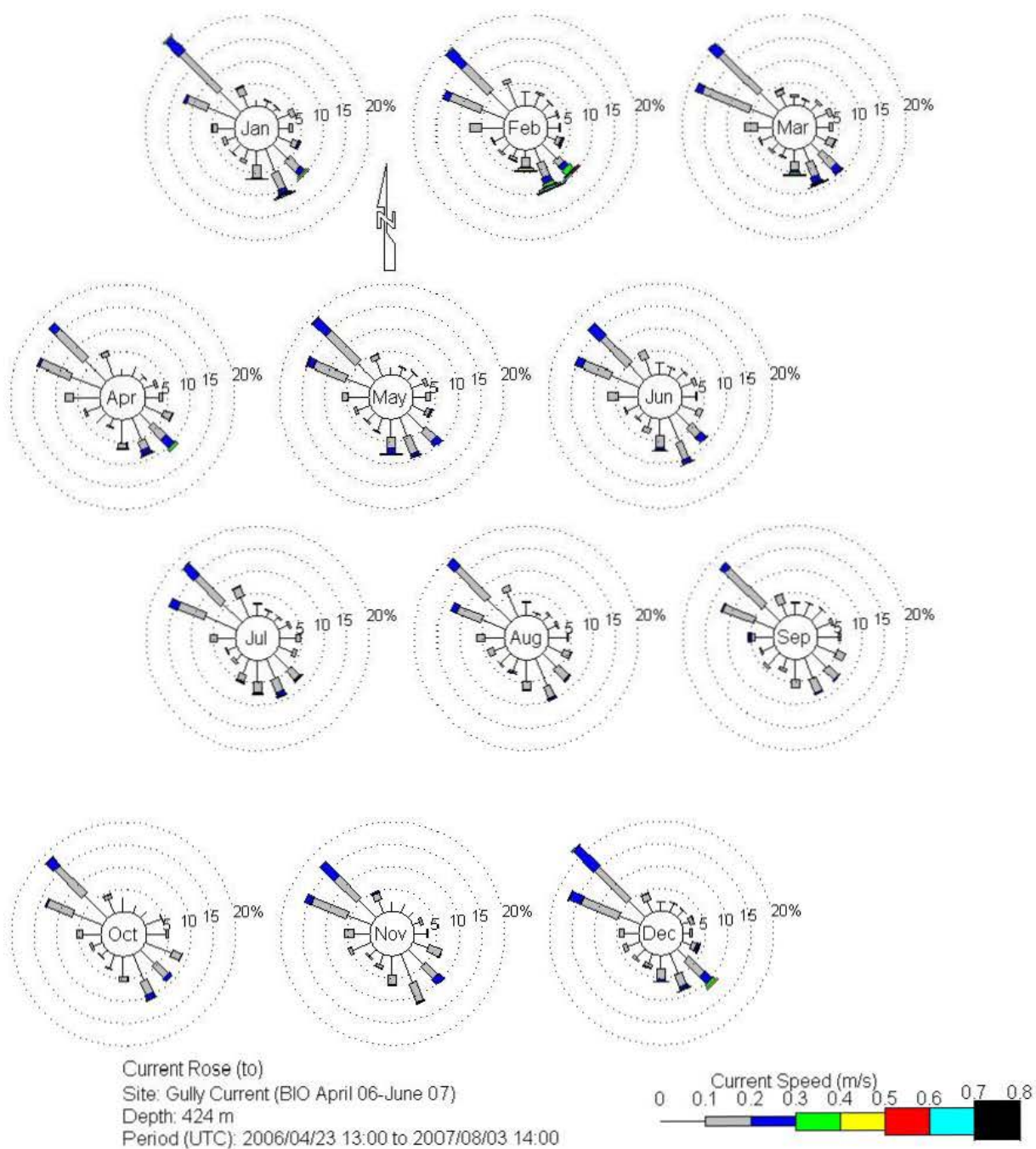
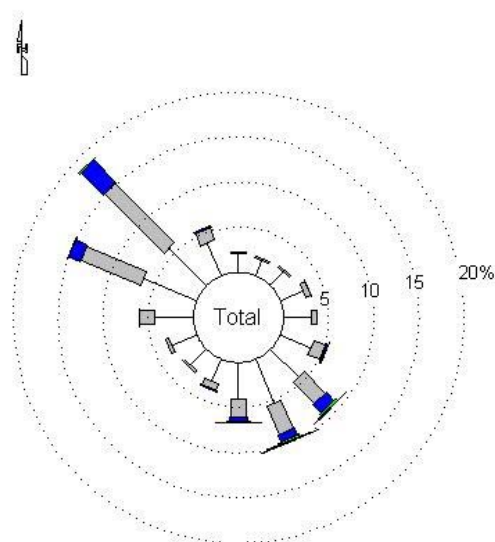


Figure A- 156: Monthly average current rose plots RCM8 Mooring 1591.



Current Rose (to)

Site: Gully Current (BIO April 06-June 07)

Depth: 424 m

Period (UTC): 2006/04/23 13:00 to 2007/08/03 14:00

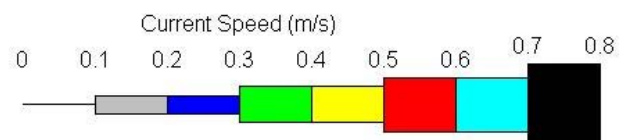


Figure A- 157: Annual average current rose plots RCM8 Mooring 1591.

Appendix 9: Tidal Analysis

Four moorings were deployed at the sites SG2 (mooring #1588), SG10 (mooring #1591), SG11 (mooring #1589), SG12 (mooring #1590), in Zone 1 of the Gully (Figure 2), which each had an RDI ADCP current profiler and several Aanderaa RCM8 current meters (Appendix 1). The moorings were deployed April 23 and 24, 2006 and recovered on August 3, 2007. The deep central mooring at SG11 when recovered was missing the upper 200 m which did not include an RCM; it went missing on 17 June, 2007. Also the two moorings on the canyon axis (#1588 and #1589) underwent vertical displacements, up to 500 m for mooring 1589.

The tidal analysis was done using T-TIDE harmonic analysis (Pawlowicz et al., 2002) of current time series from both the RCM8 and the ADCP instruments. For the ADCP time series three depth bins were chosen representing top, mid and deep ranges. Figure A- 158 to Figure A- 163, Table A- 5 and Table A- 6 summarize tidal U and V current velocity (m/s), ellipse orientation (degrees) and constituent phase (degrees relative to Greenwich) for tidal constituents with current speeds greater than 0.01 m/s.

All plots were created using MATLAB R2008b.

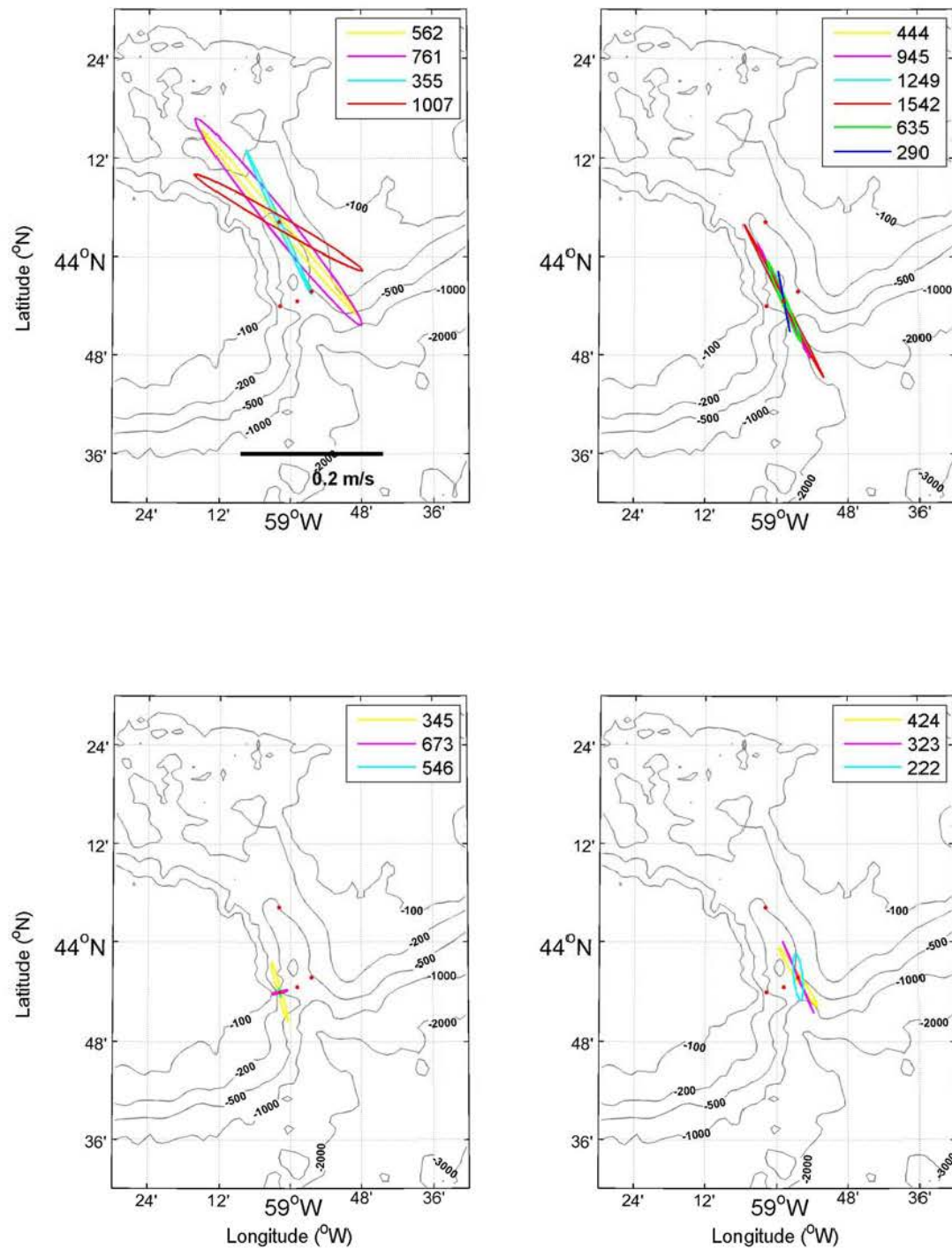


Figure A- 158: K1 tidal ellipses from the RCM8 current meters at each of the four mooring sites. Depth of the RCM8 is indicated in the upper right of each panel. A scale is provided in the upper left panel.

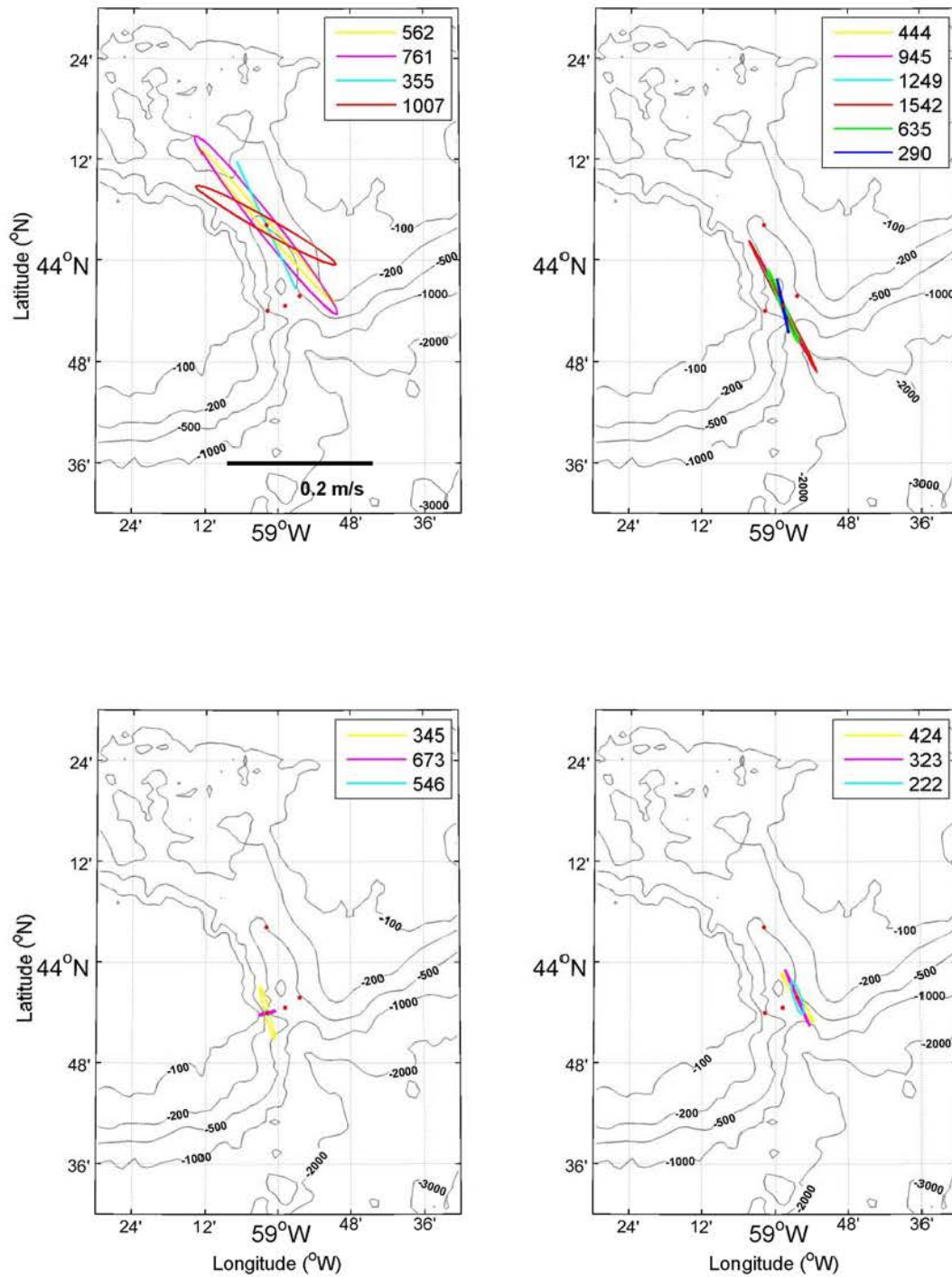


Figure A- 159: O1 tidal ellipses from the RCM8 current meters at each of the four mooring sites. Depth of the RCM8 is indicated in the upper right of each panel. A scale is provided in the upper left panel.

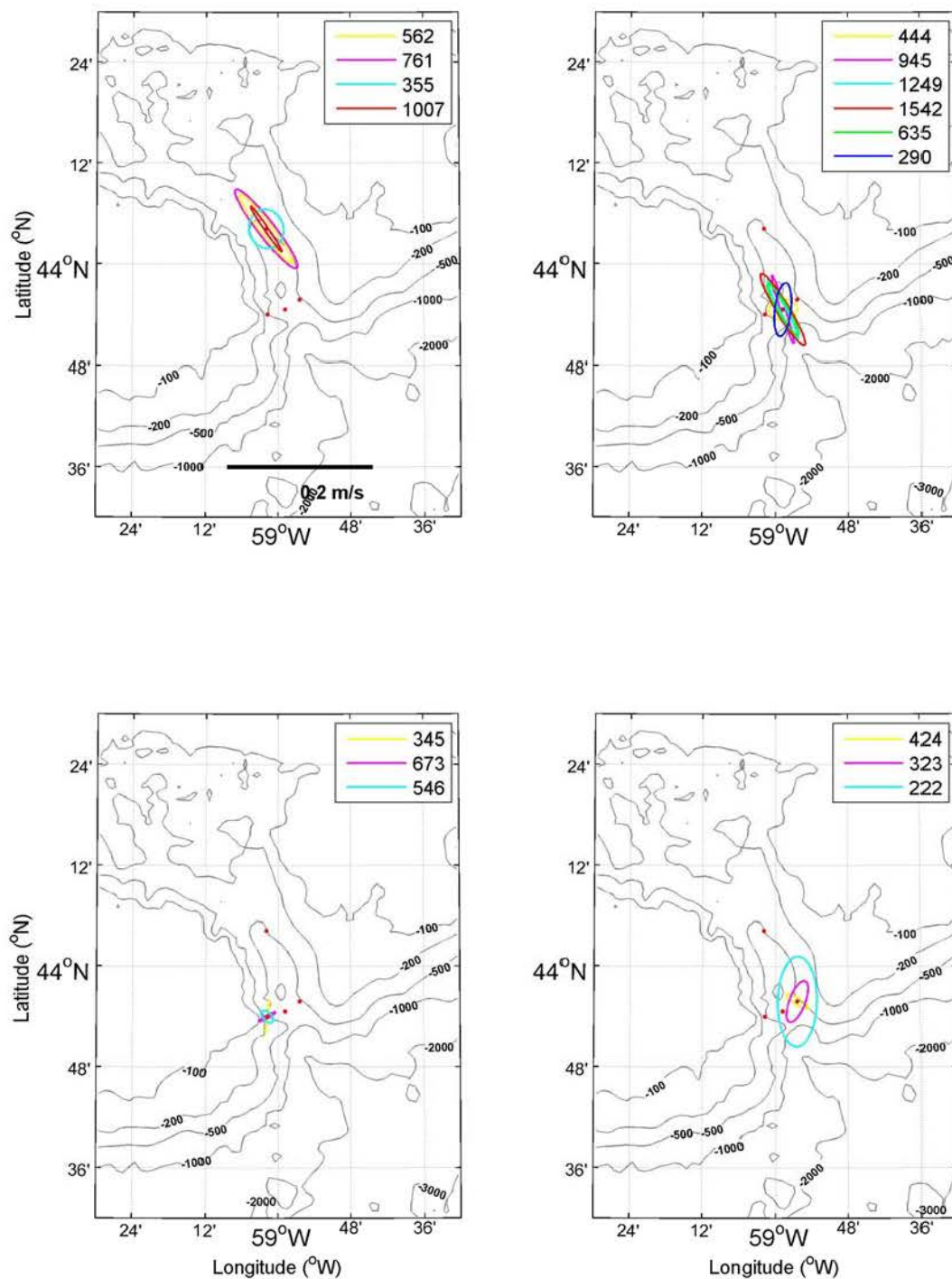


Figure A- 160: M2 tidal ellipses from the RCM8 current meters at each of the four mooring sites. Depth of the RCM8 is indicated in the upper right of each panel. A scale is provided in the upper left panel.

Table A- 5 Tidal major and minor current velocities (m/s), ellipse orientation (degrees) and phase (degrees relative to Greenwich) for tidal constituents with current speeds greater than 0.01 m/s.

Mooring # 1588 serial # 5574 depth 355 m

Major	Minor	Orientation	Phase	Constituent
0.04920	0.03913	170.15	350.59	M2
0.01462	0.00229	166.91	318.31	N2
0.01577	0.01157	164.57	20.38	S2
0.14945	0.00060	122.97	187.08	O1
0.17438	0.00515	122.35	215.41	K1
0.01778	-0.00394	144.53	57.56	MSF
0.03211	0.00057	125.61	154.07	Q1
0.02257	0.00014	128.41	215.60	J1
0.01630	-0.00875	127.15	214.94	MO3
0.01969	-0.01115	123.41	236.49	MK3
0.01128	-0.00212	176.55	317.67	M4

Mooring # 1588 serial # 5002 depth 562 m

0.09912	-0.01415	137.28	319.17	M2
0.01488	-0.00132	141.92	297.04	N2
0.02835	-0.00355	147.02	0.65	S2
0.24373	-0.00926	140.65	181.19	O1
0.28712	-0.00887	139.67	214.55	K1
0.04821	-0.00188	143.28	148.78	Q1
0.01142	-0.00104	137.49	200.97	NO1
0.02465	-0.00145	145.31	208.61	J1
0.01616	0.00103	48.20	67.90	MO3
0.02191	-0.00207	46.12	105.14	MK3
0.01759	-0.00372	98.05	216.04	M4

Mooring # 1588 serial # 5567 depth 761 m

0.11612	-0.01957	137.94	321.59	M2
0.01470	-0.00109	127.35	304.58	N2
0.03279	-0.00643	133.66	0.23	S2
0.26468	-0.02162	138.13	168.22	O1
0.31421	-0.02531	138.40	203.30	K1
0.01664	-0.00064	128.44	105.00	2Q1
0.04460	-0.00536	140.32	138.50	Q1
0.01408	-0.00268	136.23	196.57	NO1
0.02070	-0.00155	139.38	199.12	J1
0.01787	-0.00098	136.33	207.59	OO1
0.01115	0.00086	160.14	40.52	MU2
0.01053	-0.00502	126.40	55.09	L2
0.01761	0.00709	104.13	14.81	MO3
0.01883	0.00929	96.87	40.30	MK3
0.01247	-0.00080	132.90	191.51	M4

Mooring # 1588 serial # 7013 depth 1007 m

0.06269	0.00537	133.81	292.53	M2
0.00832	0.00179	130.47	232.97	N2
0.02530	0.00242	148.10	324.35	S2
0.20840	0.01549	158.00	155.95	O1
0.25720	0.01385	157.70	189.79	K1
0.01175	0.00111	159.74	220.65	MSF
0.01930	-0.00287	159.70	87.87	2Q1
0.03078	0.00593	156.82	131.68	Q1
0.01233	0.00136	161.02	186.25	NO1
0.01082	0.00117	175.32	193.74	J1
0.02223	-0.00140	161.86	186.79	OO1
0.02884	-0.00100	161.74	355.75	MO3
0.03069	-0.00300	158.50	26.88	MK3
0.01387	0.00028	136.79	159.21	M4

Mooring # 1589 serial # 7650 depth 290 m

0.05413	-0.02195	79.83	311.01	M2
0.00999	-0.00098	92.57	295.02	N2
0.01321	-0.00234	93.26	347.25	S2
0.05648	-0.00187	106.87	223.84	O1
0.06414	0.00029	105.02	244.98	K1
0.01341	0.00143	111.85	189.93	Q1
0.01055	-0.00015	109.59	238.21	J1
0.01282	-0.00629	13.90	54.64	L2

Mooring # 1589 serial # 3299 depth 444 m

0.03995	0.02074	2.48	209.53	M2
0.00856	0.00352	87.35	290.14	N2
0.00985	0.00805	78.73	324.42	S2
0.07931	-0.00366	118.62	192.39	O1
0.09392	-0.00158	119.30	217.34	K1
0.01080	-0.00053	119.03	34.66	MSF
0.01765	-0.00036	120.57	170.83	Q1
0.01128	-0.00066	115.83	214.00	J1

Mooring # 1589 serial # 4602 depth 635 m

0.06666	-0.01225	130.43	325.95	M2
0.01298	-0.00161	133.26	308.43	N2
0.01803	-0.00153	130.20	7.40	S2
0.08518	0.00559	120.63	179.92	O1
0.09623	0.00660	120.03	208.35	K1
0.02061	0.00110	121.00	146.29	Q1
0.01265	0.00106	121.81	224.29	J1

Mooring # 1589 serial # 3300 depth 945 m

0.07425	-0.00574	114.05	293.02	M2
0.01482	-0.00320	113.29	291.29	N2
0.02128	-0.00207	118.90	340.83	S2
0.11535	0.00477	124.56	162.46	O1
0.13812	0.00483	122.77	194.85	K1
0.02403	0.00048	125.08	136.81	Q1
0.01335	0.00036	123.14	189.18	J1

Mooring # 1589 serial # 3584 depth 1249 m

0.07300	0.00840	126.11	287.35	M2
0.01050	0.00344	122.65	276.27	N2
0.01997	0.00130	116.85	319.31	S2
0.12929	-0.00034	125.19	158.14	O1
0.15198	-0.00234	125.16	190.87	K1
0.02481	-0.00016	127.76	128.06	Q1
0.01685	-0.00086	129.82	171.84	J1

Mooring # 1589 serial # 4406 depth 1542 m

0.09359	-0.01562	130.71	265.12	M2
0.01506	-0.00404	134.56	236.40	N2
0.02917	-0.00417	141.21	298.27	S2
0.16016	0.00410	126.01	139.26	O1
0.19169	0.00438	125.81	175.42	K1
0.01481	-0.00226	122.32	89.23	2Q1
0.02640	0.00005	124.82	105.31	Q1
0.01245	0.00021	129.02	157.44	J1
0.01240	-0.00107	121.81	200.97	OO1
0.01115	0.00047	135.37	340.44	L2
0.01756	0.00192	170.40	315.89	MO3
0.02145	0.00356	169.61	350.27	MK3

Mooring # 1590 serial # 4349 depth 345 m

0.03462	0.00028	79.67	311.30	M2
0.00908	-0.00022	103.40	297.95	N2
0.00908	-0.00102	94.22	347.19	S2
0.05515	-0.00546	111.17	214.74	O1
0.06284	-0.00460	111.94	235.22	K1

Mooring # 1590 serial # 9607 depth 546 m

0.01871	0.00962	153.56	317.21	M2
0.00393	0.00223	101.96	274.01	N2
0.00525	0.00253	103.89	336.38	S2
0.00683	0.00245	124.58	135.97	O1
0.00974	0.00318	108.74	156.20	K1

Mooring # 1590 serial # 6409 depth 673 m

0.02490	0.00289	20.92	54.08	M2
0.00705	0.00053	18.02	54.14	N2
0.00631	0.00015	23.19	138.95	S2
0.02386	-0.00208	10.14	357.89	O1
0.02236	-0.00199	10.08	26.38	K1
0.02140	0.00115	9.70	128.99	MO3
0.02559	0.00130	8.43	168.84	MK3

Mooring # 1591 serial # 1607 depth 222 m

0.08970	-0.05410	87.83	299.97	M2
0.01595	-0.00946	106.86	261.50	N2
0.01778	-0.00942	80.91	342.99	S2
0.03600	0.00996	114.72	202.32	O1
0.04712	0.01262	98.99	205.30	K1
0.01269	0.00101	27.97	21.30	MM
0.01124	-0.00023	153.71	233.36	MSF

Mooring # 1591 serial # 1039 depth 323 m

0.04676	0.02099	58.25	253.71	M2
0.01130	0.00294	118.83	300.31	N2
0.01760	0.00249	73.98	306.53	S2
0.06522	-0.00180	121.36	174.77	O1
0.08448	0.00098	121.62	200.69	K1
0.01232	-0.00061	132.48	240.97	MM

Mooring # 1591 serial # 0786 depth 424 m

0.03378	0.00720	157.42	302.43	M2
0.00509	0.00184	116.93	261.35	N2
0.00836	0.00207	162.66	331.15	S2
0.06455	-0.00614	132.08	150.05	O1
0.08081	-0.00625	133.41	180.93	K1
0.01109	-0.00195	125.97	118.29	Q1

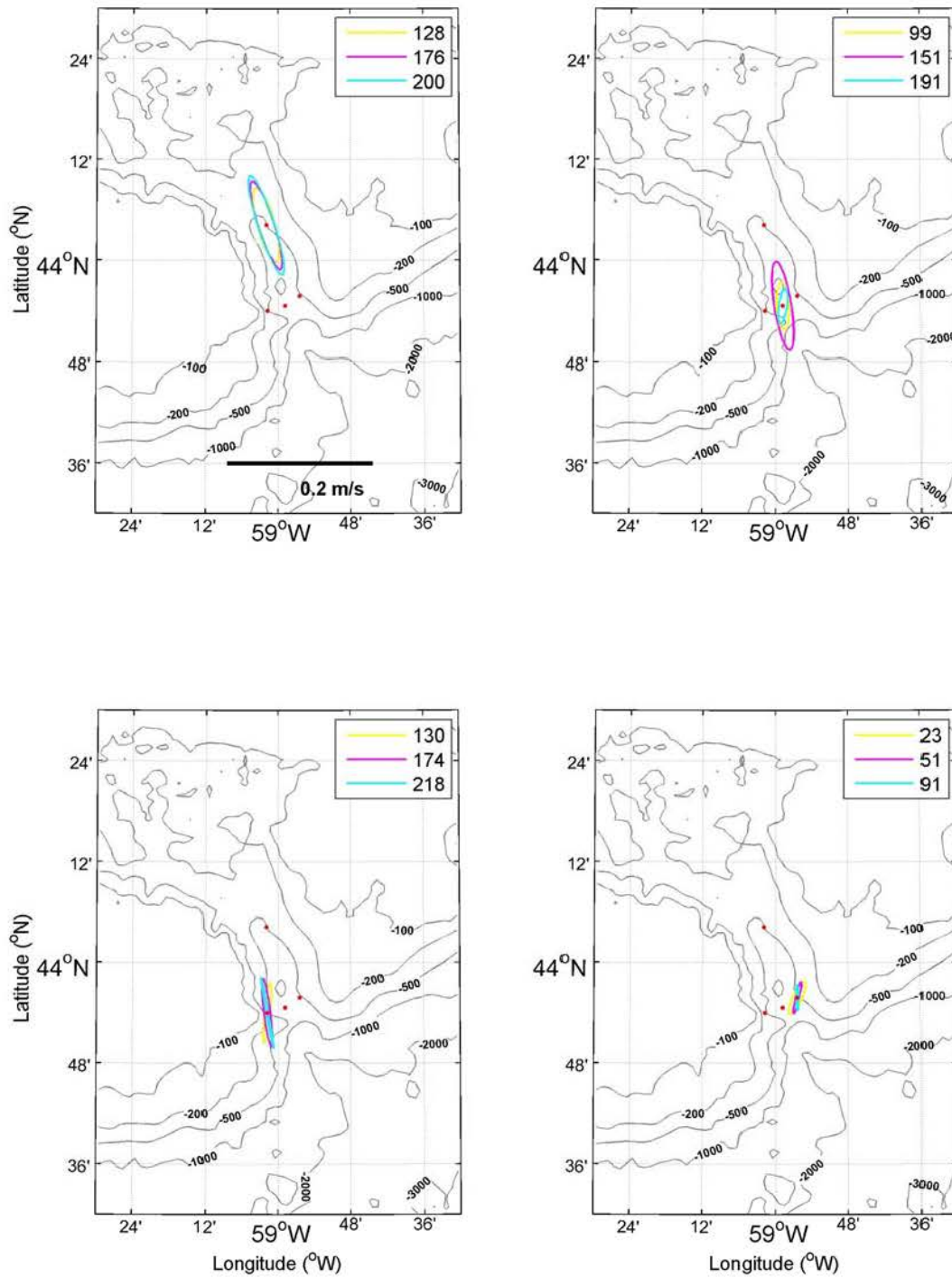


Figure A- 161: K1 tidal ellipses from the ADCPs at each of the four mooring sites. Depth of the ADCP bin is indicated in the upper right of each panel. A scale is provided in the upper left panel.

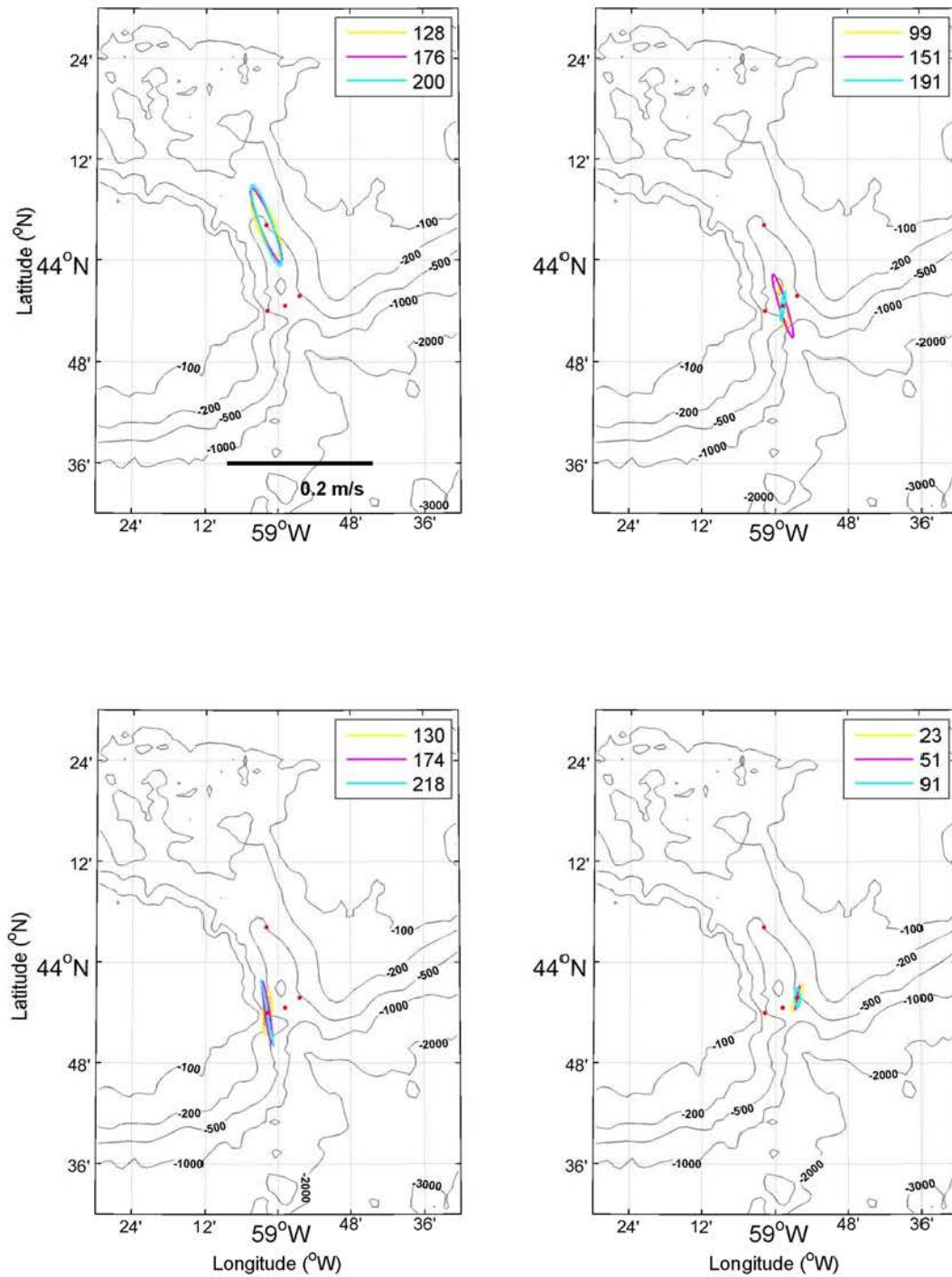


Figure A- 162: O1 tidal ellipses from the ADCPs at each of the four mooring sites. Depth of the ADCP bin is indicated in the upper right of each panel. A scale is provided in the upper left panel.

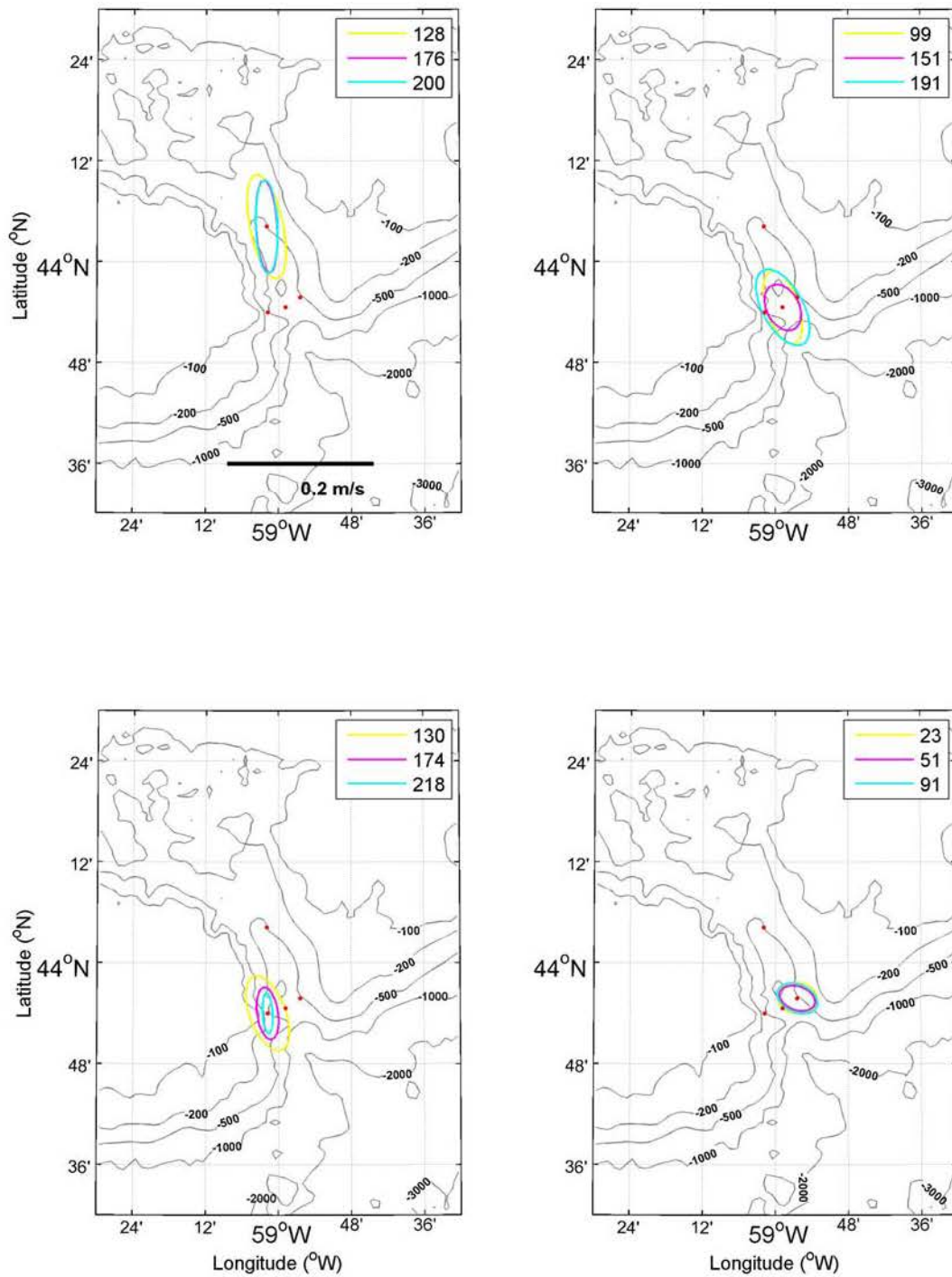


Figure A- 163: M2 tidal ellipses from the ADCPs at each of the four mooring sites. Depth of the ADCP bin is indicated in the upper right of each panel. A scale is provided in the upper left panel.

Table A- 6 Tidal U and V current velocity (m/s), ellipse orientation (degrees) and phase (degrees relative to Greenwich) for tidal constituents with current speeds greater than 0.01 m/s.

Mooring # 1588 depth bin 128 m

0.10719	-0.04456	107.53	285.16	M2
0.01981	-0.00504	102.03	251.67	N2
0.02365	-0.01007	98.62	340.41	S2
0.07090	0.02341	121.41	201.93	O1
0.07948	0.02395	112.38	214.92	K1
0.01268	0.00536	47.80	166.53	MM
0.01273	0.00333	76.06	44.73	MSF
0.02260	-0.00212	132.40	184.60	Q1
0.01154	-0.00196	125.69	250.38	MU2
0.01276	-0.00392	80.85	33.45	MK3

Mooring # 1588 depth bin 176 m

0.09197	-0.02912	94.93	276.66	M2
0.01809	-0.00500	97.99	253.45	N2
0.02501	-0.00846	97.16	315.37	S2
0.08529	0.01624	119.25	196.75	O1
0.09666	0.02140	114.98	220.01	K1
0.01698	0.00523	96.78	234.48	MM
0.01209	-0.00151	101.70	30.10	MSF
0.01660	0.00205	122.47	163.88	Q1
0.01020	-0.00426	90.66	275.35	MU2

Mooring # 1588 depth bin 200 m

0.09254	-0.02963	93.44	278.61	M2
0.01901	-0.00685	99.77	255.92	N2
0.02540	-0.00882	90.27	318.21	S2
0.09033	0.01693	115.99	191.56	O1
0.10799	0.02195	115.00	216.77	K1
0.01386	0.00458	87.26	239.60	MM
0.01303	-0.00163	127.32	24.79	MSF
0.01667	0.00286	117.91	154.40	Q1

Mooring # 1589 depth bin 099 m

0.07911	-0.04205	118.55	292.83	M2
0.01436	-0.00678	102.70	271.22	N2
0.01864	-0.00930	109.32	327.29	S2
0.04516	0.01149	101.65	221.05	O1
0.04679	0.01713	94.83	235.86	K1
0.01434	-0.00849	178.98	197.12	MM
0.01285	-0.00378	92.51	356.67	MSF
0.01454	-0.00709	0.85	153.84	L2

Mooring # 1589 depth bin 151 m

0.05565	-0.03898	144.11	256.33	M2
0.02082	-0.00577	84.50	250.98	N2
0.01152	-0.00009	39.96	351.86	S2
0.06956	0.01019	113.53	235.83	O1
0.09049	0.02374	102.85	245.22	K1
0.01385	-0.01220	83.10	283.52	MM
0.01663	-0.00573	136.97	355.13	MSF
0.01279	0.00488	104.77	180.01	2Q1
0.01396	0.00181	112.73	196.34	Q1
0.01437	-0.00579	165.51	194.09	MU2
0.01920	-0.00407	56.02	98.76	L2
0.01059	0.00745	94.07	50.45	MO3
0.01388	0.00126	94.94	168.21	M3
0.01073	0.00346	80.88	30.01	MK3

Mooring # 1589 depth bin 191 m

0.09306	-0.05005	133.83	292.69	M2
0.02420	-0.01364	108.19	262.76	N2
0.01697	-0.00657	146.81	306.27	S2
0.03029	0.00423	80.08	193.98	O1
0.03628	0.01125	78.71	205.72	K1
0.02237	0.00227	177.75	232.15	MM
0.02573	-0.00612	87.39	328.47	MSF
0.01142	-0.00683	88.91	207.24	Q1
0.01063	-0.00264	118.51	188.62	J1
0.01086	0.00505	46.91	41.62	MU2
0.01556	0.00780	177.12	50.88	L2

Mooring # 1590 depth bin 130 m

0.08342	-0.04648	123.37	282.07	M2
0.01409	-0.00824	102.55	276.11	N2
0.01542	-0.00707	123.89	312.07	S2
0.04513	0.01211	86.12	217.67	O1
0.06043	0.00806	82.07	228.39	K1
0.01537	-0.00566	136.81	216.47	MM
0.01125	-0.00013	90.14	48.72	MSF
0.01174	0.00277	91.87	204.09	Q1
0.01130	-0.00481	5.24	20.00	MU2
0.01488	-0.01110	65.64	112.14	L2
0.01002	-0.00449	170.21	160.58	MK3

Mooring # 1590 depth bin 174 m

0.05260	-0.02830	103.45	280.57	M2
0.01129	-0.00585	98.87	268.83	N2
0.01256	-0.00613	105.87	313.85	S2
0.06420	0.00639	101.78	226.74	O1
0.06945	0.00876	100.00	249.35	K1
0.01439	-0.00193	111.52	235.49	MM
0.02341	-0.00006	97.52	46.42	MSF
0.01338	0.00007	105.61	197.87	Q1

Mooring # 1590 depth bin 218 m

0.04001	-0.01356	95.36	293.18	M2
0.00866	-0.00128	88.12	262.10	N2
0.00920	-0.00173	100.20	341.07	S2
0.06770	0.00098	104.73	229.91	O1
0.07260	0.00291	103.78	251.40	K1
0.02003	0.00120	102.08	47.43	MSF
0.01345	0.00149	103.43	189.95	Q1
0.01059	0.00025	103.83	248.65	J1

Mooring # 1591 depth bin 023 m

0.05481	-0.03009	177.23	295.78	M2
0.01432	-0.00652	145.41	288.15	N2
0.01064	-0.00864	2.71	142.43	S2
0.02945	-0.00581	59.65	133.73	O1
0.03879	-0.01177	56.28	162.31	K1
0.01143	-0.00325	163.16	354.78	MSF

Mooring # 1591 depth bin 051 m

0.04987	-0.02380	169.18	285.58	M2
0.01046	-0.00591	142.84	261.89	N2
0.01524	-0.00961	0.02	131.36	S2
0.02483	0.00152	74.73	138.60	O1
0.03241	-0.00466	71.83	166.84	K1
0.01079	-0.00155	58.06	5.32	MM

Mooring # 1591 depth bin 091 m

0.05621	-0.02811	167.84	283.22	M2
0.00967	-0.00557	144.76	248.37	N2
0.01465	-0.00868	160.29	322.58	S2
0.01960	0.00752	93.56	157.15	O1
0.02590	0.00335	90.77	170.26	K1
0.01429	-0.00113	65.88	8.74	MM

Appendix 10: Spectral Analysis

A spectral analysis was conducted for each mooring with the RCM8 and ADCP 25 m binned current time series using the Hamming window of 1024 and Welch's averaged modified periodogram method in MATLAB.

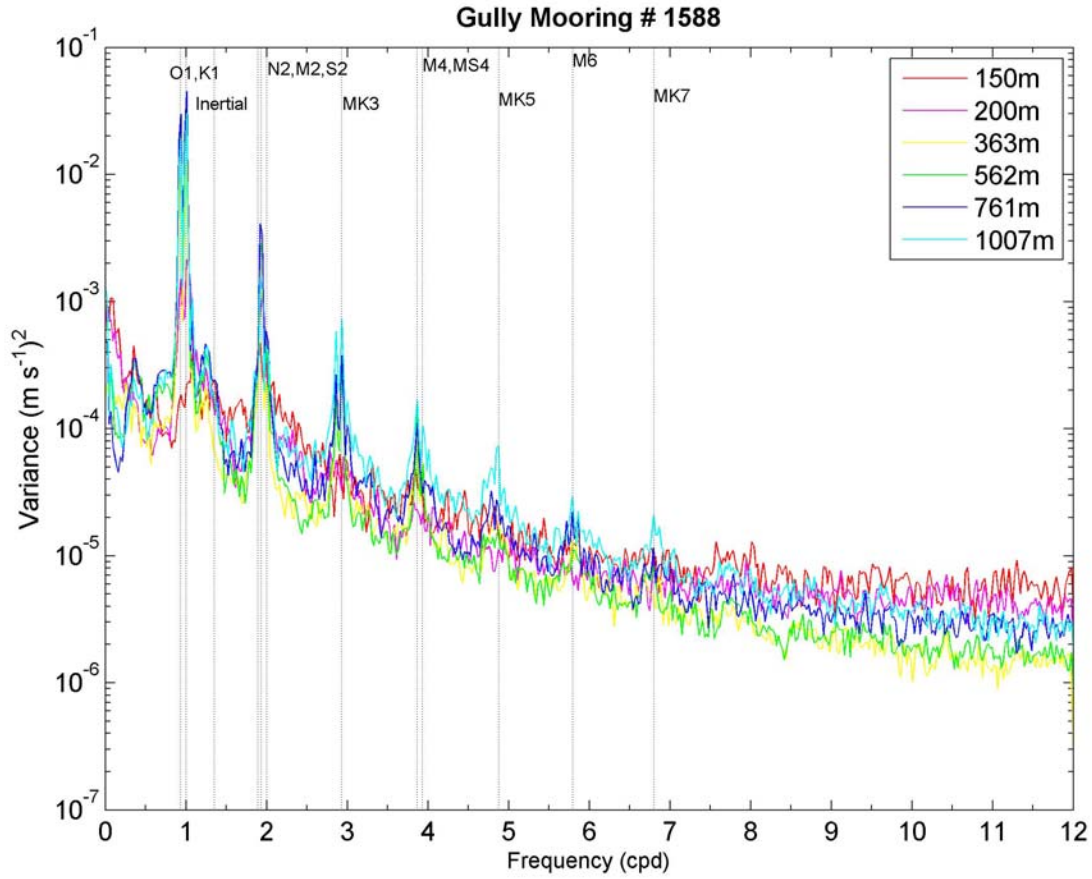


Figure A- 164: Spectra of currents for mooring 1588 (SG2). Vertical grey lines correspond to tidal and inertial frequencies. Depths of the current meter are indicated by the colour-code legend in the upper right.

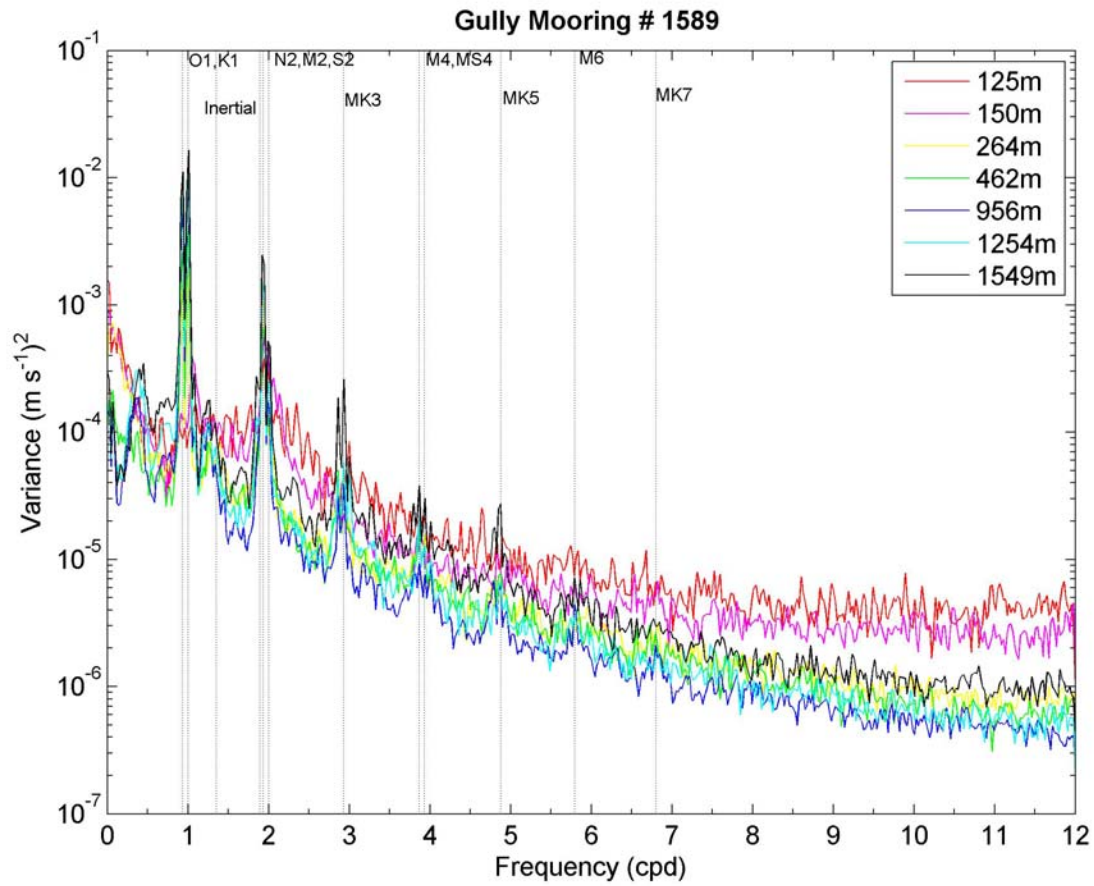


Figure A- 165: Spectra of currents for mooring 1589 (SG11). Vertical grey lines correspond to tidal and inertial frequencies. Depths of the current meter are indicated by the colour-code legend in the upper right.

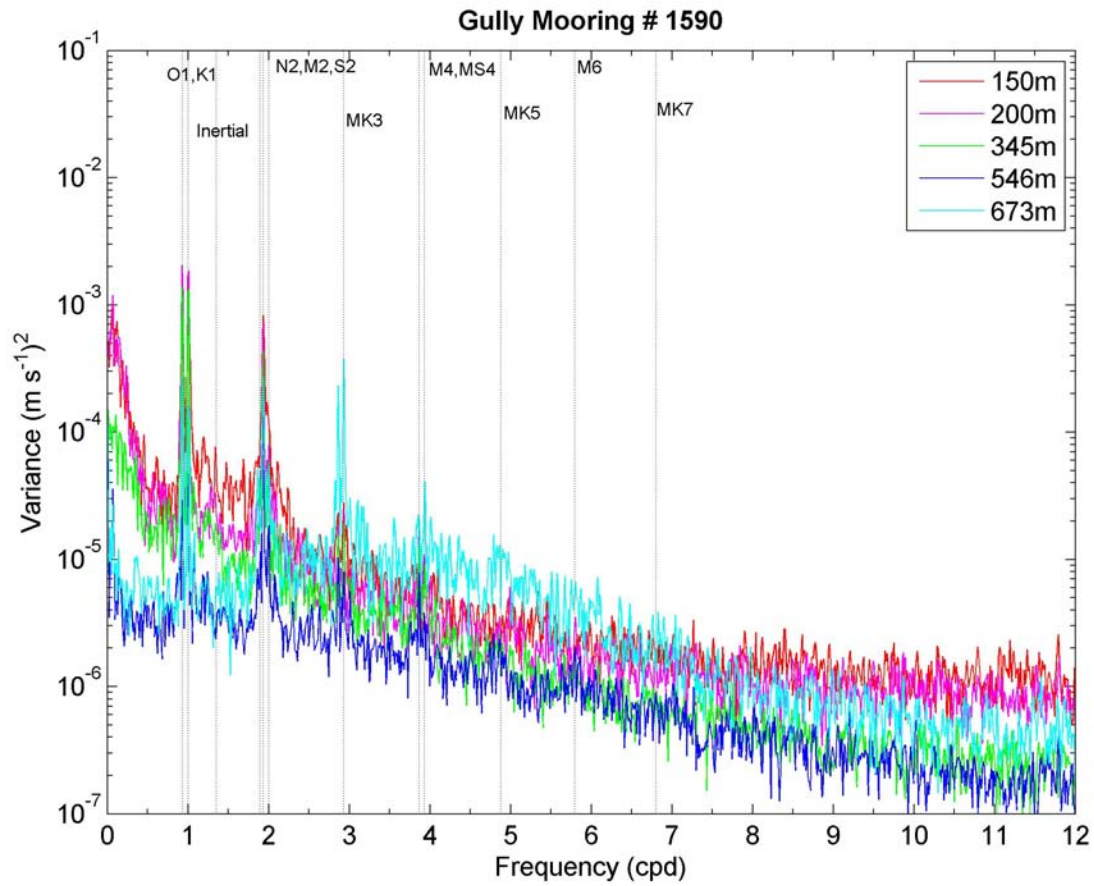


Figure A- 166: Spectra of currents for mooring 1590 (SG12). Vertical grey lines correspond to tidal and inertial frequencies. Depths of the current meter are indicated by the colour-code legend in the upper right.

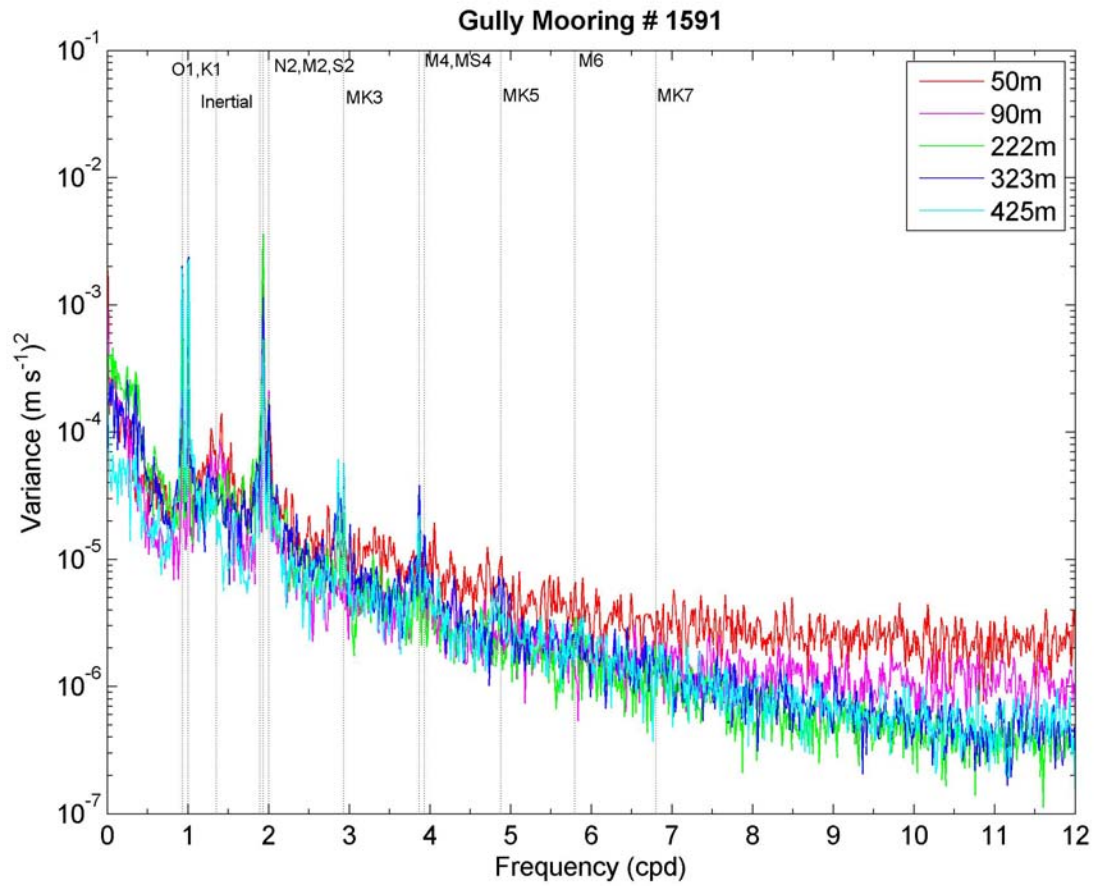


Figure A- 167: Spectra of currents for mooring 1591 (SG10). Vertical grey lines correspond to tidal and inertial frequencies. Depths of the current meter are indicated by the colour-code legend in the upper right.